The University Of Sheffield.

Botulinum Neurotoxin X: A New Tool to Study Intracellular Transport and Membrane Trafficking

Asral Wirda Binti Ahmad Asnawi

A thesis submitted in partial fulfilment of the requirements for the degree of Doctor of Philosophy

The University of Sheffield
Faculty of Science
Department of Biomedical Sciences

January 2021

Acknowledgements

Alhamdulillah, all praises to Allah S.W.T who is the Most Gracious, most compassionate for giving me the strength and perseverance to endure all the challenges encountered during my Ph.D. journey. The work contained in this thesis may have never come together without the help, continual support, and encouragement of so many people.

First and foremost, my deepest appreciation and gratitude must go to my supervisor, Dr. Andrew Peden. Thank you for accepting an old gal to be part of your lab and giving me all the opportunities to learn and grow. Despite my background that lacks the conventional laboratory skills and knowledge of basic science that is "outdated", Dr. Peden gave me a chance to obtain the skills that I would never have dreamed of learning and mastering at this stage of my career. The level of creativity, ingenuity, and insight in troubleshooting technical issues, tweezing out the science and just making sense of complex biological questions amazes me still and inspires me to do better always. I will never forget your kindness, dedication, advice, encouragement, and most of all your patience throughout the entirety of this experience. My gratitude also goes out to my advisers, Professor David Grundy and Dr. Kai Erdmann. Thank you for your invaluable advice and dedication to see me through. Both have kept me on track and always looking at the bigger picture. Thank you also to post-docs in the lab Elan and Selva for showing me the ropes in the lab. Elan literally held my hand for the first 6 months of life during my Ph.D. I will never forget your kindness.

Special thank you and loads of love to my lab mates, Amber, Jess, and Nabila. Thank you for keeping me sane, showing me how to 'lighten-up' and have single-ladies' outings. Thank you for making my nails look pretty in nail polish for the first time in my life, taking me Christmas shopping, and introducing me to the signature Sheffield Sheppard's Pie. It would have been a crime to come back to Malaysia without having one. Naturally, we bonded over food and they treated me like a superstar over simple Malaysian dishes, like curry, kurma, prata bread, and rendang. It was indeed my pleasure. Thank you guys for always lending an ear, having my back, and being my besties.

Everyone on D-floor of Alfred Denny is a superb and wonderful individual. My immediate "next-door" neighbours in Dr. Kai Erdmann's lab; Claire, Andrew Wood, and Lily. I would never have had the motivation to continue working throughout the night and spending long weekends at the lab without having you guys as great companions that I see almost 7-days a week. Andrew Wood, you are a genius, Lily; I will miss having bubble-tea with you and Claire, the first friendly face that said hello to me, set up my laptop connection to the printer, and always makes sure my calculations are spot-on. I miss all of you dearly.

This bittersweet journey would never have been realised without the support and love of my darling husband, Dr. Abdul Qahhar Abdul Wahid. He is my rock and I love him to the moon and back. He mentioned that if we went back in time and had the chance for a do-over of the time we lost this past 4 years, he would still insist I do my Ph.D.

Thank you for not clipping my wings and making my dreams a reality. He has been the voice of reason throughout this whole back-and-forth roller-coaster ride and I appreciate that he turned a deaf ear to all the negativity around our precarious living arrangements during those 4 years. My darling angels, Abdurrahman, Aila and Aufa. I could not breathe if I lost sight of all of them. Aufa, my youngest, leaving her with her father at a tender age was the hardest decision we had to make as situations evolved and changed. To my parents and in-laws, no words can describe my gratitude for all that you have done for us during this time. And not forgetting, my post-graduate students, Nadila, Alif, Syazwan, Halimah, and Jihan. I am proud of each and every one of them. I wish I could have been a better supervisor for all of them and let them know then what I know now.

I am indebted to everyone that has been mentioned and all other individuals that have been directly and indirectly involved with the project and the final thesis preparation. Lastly, the funding aid for this Ph.D. was made available from the Ministry of Higher Education and the Universiti Sains Islam Malaysia.

Preface

I, the author, confirm that the Thesis is my own work. I am aware of the University's Guidance on the Use of Unfair Means (www.sheffield.ac.uk/ssid/unfair-means). This work has not been previously been presented for an award at this, or any other, university.

Asral Wirda Binti Ahmad Asnawi January 2021

Summary

The recent discovery of a new serotype, BoNT/X has created an exciting opportunity to characterise the function of SNAREs which were not previously amenable to the action of these toxins. BoNT/X has been shown to cleave multiple R-SNAREs in vitro (VAMP1, 2, 3, 4, 5, and Ykt6) and VAMPs 2 and 4 in vivo. However, almost nothing is known about the impact of cleaving these SNAREs on intracellular trafficking. The aim of my thesis was to validate and extend BoNT/X's substrate specificity by looking at endogenous SNAREs and determine how the loss of these proteins impacts intracellular trafficking using a range of quantitative endocytic and biosynthetic transport assays. I have shown that BoNT/X is active when expressed in cells and has a similar specificity as the native toxin (cleaves endogenous VAMPs 3, 4, and Ykt6). BoNT/X intoxication leads to dramatic alterations in the localisation, morphology, and staining intensity of numerous markers of the endocytic and biosynthetic pathways suggesting that the toxin is impacting many different trafficking pathways. Using a flow cytometry-based endocytic assay I have shown that there is a significant reduction in TF-R endocytosis most likely caused by the loss of the receptor from the cell surface. I have also shown that the surface levels of many proteins are also significantly reduced (CD63, CD/CI-MPR, EGF-R, and TGN46) suggesting a global defect in cell surface trafficking. I have also examined the impact of BoNT/X intoxication on constitutive secretion using a novel flow cytometry-based assay I have developed during my Ph.D. I have found that BoNT/X intoxication blocks the delivery of soluble and membrane-anchored proteins to the cell surface by causing them to accumulate in the early biosynthetic pathway. Taken together, my data suggests that BoNT/X is a potent inhibitor of intracellular trafficking and behaves very differently from any of the well-characterized botulinum serotypes. In the future, it will be important to determine if the observed phenotypes can be rescued using cleavage-resistant SNAREs.

Abbreviations

AP	Adaptor protein complex, such as AP-1, AP-2, AP-3, and AP-4
AQP2	Aquaporin-2 channel
ARF	ADP ribosylation factors
Arg	Arginine
ATP	Adenosine triphosphate
BoNT	Botulinum toxin
BSA	Bovine serum albumin
C	Clostridium
CCAIM	Isoprenyl/lipid-anchored motif at C-terminus of human Ykt6
CD	Cluster of differentiation; example CD63
CD	Cation dependent
CI	Cation independent
CME	Clathrin-mediated endocytic
CO_2	Carbon Dioxide
COG	Conserved oligomeric golgi complex
COPI	Coat protein complex I, involved in Golgi to ER retrograde transport
COPII	Coat protein complex II, involved in ER to Golgi anterograde transport
DD	Destabilization domain
ddH2O	Double distilled water
dH2O	Distilled water
DMEM	Dulbecco's modified eagle medium
DMSO	Dimethyl sulfoxide
DNA	Deoxyribonucleic acid
E.coli	*Escherichia coli*
ECL	Enhanced chemilluminescence
EDTA	Ethylenediaminetetraacetic acid, a metal chelator
EE	Early endosome
EEA1	Early endosome antigen 1
EGFP	Enhanced Green Fluorescent Protein
EGF-R	Epidermal growth factor
EM	Electron microscopy
En	*Enterococcus faecium*
ER	Endoplasmic reticulum
ERGIC	ER/Golgi intermediate compartment
FACS	Fluorescence activated cell sorting
FBS	Fetal Bovine Serum
FSC	Forward scatter
GABA	γ-aminobutyric acid
GFP	Green fluorescent protein
GIcNAc	N-Acetylglucosamine

Gluc	Gaussia luciferase
GLUT-4	Glucose transporter type 4
GTP	Guanosine triphosphate
HA	Hemagglutinin tag, a 9 amino acid tag derived from the human influenza hemagglutinin protein
Habc	Regulatory N-terminal three-helix bundle
HC	Heavy chain
HC-C	Heavy chain C-terminal
HC-N	Heavy chain N-terminal
HeLa	Human cervical carcinoma cell line
HEPES	4-(2-hydroxyethyl)-1-piperazineethanesulfonic acid, a buffering agent
HRP	Horseradish peroxidase
IgG	Immunoglobulin G
kDa	Kilo Dalton
LB	Luria Bertani Broth
LC	Light chain
LDL	Low-density lipoprotein receptor
LE	Late endosome
MCS	Multiple cloning sites
MDCK	Madin Darby canine kidney cells, a polarized epithelial cell type
MMP	Matrix metallopeptidase
MPR	Mannose 6-Phosphate receptor
MTCs	Multisubunit tethering protein complexes
MVB	Multivesicular bodies
Nacl	Sodium chloride
NAPs	Nontoxic accessory proteins
NSF	N-ethylmaleimide sensitive factor, an ATPase which unwinds SNARE complexes
NTNHA	Nontoxic non-haemagglutinin component
Orf	Open reading frame
PBS	Phosphate buffered saline
PCR	Polymerase chain reaction
PEGFP-C3	C-terminus of enhanced GFP
PEI	Polyethyleneimine
PFA	Paraformaldehyde
pH	Scale used to specify how acidic or basic a water-based solution
PLL	Poly-L-lysine
PM	Plasma membrane
PVDF	Polyvinylidene fluoride, a membrane used for western blotting applications
Qa-SNARE	Protein with a SNARE domain resembling that of syntaxin 1, contributing a glutamine (Q) at the 0-layer of the SNARE complex

Qbc-SNARE	Protein with two SNARE domains at the N and C-termini, both contributing a glutamine (Q) at the 0-layer of the SNARE complex
Qb-SNARE	Protein with a SNARE domain resembling the N-terminal SNARE domain of SNAP25, contributing a glutamine (Q) at the 0-layer of the SNARE complex
Qc-SNARE	Protein with a SNARE domain resembling the C-terminal SNARE domain of SNAP25, contributing a glutamine (Q) at the 0-layer of the SNARE complex
Rab	Member of the Ras superfamily of small G proteins
rpm	Revolutions per minute
R-SNARE	Protein with a SNARE domain resembling that of VAMP/synaptobrevin, contributing an arginine (R) at the 0-layer of the SNARE complex
RT	Room temperature
SDS	Sodium dodecyl sulfate, a negatively charged detergent
SDS-PAGE	Sodium dodecyl sulfate polyacrylamide gel electrophoresis
SEC	Refers to yeast temperature-sensitive secretion mutants, with appended numbers indicating the general order in which they were generated/characterized
SecV	Secretory vesicle
SFA	Surface Force Apparatus
SG	Secretory granules
siRNA	Small interfering RNA
SM	Sec1/Munc1
SNAP	Soluble NSF attachment protein. Not to be confused with the SNAREs SNAP23, 25, 29, etc.
SNAREpin	A complex of four SNARE proteins
SNAREs	Soluble NSF attachment protein receptor
SSC	Side scatter
Stx	Syntaxins
SV	Synaptic vesicles
Syb	Synaptobrevin, refers to either the somatic R-SNARE of Drosophila or the neuronal mammalian R-SNAREs synaptobrevin 1 and 2
SYBR	SYBR Green is an asymmetrical cyanine dye used as a nucleic acid stain in molecular biology
TBE	Tris/borate/EDTA buffer used to run agarose gels
TeNT	Tetanus neurotoxin
TF-R	Transferrin receptor
TGN	Trans-Golgi-network
TMD	Transmembrane domain
TOPO	Refers to a ligase-free cloning strategy using pre-cut vectors with topoisomerase I ligated to the 3’ ends.
TRAPP	“Transport protein particle” complex mediating ER-Golgi transport
t-SNARE	Target membrane SNARE

Uniprot	Freely accessible database of protein sequence and functional information
V	Volts
VAMP	Vesicle associated membrane protein, all of which are R-SNAREs
Vps	Vacuolar protein sorting yeast mutants
v-SNARE	Vesicle SNARE
VSV-G	Vesicular stomatitis virus glycoprotein. The ts045 VSV-G mutant is confined to the ER at 39.5°C, but is transported out of the ER at 32°C
WGA	Wheat Germ Agglutinin
Wo-orf1	*Weissella oryzae* Open reading frame

List of Tables

List of Figures

Table of Contents

Chapter 1: Introduction

1.1 A Historical Perspective of Membrane Trafficking

A critical juncture in the prokaryote to eukaryote evolutionary transformation was the inception of the endomembrane system and the elucidation of the membrane-trafficking system. The genesis and evolution of the membrane trafficking system were initiated by models that included the endosymbiotic (Gupta and Brian Golding, 1996, Martin and Müller, 1998, Moreira and López-García, 1998) and autogenous origins (Cavalier-Smith, 1975, Cavalier-Smith, 1987). These models have since been incorporated within larger theories of eukaryogenesis (de Duve, 2007, Jékely, 2003). All eukaryotic cells contain membrane-bound organelles that separate specific functions. which constantly interact with one another. The communication of the cell with its environment is crucial for all tissue and organ function. Intracellular transport systems in eukaryotes are complex and extend beyond simple diffusion. The organelles of the endomembrane system include the endoplasmic reticulum, Golgi apparatus, early and recycling endosomes, multivesicular body or late endosomes, lysosomes/vacuoles, and the plasma membrane.

Studies of yeast *(Saccharomyces cerevisiae)* and other metazoan cells have revealed a common core of protein factors involved in transport carrier formation, compartment specificity, and membrane fusion (Bonifacino and Glick, 2004). An ensemble of proteins such as GTPases, adaptor proteins, and coat protein complexes congregate on membranes to produce cargo carriers in the form of vesicular or tubular structures to export material from one organelle for delivery to another cellular compartment in an exceptionally well-orchestrated process (McMahon and Mills, 2004, Robinson, 2004). Many protein families are essential for this task, which includes SNAREs, tethering complexes, syntaxin-binding proteins or Sec1/Munc1 (SM) proteins and Rab GTPases to ensure specificity and fusion of these carriers with the correct target membrane (Jahn et al., 2003). These protein factors can be further divided into subfamilies whereby each member performs a function that is paralogous but at a different organelle location or in a distinct transport pathway (Bonifacino and Glick, 2004). Intracellular trafficking

that involves the delivery of numerous different molecules within the cell has been a Nobel prize-winning subject in Physiology and Medicine. The work and contribution of Nobel-winning scientists such as Randy W. Schekman, James E. Rothman, and Thomas C. Südhof who have developed sophisticated tools and methodologies in breaking down the complex intracellular elements paved the way for other scientists to further advance the understanding of the various molecules and pathways associated with this dynamic network of cellular communication (Ferro-Novick and Brose, 2013).

1.1.1 Vesicular-based trafficking

The organelles involved in the membrane-trafficking system may be steady installations in the cell or represent transitional stages of maturing compartments (Pantazopoulou and Glick, 2019). The transport of material between them is to a great extent mediated by vesicle formation from a donor organelle and vesicle fusion at the succeeding acceptor organelle. The basic process of vesicle formation starts after priming of small GTPases (from the Arf family) by its guanine exchange factor (GEF) and is relocated from the cytosol to the membrane of the donor organelle while recruiting coat-forming proteins to this membrane. This undertaking is regulated by the action of GTPase-activating protein (GAP) (D'Souza-Schorey and Chavrier, 2006). Various cargo adaptors will then bound these vesicle cargo proteins (Sanger et al., 2019). The motor proteins myosin, dynein, or kinesin, interact with peptide motifs within the cargo and cargo adaptor proteins, allowing vesicles to be transported along cytoskeletal elements (Cross and Dodding, 2019). Tethering proteins that extend from the acceptor organelle will recognize the inbound vesicles. These multisubunit tethering complexes function together with Rab GTPases and their respective GEFs and GAPs to coordinate membrane tethering and fusion at different locations in the cell through their interaction with effector proteins (Luo et al., 2014, Mima et al., 2008, Ohya et al., 2009). Once tethered, vesicles are docked and later undergo membrane fusion with the target membrane. This final process is mediated by the SNARE proteins and its regulators (Carr and Rizo, 2010, Baker et al., 2015).

Palade originally hinted towards a more complex explanation of intracellular transactions, where small vesicles carry cargo between distinct compartments (Palade, 1975b). He initially focused on the role of intracellular membranes in the maturation

and secretion of proteins manufactured by cells of the exocrine pancreas. This was demonstrated by using pulse-chase autoradiographic tracings of newly synthesized zymogens, moving from the ER to Golgi complex, and storage granules to the cell surface. For sequential processing of carbohydrates and sorting of cargo to the correct destination, vesicle flow had to be directional. Evidence for a vesicular transport model of exocytosis was presented by Rothman's Lab, in which a cell-free system they developed had succeeded to reproduce the specificity of vesicle budding and sorting on the membrane exemplified by reconstitution of the transport of protein between successive compartments on the Golgi and measured by the coupled incorporation of N-acetylglucosamine (GlcNAc) (Balch et al., 1984)

To further understand the cellular mechanics of the movement of proteins from the ER through the Golgi complex, the visualization of ER to Golgi transport in living cells revealed a sequential mode of action of coat protein complexes, COPII and COPI (Scales et al., 1997). Their individual roles are still unclear. Coats are multisubunit complexes that mediate the formation of transport vesicles from donor membranes. There are three major types of protein-coated transport vesicles that have been quite well-characterized with molecular detail, which attribute to various steps along the secretory pathway. The first is COPII-coated vesicles that allow its exit from the ER (Kaiser and Schekman, 1990), the second is COPI-coated vesicles carrying proteins between the ER and Golgi complex (Malhotra et al., 1989) and thirdly, clathrin-coated vesicles for post-Golgi trafficking (Friend and Farquhar 1967). Adaptor protein complexes help coat proteins mediate the recruitment and enrichment of specific cargo into transport vesicles by recognizing linear and three-dimensional sorting signals. These transport complexes act as ER to Golgi transport intermediates from which COPI may even be involved in recycling material to the ER (Scales et al., 1997).

While, data from biochemical, morphological, and genetic approaches strongly supports the vesicular model as the general mode of intracellular transport, cisternal maturation as a model for exocytosis has also been explored. A case for extra-large cargo transport has been made for newly synthesized procollagen I. Procollagen I assembles into an oligomeric complex composed of rod-like triple helices in the ER lumen. Using serial sections of immunoelectron microscopy images, these supramolecular structures (>300 nm), travels from the ER to Golgi via tubular-saccular structures and moves to the Golgi

forming large electron-dense aggregates, where it does not leave the Golgi lumen as it traverses the stack thus supporting intracellular transport in this instance occurs by cisternal maturation (Bonfanti et al., 1998). It may be implied that cisternal maturation models apply to ultra-large cargo in specialized cell types.

1.2 SNARE proteins and membrane fusion

Proteins and lipids of the endocytic and biosynthetic pathways are transported between compartments in small transport vesicles. As described in section 1.1.1, a vesicular model to mediate complex trafficking pathways has been proposed. Vesicle-mediated membrane trafficking can be broken down into several distinct steps; vesicle formation, transport, tethering, and finally fusion. Fusion is the final step in the process and is mediated by a family of proteins called soluble N-ethylmaleimide-sensitive factor attachment protein receptors or SNAREs.

Rothman and colleagues established the SNARE (soluble N-ethylmaleimide-sensitive factor attachment protein receptor) hypothesis by studying vesicle exocytosis of neurotransmitters in brain synapses. The work began years earlier when he successfully purified the NSF protein, a 75 kDa tetramer (Block et al., 1988b). They observed that uncoated transport vesicles accumulated when NSF was withheld from incubation of Golgi stacks with cytosol and ATP, indicating that NSF was needed for membrane fusion (Malhotra et al., 1988). Subsequent to this, he discovered two other components that would bind NSF to Golgi membranes, an integral heat-sensitive membrane receptor and a cytosolic factor, which was later known as SNAP or soluble NSF attachment proteins (Weidman et al., 1989). He subsequently suggested that NSF is a general component of membrane fusion machinery involving various stages of the secretory pathway (Beckers et al., 1989). He also discovered that the NSF gene was equivalent to Sec18 gene product of yeast, known to be important for vesicle-mediated transport from the endoplasmic reticulum to the Golgi, suggesting that the mechanism is highly conserved between species and at different stages of transport (Wilson et al., 1992).

1.2.1 The SNARE superfamily

The SNARE hypothesis for vesicular fusion was developed by James Rothman (Söllner et al., 1993). He initially proposed that v-SNAREs (on vesicles) interact with t-SNAREs (on target compartment) to form a SNARE complex and that the hydrolysis of ATP by NSF drives membrane fusion (Söllner et al., 1993). Rothman's laboratory performed an affinity purification procedure where they used NSF and SNAP to extract SNAP receptors, being the SNAREs from brain homogenate. Three SNAREs proteins were purified and subsequently identified as SNAP-25, VAMP2, and Syntaxin (Söllner et al., 1993).

SNARE proteins are evolutionary conserved and found in all Eukaryotes (Kloepper et al., 2007). There are at least 24 known SNAREs in the yeast genome, 26 in the *Drosophila* genome, and 38 SNAREs encoded in the human genome (Kloepper et al., 2007, Bock et al., 2001). SNARE proteins are generally small 20-30 kDa proteins that contain a highly conserved SNARE motif (60-70 residues) that participates in forming complexes with other SNAREs. Most SNAREs are C-terminal anchored with their N-terminal and SNARE domains exposed to the cytoplasm where they are able to interact with other SNARE proteins.

Table 1.1 Classification of mammalian SNAREs

SNARE	Subtype	Members
Q-SNARE	Qa/Syn	Syn 1,2, 3, 4, 5, 7, 9 /19, 11, 13, 16, 17 and 18
	Qb/S25N	SNAP23N, SNAP25N, SNAP29N, GS27, GS28, Vti1a, Vti1b
	Qc/S25C	SNAP23C, SNAP25C, SNAP29C, Syn6, Syn10, Syn8, Bet1, GS15, Slt1/Use1, Sec20
R-SNARE	Longin	VAMP7, Sec22b, Ykt6
	Brevin	VAMP1, 2, 3, 4, 5, 8

1.2.2 The SNARE complex

SNARE proteins mediate membrane fusion events such as vesicle fusion and exocytosis. Prior to membrane fusion, SNARE complexes exist in a trans-SNARE

conformation on opposing membranes. The basic SNAREpin structure would consist of 2 or 3 t-SNARE molecules interacting with 1 v-SNARE. Each SNARE has 1 or 2 SNARE motifs, that would zipper-up on each other from the N-terminus towards the C-terminus which arranges in parallel to form a coiled-coil parallel four-helix bundle (Figure 1.2). When SNAREs on opposing membranes interact, the SNAREpin structure is known as *trans*-SNARE complex. Following vesicle fusion, the complex becomes a *cis*-SNARE configuration where the complex becomes a continuous structure that is associated with the same membrane (Jahn and Scheller, 2006, Sutton et al., 1998).

The first SNARE complex identified in the presynaptic neuron contains 3 SNARE; Syntaxin1, SNAP25, and VAMP1 necessary for neurotransmitter release (Trimble et al., 1988a, Oyler et al., 1989, Bennett et al., 1992). The crystal structure of this complex revealed that this four-helix bundle of SNARE motifs, at its longitudinal midpoint, contains a 'zero layer' that comprises four large hydrophilic residues, usually three glutamine (Q) residues contributed by syntaxin1 and SNAP25 and one arginine (R) residue by VAMP2 (Fasshauer et al., 1998, Sutton et al., 1998) (Figure 1.1).

In the current model, additional factors such as tethering complexes and Rabs found on the surface of transport vesicles would provide additional specificity to the process.

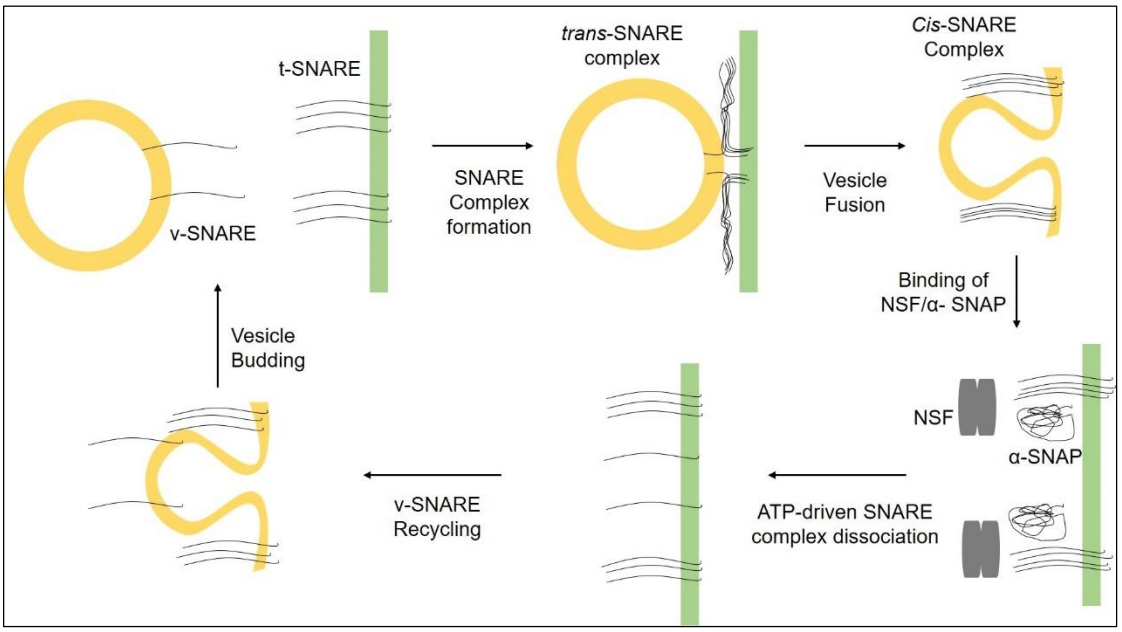

Figure 1.1 SNARE complex formation. Model for SNARE-mediated vesicle fusion and recycling. (Adapted from Banifacino and Glick, 2004).

SNAREs that reside on the vesicle and target compartment assemble to form complexes that bring two membranes closer together and mediates fusion by a zippering process. The core complex then disassembles after fusion by the ATPase activity of NSF which binds to the core complex through SNAP. The SNAREs are recycled back to their location for subsequent rounds of membrane fusion. Abbreviation: NSF; N-ethylmaleimide-sensitive fusion protein, SNAP; soluble NSF-attachment protein.

1.2.3 Classification of SNAREs

SNAREs were originally classified functionally as v-SNAREs vesicle-associated or target-membrane-associated, t-SNAREs. However, this categorization system did not help to explain the concept of homotypic fusion, when two organelles of the same type fuse with each other (Fasshauer et al., 1998) and became a problem when examining the trafficking of t-SNAREs by vesicles.

The crystal structure of the neuronal SNARE complex (syntaxin1/SNAP25 and VAMP2) allowed for a new classification of SNAREs to be developed based on the identification of key residues found in the centre of the coiled-coil termed the ‘zero layer’. The ‘zero layer’ residues are buried within the hydrophobic core of the SNARE complex and form hydrogen bonds with each other, most likely to ensure that all the four SNARE motifs are assembled properly. Therefore, Q-SNAREs were those identified as having the Q/Glutamine (Gln) residue and R-SNAREs were those having

an R/Arginine (Arg) residue. Further phylogenetic analysis of the SNARE proteins allows the subdivision of Q-SNAREs according to their degree of resemblance to syntaxin SNARE domain (Qa/Stx), SNAP25 N-terminal SNARE domain (Qb/S25N), or the SNAP25 C-terminal domain (Qc/S25C) (Bock et al., 2001, Fasshauer et al., 1998, Kloepper et al., 2007).

1.2.3.1 R-SNAREs

R-SNAREs can be classified into two main types, longins and brevins. Brevin type R-SNAREs; VAMP1, 2, 3, 4, 5, and 8 (Table 1.1) have homology to VAMP (vesicle-associated membrane protein), also known as synaptobrevin, a protein that was initially identified and enriched in synaptic vesicles (Baumert et al., 1989, Trimble et al., 1988a). Longin type R-SNAREs (VAMP7, Sec22b, and Ykt6) possess a folded N-terminal regulatory longin domains that can form a closed conformation so inhibiting their ability to form SNARE complexes. The conserved region on Sec22 and VAMP7 also mediate sorting events by coat components, indicating a possible relationship between closed/open SNARE structure and availability of sorting signals for binding of coat/coat adaptor subunits (Gonzalez et al., 2001, Mancias and Goldberg, 2007, Martinez-Arca et al., 2003, Tochio et al., 2001).

The brevins are small (11-18 kDa) R-SNAREs that localize to post-Golgi membranes and participate in post-Golgi trafficking pathways, including endosomal trafficking and fusion with the PM. The two brevins in yeast Snc1p and Snc2p, are homologs to the human form of the brevins VAMP1, 2, 3, 4, 5, and 8. The brevins have short, unstructured N- terminal regions, with the exception of VAMP4, and are likely to be sorted through accessory protein binding to their SNARE motifs (Peden et al., 2001). The N-terminal extension of VAMP4 contains a dileucine motif and acidic clusters that mediate its recycling from the endosome to the TGN (Zeng et al., 2003, Tran et al., 2007).

Scheller first reported the discovery of vesicle-associated membrane protein 1 (VAMP1) by using a polyclonal antibody raised against purified cholinergic synaptic vesicle from the electric organ of *Torpedo californica* (Trimble et al., 1988b). At this stage, he suggested that VAMP1 played an important role in the packaging, transport, and release of neurotransmitters. This protein was later cloned by Sudhof from

mammalian synaptic vesicles, naming it synaptobrevin. He also concluded that it was conserved from mammals to Drosophila (Südhof et al., 1989). The discovery of its function was made by the Montecucco laboratory using tetanus and botulinum toxin serotype B which proteolysed VAMP2 (Schiavo et al., 1992b). VAMP1 and VAMP2 or synaptobrevins are highly expressed in neuronal tissue and have been well characterized in their roles in regulated synaptic vesicle exocytosis (Baumert et al., 1989, Jahn and Scheller, 2006, Schoch et al., 2001, Trimble et al., 1988a). VAMP2 has been demonstrated to have a role in the regulated secretion of AQP2 (aquaporin-2 a channel for antidiuretic hormone action) that mediates its fusion with the apical PM in polarized cortical collecting duct medullary collecting duct, MCD4 cells (Procino et al., 2008), and insulin-stimulated translocation of glucose transporter type 4 (GLUT4) to the PM in 3T3-L1 adipocytes (Williams and Pessin, 2008).

Südhof identified the VAMP2 homologue, cellubrevin after observing the protein was cleaved by the tetanus toxin light chain. However, in contrast to VAMP1 and 2, cellubrevin or also known as VAMP3 has a wider expression profile in mammalian cells (McMahon et al., 1993). It has been proposed to function in the fusion of recycling endosomes with the cell surface. It is also one of the groups of SNAREs involved in pathways of fusion of endosome-derived carriers with the TGN. It is concentrated transiently on surface ruffles where membrane fusion is prominent. It appears transiently on destination membranes before it is reinternalized and returned to the recycling endosomes for subsequent rounds of fusion. During internalization, there is significant remodelling of the membrane and so VAMP3 can also be seen on ruffles, tubules, and vesicular structures as membrane is exchanged between the endosomes and cell surface (Wall et al., 2015). It also has been reported to contribute to the fusion of multivesicular bodies with autophagosomes (Fader et al., 2009). VAMP3 has been identified in the basolateral delivery of transferrin receptor and LDL-receptor sorting signal mutant LDLR-CT27 in polarized MDCK cells and mediates MMP (matrix metallopeptidase) secretion from an invasive human fibrosarcoma cell line (Fields et al., 2007). However, VAMP3 knockout mice were normal in most endocytic and exocytic pathways including constitutive exocytosis other than a minor decrease in phagocytic uptake of Zymosan by macrophages. This indicates that the functions

mediated by VAMP3 are likely redundant with other post-Golgi R-SNAREs (Allen et al., 2002, Schraw et al., 2003, Yang et al., 2001b).

VAMP4 is widely expressed and is known to mediate vesicle fusion between the TGN, endosomes, and homotypic fusion of endosomes (Steegmaier et al., 1999, Brandhorst et al., 2006). VAMP4 is also enriched in neurons and contributes to asynchronous synaptic vesicle exocytosis, enlargeosome exocytosis, and activity-dependent bulk endocytosis in neurons (Raingo et al., 2012, Cocucci et al., 2008, Nicholson-Fish et al., 2015). One physiologically important hormone-regulated trafficking event is the insulin-stimulated translocation of the glucose transporter (GLUT4) from intracellular vesicle compartments to the plasma membrane in adipocytes and skeletal muscle (Watson and Pessin, 2001). VAMP4 is also thought to play a role in endosomal trafficking and the delivery of GLUT4 to regulated storage compartments by binding to the AP-1 adaptor complex via a conserved acidic di-leucine (Peden et al., 2001). VAMP4 is required for the initial biosynthetic entry of GLUT4 from the Golgi into the insulin-responsive vesicle compartment. Knockdown of VAMP4 with VAMP3, 5 or 8 had no effect on GLUT4 trafficking, with the exception of a reduction of basal state trafficking of newly synthesized GLUT4 to the plasma membrane with knockdown of VAMP4 and 7 (Williams and Pessin, 2008).

VAMP5 regulates the docking and fusion of membrane vesicles. Ubiquitous expression of this protein has been reported in muscle and various other organs except for the brain and small intestine (Zeng et al., 1998, Takahashi et al., 2013). Every post-Golgi R-SNARE mentioned has been shown to play a role in the fusion of secretory carriers at the PM, except for VAMP5 (Zeng et al., 1998). VAMP5 knockout mice showed low birth rate and low body weight with abnormalities of the urinary and respiratory systems development suggesting its importance in growth and development (Ikezawa et al., 2018).

VAMP7 has been identified to function in endosome-lysosome trafficking including endosome/lysosome fusion and Ca2+-triggered lysosome fusion with the PM in mammalian cells (Advani et al., 1999, Pryor et al., 2004, Rao et al., 2004, Ward et al., 2000). It has also been shown to function in the direct delivery of cargo to the apical PM in polarized cells, and is required for efficient osmotic shock-induced translocation of GLUT4 to the PM in 3T3-L1 adipocytes (Williams and Pessin, 2008). However,

despite many proposed functions of VAMP7, knockout mouse models of this protein did not show any significant physiological phenotype where normal lysosomal exocytosis was still preserved in different types of mammalian tissues. This was highly indicative that its function was easily replaced by other post-Golgi R-SNAREs with its absence (Sato et al., 2011).

VAMP8 or also known as endobrevin also has a wide expression profile and has been mapped to play a role in regulated secretion and the terminal step of cytokinesis in mammalian cells (Low et al., 2003, Pryor et al., 2004, Wang et al., 2004). It has also been suggested that VAMP8 mediates homotypic fusion (granule-to-granule) (Behrendorff et al., 2011).VAMP8 has also been identified as an important molecule for transcytosis delivery of proteins from the basolateral to the apical PM in polarized cells (Pocard et al., 2007). VAMP8 knockout mouse showed defects in pancreatic granule secretion which proves its role in regulated secretion (Wang et al., 2004, Cosen-Binker et al., 2008).

Ykt6 is an essential protein that is highly conserved from yeast to man. Ykt6 is different from the other R-SNAREs in that it does not have a transmembrane domain. Instead, it is lipid-anchored to the membrane and therefore lacking the usual hydrophobic anchor sequence. In its place, Ykt6 contains a prenylation consensus motif (CAAX box), where the addition of hydrophobic molecules to the protein facilitates membrane attachment. Prenylation controls the localization and activity of a protein. Ykt6 can exist in two forms; an inactive cytosolic form and an active membrane-bound form. Both the inactive and active forms undergo the post-translational modification step, farnesylation by addition of an isoprenyl group to the cysteine residue at the carboxyl-terminal of the CCAIM sequence (Fukasawa et al., 2004). This step is crucial as it is a prerequisite for subsequent palmitoylation of the upstream cysteine, which permits stable membrane association of Ykt6. The membrane recruitment and palmitoylation are controlled by the N-terminal domain which interacts with the SNARE motif, keeping it in its closed inactive state (Daste et al., 2015b). Many studies support its role in different intracellular membrane trafficking events at the Golgi, endosome, autophagosome, and vacuole (Hasegawa et al., 2003, Bas et al., 2018, Matsui et al., 2018, Dietrich et al., 2005). This unconventional R-SNARE in complex with Sed5, a Q-SNARE, was first identified in yeast (Søgaard et al., 1994). The role of Ykt6-dependent membrane

trafficking was confirmed when yeast depleted of Ykt6 showed a block in the early stages of exocytosis (McNew et al., 1997). This initial model showed Ykt6 mediated retrograde trafficking from *cis*-Golgi to the ER (McNew et al., 1997, Kweon et al., 2003). Various Ykt6 mutants in yeast have since elucidated its role in both protein secretion and protein transport to the vacuole (Dilcher et al., 2001, Kweon et al., 2003). Ykt6 (and Sec22b) may also act as part of the t-SNARE subcomplex (Hong and Lev, 2014). Complete loss of Ykt6 has been shown to be lethal in eukaryotes (Takáts et al., 2018, McNew et al., 1997).

1.2.3.2 Q-SNAREs

The original v/t nomenclature is problematic as it was neither specific nor broadly applicable as t-SNAREs are also found in vesicles. A t-SNARE is generally assembled from one heavy chain and two light chains of the SNARE domains. The two light chains can come from one or two proteins. The Qa/Stx -type of SNARE is considered to be the heavy chain, and Qb and Qc SNAREs, either from the same protein such as SNAP25 or from two different proteins are considered to be the light chains. The Q-SNAREs identified in humans are listed in Table 1.1.

As illustrated in Figure 1.2, all the syntaxins (Stx) as well as GS27, GS28, Vti1a, and Vti1b contain a regulatory N-terminal three-helix bundle (Habc) domain. Many Stx also possesses short, unstructured regulatory sequences around 30aa located at the N-terminal of the Habc domain, which is known to mediate interaction with accessory proteins such as the SM proteins that are required for SNARE-mediated vesicle fusion (Hong, 2005). The syntaxins display different modes of binding with their partner regulatory SM proteins (Dietrich et al., 2003, MacDonald et al., 2010). A majority of SNAREs will contain only one SNARE motif near the C-terminal tail anchor. However, SNAP23, SNAP25, SNAP29, and SNAP47 would contain two tandem SNARE motifs separated by a linker region. Most SNAREs are anchored to the membrane by a C-terminal transmembrane domain (TMD), while some are associated with the membrane through palmitoylation (Figure 1.2). The function of lipid modifications on some of its family members is still unclear, however suggests its versatility and may represent a more diverse role in cellular trafficking.

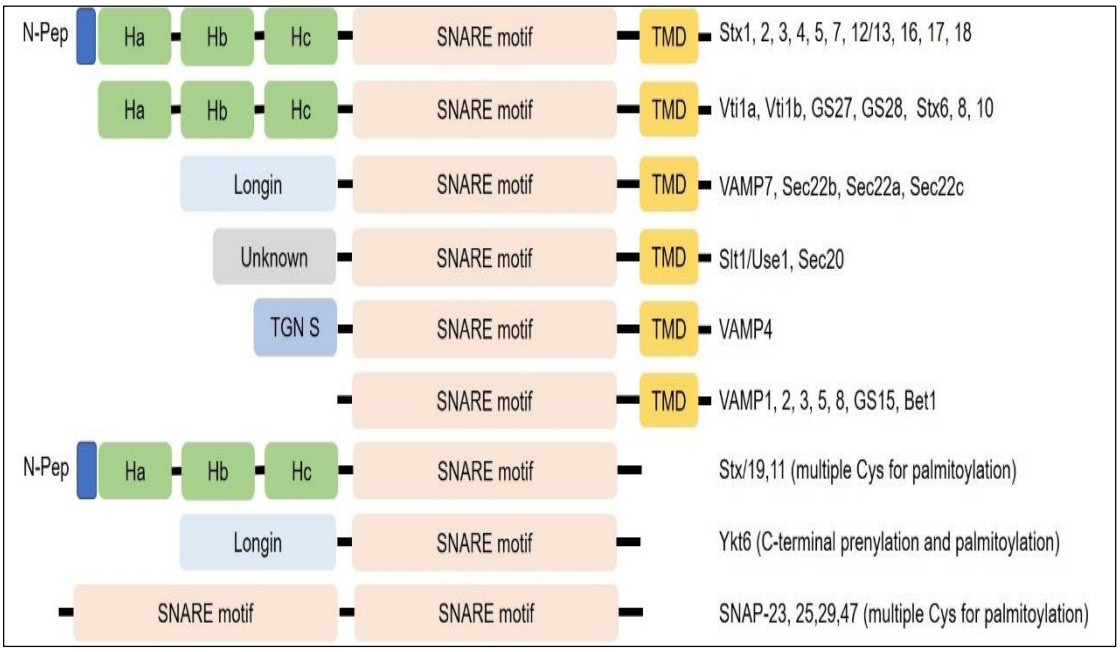

Figure 1.2 Domain organization and structure of human soluble N-ethylmaleimide-sensitive factor attachment protein receptor (SNARE).

Indicated SNAREs along with their corresponding domains are shown. Abbreviation: TMD, transmembrane domain.

1.2.4 Regulation of SNARE complex formation

Many in vitro studies have demonstrated that SNAREs are promiscuous and can form a diverse array of SNARE complexes. However, only certain combinations enable membrane fusion and cargo delivery. Thus, this suggests that additional machinery which regulates their activity is required (Waters & Hughson, 2000; Whyte & Munro, 2002).

Intracellular targeting of SNAREs to specific compartments represents one of the first steps for regulation for the formation of specific complexes. For example, VAMP7 is enriched in the late endosome-lysosomal compartments (Martinez-Arca et al., 2003). VAMP4 is enriched in the TGN via a targeting motif on its N-terminal extension (Zeng et al., 2003, Gordon et al., 2009). Distribution and internalisation of VAMP4 to the TGN for example is achieved via its dileucine motif, while VAMP3 and 8 are determined by the conserved mechanism of coiled-coil interaction (Gordon, Mirza, Sahlender, Jakovleska & Peden, 2009). In polarized epithelial cells, for example, Stx3 and Stx4 are specifically enriched in the apical and basolateral domain of the plasma

membrane respectively (Sharma et al., 2006, Reales et al., 2011). However, the detailed molecular motif and underlying molecular machinery regulating the trafficking and targeting is known for a few SNAREs (Pryor et al, 2008; Miller et al, 2011). Figure 1.3 summarises the location and function of the known SNARE complexes along the secretory and endocytic pathways.

1.2.4.1 Assembly by tethering factors and SM proteins

SNARE complex formation is highly regulated by multiple proteins such as tethering factors and SM (Sec1/Munc) proteins. Tethering factors and SM proteins can interact directly with individual SNAREs or the SNARE complex in order to regulate specific SNARE assembly and stabilize SNARE complexes. There are two broad categories of tethering structures: long coiled-coil tethering proteins that mediate vesicles targeting to membranes over long distances and large multisubunit tethering protein complexes also called MTCs (Whyte and Munro, 2002) which can associate with different cellular compartments to mediate specific membrane trafficking over shorter distances (Bröcker et al., 2010, Yu and Hughson, 2010).

The tethering complex binds specific SNAREs to promote the formation of a fusogenic *trans*-SNARE complex. In this instance, tethering factors fine-tune the specific availability and accessibility of SNAREs so that correct complexes are formed for the specific fusion event. The first example can be attributed to p115 (yeast homologue is Uso1p) as a docking site of COPII vesicles on *cis*-Golgi side of the Golgi complex. Example of MTCs are the exocyst complex that mediates fusion of vesicles with the PM (Guo et al., 1999, He and Guo, 2009) and the TRAPP (transport protein particle) complex that mediates COPII vesicle docking to the Golgi (Sacher et al., 1998). A compilation of known tethering complexes and their interactions with SNARE proteins is shown in Table 1.2. The specific interaction of MTC with SNAREs also prevents the assembly of a non-fusogenic SNARE complex, which is seen in-vitro. It has been shown that the conserved oligomeric Golgi complex (COG) complex preferentially binds to fusogenic Golgi SNARE, preventing non-fusogenic SNARE pairing (Laufman et al., 2013). The stability of SNARE complexes is also influenced by tethering complexes by conferring protection against proteosomal degradation. It was observed that depletion of COG subunits caused the degradation of Stx6-GS28-GS15 SNARE complex (Oka et

al., 2004). MTCs also work with SM proteins to trigger the assembly and stabilization of the SNARE complex.

Table 1.2 Tethering factors and interaction with SNARE proteins

Tethering factors	Components	Subcellular association	SNARE interaction	Function
Multisubunit tethering complex				
DSL1	Dsl1, Tip20,Dsl3/Sec39	ER	Use1,Sec20	Golgi to ER retrograde transport
COG	Cog(1-8)	Golgi	Stx5,Stx6, STx16,GS28	Transport within the Golgi apparatus and Golgi to ER retrograde transport
GARP	Vps(51-54)	TGN	Stx6,Stx16,Vamp4	Endosome to TGN retrograde transport
HOPS	Vps11, Vps16, Vps18, Vps33, ps39, Vps41	Late endosome	Vamp3,Vamp7,Nyv1	Late endosome to lysosome transport
CORVET	Vps11, Vps16, Vps18, Vps33, Vps3, Vps8	Early endosome		Early endosome to late endosome transport
EXOCYST	Sec3, Sec5, Sec6, Sec8, Sec10, Sec15, Exo70, Exo84	PM	Sec9, Snc2	Secretory vesicle fusion with PM
TRAPP			Unknown	ER to Golgi transport, autophagy
TRAPP I	Bet3A, Bet3B, Bet5, Trs20, Trs23, Trs31, Trs33	ER, Golgi		
TRAPP II	TRAPPI subunits and Trs65, Trs120, Trs130	Golgi		

TRAPP III	TRAPPI subunits and Trs85	TGN		
Long coiled-coil tethers				
p115	115kDa protein	*Cis*-Golgi	Stx5, GS28, GS15, Sec22, GS27, Ykt6	ER to Golgi transport
Giantin	400kDa protein	Golgi		ER to Golgi transport
CASP	160kDa protein	Golgi		Retrograde transport within the Golgi
GM130	130kDa protein	*Cis*-Golgi		ER to Golgi transport
Golgin-97	97kDa protein	TGN		TGN to endosome transport
Golgin-245	245kDa protein	TGN		TGN to endosome transport
GCC185	185kDa protein	TGN		Endosome-to-TGN trafficking
EEA1	16kDa protein	Early endosome		Transport through the early endosome

SM proteins are conserved soluble peripheral membrane proteins of 60-90 kDa. They are considered as key universal components of the fusion machinery that function in distinct intracellular transport steps to physically interact with either individual SNAREs or the SNARE complex itself. There are four major classes of SM proteins identified in mammals: Sly1, VPS45, VPS33 (VPS33A and VPS33B), and Munc18 (Munc18-1, Munc18-2, and Munc18-3) (Hong, 2005, Südhof and Rothman, 2009). Sly1 regulates SNARE assembly at the ER-Golgi region, VPS45 at the endosome-TGN, VPS33 at the endocytic/lysosomal system, and Munc18 at the plasma membrane. SM proteins are required for all SNARE-mediated fusion. In-vitro reconstitution studies showed that SM proteins strongly accelerate the rate of SNARE-mediated fusion and

contribute to the specificity of various fusion events (Shen et al., 2007, Scott et al., 2004, Rodkey et al., 2008). However, there have also been many studies that contradict these findings and suggest SM proteins act to inhibit membrane fusion (Südhof and Rothman, 2009, Jun and Wickner, 2019, Yu et al., 2013).

Other regulating factors such as complexins, Munc13, and synaptotagmins have been described in the regulated release of neurotransmitters by synaptic vesicles. Complexins are small (15-18 kDa) helical proteins that bind to the surface of assembled SNARE complex and act together with other SNARE regulatory proteins in regulating the late stages of stimulated vesicle fusion (Chen et al., 2002, Jahn and Scheller, 2006). Munc13 are large proteins that localize to zones of synaptic vesicle fusion. Genetic ablation of Munc13 protein impairs both regulated and spontaneous vesicle fusion events in neurons (Augustin et al., 1999, Varoqueaux et al., 2002).

1.2.4.2 SNARE complex disassembly by NSF and SNAP

N-ethylmaleimide sensitive factor (NSF) was first identified as a protein that is required for the transport of VSV-G in a cell-free system (Malhotra et al., 1988) (Block et al., 1988a). Around the same time, NSF was also identified in a genetic screen for genes that are required for constitutive secretion in yeast (named Sec18p). The loss of the NSF in yeast caused the accumulation of docked transport vesicles that were unable to fuse with their target membranes (Wilson et al., 1989). In the original hypothesis, Rothman proposed that NSF and ATP hydrolysis drove membrane fusion. However, this was later proven to not be the case, and that NSF and SNAP would in fact allow disassembly of the core complex (Sollner, Bennett, Whiteheart, Scheller & Rothman, 1993).

NSF is a cylindrical oligomeric ATPase with a three-domain organization. The disassembly of the SNARE complex requires the cooperation of two molecules; NSF (N-ethylmaleimide sensitive factor) and SNAP (soluble NSF attachment proteins); α-SNAP, β-SNAP, and γ-SNAP. SNAP interacts with the SNARE complex with an opposite structural twist. The α-SNAP binds the cis-SNARE complex and the N-terminal domain of the NSF to form a 20s supercomplex. The C-terminal domains are involved in ATP hydrolysis and ATP-dependent oligomerization, both of which are essential for NSF's role in promoting membrane fusion. The transformation of ATP-bound NSF to ADP via hydrolysis forces the conformational alteration of SNAP to

unwind the SNARE complex (Zhao et al., 2015) which relieves the SNARE complex in a burst through a "spring-loaded" mechanism (Ryu et al., 2015) and releases the individual SNARE proteins for further cycles of vesicle transport. Disassembly of the cis-SNARE complex is an important step in the membrane fusion cycle because it frees the individual SNAREs to be used for subsequent rounds of vesicle transport (Bombardier and Munson, 2015, Hong, 2005).

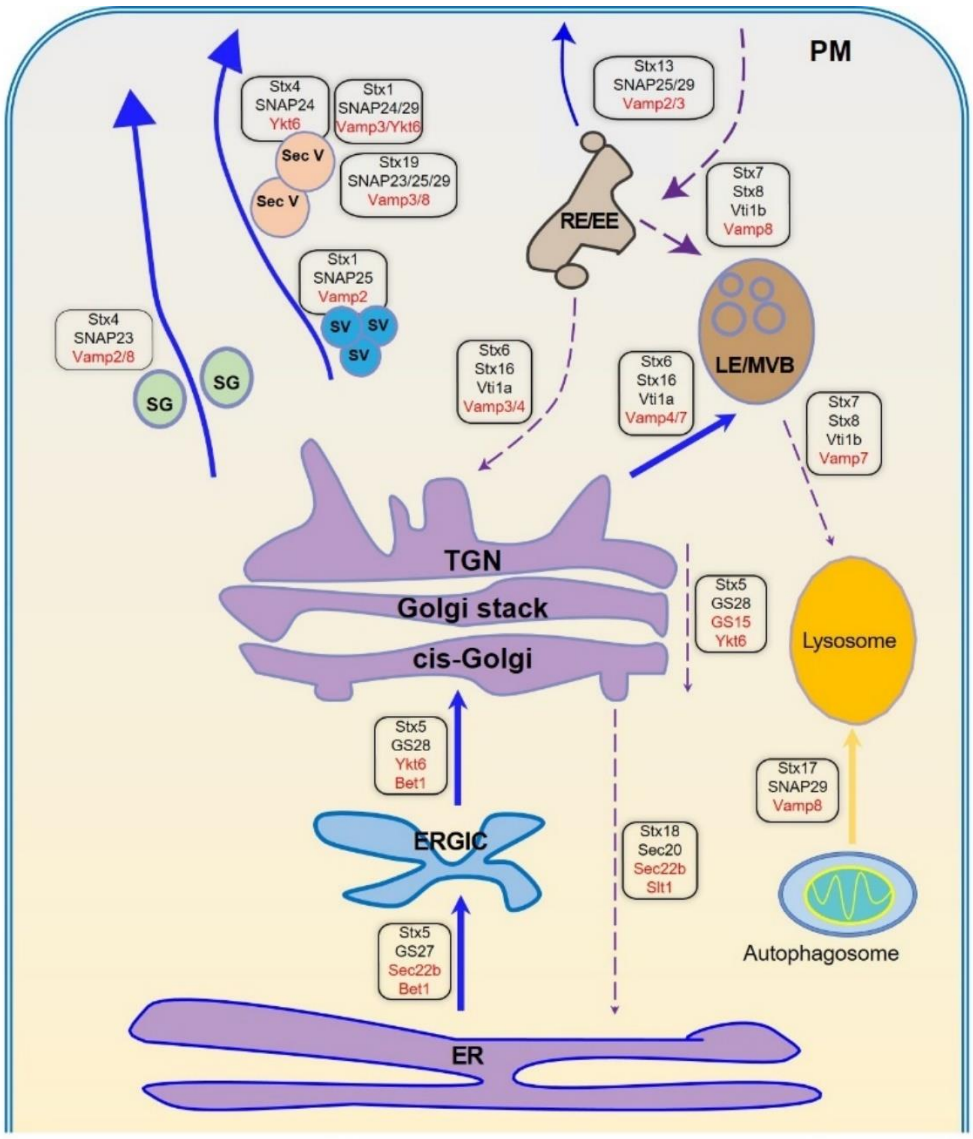

Figure 1.3 Schematic showing some of the known SNARE complexes that act along the secretory and endocytic pathways in mammals.

R-SNAREs are labelled in red. Abbreviation: ER, endoplasmic reticulum; ERGIC, ER-Golgi intermediate compartment, LE/MVB, late endosome/multivesicular body; TGN,

trans-Golgi network; PM, plasma membrane; RE/EE, recycling endosome/early endosome; SG, secretory granules; SV, synaptic vesicles; SecV, secretory vesicles.

1.3 An Overview of Botulinum Neurotoxins

Botulinum neurotoxin (BoNT) was identified as the sole cause of botulism over a century ago, after the discovery of the anaerobic and spore-forming bacteria of the genus Clostridium (Rossetto, Pirazzini, & Montecucco, 2014). Some of the earliest evidence of the role of SNARE proteins in vesicle fusion has come from the pathophysiology caused by Botulinum and Tetanus toxins.

1.3.1 Botulinum toxin and botulism

The German scientist Justinus Kerner (1786-1862) described botulism as 'sausage poisoning'. Several years later, Emile Pierre van Ermengem discovered the causative agent as *Clostridium botulinum*. Botulism is a severe neuroparalytic illness, most commonly caused by foodborne ingestion contaminated by the intoxication with neurotoxins produced by this anaerobic gram-negative bacteria. It is a rare but severe disease and potentially fatal for vertebrates which cause neuroparalysis targeting the peripheral nerve endings (Pirazzini et al., 2017, Rossetto et al., 2014, Johnson and Montecucco, 2008). This neuroparalytic event is a result of a disruption of vesicles trafficking neurotransmitters to the neuromuscular junction. Synaptobrevin is the target of the clostridial neurotoxin, which demonstrated for the first time the functional importance of SNARE protein for neurotransmitter release (Link et al, 1992; Shiavo et al, 1992). Typical symptoms are flaccid muscle paralysis, often initiated by a blurring of vision, which is quickly followed by an acute symmetrical descending bilateral paralysis. If left untreated ultimately paralyses the respiratory and cardiac muscles causing death. It remains one of the most toxic substances for humans and is classified as one of the six most dangerous potential bioterrorism agents (Arnon et al., 2001). The estimated lethal dose in humans is in the low ng/kg range (Pirazzini et al., 2017).

BoNTs are a genetically diverse group of toxins that are the aetiological agents of botulism. Apart from the potentially lethal properties, BoNTs have been considered a valuable and sophisticated tool for studying neuron physiopathology and in the broader context of intracellular vesicle trafficking in non-neuronal cell types. As such, its properties of promoting relaxation at the neuromuscular junction have been exploited for cosmetic purposes and an increasing number of hyperfunction disorders of peripheral nerve endings (Hallett et al., 2013, Naumann et al., 2013, Jankovic, 2017).

Tetanus neurotoxin (TeNT) is another highly potent toxin produced by the clostridial family, C. tetani. TeNT initially binds at the presynaptic terminals of the neuromuscular junction. Unlike BoNTs, it is then transported by motor neurons to the spinal cord where it is then transferred to inhibitory presynaptic terminals, surrounding the motor neurons. The toxin cleaves VAMP1, 2, and 3 (Schiavo et al., 1992a, Schiavo et al., 1992b) resulting in the failure of inhibitory neurotransmitters, γ-aminobutyric acid (GABA) and glycine delivery, that would normally suppress motor neurons and muscle activity. This results in the opposite effect of BoNTs, with enhanced excitability causing continuous involuntary muscle contraction resulting in generalized tetanus, a spastic form of paralysis (Brooks et al., 1955).

1.3.2 Botulinum neurotoxin serotypes

Historically, BoNTs are classified into seven different serotypes A through G, based on their reactivity with polyclonal serum (Hatheway, 1994). BoNTs are produced primarily by different strains of the *C. botulinum* consisting of four phylogenetically distinct groups, and is also produced by related *Clostridium* species; *C. butyricum* (BoNT/E) (Aureli et al., 1986, McCroskey et al., 1986), *C. baratii* (BoNT/F) (Hall et al., 1985) and *C. argentinense* (BoNT/G) (Gimenez and Ciccarelli, 1970). Botulinum toxin serotype A-G are quite well characterized (Schiavo et al., 2000, Montal, 2010, Rossetto et al., 2014), in which all serotypes block the release of the principal neurotransmitter, acetylcholine at the neuromuscular junction by cleaving specific SNAREs involved in SNARE complex formation and vesicle trafficking. Table 1.3 summarizes the different characteristics of BoNT serotypes.

To further characterise the relationship between different serotypes next-generation sequencing and sophisticated bioinformatics analysis have been performed on

published genomic sequences obtained from clostridial strains responsible for human and animal botulism. It has been discovered there is significant heterogeneity in genome organization and amino acid sequence composition of the toxins which has led to the identification of several new subtypes and mosaic toxins. For example, BoNT/A1 and BoNT/A2 can be recognized by the same antiserum but show substantial sequence variation (Smith et al., 2005, Hill et al., 2007, Montecucco and Rasotto, 2015).

In addition, this approach has also led to the identification of new serotypes and botulinum-like molecules in non-clostridial strains. Other than seven serotypes that have been quite well studied, non-clostridial organisms producing botulinum-like toxin have also been characterized. The first non-clostridial botulinum-like toxin was discovered in a gram-positive bacteria *Weissella oryzae*, where an open-reading frame, then dubbed *Wo-orf1* shared substantial nucleotide sequence homology with the *bont* gene. However, the sequence lacked some essential features of BoNTs as well as the additional genes encoding the neurotoxin accessory proteins typically encoded in the *bont* gene cluster (Mansfield et al., 2015). It was first isolated from fermented rice and grains. The toxin has several domains which were similar to BoNT/B, including the light chain domain. This novel BoNT-like molecule has tentatively been named BoNT/Wo. However, it is unclear if it has any activity towards R-SNAREs in vivo. Recent reports have shown the presence of a complete *bont* gene cluster in the genome of *Enterococcus faecium*, a commensal bacterium often found in the gut of animals and humans (Brunt et al., 2018, Williamson et al., 2017). The predicted neurotoxin, now dubbed BoNT/En, includes all the functional domains and shares many features of typical BoNT. It has been shown to cleave VAMPs 1-3 and less efficiently STX1B and STX4.

Table 1.3 BoNT serotypes and variants characteristics

Serotype	Protein receptor	Ganglioside receptor	Metallo-protease motif (HExxH)	Substrates	Cleavage sites
BoNT/A	N-glycosylated SV2A-B-C	GT1b GD1a	HELIH	SNAP25	Q197-R198
BoNT/B	Synaptotagmin-1/2	GT1b GD1a	HELIH	VAMP1 VAMP2 VAMP3	Q78-F79 Q76-F77 Q63-F64
BoNT/C	none	GT1b	HELNH	SNAP25	R198-A199

		GD1a		Syntaxin1A, -2, 3 Syntaxin1B	K253-A254 K252-A253
BoNT/D	N-glycosylated SV2A-B-C	GT1b GD1a GD2	HELTH	VAMP1 VAMP2 VAMP3	K61-L62 K59-L60 K46-L47
BoNT/DC	Synaptotagmin-1/2	Sialic acid residue	HELTH	VAMP1 VAMP2 VAMP3	K61-L62 K59-L60 K46-L47
BoNT/E	N-glycosylated SV2A-B	GT1b GD1a	HELIH	SNAP25	R180-I181
BoNT/F	N-glycosylated SV2A-B-C	GT1b GD1a	HELIH	VAMP1 VAMP2 VAMP3	Q60-K61 Q58-K59 Q45-K46
BoNT/F5	Unknown	Unknown	HELIH	VAMP1 VAMP2 VAMP3	L56-E57 L54-E55 L41-E42
BoNT/H (BoNT/HA, BoNT/FA)	N-glycosylated SV2C	Unknown	HELIH	VAMP1 VAMP2 VAMP3	L56-E57 L54-E55 L41-E42
BoNT/G1	Synaptotagmin-1/2	GT1b GD1a	HELIH	VAMP1 VAMP2 VAMP3	A83-A84 A81-A82 A68-A69
BoNT/X	Unknown	Unknown	HELVH	VAMP1 VAMP2 VAMP3 VAMP4 VAMP5 Ykt6	R68-A69 R66-A67 R53-A54 K86-S87 R40-R41 K173-S174
BoNT/Wo	Unknown	Unknown	HEMTH	VAMP2	W89-W90
BoNT/En (eBoNT/J)	Unknown	Unknown	HELCH	SNAP25 VAMP1 VAMP2 VAMP3 Syntaxin1B Syntaxin4	K69-D70 A69-D70 A67-D68 A54-D55 K145-D146 K191-D192

1.3.3 Botulinum neurotoxin molecular architecture

All BoNTs have a similar domain structure and show a high degree of structural similarity despite a low level of sequence identity. Structurally, the toxin comprises two chains, the light chain and the heavy chain that is linked by a disulfide bond (Figure 1.4).

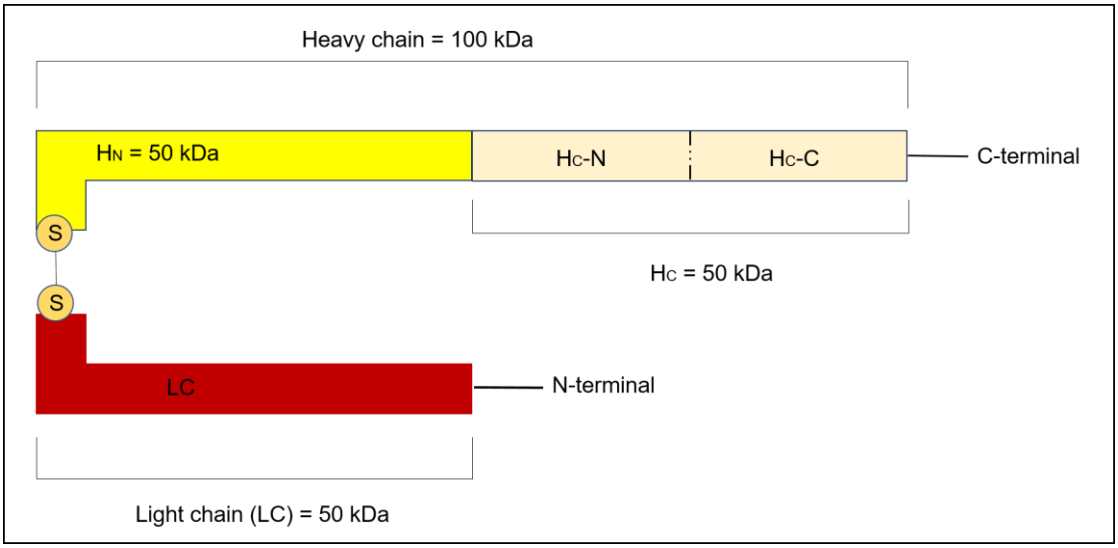

Figure 1.4 Schematic representation of BoNT domains.

The BoNT comprises a single polypeptide which is nicked to form a di-chain active BoNT. The HC mediates entry into the cell and subsequent LC translocation into the cytosol. The LC contains the metalloprotease motif. Abbreviation: LC; light chain, HN; translocation domain, HC; ganglioside-binding motif; HC-N; heavy chain N terminal, HC-C; heavy chain C terminal.

The heavy chain (100 kDa) comprises two functional domains responsible for ganglioside receptor binding for initial entry into the cell, HC, and the other for light chain translocation or HN. A smaller subdomain of the HC, heavy chain C-terminal (HC-C) of 25 kDa mediates the presynaptic binding and in subsequent internalization of the toxin within the transport vesicle (Rummel, 2017, Binz and Rummel, 2009a) and heavy chain N-terminal (HC-N) domain about 25 kDa contributes to binding by interacting with the membrane lipid microdomains (Muraro et al., 2009).

The HN domain (50 kDa) is linked to the catalytic LC (50 kDa) by an interchain disulfide bond, which assists with translocation of the catalytic domain from the vesicle into the cytosol (Fischer, 2013, Montal, 2010, Pirazzini et al., 2016). The LC has a zinc metalloprotease motif, which specifically cleaves SNARE proteins and inhibits neuroexocytosis (Pantano et al., 2014, Binz, 2013, Schiavo et al., 1992a).

1.3.4 Botulinum neurotoxin mechanism of action

BoNTs selectively bind irreversibly to high-affinity receptors at the presynaptic surface of the cholinergic neurons via their receptor targeting domain and are internalized through clathrin and non-clathrin mediated endocytosis (Simpson, 2000, Verderio et al., 2006). Once the toxin is endocytosed, it is reduced in the lumen of the vesicle and undergoes a conformational change which allows the toxin to translocate into the cytoplasm of the intoxicated cell (Binz and Rummel, 2009b, Poulain and Humeau, 2003). Once in the cytoplasm, the light chain domain can then target SNARE molecules. For example, BoNT serotype, A, C, and E cleave at distinct sites on a peripheral membrane protein SNAP25, while BoNT/B, D, F, and G cleave at different sites on homologous vesicle-associated membrane proteins 1, 2, and 3 (VAMP); and BoNT/C also cleaves the plasma membrane protein syntaxin 1 (Schiavo et al., 1992b, Montecucco and Schiavo, 1994). Cleavage of these proteins blocks SNARE complex formation that leads to the inhibition of neurotransmitter release and causes potent neurotoxic effects (Figure 1.5).

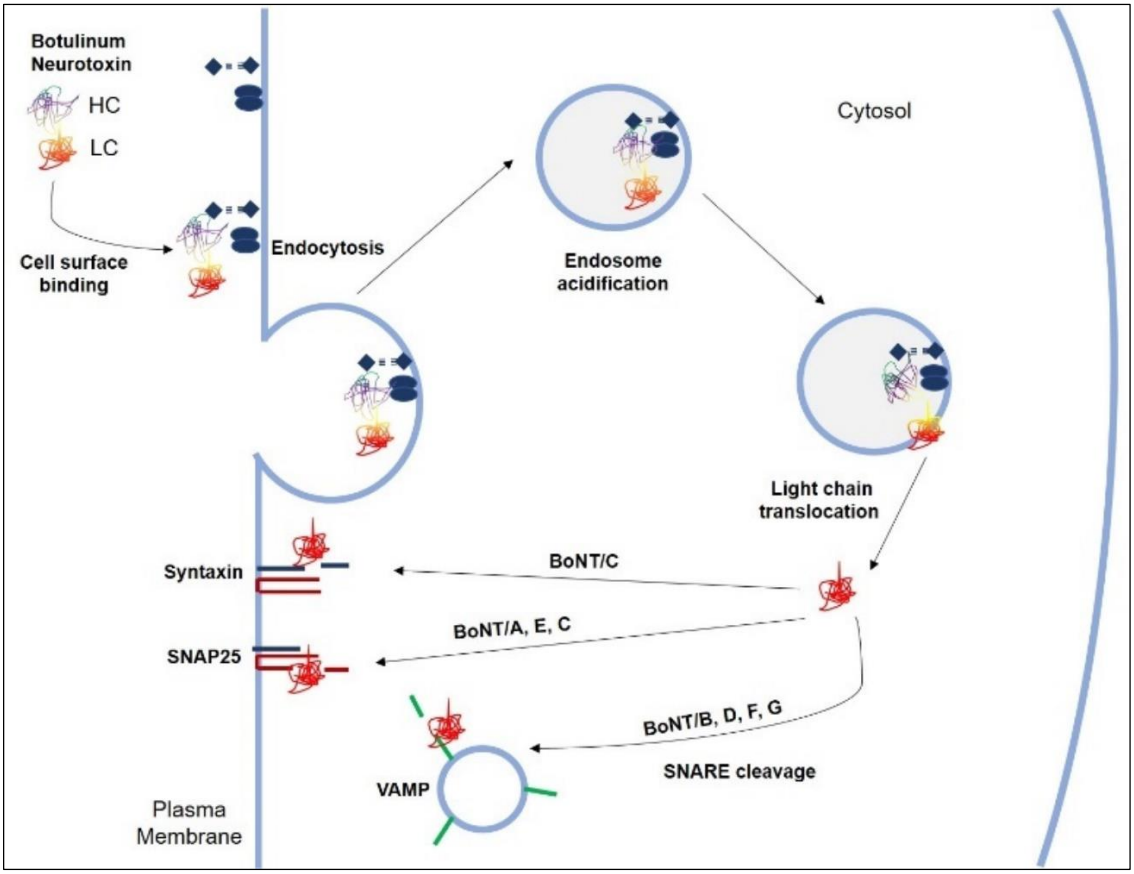

Figure 1.5 Schematic model of BoNT mechanism of action.

BoNTs associates themselves with specific ganglioside receptors on the plasma membrane via its receptor-targeting domain located on the HC. After endosomal acidification, the disulfide bond between the two chains is cleaved and the endopeptidase LC translocates into the cytosol. Translocation across the intraneural vesicle membrane to the cytosol is assisted by the translocation domain on the HN terminal. The LC then cleaves specific SNAREs and perturbs intracellular trafficking of vesicles and inhibition of neurotransmitter delivery.

1.4 The discovery of Botulinum Neurotoxin X

The last serotype, BoNT/G was discovered in 1969 and since then, no new BoNT serotypes have been added. Zhang and colleagues set out to survey the evolutionary landscape of BoNT by performing repeated rounds of computational analysis on BoNT sequences deposited in public databases (Zhang et al., 2017). By using this strategy, they were able to identify all of the known BoNT serotypes, subtypes, and mosaic toxins. The search landed on a breakthrough when they discovered a potentially new BoNT designated BoNT/X (GenBank no: BAQ12790.1). BoNT/X origin was traced back from the sequencing of the *C.botulinum* strain 111, a strain which was originally identified as BoNT/B2 and reported as a case of infant botulism in Japan (Kakinuma et al., 1996).

1.4.1 Key characteristics of BoNT/X

BoNt/X has the least sequence identity with other BoNTs suggesting that it is a novel serotype. In support of this statement: 1) it displayed a low sequence similarity evenly distributed along its entire sequence suggesting that it was not a mosaic toxin; and 2) none of the known antisera were able to neutralize the toxin in dot-blot assays (Zhang et al., 2017)

The overall domain arrangement of the toxin is conserved in BoNT/X, which includes the zinc-dependent protease motif HExxH (residues 227-231, HELVH) in the LC and a SxWY motif in the HC (residues 1274-1277, SAWY) which carries the receptor binding sub-domain that recognizes the lipid receptor gangliosides (Rummel et al., 2004). As with other BoNT serotypes, Zhang and colleagues found it is expressed in a gene cluster, with co-expression of NAP which consists of the NTNHA and HA clusters. The Orf gene cluster that hosts the BoNT/X gene has two distinct features compared with

other known OrfX clusters in other BoNTs; 1) an additional OrfX2 protein which is designated OrfX2b is located next to the BoNT gene and, 2) the reading frame of the OrfX genes has the same direction as the BoNT/X gene. The reading frame of OrfX genes is usually opposite to BoNT/NTNHA genes. These features make the BoNT/X a unique serotype of the BoNT family.

1.4.2 SNAREs cleaved by BoNT/X

To determine the substrate specificity of BoNT/X the light chain of the toxin was expressed recombinantly and incubated with cell extracts expressing recombinant SNAREs. BoNT/X was found to cleave an extensive number of recombinant R-SNAREs including VAMPs 1-5 and Ykt6 (Zhang et al., 2017). To identify the cleavage site recombinant SNAREs were incubated with the light chain and mass spectrometry performed on the proteolytic fragments. Surprisingly, BoNT/X did not cut the R-SNAREs at any of the previously identified sites but cleaved them at a unique position in the SNARE motif (VAMP4: K87-S88; Ykt6: K173-S174 and VAMP3: R53-A54). Other R-SNAREs in the family namely VAMP7, VAMP8, and Sec22b were resistant to cleavage.

All of the SNAREs that are cleaved by BoNT/X are ubiquitously expressed and are not directly involved in classical neuroexocytosis. Thus, this new serotype offers a unique opportunity to dissect the function of VAMPs and pathways which have until recently be inaccessible to toxin treatment. BoNT/X will be useful tools to investigate the function of less characterized SNAREs such as VAMPs 4, 5, and Ykt6 and the related trafficking events associated with them.

1.4.3 Structural characterization of the catalytic domain of BoNT/X

To gain an insight into the substrate specificity of BoNT/X the crystal structure of the light chain has been solved (Masuyer et al., 2018). The BoNT/X light chain (LC/X) shares the core fold common to other BoNTs, which shows that BoNT/X is a true member of the BoNT family. The LC/X had the highest sequence similarity to BoNT/B and tetanus neurotoxin (TeNT) of about 36% and 34% respectively. However, the LC/X has the closest structural resemblance to LC/D. The group discovered that access to the

catalytic pocket of LC/X has a narrower entrance composed of polar residues (Thr-Asn-Asn-Thr) and therefore is more restricted than other toxins. In addition, sequence alignment of LC/X with other VAMP-cleaving toxins showed that this region is not well conserved. Thus, this difference in sequence may contribute to substrate recognition and allow LC/X to cleave VAMPs in a unique position (Sikorra et al., 2008). BoNT/Xs tolerance for residue changes at the cleavage site is unusual. Besides, this structure also suggests that the exosite /LC interactions for BoNT/X are very different from that of other light chains so potentially explaining why it cleaves VAMPS at a distinct cleavage site (Masuyer et al., 2018).

1.4.4 BoNTs as a tool to study SNARE function

The role of SNAREs in regulated exocytosis has been extensively defined using BoNTs. Neuronal intoxication with these proteins occurs within minutes of their application. Their acute action, exquisite specificity, and long duration make them attractive alternatives to RNAi or CRISPR/Cas9 based strategies to study SNARE proteins. However, the neuronal specificity of the toxins and the small number of SNAREs they cleave has limited their application. Thus, there has been significant interest in developing new are altered versions of these molecules so they can target non-neuronal cells. The first indication that this may be possible came from some early work where a fragment of BoNT/A comprised of LC and HN domains was discovered following treatment of the full-length toxin by trypsin (Shone et al., 1985). While this protein inefficiently binds to neuronal cells, it retains a fully active catalytic and translocation domain. This protein is able to directly form pores in membranes and translocate the LC into the cytosol (Shone et al., 1987).

Later efforts have focused on reengineering or replacing the binding domain of the toxins, so they have altered specificity for cell binding. For example, a version of BoNT/A has been created where the neuronal binding domain has been replaced by the epidermal growth factor (EGF). This molecule binds to EGF receptors (EGF-R) at the cell surface cells and co-localises with the EGF-R in early endosomes following cellular internalization (Fonfria et al., 2016). The toxin does show some activity but is inefficiently released from endosomes.

It is also possible to overcome the neuronal specificity of these toxins by simply expressing the LC domain in cells. For example, the LC of tetanus has been used for this purpose. One potential drawback of this approach is a large number of toxin molecules are expressed in the cell which possibly could result in non-specific protease activity. Under normal conditions, only a very small number of toxin molecules are delivered per cell.

In addition to altering the binding properties of these toxins, work has also been performed to modify the substrate specificity of these. For example, a mutated BoNT/E LC (K224D), showed extended substrate specificity to cleave SNAP23 (Chen and Barbieri, 2009). This non-neuronal SNARE mediates vesicle-to-plasma membrane fusion affecting the secretion of mucus in the airways, antibodies, insulin, gastric acids, and ions. Cleaved endogenous SNAP23 in culture, inhibited secretion of mucin and IL-8 (Chen and Barbieri, 2009), suggesting potential therapeutic value for the treatment of hypersecretory disorders.

1.4.5 The application of BoNTs in Medicine

BoNTs have been used as therapeutic agents in clinical treatment for an array of neurotransmission disorders and the list of indications has dramatically expanded over the years (Craik et al., 2011). Neurotoxins have been exploited for their cosmetic value and benefits in pain management. Since the pioneering work of Alan Scott, applying BoNT/A to initially treat strabismus or “cross-eye” disorder allowed for the accidental discovery of its effective and most well-established use for cosmetic application (Scott et al., 1973). BoNT/A1 has been widely studied and is currently used to treat a number of movement disorders such as focal and segmental dystonia and spasticity. BoNT/A cleaves SNAP25 which disrupts vesicle fusion required for neurotransmitter release at the neuromuscular junction (Blasi et al., 1993). This highly specific action and its long-acting effect have inspired researchers to expand the list of indications (Montecucco and Molgó, 2005). From then on, the clinical use of BoNT/A has continuously evolved. Retargeting the delivery or substrate selectivity of BoNT/A has the potential to expand its therapeutic uses. The fusion of antibody fragments, growth factors, lectins, and other proteins to the HC/A translocation domain could successfully deliver BoNT subtypes to new cell types to potentially treating pain, neuroendocrine disorders, and cancers (Ma

et al., 2014, Nugent et al., 2017, Leggett et al., 2013, Duggan et al., 2002, Arsenault et al., 2013). Non-neuronal SNAREs such as SNAP23 appear to be an attractive therapeutic target by reengineering the proteolytic specificity of LC/A because of its homologous nature to the substrate of wild-type LC/A. SNAP23 mediates the release of proinflammatory molecules, secretion of matrix metalloproteases that promote tumour invasion, and hypersecretion of mucin in asthma (Pagan et al., 2003, Frank et al., 2011, Kean et al., 2009, Ren et al., 2015).

In addition to their pharmaceutical uses BoNT is also being used in a wide range of animal and human vaccines. For example, BoNT/C1 was developed with LC mutations H229G, E230T and H233N expressed in *E. coli* and purified via an amino-terminal 6X polyhistidine affinity tag (Kiyatkin et al., 1997). The most notable application of this recombinant technology is the application of these atoxic BoNT derivatives to elicit humoral immunity and generate protective antibodies. Because BoNT exclusively targets and enters a specific set of neuronal cells, this has made them an attractive method as a vehicle to deliver cargoes of therapeutic molecules. Functional LC-HN domains retain their catalytic activity when ligated or expressed as a recombinant protein with a wide variety of different cell types or receptor-specific targeting domains. Some BoNTs that have been reported to become drug delivery vehicles include recombinant BoNT/D proteins with four individual amino-terminal fusion proteins where it enabled the cytosolic delivery of enzymatically active cargo proteins to neurons via unfolded translocation intermediates (Bade et al., 2004). Recombinant BoNT/B1 was also reported as a successful drug delivery vehicle with LC neutralizing mutations E231A and H234Y (O'Leary et al., 2011, Edupuganti et al., 2012). Other atoxic derivatives that have been developed are the LC of BoNT/C with three amino acid substitutions (E238A, H241G, Y383A), which was rapidly internalised without cleaving the SNARE proteins in neuronal cell culture or disrupting neurotransmitter release in mice (Vazquez-Cintron et al., 2017). Given the low toxicity and high specificity of its neuron-targeting properties, this strategy could be useful as a molecular vehicle for drug delivery into neuronal cytoplasm.

BoNT has become very successful therapeutic agents mostly due to their exceptional specificity, acute action, and potency. With the development of novel recombinant

toxins, their therapeutic potential is significantly expanded and will only grow further if they can be developed to target non-neuronal cell types.

1.5 Aims of this Thesis

The identification of a new botulinum serotype, BoNT/X with novel substrate specificity is very significant. However, almost nothing is known about its impact on intracellular trafficking. This study aimed to determine if the toxin could be expressed recombinantly and explore its effect on intracellular trafficking using a range of quantitative endocytic and biosynthetic assays.

Chapter 2: Materials and Methods

2.1 Materials

All common reagents and antibodies used are described in the following sections. All restriction enzymes were purchased from New England BioLabs and used according to the manufacturers' instructions unless otherwise noted. Antibodies were purchased from suppliers, requested from colleagues, or made in-house.

2.1.1 Consumables and kits

Table 2.1 lists consumables and kits used in this study.

Table 2.1 Consumables and kits

Amersham™ PVDF 0.45 µm	GE Healthcare Life Sciences
EDTA-free protease inhibitor cocktail	Roche
Protease inhibitor	Sigma
Gel loading dye (6X)	New England BioLabs
PEI	Polysciences Inc.
Quick-Load Purple 1kb DNA ladder	New England BioLabs
Western C ladder	Bio-Rad
Trypsin	Sigma
RNase-free water	Sigma
Trypan Blue 0.4%	BioRad
Cell Counter dual chamber	BioRad
SYBR®Safe DNA Gel Stain	Thermo Fisher Scientific
StarSeal sealing tape Polyolefin film	STARLAB International GmbH
Prolong Gold anti-fade	Invitrogen
Whatman™ chromatography paper, 3mm	GE Healthcare Life Sciences
GeneJET Gel Extraction Kit	Thermo Fisher Scientific
GeneJET Plasmid Miniprep Kit	Thermo Fisher Scientific
GeneJET Plasmid Maxiprep Kit	Thermo Fisher Scientific
ECL Western Blot detection system	BioRad
Protein quantification kit	Thermo Fisher Scientific
TOPO cloning	Invitrogen, Thermo Fisher Scientific
Rapid DNA Ligation Kit	Thermo Scientific

2.1.2 Chemicals

Chemicals used in the experimental work for this thesis were purchased from reputable suppliers including Sigma-Aldrich and ThermoFisher Scientific.

2.1.3 Antibodies

Listed in Table 2.2 are antibodies used in the current work. All antibodies were used according to the manufacturer's instructions in the recommended dilution. However, optimization of reactions was done if required.

Table 2.2 Antibodies

Antigen	Host	Application	Source	Notes
Primary Antibodies				
Calreticulin	Rabbit	IF (1:50)	ThermoFisher	Rabbit polyclonal
CD-MPR	Mouse	IF (1:100) FC (1:100)	22D4	Anti-human monoclonal
CI-MPR	Mouse	IF (1:100) FC (1:100)	Abcam	Anti-human monoclonal
CD8	Mouse	IF 1:100 FC 1:20	Serotec	Anti-rat monoclonal antibody
CD63	Mouse	IF (1:1000) FC (1:1000)	H5C6	Anti-human monoclonal
CD63	Rat	IF (1:100) FC (1:100)	Biolegend	Anti-mouse CD63
EEA1	Mouse	IF (1:1000)	BD transduction Lab	Anti-human monoclonal
EGF-R AF647	Rabbit	IF 1:100 FC 1:100	Clone 5G3 Genentech Inc.	Anti-human monoclonal
ERGIC53	Mouse	IF (1:100)	Sigma Aldrich	Mouse anti-human monoclonal
γ-adaptin	Mouse	WB (1:1000)	(Ahle et al, 1988) MAB100.3	Mouse monoclonal crude ascites
GM130	Mouse	IF (1:1000)	BD transduction Lab	Mouse anti-human monoclonal
Green Fluorescent Protein (GFP)	Rabbit	IF (1:1000) WB (1:1000)	Abcam	Rabbit polyclonal
Sec22b	Rabbit	WB (1:2000)	Synaptic Systems	Rabbit polyclonal raised against human protein
TGN46	Rabbit	IF (1:1000)	M. Seaman	Rabbit polyclonal
Transferrin receptor (TF-R), CD71	Mouse	IF (1:200)	Santa Cruz	Mouse anti-human monoclonal
Transferrin AF647	Human	FC (20-50 µg/ml; 1:200)	ThermoFisher Scientific	Alexa Fluor 647 conjugated human transferrin
Transferrin receptor (TF-R), CD71 APC	Human	FC 20-40 µg/µl; 1:200)	BD (M-A712)	APC conjugated human CD71
Vamp2	Mouse	WB (1:500) IF (1:100)	Synaptic systems	Mouse monoclonal (cell line 69.1)
Vamp3	Rabbit	WB (1:500) IF (1:200)	In house	Rabbit polyclonal raised against human protein minus TM domain

Vamp4	Rabbit	IF (1:500)	In house	Rabbit polyclonal raised against human protein minus TM domain
Vamp4	Hamster	WB (1:1000)	In house	Hamster monoclonal (3H4) raised against human protein minus TM domain
Vamp7	Mouse	WB (1:1000)	In house	Mouse monoclonal (6C3 IgG2B) raised against first 100 amino acid of human protein
Vamp7	Rabbit	IF (1:50)	In house	Rabbit polyclonal raised against human protein minus TM domain
Vamp8	Rabbit	WB (1:100) IF (1:100)	In house	Rabbit polyclonal raised against human protein minus TM domain
Wheat Germ Agglutinin AF647	Lectin	IF 1:2000 FC 1:5000	ThermoFisher Scientific	Wheat germ agglutinin, a lectin used in cell biology conjugated with Alexa Fluor 647
Wheat Germ Agglutinin 350	Lectin	IF 1:100 FC 1:2000	ThermoFisher Scientific	Wheat germ agglutinin, a lectin used in cell biology conjugated with Alexa Fluor 350
Ykt6	Rabbit	WB (1:200) IF (1:200)	J. Hay	Rabbit polyclonal raised against human protein
Secondary Antibodies				
Alexa Fluor 594 Goat anti-Rabbit IgG	Goat	IF (1:1000)	Invitrogen, Thermo Fisher Scientific	Alexa Fluor 594 Goat anti-Rabbit IgG (H+L)
Alexa Fluor 594 Goat anti-Mouse IgG	Goat	IF (1:1000)	Invitrogen, Thermo Fisher Scientific	Alexa Fluor 594 Goat anti-Mouse IgG (H+L)
Alexa Fluor 488 Donkey anti-Rabbit IgG	Donkey	IF (1:1000)	Life Technologies	Alexa Fluor 488 donkey anti-rabbit IgG (H+L)
Alexa Fluor 488 Goat anti-Mouse IgG	Goat	IF (1:1000)	Invitrogen, Thermo Fisher Scientific	Alexa Fluor 488 Goat anti-Mouse IgG (H+L)
Anti-Mouse HRP conjugate FC specific	Goat	WB 1:10,000	Jackson ImmunoResearch Laboratories	Peroxidase-conjugate AffiniPure Goat Anti-Mouse IgG, Fc-specific
Anti-Rabbit HRP conjugate FC specific	Goat	WB 1:10,000	Jackson ImmunoResearch Laboratories	Peroxidase-conjugate AffiniPure Goat Anti-Rabbit IgG, Fc-specific
Anti-Armenian Hamster HRP conjugate	Goat	WB 1:10,000	Jackson ImmunoResearch Laboratories	Peroxidase-conjugated AffinityPure Goat Anti-Armenian Hamster IgG (H+L)
Anti-Rat HRP conjugate	Goat	WB 1: 10,000	Jackson ImmunoResearch Laboratories	Peroxidase-conjugated AffinityPure anti-Rat IgG Light Chain Specific
Anti-Rat Cy5	Goat	IF 1:250 FC 1:250	Jackson ImmunoResearch Laboratories	Alexa Fluor 650 Goat anti-Rat IgG (H+L)

WB-western blot; IF-immunofluorescence; FC-flow cytometry

2.1.4 Primers

Table 2.3 lists primers used for mutagenesis and sequencing. DNA sequencing was performed by the Research Core Facility based at the Medical School, University of Sheffield (Applied Biosystems' 3730 DNA Analyzer). Primers for sequencing were provided with sequencing services unless specified. All primers were purchased from Sigma.

Table 2.3 Primers used for molecular cloning

Primer name	Sequence	Notes
Molecular cloning		
Ykt6 VWmutant	CTTGGTATCCGTATGGGAAGTCCTGGCAACAC TCATCAAGCTTCTCGCCT	Substitution of nucleotides K173V/S174W in the Ykt6 protein at the cleavage site to create a SNARE that is resistant to BoNT/X light chain
DNA Sequencing		
CMV-F	CGCAAATGGGCGGTAGGCGTG	Ykt6 VW mutant constructs
GFP reverse seq	GGGCACCACCCCGGTG	Palmitoyl-tail and ER anchor BoNT/X
GFP(N3)	CCGGACTCAGATCTCGAG	Ykt6 VW mutant constructs

2.1.5 Plasmid DNA

Table 2.4 lists the plasmids used in the study. Plasmids either custom-made or synthesized in-house are as indicated.

Table 2.4 Plasmids

Plasmid name	Description	Source
pEGFP-C3	Kanamycin selection	Clontech
mCherryC1	Kanamycin selection	Clontech
pIRESneo CD8		Sean Munro
pLXIN	Gamma-retrovirus transfer plasmid	Clontech

pEGFP-C3-wild type BoNT/X light chain	Construct with GFP tag at N-terminus and wild type BoNT/X light chain sequence on C-terminal end (GeneScript)	GenScript
pEGFP-C3-mutant BoNT/X light chain	Construct with GFP tag on N-terminal and mutant BoNT/X light chain sequence on C-terminal end (GeneScript)	GenScript
pEGFP-C3-wild type BoNT/D light chain	Construct with GFP tag on N-terminal and wild type BoNT/D light chain sequence on C-terminal end (GeneScript)	GenScript
pEGFP-C3-mutant BoNT/D light chain	Construct with GFP tag on N-terminal and mutant BoNT/D light chain sequence on C-terminal end (GeneScript)	GenScript
mCherryC1-wild type Bont/X light chain	EGFP was swapped with mCherry ushing Nhe1/BsrG1.	Made in-house by myself
mCherryC1-mutant Bont/X light chain	EGFP was swapped with mCherry ushing Nhe1/BsrG1	Made in-house by myself
pCMV3-mCD63-GFPSpark	Mouse CD63 ORF in mammalian expression plasmid with C-terminal GFPSpark tag	Sino-biological
CD8α-pEGFPC3	CD8α in expression plasmid with C-terminal GFP tag	Sino-biological
pEGFPC3-HA-wild type VAMP3	HA-tagged VAMP3 in mammalian expression plasmid with N-terminal GFP-tag	GenScript
pEGFPC3-HA-mutant VAMP3	HA-tagged cleave-resistant VAMP3 in mammalian expression plasmid with N-terminal GFP-tag	Genscript
pEGFPC3-myc-wild type Ykt6	Myc-tagged Ykt6 in expression plasmid with N-terminal GFP-tag (cytoplasmic)	Jesse Hay
pCMV-myc-wild type Ykt6-Sec22b TM	Myc-tagged Ykt6 in expression plasmid with N-terminal Sec22b transmembrane domain (membrane-anchored)	Jesse Hay
pEGFPC3-myc-mutant Ykt6	Myc-tagged cleave-resistant Ykt6 in expression plasmid with N-terminal GFP-tag (cytoplasmic expression) Residues mutated by substituting the K173V-S174W	Made in-house by myself

pCMV-myc-mutant Ykt6-Sec22b TM	Myc-tagged cleave-resistant Ykt6 in expression plasmid with N-terminal Sec22b transmembrane domain (membrane-anchored)	Made in-house by myself
pEGFPC3-STX19 palmitoylation tail-wild type BoNT/X	Syntaxin 19 palmitoylation sequence fused on the active BoNT/X light chain in expression plasmid at N-terminus of GFP-tag	Made in-house by project student
pEGFPC3-STX19 palmitoylation tail-mutant BoNT/X	Syntaxin 19 palmitoylation sequence expressed on inactive BoNT/X light chain in expression plasmid with N-terminus of GFP	Made in-house by project student
pIRESneo CD8-GFP-wild type BoNT/X light chain	Construct with CD8 in expression plasmid with C-terminal GFP tag and active BoNT/X light chain	Made in-house by myself
pIRESneo CD8-GFP-mutant BONT/X light chain	Construct with CD8 in expression plasmid with C-terminal GFP tag and inactive BoNT/X light chain	Made in-house by myself
pEGFPC3-ER Anchor-wild type BoNT/X	Endoplasmic reticulum P450 signal peptide expressed at the N-terminus of GFP with active BoNT/X light chain	Made in-house by project student
pEGFPC3-ER Anchor-mutant BoNT/X	Endoplasmic reticulum anchor signal expressed at the N-terminus of GFP with inactive BoNT/X light chain	Made in-house by project student
pLXIN-GFP-DDBONT/X LC	Construct with GFP tag on N-terminal with destabilization domain attached to BoNT/X light chain sequence	Made in-house by myself

2.1.6 Mammalian cell lines

Table 2.5 lists the cell lines used in this study.

Table 2.5 Cell lines

Name	Description	Morphology	Source
HeLa-M	Human Cervical Cancer cell line	Epithelial	Scottie Robinson
HeLa-C1	Soluble secretory reporter cells	Epithelial	(Gordon et al., 2010b)

HEK293T	Human Embryonic Kidney cell line	Epithelial	ATCC

2.1.7 Culture media

Table 2.6 lists the media used for mammalian cell culture and bacterial culture growth

Table 2.6 Media

Media	Supplier	Content
DMEM	Sigma-Aldrich	Dulbecco's Modified Eagle Medium [+] L-Glutamine [+] 4.5 g/L D-glucose [-] Pyruvate Supplemented with: 10% Fetal calf serum (PAN Biotech) 1% Penicillin-Streptomycin; 100 U Penicillin; 0.1 mg Streptomycin /ml (Hyclone)
Opti-MEM	Supplier; Gibco, Life Technologies	Opti-MEM® I (1X) – Reduced Serum Medium [+] HEPES [+] 2.4 g/L Sodium bicarbonate [+] L-Glutamine No supplements required
Transfection media (Antibiotic-free)	Sigma-Aldrich	Dulbecco's Modified Eagle Medium [+] L-Glutamine [+] 4.5 g/L D-glucose [-] Pyruvate Supplemented with: 10% Fetal calf serum (PAN Biotech)
Media used for bacterial growth		
Luria-Bertani (LB) broth	Prepared as needed	5 g/L tryptone 2.5 g/L yeast extract 5 g/L NaCl In 500L of ddH2O For bacterial TYE culture plates (1% tryptone, 0.5% yeast extract, 1% NaCl and 1.5% agar at pH7.4) add 7.5 g of agar to the mixture above Add antibiotics accordingly: Ampicillin 100 mg/ml use 1 in 1000 Kanamycin 50 mg/ml use 1 in 1000

2.2 Methods

2.2.1 Cell line culture and maintenance

2.2.1.1 Thawing cryopreserved cells.

Cryopreserved cells were transported from storage to the laboratory on dry ice. On rare occasions, the vials may explode on warming due to the expansion of trapped residual liquid nitrogen. The vial is opened under sterile conditions in a biohazard cabinet. A tissue soaked in 70% ethanol is held around the cap and quarter-turned to release any residual liquid nitrogen. The cap is then retightened and quickly transferred to a water bath at 37ºC for 1-2 minutes. The vial is not immersed to minimize the risk of contamination. Once thawed, the vial was wiped down with a tissue soaked in 70% ethanol. The whole content of the vial is transferred into a 10 cm dish containing 10 ml of prewarmed media. Then the cells were incubated in a humidified incubator at 37ºC at 5% CO_2 overnight. The next day, all unattached dead cells were aspirated and the medium was changed. The description of cell lines is listed in Table 2.7.

Table 2.7 Culture condition

Cell line	Species	Tissue	Incubation	Complete growth medium
HEK293T	Human	Embryonic kidney	37ºC with 5% CO2	DMEM + 10% FBS + 1% Penicillin/Streptomycin
HeLa-M	Human	Cervix		
HeLa-C1	Human	Cervix		

2.2.1.2 Sub-culturing adherent cell lines

HEK293T and HeLa-M cells are maintained similarly. Cells were grown in a 10 cm culture dish in a humidified incubator at 37ºC with 5% CO_2 (Table 2.7). After the cells have reached 80-100% confluency, the medium was removed and cells rinsed 1-2 times with 10 ml sterile 1xPBS to remove any residual media which may inhibit trypsinisation. 1 ml of trypsin was added to the cells and spread across the surface by swirling the dish. It was then placed back into the humidified incubator for 3-5 minutes to allow for the trypsin to work. After the cells have detached, 10 ml of medium was

added to the dish. Cells were pipetted up and down repeatedly to break up visible clumps. The medium was aspirated and the remaining cell pellet was resuspended in 1 ml fresh complete media. Cells were split 1:5 to 1:20 depending on the requirements of the experiments planned.

When cells were cultured for microscopy, coverslips were placed in a 12-well culture vessel under sterile conditions, and 60-80 thousand cells pipetted into each well. For HEK293T cells, to ensure the cells properly adhere to the coverslips, coverslips were coated with poly-L-lysine (PLL) for one hour before washed with 1xPBS six times. The plates were left to completely dry under the biohazard cabinet for a few hours before sealed and stored. Before usage, the PLL-coated coverslips were washed again with 1xPBS three times.

2.2.1.3 Counting cells using the TC20 automated cell counter (BioRad)

To count the number of cells in the culture cells were trypsinised as in section 2.2.1.2. 20 µl of cell suspension was added to 20 µl of 0.4% Trypan blue dye (BioRad) in a 0.5 ml Eppendorf tube. The cells and trypan blue were mixed by pipetting. Ten microlitres of the cell mixture were pipetted into one chamber of the cell counting slide at a 45º angle. This allows the entire chamber to be filled and eliminates air trapping. The readout of the number of cells in cells/ml can be multiplied by the total volume of the cell suspension to obtain the final total cell count. Cells were then calculated for the number of cells required for the different culture vessels used (Table 2.8).

Table 2.8 Seeding density for different culture vessels

Cell line	10 cm culture dish	6-well plate	12-well plate
HEK293T	1.0-2.0 x 10^6	1.0-3.0 x 10^5/well	1.0-3.0 x 10^5/well

2.2.1.4 Cryopreservation

During the sub-culturing step, cells were resuspended with the appropriate freezing media (10% DMSO in FBS-containing media). The cell suspension was transferred to 1.8 ml cryovials and placed in an isopropanol bath at RT. The whole container was then

placed in -80ºC. The cryovials were either stored at -80ºC for short-term or in liquid nitrogen for longer storage.

2.2.2 Transient transfection

Successful transfection depends upon striking a balance between transfection efficiency and toxicity. The standard protocol used for most transfections is as follows:

Day 1: Cells were seeded so they are 70%-80% confluent at the time of transfection (Table 2.9).

Table 2.9 Culture conditions for transient transfection

Cell line	**10 cm culture dish**	**6-well plate**	**12-well plate**
HEK293T	1.0-2.0 x 10^6	1.0-3.0 x 10^5/well	1.0-3.0 x 10^5/well
HeLa-M	0.7-0.8 x 10^6	1.0 x 10^5/well	0.7-0.8 x 10^5/well
Volume of complete medium/well	10 ml	2 ml	1 ml

Day 2: Before transfection, all reagents are brought to room temperature. The medium was removed from the cells and replaced with an antibiotic-free medium (Table 2.10). The DNA to PEI ratio is calculated for each culture condition. In a sterile tube, the plasmid DNA and PEI are diluted in Opti-MEM separately and incubated for 5 minutes at room temperature (Table 2.11).

Table 2.10 Volume of transfection medium added prior to transfection

Cell line	**10 cm culture dish**	**6-well plate**	**12-well plate**
HEK293T	1.0-2.0 x 10^6	1.0-3.0 x 10^5/well	1.0-3.0 x 10^5/well
HeLa-M	0.7-0.8 x 10^6	1.0 x 10^5/well	0.7-0.8 x 10^5/well
Volume of transfection medium/well	7 ml	1 ml	0.5 ml

Table 2.11 Preparation of transfection mixture

Culture vessel	**Cell type**	**Tube 1 (PEI; 1mg/ml)**		**Tube 2 (DNA)**		**Final volume of DNA-PEI complex per well**
	HeLa-M	Opti-MEM	400 µl	Opti-MEM	400 µl	800 µl

10-cm dish	HeLa-C1	DNA to PEI (1:3)	24 µl	DNA	8 µg	
	HEK293T	Opti-MEM	400 µl	Opti-MEM	400 µl	800 µl
		DNA to PEI (1:3)	33 µl	DNA	11 µg	
6-well plate	HeLa-M HeLa-C1	Opti-MEM	100 µl	Opti-MEM	100 µl	200 µl
		DNA to PEI (1:5)	7.5 ul	DNA	1.5 µg	
	Co-transfection	DNA to PEI (1:5)	15 µl	DNA 1 DNA 2	1.5 µg 1.5 µg	200 µl
12-well plate	HeLa-M HeLa-C1	Opti-MEM	50 µl	Opti-MEM	50 µl	100 µl
		DNA to PEI (1:3)	3 µl	DNA	1 µg	
	Co-transfection	DNA to PEI (1:3)	6 µl	DNA 1 DNA 2	1 µg 1 µg	100 µl

After incubation, Tube 1 is added to Tube 2 and mixed by pipetting. The DNA-PEI complex is incubated for 20 minutes at room temperature. The DNA-PEI complex was then added dropwise to the cells. The cells were incubated at 37°C in a 5% CO_2 humidified incubator overnight.

Day 3: The transfection efficiency of the cells was examined using the ZOE Fluorescence Imager (BioRad). If the transfection efficiency was satisfactory the cells were then used for downstream analysis.

2.2.3 Plasmid DNA isolation

The DNA constructs used in this thesis were either purchased, obtained from colleagues, or custom-made using GeneScript (https://www.genescript.com). A few constructs were made in the lab using standard cloning and mutagenesis procedures.

2.2.3.1 Restriction digest

All restriction endonucleases were purchased from New England BioLabs. Restriction digest was performed following manufacturer recommendations. The reaction condition used is stated in Table 2.12. The restriction digest was performed for 1 hour at 37°C. To stop the digestion, samples were added with 6X DNA loading dye.

Subsequently, digested DNA insert and vector were run on an agarose gel and purified GeneJet Extraction kit (Thermo Scientific).

Table 2.12 Restriction digest reaction components

Reaction component	Sequential digest	Double digestion
DNA (vector or insert or PCR product)	1-3 µg	1-3 µg
10X reaction buffer	5 µl	5 µl
Enzyme I	1-3 units	1-3 units
Enzyme II		1-3 units
dH_2O	Make up to 50 µl	Make up to 50 µl

2.2.3.2 Agarose gel electrophoresis

Gel electrophoresis was performed to visualise DNA fragments after digestion and gel purify DNA for ligations. Table 2.13 shows the protocol to make 1% agarose gel.

Table 2.13 Buffers

1 X TBE buffer	40 mM Tris, 20 mM acetic acid, 1 mM EDTA
Agarose gel	1% agarose in 1x TBE buffer

Agarose was dissolved in 1X TBE buffer by heating in a microwave (Table 2.14). To visualize the DNA, SYBR® safe DNA Gel Stain was added to the agarose at 1:10,000 dilution. The agarose mixture was then transferred into a gel tray and the appropriate comb was inserted and left to solidify at RT for about 20-40 minutes. The solidified gel was then placed in the electrophoresis chamber and 1X TBE buffer was added until the gel is completely submerged. Samples (pre-mixed 6X DNA loading dye) were then loaded onto the gel. The gel was run for about one hour at 100V till loading dye had run approximately 2/3 of the gel. The DNA was then visualized using the Gel Doc™ EZ system.

When the correct fragment size has been identified, the DNA is visualized under the Blue LED illuminator and the desired fragment is excised from the gel. The DNA fragment was purified using the GeneJet Gel Extraction kit according to the manufacturer's instructions. Alternatively, the amount of DNA obtained can be measured using the Nanodrop on the dsDNA setting.

2.2.3.3 Ligation

Purified DNA insert and vector were ligated using Rapid DNA Ligation Kit. Once properly mixed, the mixture is incubated at RT for 1 hour (on the bench). Subsequently, the ligation mixture was transformed into bacteria (Table 2.14).

Table 2.14 Ligation reaction component

Reaction component	Insert	Linear Vector
Linear cloning vector	250 ng	50 ng
DNA insert	5:1 (insert:vector)	-
5X Rapid Ligation buffer	4 µl	4 µl
T_4 DNA ligate, 5 U/µL	1 µl	4 µl
ddH_2O	Make up to 20 µl	Make up to 20 µl

The amount of DNA insert and linear cloning vector was calculated as a molar ratio 5:1 (insert over vector) according to the formula;

ng of linearized vector = $\frac{length\ of\ insert\ (kb)}{length\ of\ vector\ (kb)}$ = ng of insert x 5

2.2.3.4 Bacterial culture and transformation

Plated bacterial cultures were grown at 37ºC in a Heraeus B12 incubator (Thermo Fisher, Ely, UK) and all liquid cultures were grown at 220 rpm at 37ºC in a shaker incubator. Small bacterial cultures (2-50 ml) were pelleted by centrifugation for 5 minutes at 5000rpm in a Beckman Allegra 21R centrifuge (Beckman Coulter, High Wycombe, UK), while larger bacterial cultures (>50 ml) were pelleted by centrifugation for 5 minutes at 5000 rpm in the Beckman Avanti J-20i centrifuge.

Plated bacterial cultures were maintained on LB culture plates. Bacterial cultures were grown in Lysogeny broth. Where required, the appropriate antibiotic (Ampicillin 100 mg/ml; at 1 in 1000 or Kanamycin 50 mg/ml; at 1 in 1000) was added. Competent bacteria were transformed with plasmid DNA. Competent bacteria were thawed on ice. 2 µl of DNA (no more than 100 ng) to 100 µl of competent bacteria. The tube was flicked several times to mix the contents and incubated on ice for 3 minutes. The DNA-competent bacteria mix was subjected to heat-shock at 42ºC for 42 seconds. When using Kanamycin-resistance plamids, a recovery step is required, where the cells are pelleted

at 8000 x g for 30 seconds at room temperature and resuspended in 200 µl of LB (without antibiotics). The mixture is then incubated in a 37^{o}C shaker incubator for 40 minutes. Then, a sterile plastic spreader was used to spread cells on bacteria culture plates containing the appropriate antibiotic selection and incubate overnight at 37^{o}C.

2.2.4 Microscopy

Adherent cells were cultured in 12-well plates containing glass coverslips. Appropriate cell density was determined for each cell type depending on its' rate of growth. All images were captured at the Wolfson Light Microscopy Facility using the upright Olympus BX61 motorised wide-field epifluorescence microscope (60x Oil objective) or a Zeiss LSM880 AiryScan (63x Oil objective). Image processing was performed using the latest version of Image J software.

2.2.4.1 Fixation and staining of cells

Table 2.15 lists the buffers, fixatives, and permeabilising solutions used to prepare cells on coverslips for microscopy.

Table 2.15 Buffers, fixatives, and permeabilising solutions used for microscopy

Buffer	**Working concentration**	**Description**
1xPBS		
Blocking solution (if using Triton X-100 permeabilizing reagent)	1% BSA in 1xPBS	1 g BSA in 100 ml 1xPBS
Fixative	**Working concentration**	**Description**
Paraformaldehyde (PFA)	4% PFA in 1xPBS	20 ml of 10% Formaldehyde was added to 5 ml of 10X PBS and made up to a volume of 50 ml with 25 ml of distilled water (under fume hood)
Quenching solution for PFA	0.1M glycine in 1xPBS	0.375 gm of glycine was added to 50 ml of 1xPBS
Permeabilizing solution	Working concentration	Description
saponin	0.1% saponin	1gm saponin was added to 50 ml of 10xPBS, 50 ml of FBS, and made up to a

		volume of 1 litre with 900 ml of distilled water. The solution is filtered under sterile conditions and stored in a cool and dark place.
Triton-X 100	0.1% Triton-X 100	Make 1% Triton-X 100 stock solution by adding 500 ul of concentrated Triton-X 100 into 49.5 ml of 1xPBS Stock is kept in a cool and dark place. 1 ml of 1% Triton-X 100 was diluted into 9 ml 1xPBS to achieve a working dilution of 0.1% Working concentrations should be prepared fresh every time.

Cells grown on coverslips were removed from the CO_2 incubator and fixed immediately either using PFA.

2.2.4.2 Fixation in 4% PFA

To reduce the risk of osmotic shock, an equal volume of 4%PFA was directly added to cells. The media was aspirated and replaced with fresh 4%PFA and incubated for a further 15 minutes at RT. After fixation, cells were washed twice with PBS and any remaining PFA was quenched using 0.1M glycine in PBS for 5 minutes at RT. The quenching solution was then removed and the cells were washed twice with PBS.

2.2.4.3 Permeabilisation with saponin and staining

After fixation, 0.1% saponin was added to the cells and incubated at RT for 15 minutes. The solution was removed and the primary antibody diluted in 0.1% saponin was added

and incubated for 30 minutes at RT. The cells were washed with 0.1% saponin three times before an appropriate secondary antibody diluted in 0.1% saponin was added and incubated for 30 minutes at RT. Cells were washed with 0.1% saponin twice and once with PBS before coverslips were mounted onto glass slides in Prolong Gold mounting media.

2.2.4.4 Permeabilisation with Triton-X 100 and staining

After fixation, the cells were permeabilised with 0.1% Triton-X 100 for 10 minutes at RT. The solution was removed and the samples blocked using 1% BSA in PBS. for 30 minutes at RT. The primary antibodies were diluted in blocking solution and incubated for 1 hour at RT. Cells were washed 3 times with PBS. The cells were incubated with a secondary antibody prepared in blocking solution for 30 minutes at RT. Cells were washed 3 times with PBS and the coverslips mounted onto glass slides.

2.2.5 SDS Page and Immunoblotting

2.2.5.1 Sample preparation

Cell lysates were prepared by washing cells three times with PBS and then adding the appropriate amount of Laemlli buffer supplemented with β-mercaptoethanol (under fume hood). The lysed cells were harvested from the dishes using a cell scraper and the cell lysate was transferred to a QIAshredder (Qiagen). The cell lysate was centrifuged at speeds >10,000 x g for 2 minutes. The supernatant collected was transferred to a new 1.5 mL tube. The samples were boiled for 5 minutes at 100ºC. Before samples were loaded onto the gel, they were briefly centrifuged and left to equilibrate to RT. If not used immediately, samples are placed at 4ºC for later analysis.

2.2.5.2 SDS-PAGE and protein transfer by immunoblotting

2.2.5.2.1 Casting SDS-PAGE gels

Table 2.16 lists the chemicals and protocol for making SDS-PAGE gels for western blotting.

Table 2.16 SDS-PAGE recipes

Separating Gel (4 gels)					Staking Gel (4 gels)	
10%	**12%**	**15%**	**Recipe**			**Recipe**
4.8 ml	3.4 ml	1.4 ml	H_2O		3.5 ml	H_2O
8.4 ml	8.4 ml	8.4 ml	Separating buffer		0.63 ml	Stacking buffer
6.6 ml	8.0 ml	10 ml	30% Acrylamide		0.83 ml	30% Acrylamide
100 µl	100 µl	100 µl	20% SDS		25 µl	20% SDS
100 µl	100 µl	100 µl	10% APS		50 µl	10% APS
20 µl	20 µl	20 µl	TEMED		5 µl	TEMED

Buffer Stock	Composition	Recipe (source)
Separating buffer	3 M TRIZMA Base pH 8.9	183 g TRIZMA (Sigma) 20 ml of 11.6 M HCl Total to 500 ml with H_2O and pH adjusted
Stacking buffer	1 M TRIZMA Base pH 6.8	61 g TRIZMA (Sigma) 30-40 ml 11.6 M HCl Total to 500 ml with H_2O and pH adjusted
30% Acrylamide	30% stock acrylamide:bis-acrylamide (37:5:1)	As supplied (Bio-Rad)
20% SDS	20% Sodium Dodecyl Sulfate in H_2O	As supplied (Thermo Fisher Scientific)
10% APS	10% Ammonium Persulfate in H_2O	Weigh empty microtube. Add solid APS (Sigma) into the microtube and weigh the tube again. Add H_2O to a total of 10% APS Make fresh or store at -20ºC
TEMED	N,N,N',N'-Tetramethyl-ethylenediamine	As supplied (Sigma)

Sodium-dodecyl-sulfate polyacrylamide gel electrophoresis (SDS-PAGE) gels varying from 10-15% acrylamide were cast according to the recipes in Table 2.18 using a Mini-PROTEAN-3 electrophoresis system (BioRad) with 0.75 mm spacer plates.

Glass plates were washed with liquid detergent, rinsed with distilled water followed by 70% ethanol, and left to dry. The spacer and short plates were assembled and into the casting chamber and the separating gel was added (approximately 3.5-4 mL). Isopropanol was laid on top of the separating gel to get rid of any bubbles trapped

between the spacers. The gel was left to sit for about 30 minutes. After the separating gel has set, the isopropanol was poured off the top of the gel and washed 5-6 times with distilled water. The gels were then turned sideways and tissue was used to drain the remaining water. The stacking gel was prepared and poured on top of the short plate (approximately 1 mL of stacking gel mixture). Then, the comb was inserted. The gel was left to sit for 30 minutes. The comb is removed only prior to running the gel. If not used immediately, the spacer plates can be wrapped in a damp absorbent towel and kept at 4ºC till used (not more than 1 week).

2.2.5.2.2 Loading and running of SDS-PAGE gels

Before samples were loaded onto the gels, wells were briefly inspected for deformities and/or other physical distortions. Irregular wells are marked with a black marker and loaded with 1 times sample buffer. The comb was removed from the gel under a running tap by pushing out the sides of the combs gently. The gels are then fitted into the Mini-PROTEAN-3 electrophoresis cassette ensuring a good seal. The cassette was then loaded into the buffer tank and the inner side of the cassette was filled with premixed running buffer (Bio-Rad) (Table 2.17). The wells can hold a maximum sample volume of 15 µl (to avoid overspill into other wells). Wells at either end of the gel and any empty wells were loaded with 1x sample buffer to avoid splaying of the protein bands throughout the gel. Western C (Bio-Rad) broad range molecular weight standard was loaded alongside experimental samples. After samples and buffers have been loaded, the buffer tank was filled completely with running buffer. The gel was initially run at a constant voltage of 120 V, while the loading dye runs through the stacking gel. Once the dye enters the separating gel the voltage was increased to 200V (EC135-90 power supply). The gels were run until the loading dye exited the bottom of the gel.

2.2.5.3 Staining SDS-PAGE protein gels with protein stains

For newly prepared protein lysates, a Coomassie stain was performed at the end of the run to ensure standard loading of all samples, before proceeding to protein transfer. If a Coomassie stain was intended, PageRuler Prestained Protein Ladder (Thermo Scientific) was used. The SDS-PAGE gel was removed from the gel cassette and placed in a square plastic dish. The gel was immersed in Quick Blue (Avidity Science), Coomassie stain, and incubated on a Stuart See-saw Rocker (Bibby Scientific,

Staffordshire, UK) for 15 minutes. The gel was washed with distilled water and scanned using a Gel Doc EZ Imaging system (Bio-Rad) with Image Lab software.

2.2.5.4 Protein transfer

Table 2.17 SDS-PAGE Transfer, Running buffer conditions and Immunoblotting buffers

Buffer Stock	Composition	Recipe (source)
Running buffer (5 L)	25 mM TRIZMA 192 mM Glycine 0.1% SDS pH 8.3	Bio-Rad
Low molecular weight transfer buffer (5 L)	50 mM TRIZMA 40 mM Glycine 20% Methanol	30 g TRIZMA (Sigma) 15 g Glycine (Fisher Scientific) 1 L Methanol (Fisher Scientific) Make up to 5 L with distilled water
High molecular weight transfer buffer (5 L)	50 mM TRIZMA 40 mM Glycine 20% Methanol 0.1% SDS	30 g TRIZMA (Sigma) 15 g Glycine (Fisher Scientific) 1 L Methanol (Fisher Scientific) 25 ml 20% SDS Make up to 5 L with distilled water
PBS-Tween (0.1%)	1xPBS made by 100 ml of PBS (10X) made up to 1 L with dH2O 1 ml of Tween 20	PBS (10X), pH 7.4 (Fisher Scientific) Tween 20 (Sigma-Aldrich)
5% milk solution in PBST	5 g in 100 ml of PBS-T	Skim Milk Powder (Sigma-Aldrich)

Proteins were transferred using either high or low molecular weight transfer buffer to PVDF membranes (0.45 µm, GE Healthcare Life Sciences) using a wet blotting method (Towbin et al., 1979) (Table 2.17). Specifically, the gels were removed from the gel cassette and placed in a square plastic dish containing the appropriate transfer buffer. A transfer cassette sandwich was prepared using wet transfer sponges, Whatman paper, the SDS-PAGE gel, and the PVDF membrane in a tray filled with transfer buffer. The PVDF was first activated by soaking in methanol for 1 minute. The methanol was drained and the PVDF was kept wet by soaking in the appropriate transfer buffer. All elements were stacked and assembled on the transfer overnight at 4ºC with 100 mA current running per transfer tank using a BioRad PowerPac HC (BioRad, Hercules, CA, USA).

2.2.5.5 Immunoblotting

Membranes were blocked with 5% non-fat dry skimmed milk in 0.1% PBS-T (Table 2.17) by immersing the membranes in the solution for one hour at RT with gentle agitation. Subsequently, the membrane was incubated with primary antibody diluted in blocking solution, overnight at 4ºC. After incubation with the primary antibody, the membrane was washed three times with wash buffer (0.1% Tween-20 in 1xPBS) for five minutes for each wash. Then the membrane was incubated with the secondary antibody which is HRP-conjugated (species-specific) and the anti-Streptactin (BioRad) to visualize the molecular weight marker at RT diluted in wash buffer for 1 hour. All incubations were at RT and were performed with constant rotation to ensure adequate coverage of the membrane. The membrane was then washed again three times for five minutes with wash buffer. The protein was detected using the (BioRad illumination kit) on the LI-COR Imaging System.

2.2.6 Flow cytometry

2.2.6.1 Preparation of cells for flow cytometry

2.2.6.1.1 Cell dissociation using trypsin

Cells were washed twice with PBS and the appropriate amount of trypsin was added. Cells intended for surface staining were trypsinized on ice for 3-5 minutes, while cells intended for intracellular staining or uptake assays were incubated with trypsin at 37ºC for 2-3 minutes. Cells were collected into microcentrifuge tubes or FACs tubes by pipetting up and down. Approximately $1.5 \times 10^5 – 3.0 \times 10^5$ cells were used per sample.

2.2.6.1.2 Labelling surface protein

The antibody was diluted to achieve 0.1-10 µg/ml in cold media and 50-100 µl of this solution was added to each tube. Cells were incubated for 30 minutes at 4ºC in the dark and intermittently vortexed every 10 to 15 minutes. After incubation, cells were washed three times with cold media or cold PBS by centrifugation at 400 g for 5 minutes. After the last wash, cells were resuspended in 400 µl of cold media. Cell suspension should be kept on ice in the dark till acquired by flow cytometer.

2.2.6.1.3 Intracellular protein labelling

HeLa-M cells were harvested by trypsinization and fixed with 0.5ml freshly prepared 4% PFA. After fixation, cells were washed twice with PBS and any remaining PFA was quenched using 0.1M glycine in PBS for 5 minutes at RT. The quenching solution was removed and the cells were washed twice with PBS. Approximately 1.5 x 10^5 – 3.0 x 10^5 cells for each sample were calculated and placed into individual microcentrifuge tubes. The cells were then resuspended in 200 µl of permeabilizing solution (0.1% saponin or 0.1% Triton-X 100). Cells were incubated for 15 minutes at RT. During the incubation period, the cells are intermittently vortexed to maintain the cells in single-cell suspension. 10-30 µl of primary antibody diluted in 0.1% saponin was added to resuspend the cells and vortexed to ensure adequate mixing. The cells were incubated for 30 minutes in the dark at RT. Cells were intermittently vortexed to keep cells resuspend in the solution. The cells were washed twice with 0.1% saponin. For unconjugated primary antibodies, the appropriate secondary antibody diluted in 0.1% saponin was added and incubated for 30 minutes in the dark at RT. Cells were intermittently vortexed to keep cells in the solution. After incubation, cells were washed twice with 0.1% saponin and resuspended in 400 µl of PBS.

2.2.6.2 Sample Acquisition

Sample acquisition was performed either on the BD FACS LSRII (BD Biosciences) from the Flow Cytometry Core Facility or Attune (Life Technologies) Bateson Centre, University of Sheffield. Forward and side scatter gating was used to separate the cell population from debris and dead cells. A total of 10,000 events were acquired for each sample unless a GFPA gate was used (minimum of 1000 GFP positive cells per sample). A minimum of 3-4 independent experiments was performed.

2.2.6.3 Flow Jo analysis

All flow cytometry data were analysed using Flow Jo software. This software was used to gate the cells and determine their mean fluorescent intensity of the samples.

2.2.7 Functional transport assays

2.2.7.1 Alexa647-transferrin uptake assay

HeLa-M cells expressing various constructs were serum-starved for 30 minutes at 37ºC. The cells were incubated with media containing 50 µg/ml of Alexa647-transferrin in a serum-free medium for 5 minutes at 37ºC. The cells were then washed with a warm medium and immediately fixed with 4% PFA. The coverslips were then mounted onto glass slides using Prolong Gold anti-fade reagent.

2.2.7.2 Antibody uptake assay

HeLa-M cells expressing various constructs were serum-starved for 30 minutes at 37ºC. The cells were then incubated with media containing the appropriate antibody for uptake in a serum-free medium for 20 minutes at 37ºC. The cells were then washed with a warm medium three times and fixed with 4% PFA. The coverslips were then mounted onto glass slides using Prolong Gold anti-fade reagent. Table 2.18 shows the antibodies used for the antibody uptake assay.

Table 2.18 Antibodies used for antibody uptake assay

Antibody	Species	Dilution	Compartment
CD63	mouse	1:100	Lysosome
CD-MPR	mouse	1:100	Lysosome
CI-MPR	mouse	1:100	lysosome
TGN46	rabbit	1:100	Golgi

2.2.7.3 Wheat Germ Agglutinin (WGA) binding and internalization assay

2.2.7.3.1 Preparation for immunofluorescence microscopy

HeLa-M cells were cultured in 12-well plates containing glass coverslips (Table 2.9) and transfected as outlined earlier (see method 2.2.2). For WGA uptake experiments, HeLa-M cells expressing the various constructs were chilled on ice and incubated with media containing Alexa350-WGA (1:50) for 15 minutes at 4ºC. After incubation the cells were washed with cold PBS three times and either: 1) fixed with 4% PFA for 10 minutes; 2) incubated with pre-warmed serum-free media for 15 minutes at 37ºC, washed with PBS and fixed with 4% PFA or 3) treated with 0.1M D-GlcNAc at 4ºC for

5 minutes, washed with cold PBS and fixed with 4% PFA. Table 2.19 outlines the experimental conditions used.

Table 2.19 Summary of experimental conditions for visualizing WGA

	Conditions	Localization of WGA
1.	WGA added and incubated at 4°C for 15 minutes	Surface only
2.	WGA added and incubated at 37°C in a humidified incubator for 15 minutes	Internalized in endosomes
3.	WGA added and incubated at 4°C for 15 minutes, washed then incubated at 37°C in a humidified incubator for 15 minutes	Movement of WGA from the surface to being internalized in endosomes
4.	Repeat No.3 then add GlcNAc and incubated at 4°C for 5 minutes	Stripping off WGA on the cell surface

2.2.7.3.2 Preparation for flow cytometry acquisition

HeLa-M cells previously incubated with WGA were harvested by using 300 µl (for a 12-well plate) enzyme-free cell dissociation buffer (Gibco, Life Technologies). The cells were left to incubate in this solution at RT while intermittently checking for dissociation under an inverted microscope. The plate can be firmly tapped against the palm of the hand to dislodge the cells. When this has occurred, 100 µl of serum-free media is added to the wells, and cells were collected into microcentrifuge tubes or FACs tubes by pipetting up and down. All cells were kept on ice in the dark until acquired by flow cytometry.

2.2.7.4 Soluble secretor reporter assay

The secretion assay was performed using previous methods established in our lab (Gordon et al, 2010).

2.2.7.4.1 Preparation for immunofluorescence microscopy

HeLa-C1 cells were cultured in 12-well plates containing glass coverslips (Table 2.9). Preparation of cells for transfection was performed as outlined earlier (see method 2.2.2) using these plasmids:

1. Untransfected (PEI only)
2. mCherry WT BoNT/X

3. mCherry MUT BoNT/X

Paired observation of the effect of the constitutive secretion was recorded after exposure to 1-2 µM of Rapamycin prepared in complete media at two time-points; 0 minutes and 120 minutes. At the end of each time point, the cells were washed twice with cold PBS. The cells were fixed with 4% PFA, washed with PBS, and quenched with 0.1M Glycine. Then, coverslips were mounted with an Anti-fade ProlongGold reagent.

2.2.7.4.2 Preparation for acquisition by flow cytometry

After transfection, the cells were trypsinized and collected in individual microcentrifuge tubes. Rapamycin was added to the cells in suspension at similar time points. At the end of each time point, the cells were washed with cold PBS twice by centrifuging at 400 x *g* for 5 minutes. Cells were then resuspended in 400 µl of complete media and acquired using a 2-colour flow cytometry assay using the Attune (Life Technologies). GFP signal was detected after excitation with the 488 nm blue laser and collected with a 530/30 nm bandpass filter. mCherry was excited with the 561 nm yellow-green laser and collected with a 610/20 bandpass filter. Settings and analysis can be seen in Methods section 2.2.6.2 and 2.2.6.3.

2.2.7.5 Membrane anchored secretion assay

HeLa-M cells were cultured in 12-well plates containing glass coverslips (Table 2.9) and transfected as outlined earlier (see method 2.20).

Table 2.20 Summary of co-transfection experiments

Co-transfection experiment
1. Non-fluorescent-WT BoNT/X + eGFP-CD8a
2. Non-fluorescent-MUT BoNT/X + eGFP-CD8a
3. Non-fluorescent-WT BoNT/X + pCMV3-CD63-GFPSpark
4. Non-fluorescent-MUT BoNT/X + pCMV3-CD63-GFPSpark

2.2.7.5.1 Surface staining for immunofluorescence microscopy

HeLa-M cells expressing various constructs in Table 2.22 were washed with cold PBS three times. The cells were chilled for 5 to 10 minutes on ice or in the cold room. Rat

anti-human CD8 antibody (Serotec) and rat anti-mouse CD63 antibody (Biolegend) were diluted at 1:100 in cold media and added onto the respective coverslips and incubated on ice for 30 minutes. Coverslips were washed with cold PBS four times, fixed with cold 4% PFA for 15 minutes. After fixation, cells were washed twice with PBS and any remaining PFA was quenched using 0.1M glycine in PBS for 5 minutes at RT. The quenching solution was removed and the cells were washed twice with PBS. and blocked with 1% BSA blocking buffer for 15 minutes. The appropriate secondary antibody in blocking buffer was prepared and incubated for 30 minutes at RT. Coverslips were washed with PBS four times and mounted onto glass slides using prolong gold mounting medium. Reagents/solutions and cells are kept at 4^{o}C to prevent internalization of surface antigens which could result in a loss of fluorescence intensity.

2.2.7.5.2 Surface staining for flow cytometry

HeLa-M cells expressing various constructs in Table 2.20 were prepared according to methods outlined earlier (see method 2.2.6.1). Cells were dissociated using trypsin (see method 2.2.6.1.1). Approximately 1.5 x 10^5 – 3.0 x 10^5 cells were used per sample. Rat anti-human CD8 antibody (Serotec) and rat anti-mouse CD63 antibody (Biolegend) was used for labelling surface CD8 and CD63 respectively and prepared according to methods outlined earlier (see method 2.2.6.1.2). GFP signal was detected after excitation with the 488 nm blue laser and collected with a 530/30 nm bandpass filter. Cy5 was detected after excitation with a 633 nm red laser and collected with a 660/20 bandpass filter. Settings and Flow Jo analysis can be seen in Methods section 2.2.7.

Chapter 3: The recombinant light chain of BoNT/X is capable of cleaving multiple R-SNAREs in vivo

3.1 Introduction

BoNTs have been widely used to study neurotransmitter exocytosis due to their ability to inhibit neuronal SNARE function (cleave VAMPs1/2, syntaxin, and SNAP-25). However, their broader use has been limited by the fact that they are unable to intoxicate non-neuronal cells as they do not express the correct surface receptors and SNARE proteins. The recent discovery of BoNT/X has opened the opportunity to study the function of non-neuronal R-SNAREs. However, very little is known about the action of this toxin as its activity has been predominantly tested on recombinant R-SNAREs.

3.2 Chapter aims

The aim of this chapter was to extend the characterisation of BoNT/X and determine if it is capable of cleaving R-SNAREs in vivo and determine what impact their loss has on cellular trafficking. In order to achieve this, we sought to:

1) determine if the light chain of BoNT/X is active when expressed recombinantly.

2) assess if its specificity matches what has been claimed by other research groups.

3) determine the impact of BoNT/X intoxication on endocytic and biosynthetic compartment morphology.

3.3 Results

3.3.1 The recombinant light chain of BoNT/X cleaves a wide range of post-Golgi R-SNAREs

Botulinum toxins have been classified as a category A bioterror agent due to their extreme toxicity (Arnon et al., 2001). Therefore, the study of the full-length toxin is limited to specialized laboratories which have been granted specific safety clearance. In addition, these toxins only have the ability to intoxicate neuronal cell types so limiting

their application. To overcome these limitations several groups have recombinantly expressed BoNT light chain in non-neuronal cells (Yamamoto et al., 2012, Aguado et al., 1997, Grando and Zachary, 2018). Thus, we took a similar approach and synthesized the metalloprotease domain (1–439 aa) of BoNT/X and tagged it with enhanced GFP (Figure 3.1A). This construct will be referred to as wild type BoNT/X (WT BoNT/X). As a control, an inactive mutant form of the construct was also made by mutating Arg360 and Tyr363 (R360A/Y363F), which will be referred to as mutant BoNT/X (MUT BoNT/X). We also thought that it would useful to use a well-characterised BoNT serotype as control. Therefore, I generated wild-type and mutant BoNT/D expression constructs (residues 1-430 aa and inactive mutant [Y168D/L200D]). BoNT/D cleaves VAMPs 1, 2, and 3 but does not cleave VAMPs 4, 7, 8, and Ykt6 (Yamamoto et al., 2012, Guo and Chen, 2013).

To assess the activity of the recombinant constructs we transiently transfected HeLa-M cells with the indicated plasmids and performed immunostaining for several R-SNAREs. In the cells transfected with the active BoNT/X and D constructs, it was very obvious that the signal intensity of VAMP3 had been dramatically reduced compared to cells either expressing GFP or the inactive mutants. In addition, VAMP4 and Ykt6 also showed a reduction in signal intensity in cells expressing the active BoNT/X construct. Our results suggest that active BoNT/X is cleaving VAMPs 3, 4, and Ykt6 and causing these SNAREs to become unstable and degraded (Figure 3.1B). In contrast, no loss of signal was observed for VAMP7, 8, and SEC22b suggesting that they are not being cleaved by BoNT/X. Interestingly the localisation of VAMP8 appeared to be significantly altered in cells expressing BoNT/X suggesting its trafficking may be being affected by the expression of the toxin (Figure 3.1B). As expected, the expression of the active BoNT/D construct did not affect the levels and/or localization of any SNARE other than VAMP3 (Figure 3.1B).

To validate our microscopy-based findings we repeated the transfections and performed immunoblotting for the indicated SNAREs (Figure 3.1C). As expected we observed a clear reduction in signal intensity for VAMPs 3, 4, and Ykt6 in cells transfected with active BoNT/X. In addition, we also observed the appearance of a lower molecular weight band for Ykt6 suggesting that the protein had been proteolytically cleaved by the protease domain of BoNT/X. No changes in signal intensity were observed for

Sec22B suggesting that BoNT/X is unable to target this SNARE. No change in signal intensity for VAMPs 3, 4, and Ykt6 was observed in cells expressing GFP or the inactive toxin indicating that this phenotype requires the catalytic activity of BoNT/X (Figure 3.1C).

3.3.2 Expression of the BoNT/X light chain perturbs intracellular trafficking

Our data suggest that BoNT/X cleaves a substantial number of VAMPs including Ykt6. Thus, it is likely that the transport of lipids and proteins between the endocytic and biosynthetic pathways has been perturbed in these cells. To investigate this, we have examined the localisation of a panel of well-characterised proteins that define important compartments of the endocytic and biosynthetic pathways (Table 3.1).

HeLa-M cells were seeded and grown on coverslips and transiently transfected with the indicated plasmids and incubated overnight. The cells were fixed, permeabilised, stained with different compartment markers, and examined with immunofluorescence microscopy (Figure 3.2). The majority of compartment markers examined appeared perturbed, with the intensity of signal significantly reduced or their localization altered. Interestingly, the localisation of calreticulin was not dramatically affected and its reticular expression was maintained. Table 3.1 summarises the expression pattern of the main trafficking compartment. Comparison of WT BoNT/X-transfected cells was made with cells that were not transfected in the same microscopic field, cells transfected with MUT BoNTX, and BoNT/D plasmids.

Table 3.1 Summary of the expression pattern of main trafficking compartment markers in cells transfected with the active BoNT/X-LC based on immunofluorescence images.

Compartment	Marker	Expression pattern in active BoNT/X light chain
Early endosomes	EEA1	Reduced staining intensity, abnormally small vesicles with altered localization
TGN	TGN46 GM130	Golgi appears smaller and fragmented Golgi appears smaller and fragmented
Late endosomes and lysosomes	CD63	Reduced staining intensity
TGN and late endosomes	CIMPR CDMPR	Reduced staining intensity Reduced staining intensity
ER	Calreticulin	Reticular expression maintained

3.3.3 BoNT/X expression reduces cell proliferation and in some cells may induce apoptosis

While performing my initial BoNT/X characterisation experiments I observed that some of the transfected cells became smaller and rounder suggesting that the BoNT/X construct was possibly cytotoxic. In addition, there also appeared to be a reduction in cell number. To address this, I measured the viability of cells transfected with WT BoNT/X, MUT BoNT/X, and eGFP using a TC20 automated cell counter (BioRad) and flow cytometry.

After normalizing the cell counts of each condition against untransfected control cells, a significant drop in total cell count could be seen in WT BoNT/X-transfected cells. (Figure 3.3A) The cells were viable in all the characterisation experiments performed. and only a very small decrease in cell viability was detected with trypan blue (mean: 90%) and none by TO-PRO-3 staining (mean: 100%). To explore the mild decrease in cell viability further, I investigated whether apoptosis was being induced in the BoNT/X

transfected cells by staining them for Caspase 3 (Figure 3.3B). I observed that there were Caspase 3 positive cells in the BoNT/X transfected samples. However, caspase 3 positive cells were also present in the GFP and inactive mutant control samples.

3.4 Discussion

3.4.1 The GFP tagged light chain of BoNT/X is active when expressed in cells

It has previously been shown that the light chain of BoNT/X is capable of cleaving recombinant R-SNAREs in vitro (VAMPs 1-5, and Ykt6) and VAMP2 and VAMP4 in vivo (Zhang et al., 2017). However, it was not known whether BoNT/X can be tagged and still retain its activity and/or specificity. In addition, it was also unclear whether it cleaves Ykt6 in vivo. To address this, I tagged the light chain at the N-terminus with GFP and it expressed it transiently in HeLa-M and HEK cells. Based on our blotting and immunostaining experiments it is clear that the tagged protein is still active (cleaves VAMPs 3, 4, and Ykt6) and retains its specificity (no apparent cleavage of Sec22B). My data suggests that the recombinant construct is very active and highly efficient as its intoxicating effect can be evaluated within 16 hours of transfection. To our knowledge, we are the first group to show that the toxin cleaves Ykt6 in vivo. As HeLa-M and HEK cells do not express VAMP5 we did not determine whether this protein was targeted by the toxin in my experiments.

One potential limitation of my studies is that I was unable to detect cleavage products for VAMPs 3 and 4. I only observed a decrease in signal for these proteins. Thus, it is possible that the phenotype I am observing is indirect. However, I feel that this interpretation is unlikely because a similar phenotype is seen when VAMP2 is cleaved by BoNT/B (Rust et al., 2017). It is thought that VAMP2 becomes unstable when cleaved and the cleavage product is rapidly degraded. As mentioned earlier my data suggests that the overall specificity of the tagged light chain construct is similar to that of the untagged protein. For example, I observed no change in signal intensity for Sec22B, VAMPs 7 and 8. However, it should be noted that the steady-state distribution of VAMP8 became dramatically altered in the intoxicated cells. This observation

suggests that the VAMP8's trafficking may be dependent on one of the cleaved SNAREs.

3.4.2 The simultaneous cleavage of multiple R-SNAREs alters the morphology of the endocytic and biosynthetic pathways

BoNT/X expression led to major changes in the localisation of intracellular markers across a range of compartments and pathways. Based on my experimental data it is likely that BoNT/X is cleaving VAMPs 3, 4, and Ykt6 in Hela-M cells. Ykt6 is an essential SNARE implicated in various fusions including, ER to Golgi transport, vesicle fusion with the PM, and endosome-lysosome fusion (Gordon et al., 2017, Gross et al., 2012, Ruiz-Martinez et al., 2016). VAMPs 3 and 4 have been implicated in endosome fusion, endosome to Golgi transport, and vesicle fusion with the PM (McMahon et al., 1993, Galli et al., 1994, Advani et al., 1998, Mallard et al., 2002). Thus, it is not surprising that pleiotropic defects in intracellular trafficking are observed in intoxicated cells. Interestingly, depletion of VAMPs 3 and 4 using RNAi does not lead to dramatic alterations in endocytic trafficking (Luftman et al., 2009) (Shitara et al., 2017). Thus, it is possible that the observed phenotypes are predominantly caused by the loss of Ykt6. It is also possible that the acute disruption of these SNAREs may cause more dramatic alterations in trafficking than that observed with RNAi. In the future, it will be of interest to rescue these phenotypes using toxin-resistant SNARES and/or express versions of the toxin with altered substrate specificity.

3.4.3 Why is BoNT/X reducing cell proliferation?

In my experiments, I observed a reproducible reduction in cell proliferation and a very small decrease in cell viability in intoxicated cells. At present, it is unclear whether this toxicity is due to the light chain cleaving multiple SNAREs and thus inhibiting several pathways, or it is acting non-specifically and cleaving other molecules. The only way to directly address this would be to perform rescue or reconstitution experiments where one expresses cleavage-resistant SNAREs. These experiments have proven to be technically challenging as the cleavage-resistant SNAREs appear to be non-functional and/or are miss-localised.

When full-length toxins such as BoNTs A-G are used in vivo and in vitro only a small number of molecules are delivered per cell and very little cytotoxicity is observed. However, when higher doses are used, cytotoxicity is observed (BoNT/C >10 pM and BoNT/E >100 pM in cultured neuronal cells (Peng et al., 2013) suggesting that prolonged and complete SNARE cleavage can be detrimental to cells. Thus, the cytotoxicity I am observing could be explained by the complete cleavage SNAREs. In the future, it will be important to optimise the amount of DNA used in these experiments. Work by a subsequent student in the lab has shown that it is possible to achieve the same level of SNARE cleavage by using 1/10 the amount of DNA.

Since leaving the lab it has been observed that many of the intoxicated cells have cytokinetic bridges suggesting that SNARE cleavage is leading to a defect in cytokinesis. This could possibly explain the significant drop in total cell count seen within 24 hours of transfection in the WT BoNT/X cell population. Membrane traffic is crucial for the abscission of the cytokinetic bridge (Montagnac et al., 2008) and VAMP8 has been implicated in this process (Neto and Gould, 2011). BoNT/X does not cleave VAMP8 in vitro or in vivo suggesting BoNT/X is not directly acting on this SNARE. However, VAMP8's localisation is dramatically altered in the intoxicated cells suggesting that BoNT/X may be indirectly affecting VAMP8 function. We have also observed the activation of Caspase3 in a small percentage of cells transfected with the toxin. This data suggests that some intoxicated cells undergo apoptosis. To be sure, cells expressing Caspase3 in control, WT BoNT/X, and MUT BoNT/X transfected cells should be repeated and counted. However, we are not entirely sure what triggers caspase activation. It is possible that the defect in cell division may be triggering this process. In the long term, it will be informative to determine if the cell cycle has been altered in the intoxicated cells.

Figure 3.1 Active BoNT/X light chain cleaves an extended number of R-SNAREs.

(A) Schematic of the active and inactive recombinant Botulinum D and X constructs used in this study. Numbers represent amino acids.

(B) To characterize the SNARE-cleaving profile of the active BoNT/X, HeLa-M cells were grown on coverslips and were transiently transfected with recombinant WT BoNT/X or MUT BoNT/X. As a control, cells were also transfected with WT BoNT/D or MUT BoNT/D constructs overnight. The cells were then fixed and stained with the indicated R-SNARE antibodies and imaged using a fluorescence microscope. Scale bar 20 μm.

(C) HEK293T cells were transiently transfected with GFP-tagged WT BoNT/X, MUT BoNT/X, or with GFP vector and incubated overnight on poly-L-lysine-coated plates. Protein lysates were prepared in Laemmli lysis buffer and resolved on SDS-PAGE gels, transferred onto PVDF membrane, and immunoblotted for GFP and the indicated SNARE proteins. An antibody against γ-adaptin was used as a loading control.

(A)

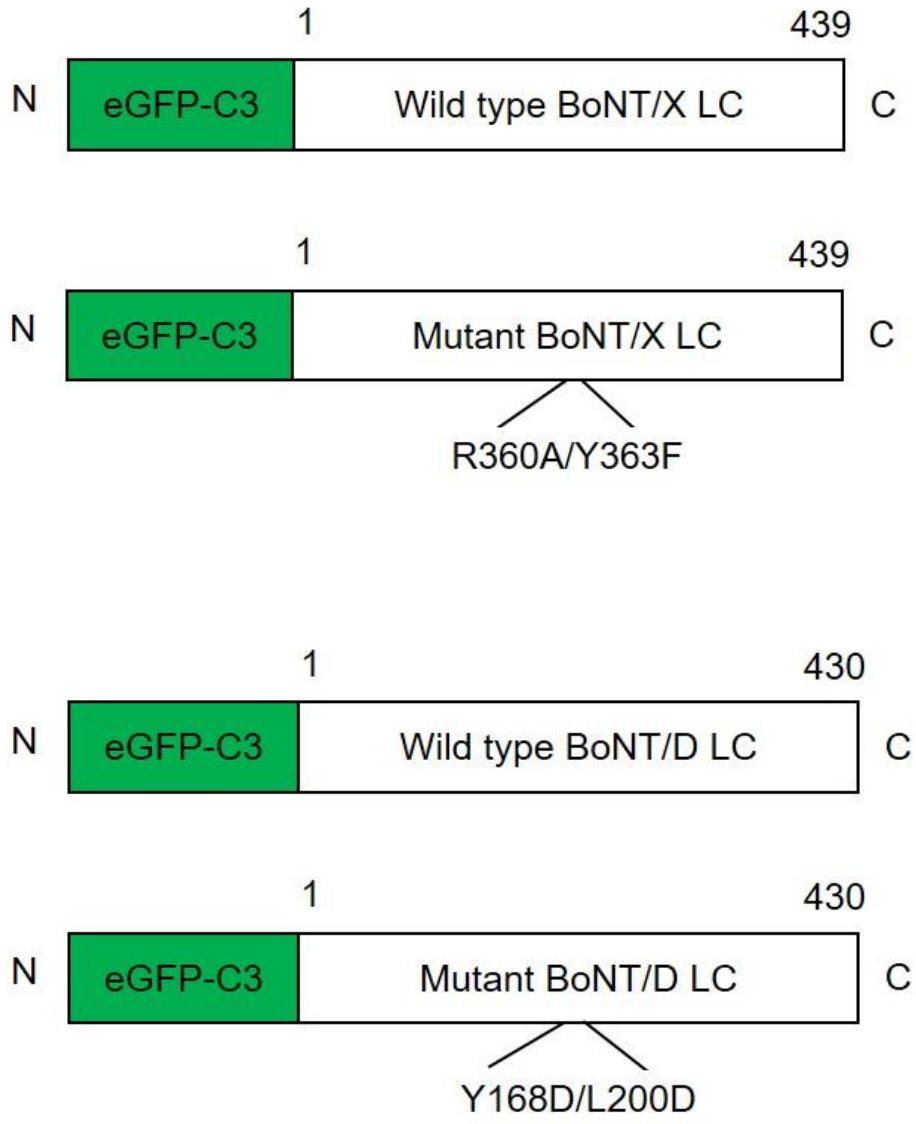
1
439
N
eGFP-C3
Wild type BoNT/X LC
C
1
439
N
eGFP-C3
Mutant BoNT/X LC
C
R360A/Y363F
1
430
N
eGFP-C3
Wild type BoNT/D LC
C
1
430
N
eGFP-C3
Mutant BoNT/D LC
C
Y168D/L200D

(B)

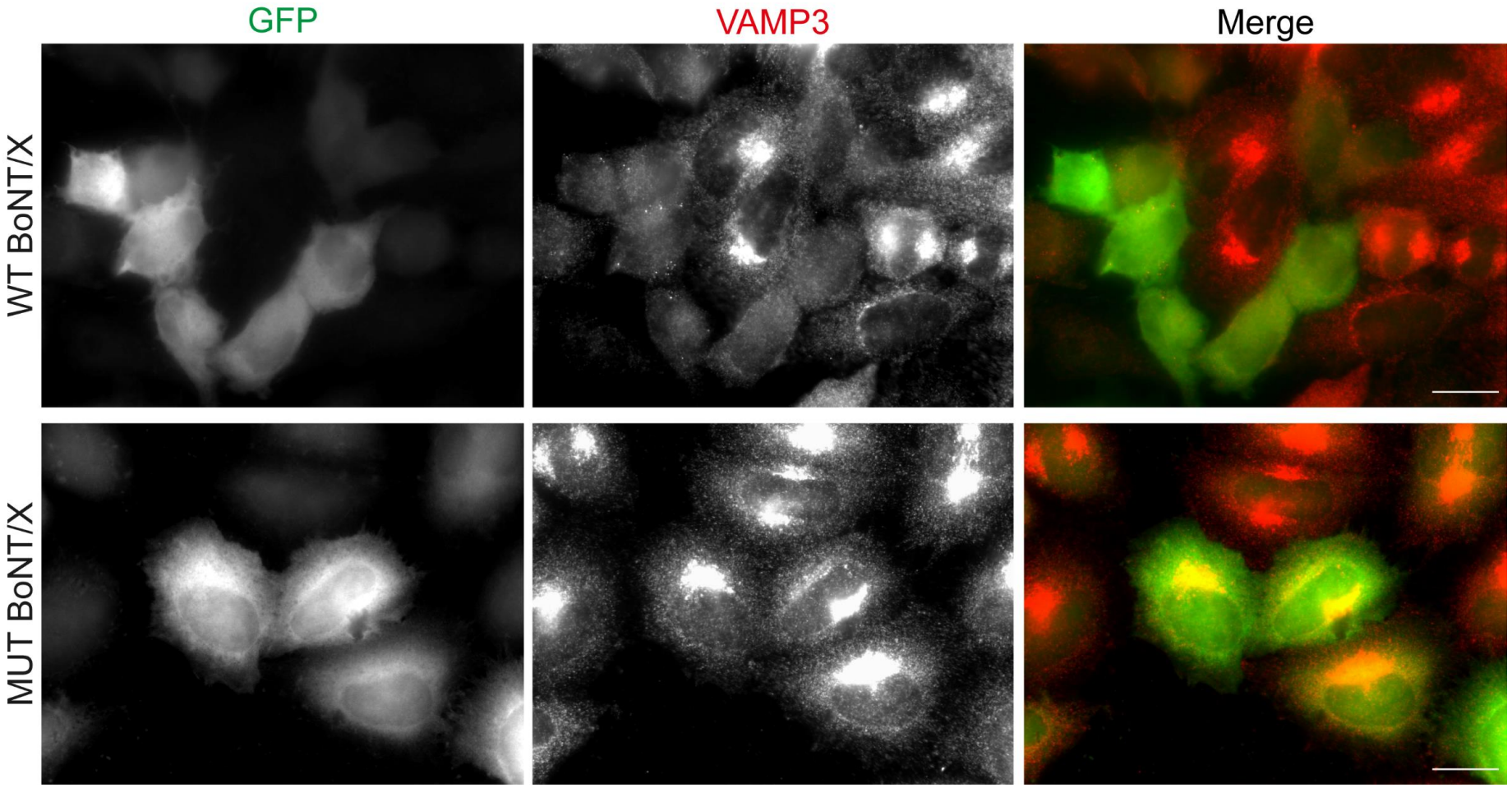

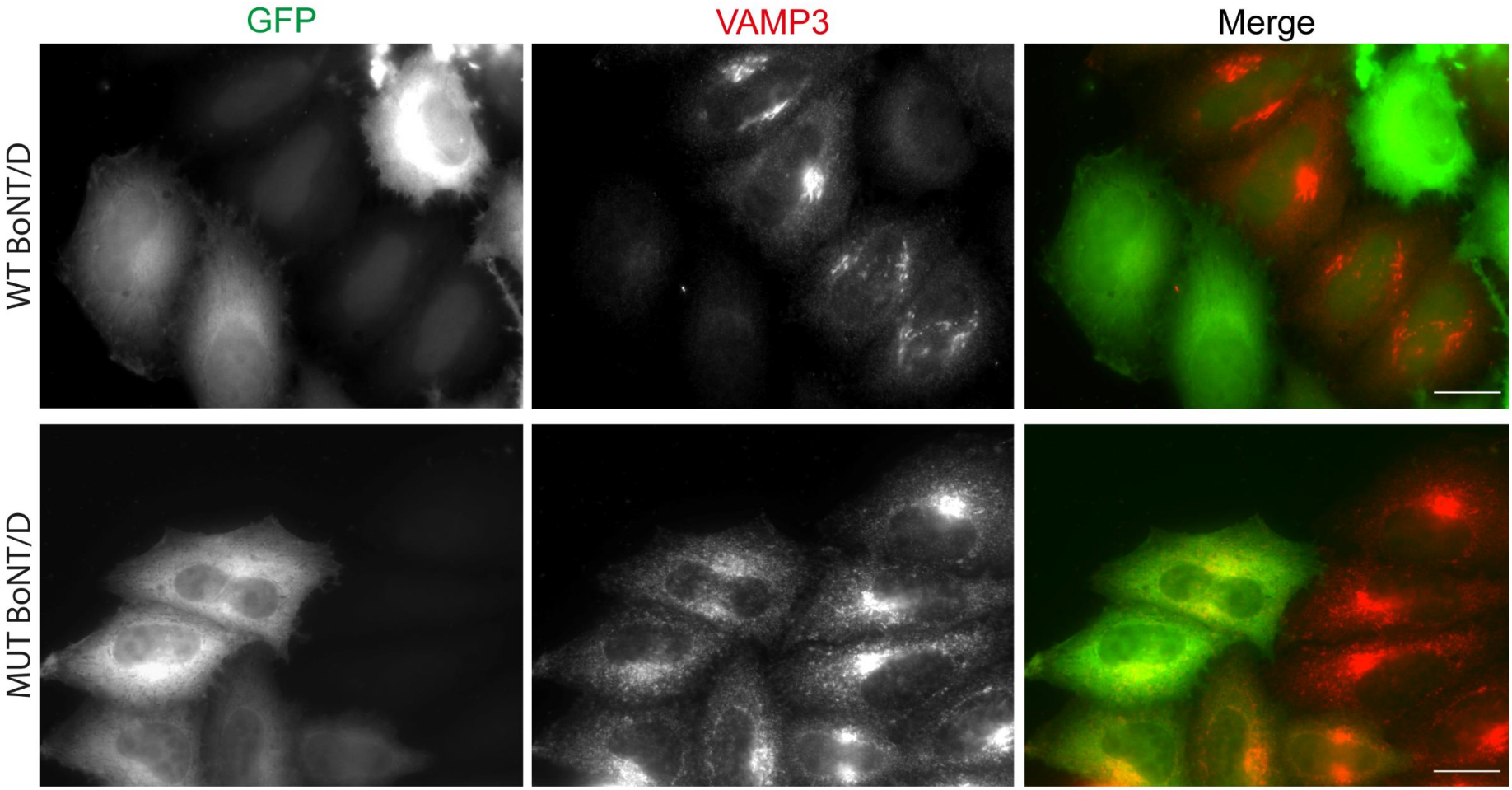
GFP
VAMP3
Merge
WT BoNT/D
MUT BoNT/D

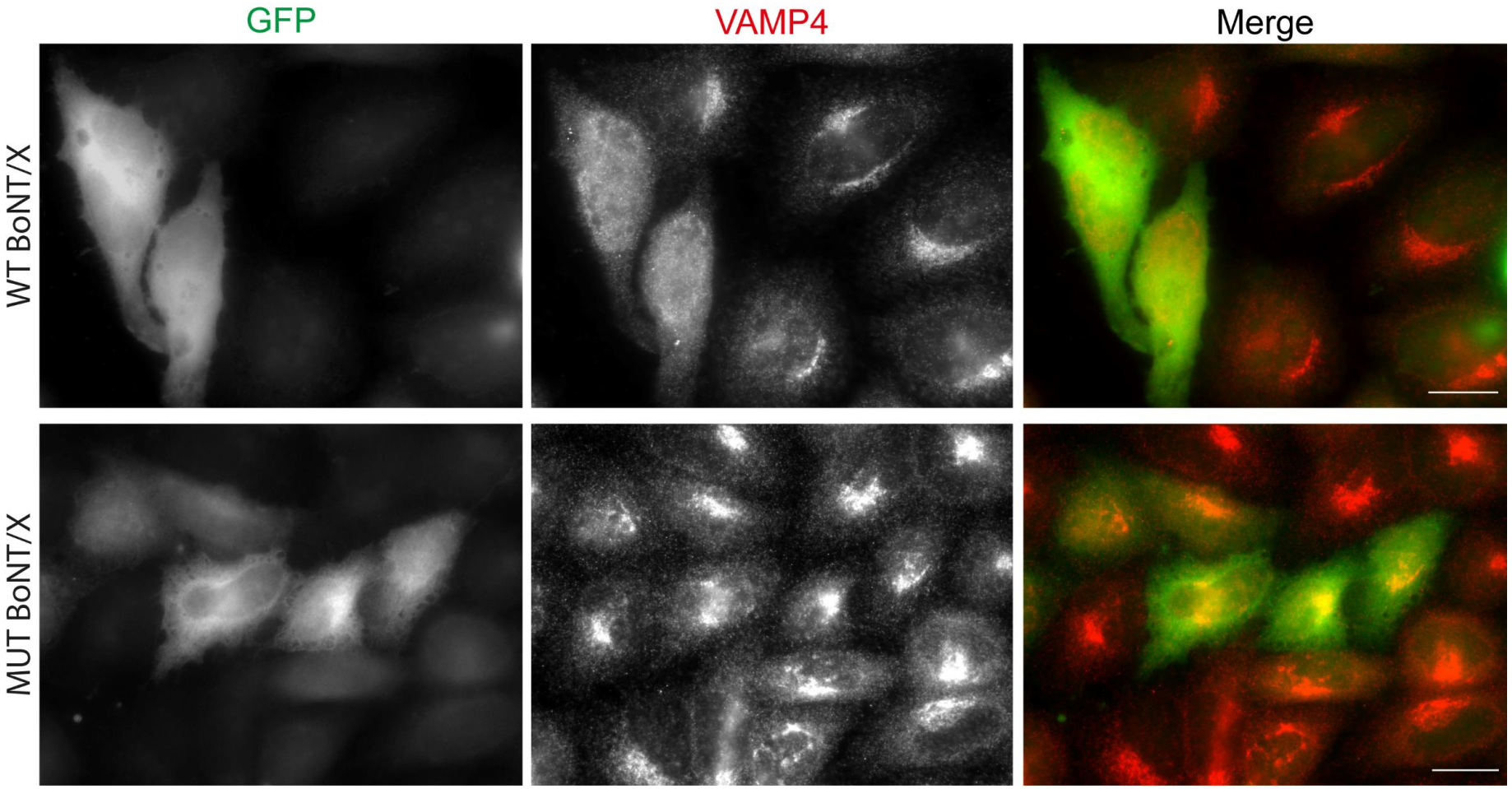
GFP
VAMP4
Merge
WT BoNT/X
MUT BoNT/X

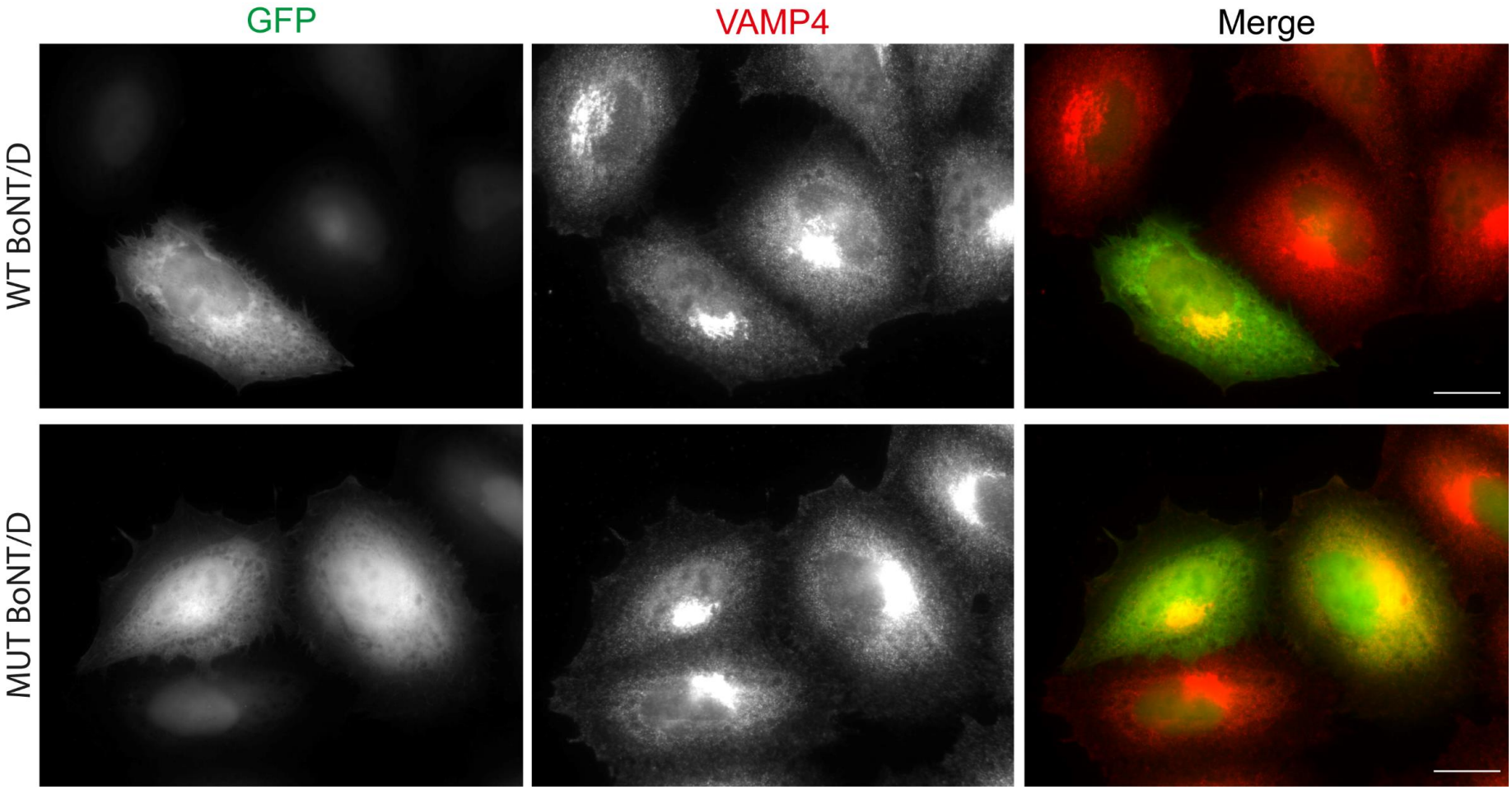
GFP
VAMP4
Merge
WT BoNT/D
MUT BoNT/D

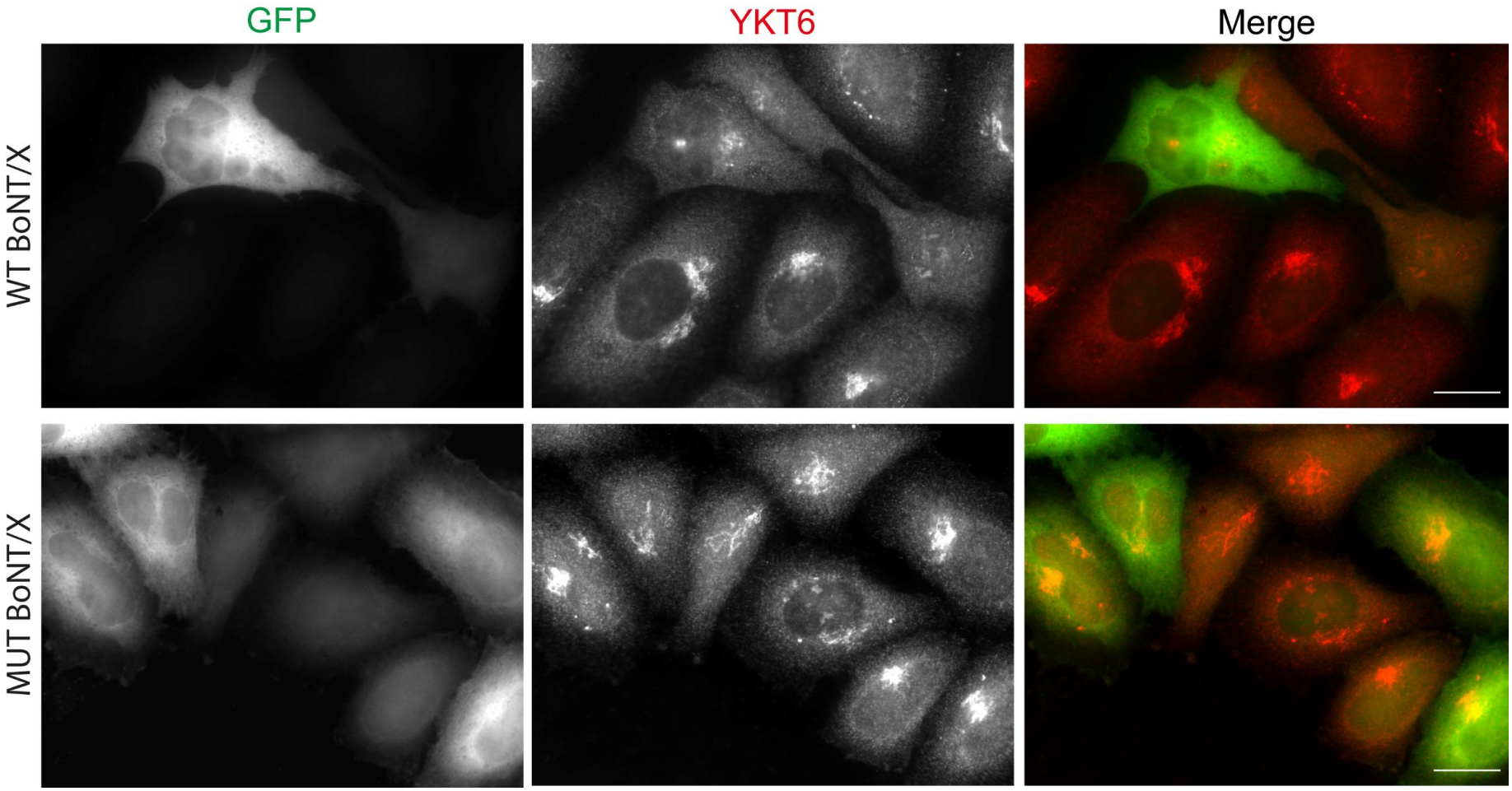
GFP
YKT6
Merge
WT BoNT/X
MUT BoNT/X

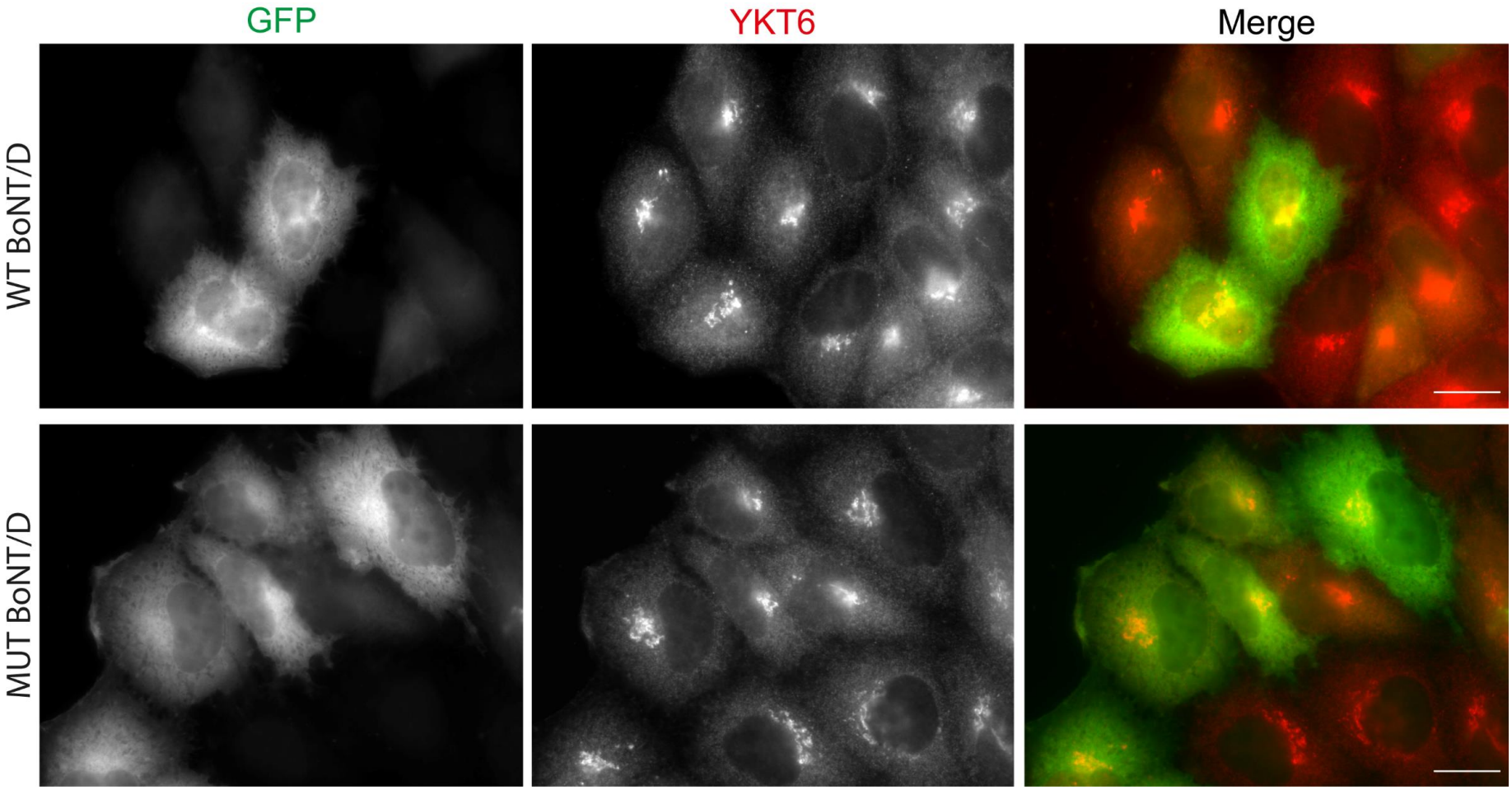
GFP
YKT6
Merge
WT BoNT/D
MUT BoNT/D

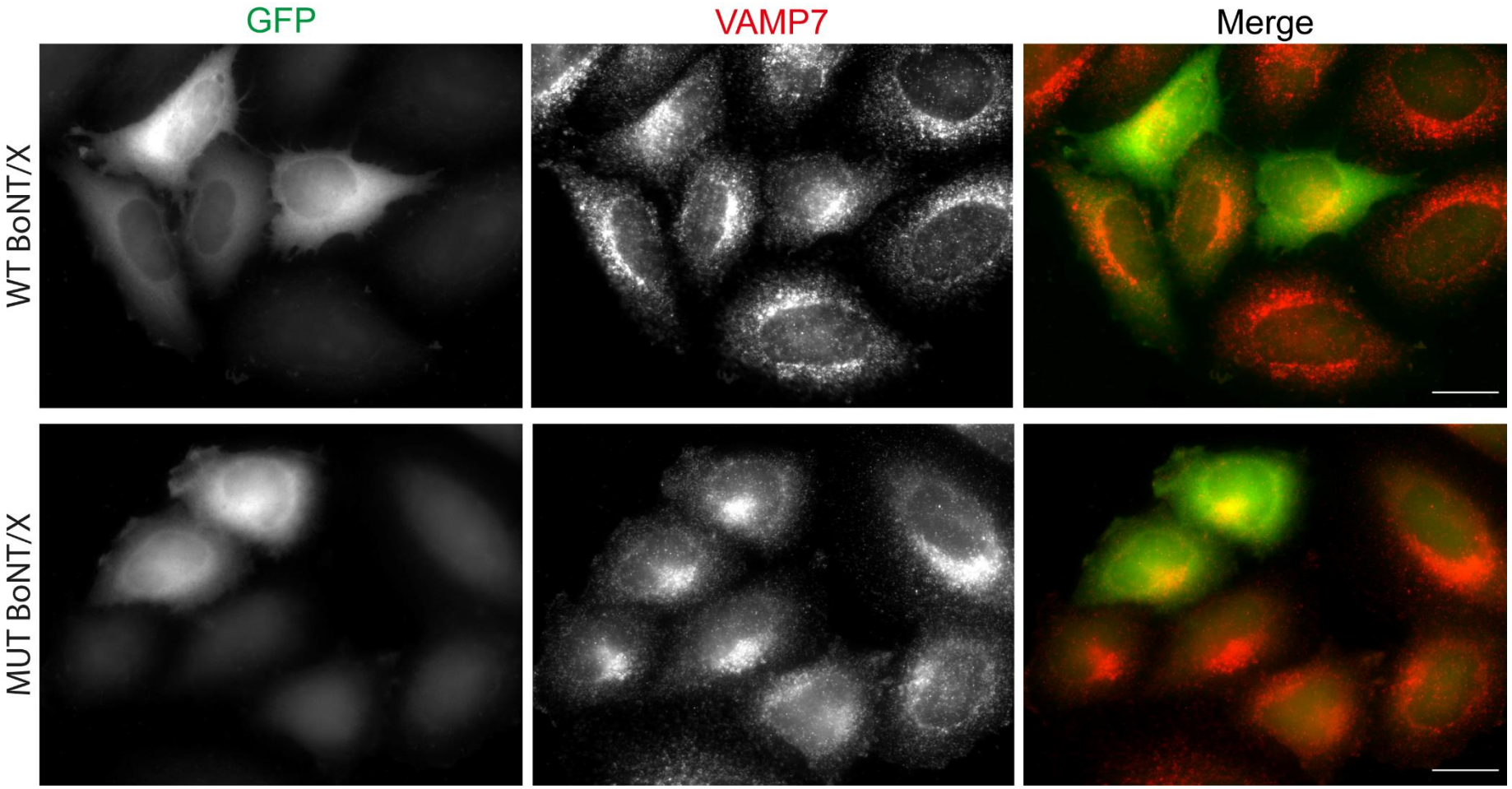
GFP
VAMP7
Merge
WT BoNT/X
MUT BoNT/X

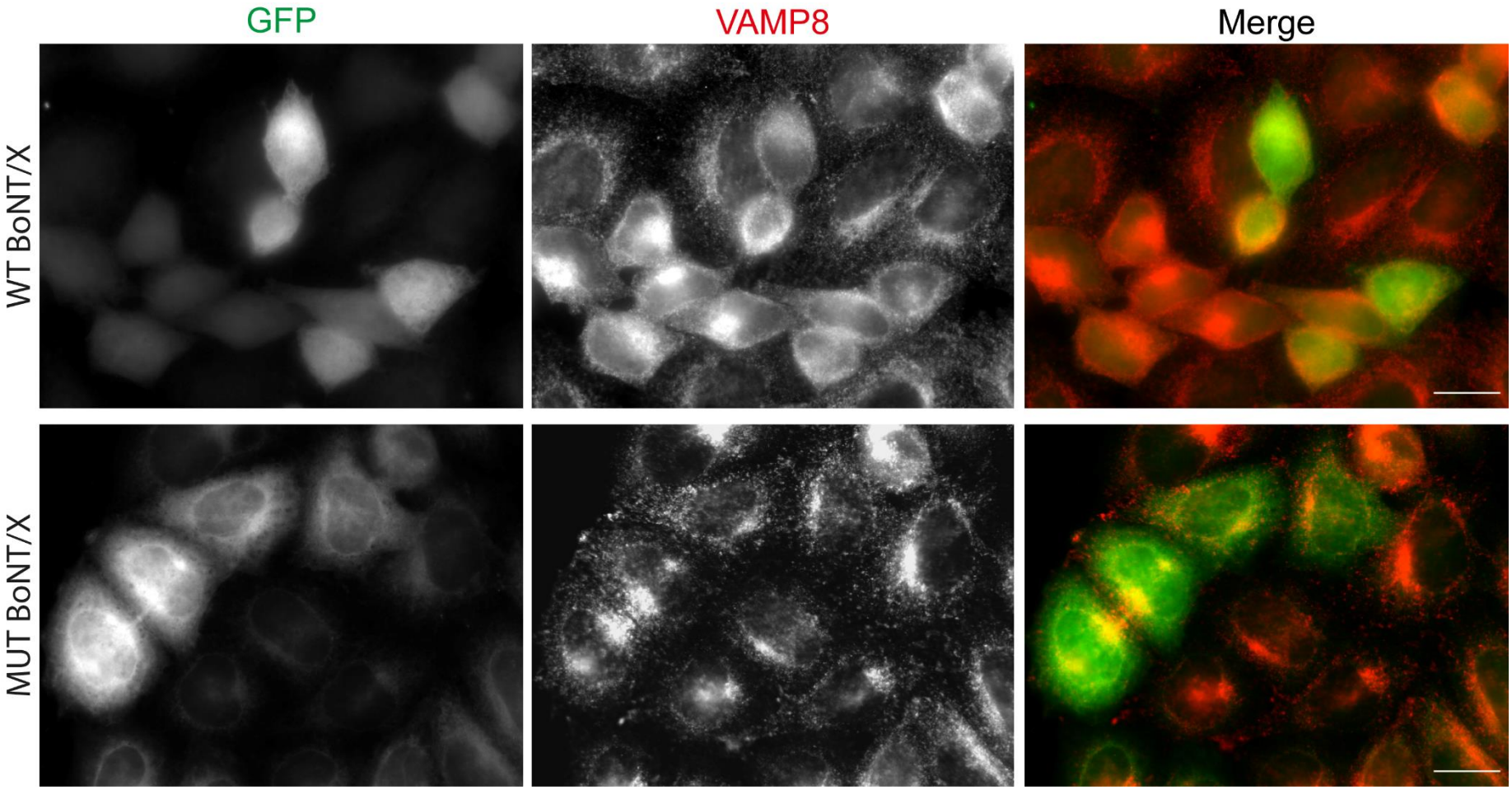
GFP
VAMP8
Merge
WT BoNT/X
MUT BoNT/X

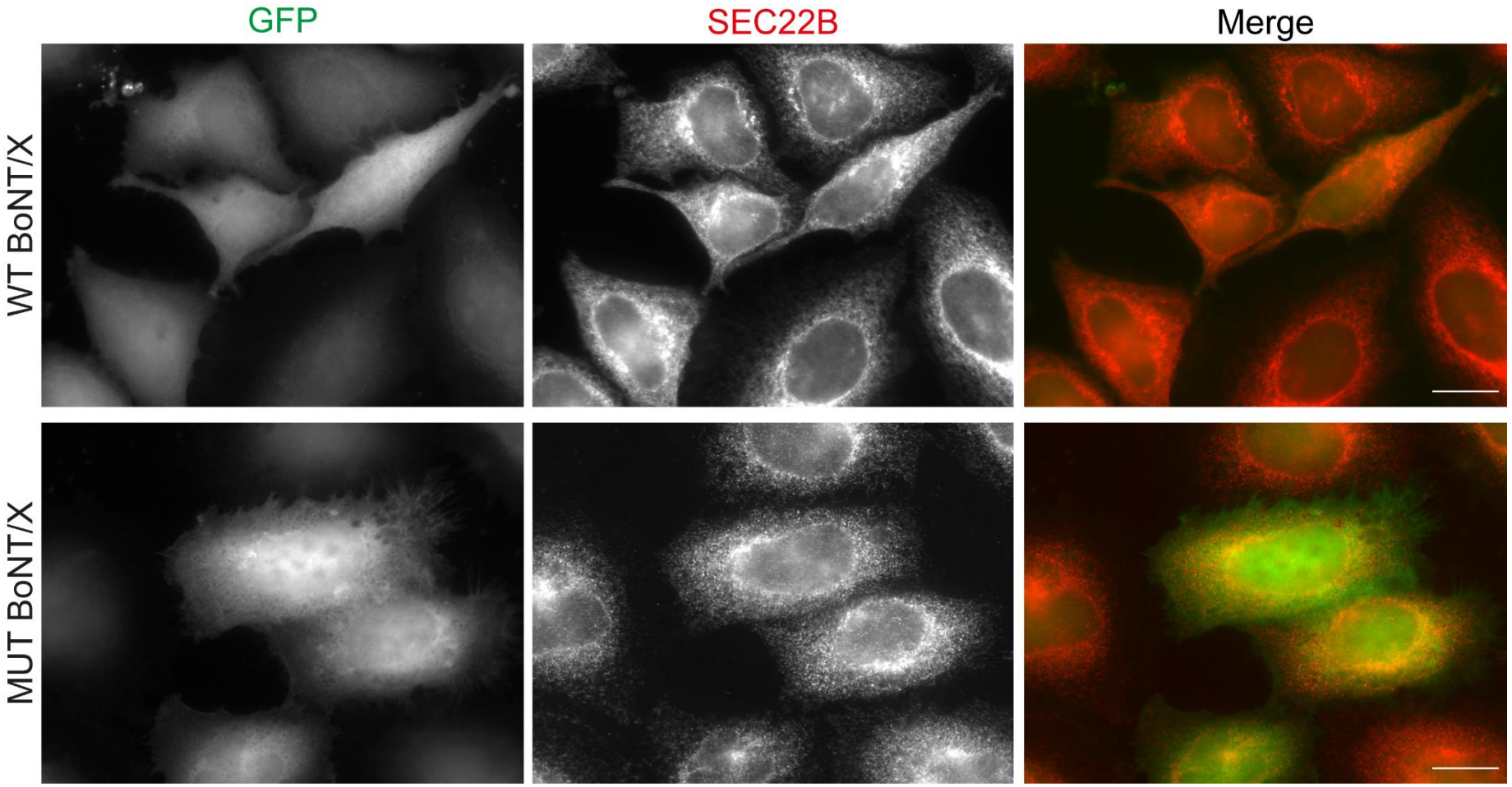
GFP
SEC22B
Merge
WT BoNT/X
MUT BoNT/X

(C)

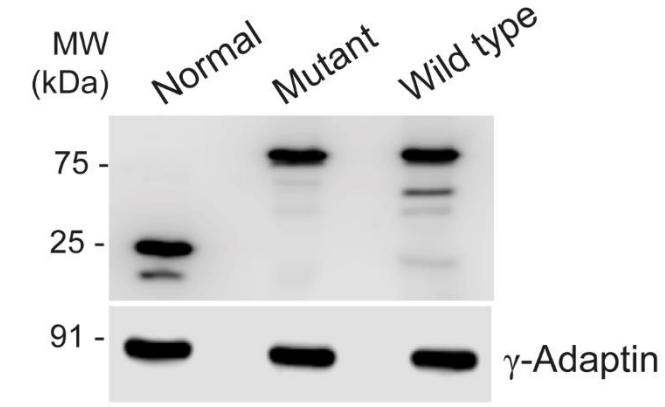
MW
(kDa)
Normal
Mutant
Wild type
75 -
25 -
91 -
γ-Adaptin

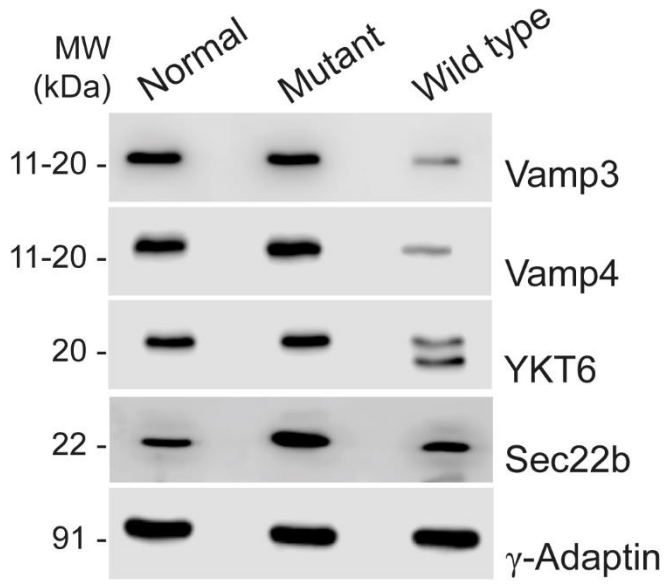
MW
(kDa)
Normal
Mutant
Wild type
11-20 -
Vamp3
11-20 -
Vamp4
20 -
YKT6
22 -
Sec22b
91 -
γ-Adaptin

Figure 3.2 BoNT/X intoxication dramatically alters the morphology of multiple organelles.

To determine the effect of BoNT/X intoxication on intracellular trafficking, HeLa-M cells were grown on coverslips and transiently transfected with recombinant WT BoNT/X or MUT BoNT/X. The cells were then fixed and stained with the indicated compartment-specific markers and imaged using fluorescence microscopy. Scale bar 20 µm. Microscopy images for WT- and MUT BoNT/D transfected cells are presented as supplemental figures.

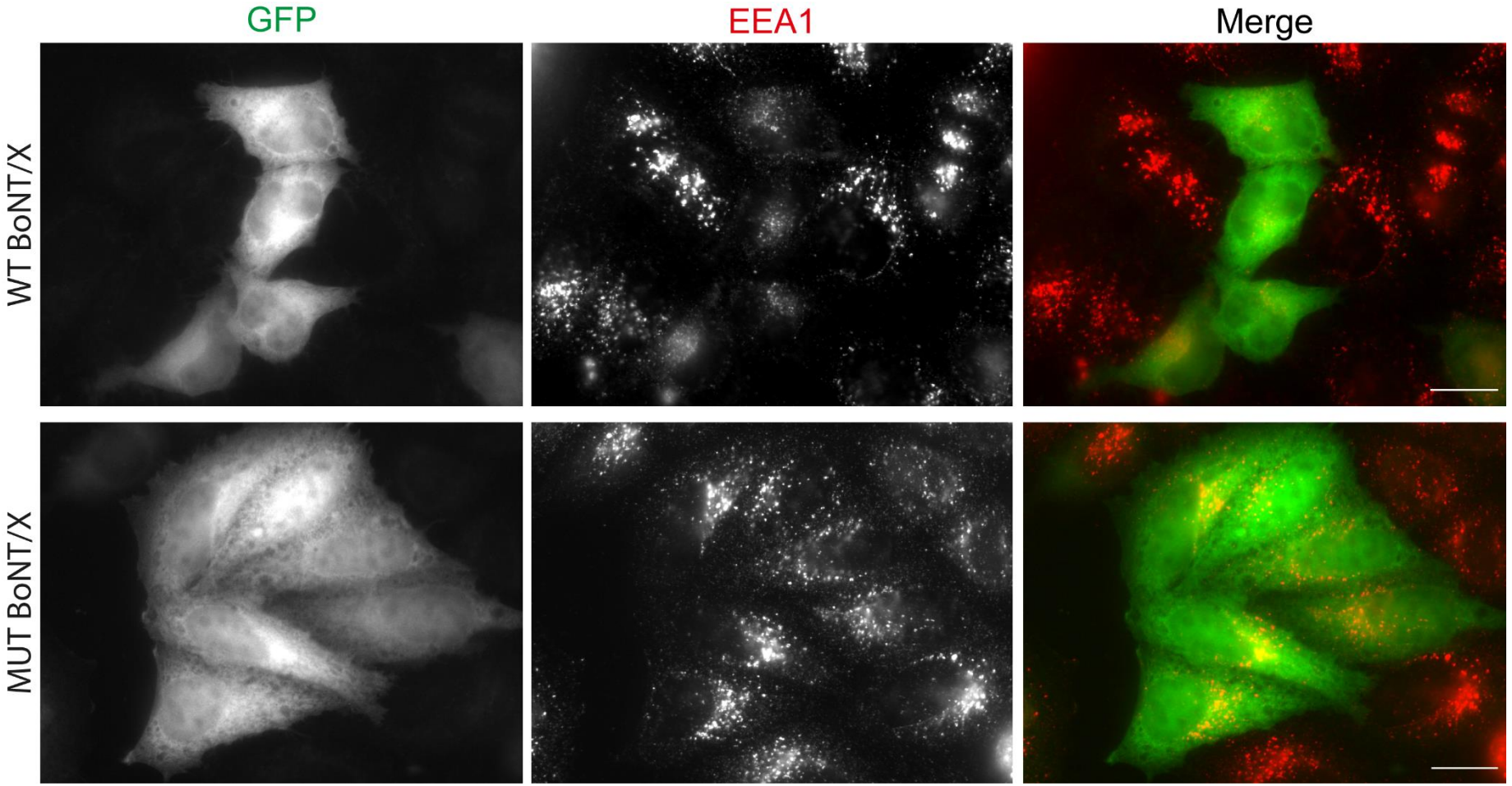
GFP
EEA1
Merge
WT BoNT/X
MUT BoNT/X

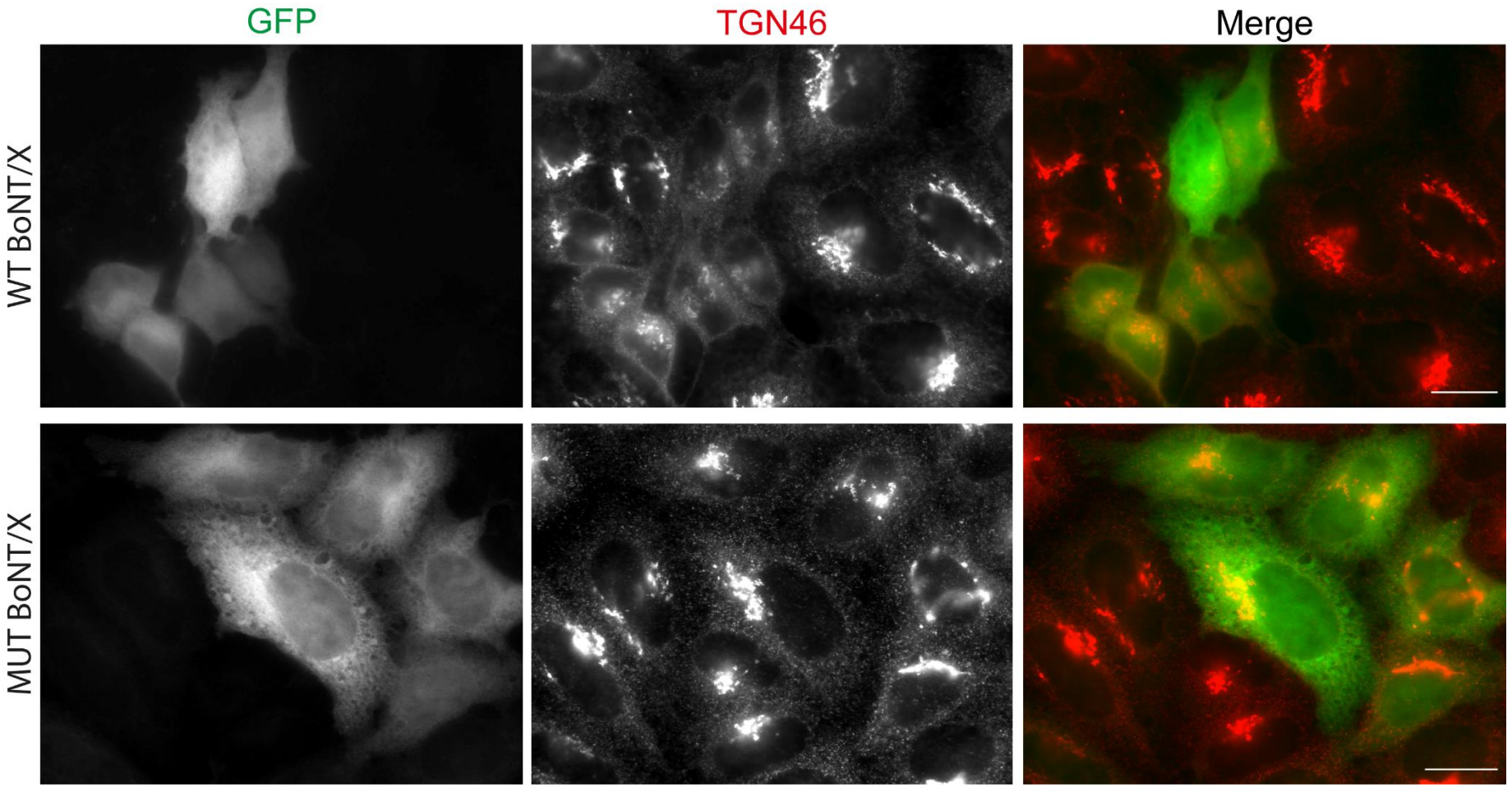
GFP
TGN46
Merge
WT BoNT/X
MUT BoNT/X

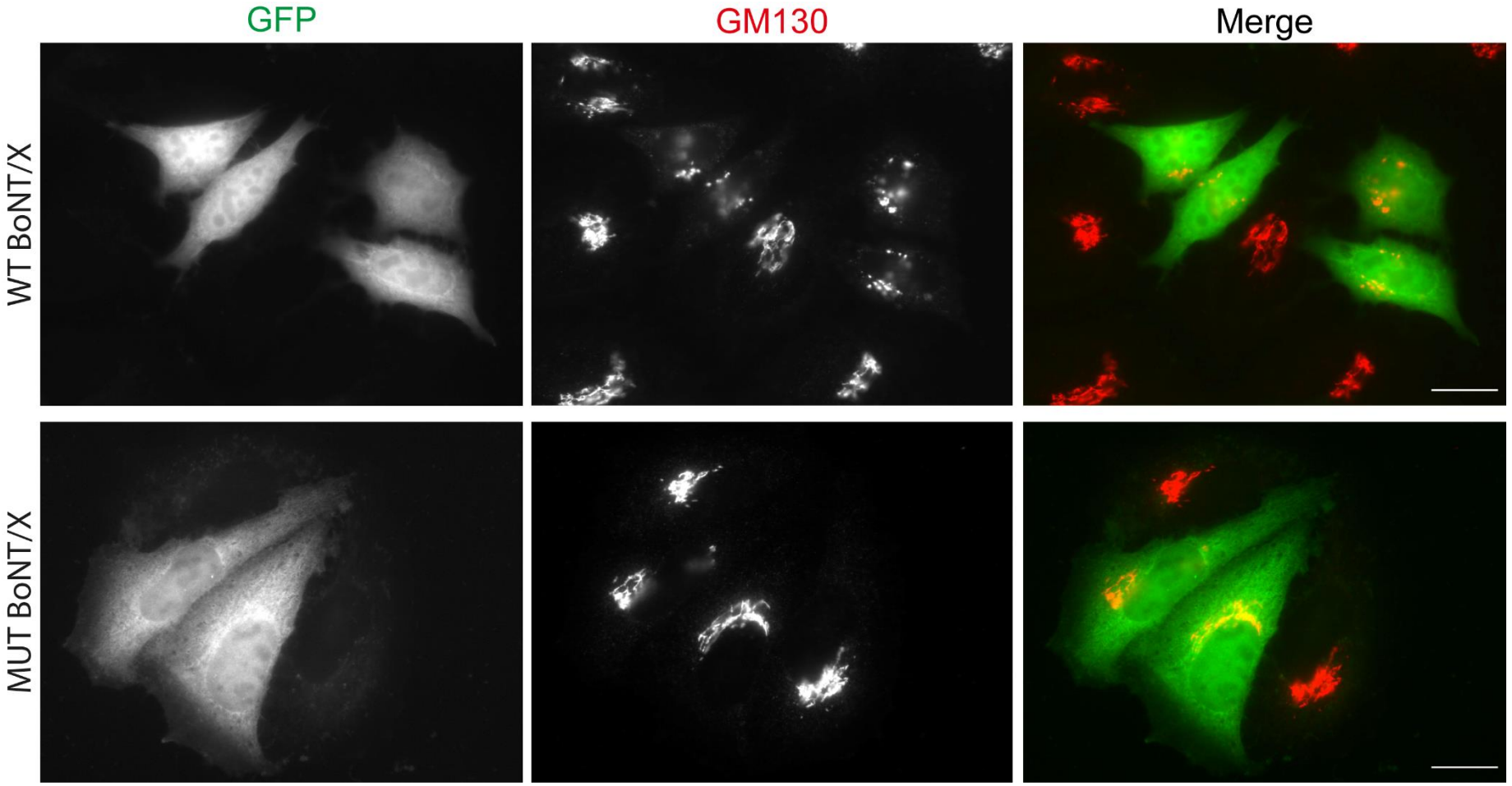
GFP
GM130
Merge
WT BoNT/X
MUT BoNT/X

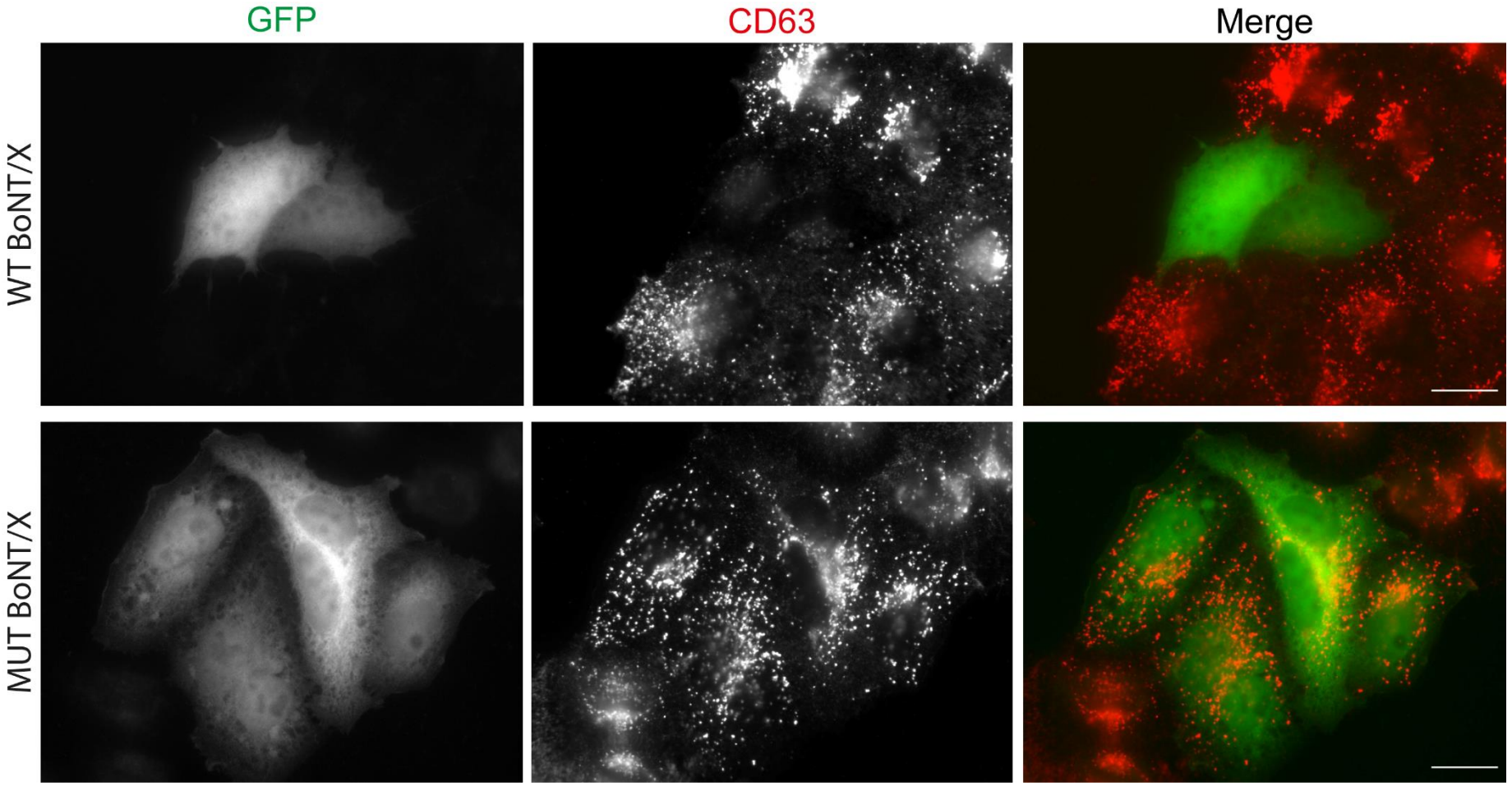
GFP
CD63
Merge
WT BoNT/X
MUT BoNT/X

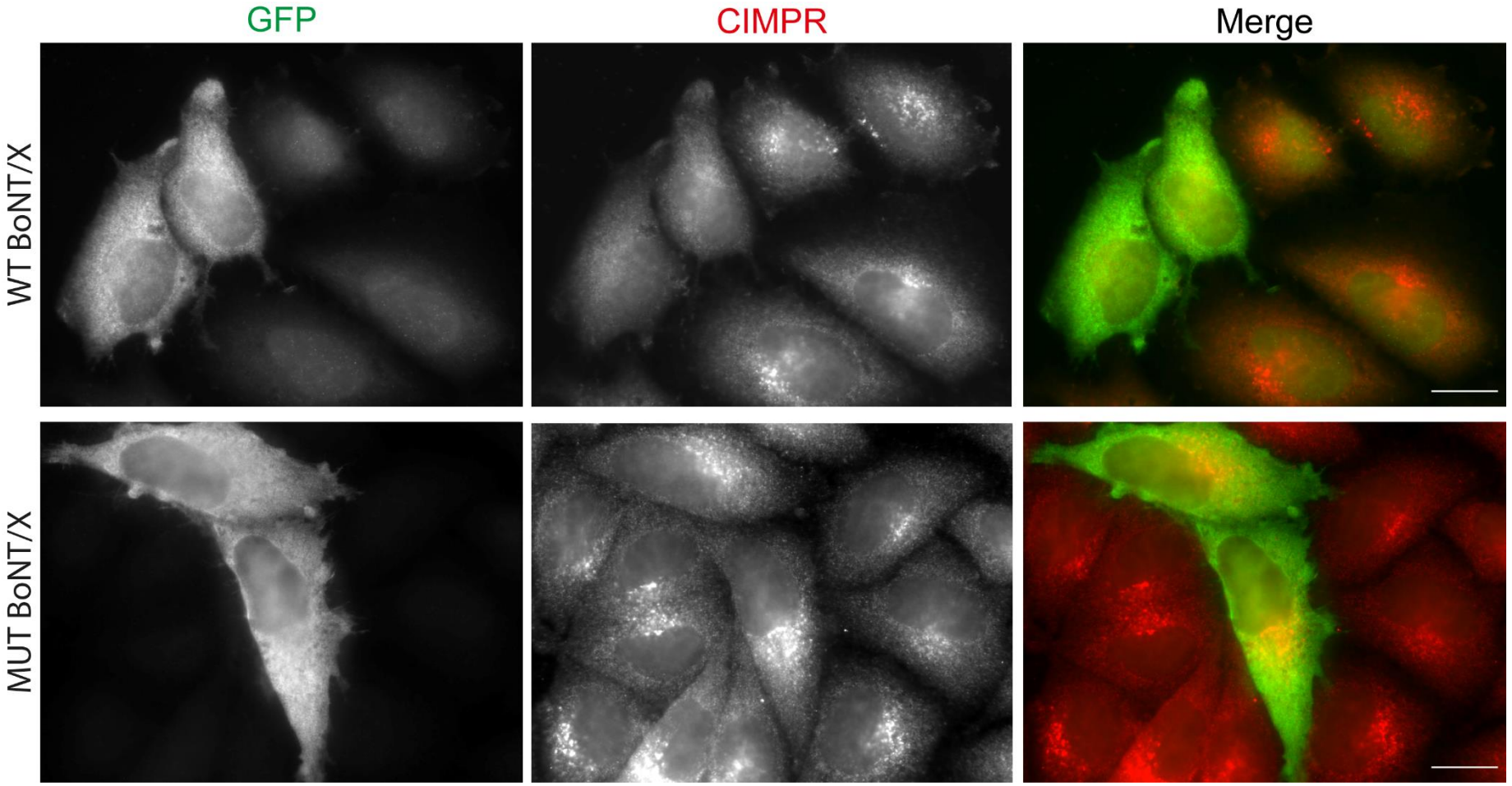
GFP
CIMPR
Merge
WT BoNT/X
MUT BoNT/X

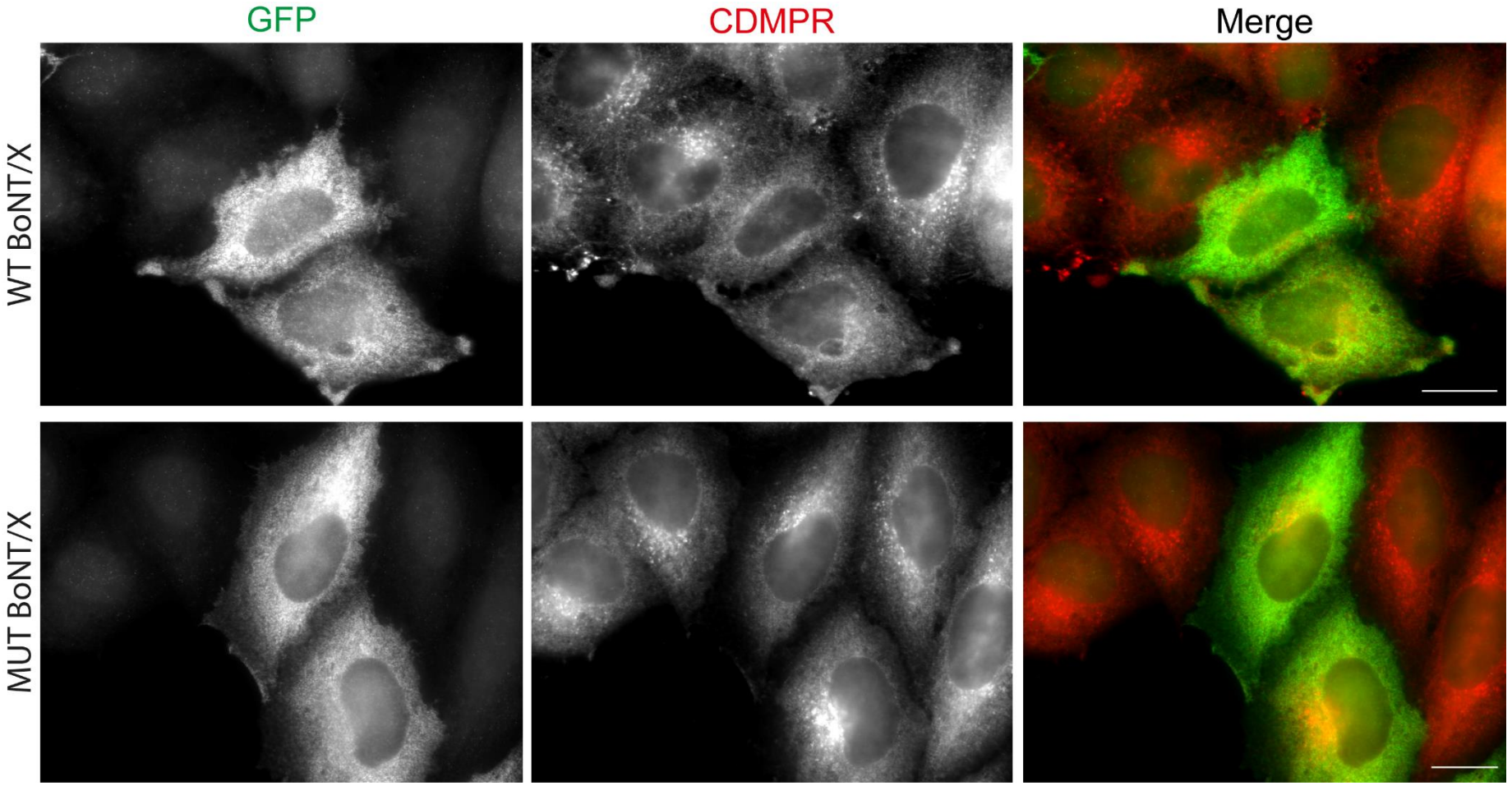
GFP
CDMPR
Merge
WT BoNT/X
MUT BoNT/X

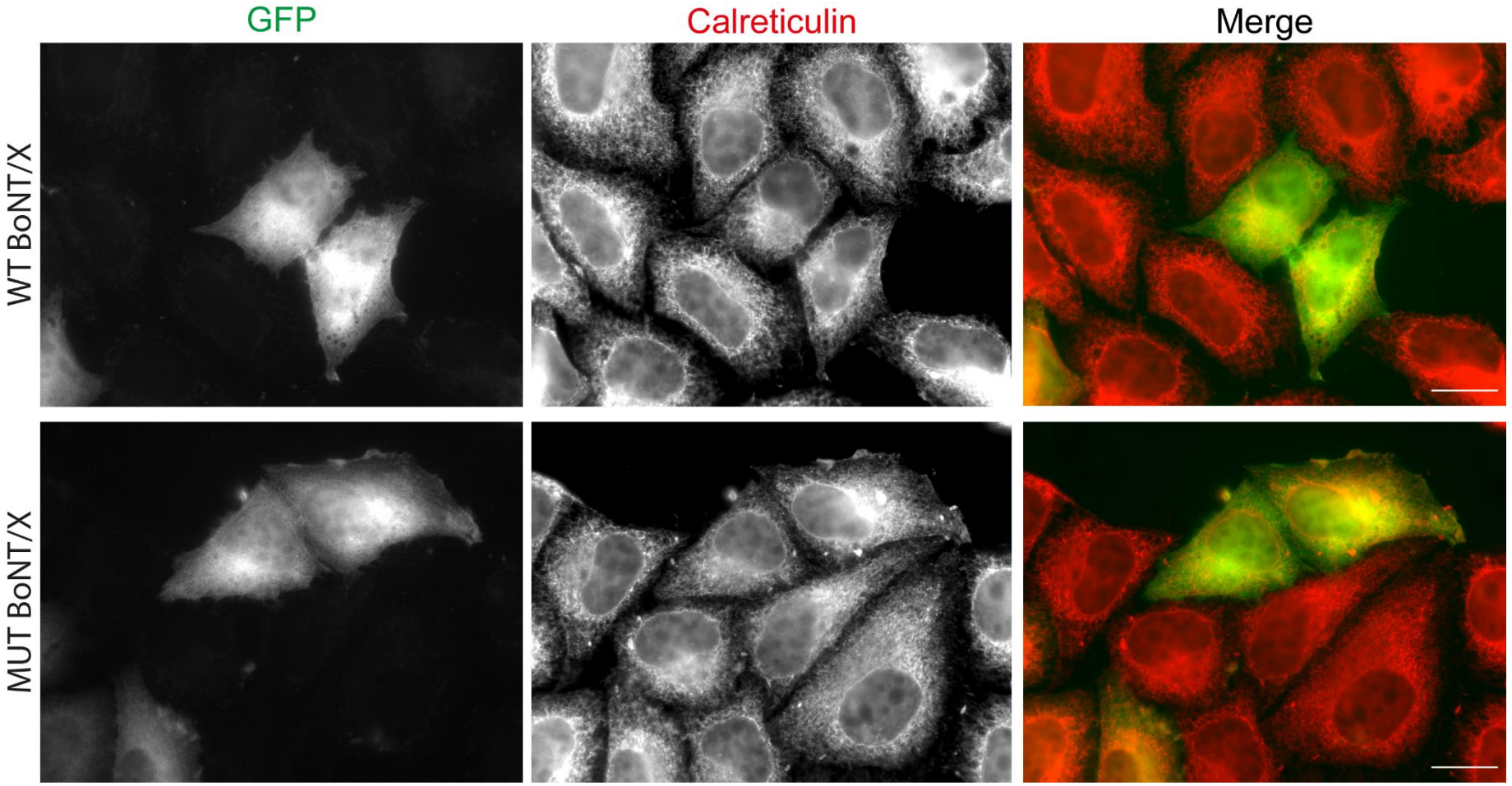
GFP
Calreticulin
Merge
WT BoNT/X
MUT BoNT/X

Figure 3.3 BoNT/X reduces the proliferation rate of transfected cells without drastically reducing cell viability.

(A) The cell number and viability of cells transfected with WT BoNT/X, MUT BoNT/X, or GFP was measured 24 hours' post-transfection by trypan blue (n= 5) or TO-PRO®-3 using flow cytometry (n=4). Error bars represent SEM. ***P*≤0.01; ns, not significant

(B) HeLa-M cells were cultured on coverslips and transiently transfected with recombinant WT BoNT/X, MUT BoNT/X, or GFP vector. 24 hours post-transfection they were fixed with 4% PFA and stained for the apoptotic marker, Caspase 3. Scale 20 µm.

(A)

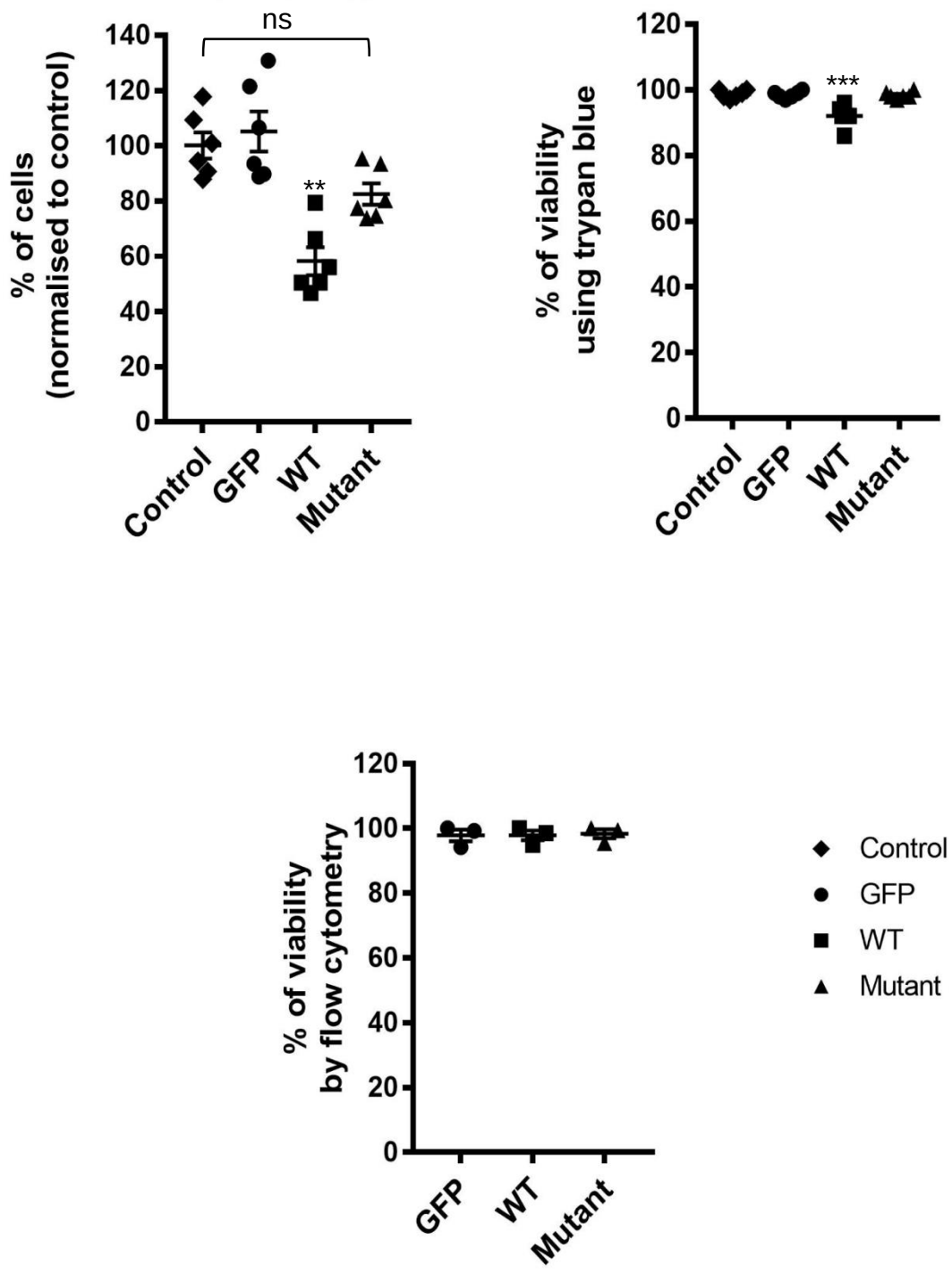
ns
**
***
% of cells
(normalised to control)
% of viability
using trypan blue
% of viability
by flow cytometry
Control
GFP
WT
Mutant
0
20
40
60
80
100
120
140

(B)

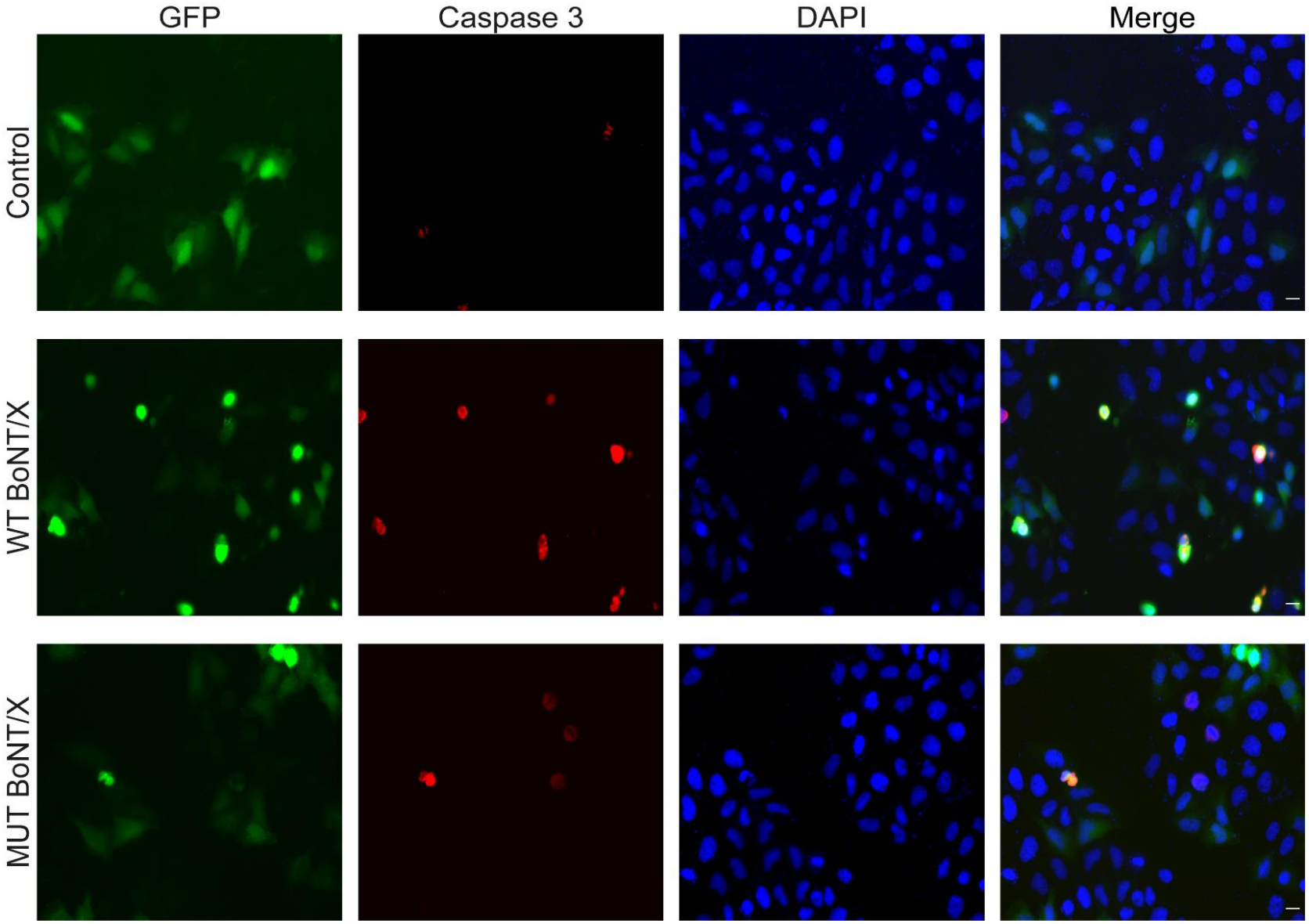

Chapter 4: BoNT/X perturbs endocytic trafficking

4.1 Introduction

In the previous chapter, I have shown that endogenous VAMPs 3, 4, and Ykt6 are cleaved by the light chain of BoNT/X. The loss of these SNAREs led to a dramatic alteration in the localisation, morphology, and staining intensity of markers of the endocytic and biosynthetic pathways. VAMP3 resides on recycling endosomes and has been implicated in the trafficking of the transferrin receptor (TF-R) (McMahon et al., 1993, Galli et al., 1994, and and Scheller, 2000) and VAMP4 has been implicated in endosome fusion (Advani et al., 1998, Mallard et al., 2002). Ykt6 has also been implicated in endocytic trafficking and is thought to have a role in the late endosome and lysosome fusion (Søgaard et al., 1994) (McNew et al., 1997) (Hasegawa et al., 2003). Thus, it is likely that endocytic trafficking has been perturbed in the intoxicated cells. Therefore, I have set out to quantitatively measure endocytic trafficking in cells expressing BoNT/X.

4.2 Chapter aims

The aim of this chapter was to determine if BoNT/X intoxication alters endocytic trafficking. Based on the observation that VAMP3 and VAMP4 are cleaved by the toxin I would predict that endocytic trafficking would be perturbed. In addition, the alteration in EEA1 staining also supports this hypothesis.

To address this, I have:

1) measured TF endocytosis.
2) measured total and surface levels of TF-R in BoNT/X intoxicated cells.
3) measured total and surface levels of a panel of late endosome and lysosomal markers in BoNT/X intoxicated cells.
4) measured the global surface levels and endocytic rates of glycosylated proteins in BoNT/X intoxicated cells.

4.3 Results

4.3.1 Transferrin receptor (TF-R) trafficking is severely perturbed in BoNT/X intoxicated cells

Transferrin is an iron-binding protein that binds the transferrin receptor (TF-R) and is taken up into cells by clathrin-mediated endocytosis. It has become an effective model for measuring clathrin-mediated endocytosis and endocytic recycling (Simons and Toomre, 2000, Hopkins, 1983) (Mayle et al., 2012, Calzolari et al., 2010, Pearse and Robinson, 1990). To determine if BoNT/X is inhibiting TF-R trafficking, I transfected cells with the indicated constructs and incubated the cells with transferrin conjugated to Alexa594 for 10 minutes at 37C° (Figure 4.1A). In the cells transfected with the active toxin, I observed that there was virtually no transferrin taken up into the cells. In cells expressing MUT BoNT/X, the uptake of transferrin was unaffected and numerous endosomal structures were apparent in the cells. In addition, I also tested WT and MUT BoNT/D as a control to evaluate the effect of cleavage of VAMP3 on transferrin internalization. Neither constructs impacted transferrin internalisation even though VAMP3 was being cleaved (Figure 3.1C). To quantify transferrin uptake in the transfected cells I repeated the experiments in suspension and analysed them by flow cytometry. In support of my previous observations, there was a significant reduction in transferrin uptake in cells expressing WT BoNT/X (Figure 4.1B).

One possible interpretation of this data is the transferrin receptor is absent from the cell surface so cannot bind transferrin. To determine if this is the case I used flow cytometry to measure its levels in cells transfected with GFP, WT, and MUT BoNT/X constructs. The cells were stained with fluorochrome-conjugated anti-TF-R antibody and incubated at 4℃ to halt endocytosis. As predicted, the level of the receptor on the surface was markedly reduced (20% of the signal compared to the GFP control and inactive BoNT/X). In addition, I also used flow cytometry to measure the total levels of the TF-R in cells expressing BoNT/ X constructs. In these experiments, I fixed and permeabilised the cells before performing the staining. The levels of the TF-R were also significantly reduced in BoNT/X intoxicated cells (40% of the GFP control) (Figure 4.1C). Taken together, these results suggest that not only is there a failure in TF-R

recycling but also a potential re-routing of the receptor to lysosomes where it is degraded.

To validate the flow cytometry experiments I also determined the steady-state subcellular localization of the TF-R in BoNT/X intoxicated cells (Figure 4.1B). HeLa-M cells were transiently transfected with WT and MUT BoNT/X constructs. In BoNT/X intoxicated cells, the TF-R was localized in small vesicles which were distributed throughout the cytoplasm. In the control cells, the vesicles were larger and showed a greater concentration in the perinuclear region.

4.3.2 Evaluation of global endocytosis in WT BoNT/X transfected cells using lectins

As BoNT/X intoxication causes a dramatic alteration in TF-R trafficking I decided to determine if this was a more general phenotype. Thus, I decided to measure global endocytosis by analysing the internalization of wheat germ agglutinin (WGA) a lectin that binds glycosylated proteins. WGA binds proteins that have N-acetyl-D-glucosamine (D-GlcNAc)-linked residues and N-acetylneuraminic acid (sialic acid) (Figure 4.2A). This modification is very abundant on proteins found at the cell surface and endosomes so can be used as a generic tool to follow their trafficking.

We first validated this approach using fluorescence microscopy. HeLa-M cells were grown on coverslips and transfected with GFP, WT, and MUT BoNT/X constructs. The following day, the cells were incubated with WGA-Alexa350 for 15 minutes at 4°C or 15 minutes at 37°C. The cells were then fixed and imaged using immunofluorescence microscopy. As expected, the WGA strongly labelled the cell surface at 4°C (Figure 4.2B) and was endocytosed at 37°C (Figure 4.2C) as defined by the presence of punctate/vesicular structures that are most likely endosomes. However, the intracellular staining was difficult to observe so I developed a stripping protocol where excess D-GlcNAc was used to remove surface-bound WGA (Figure 4.2D). My pilot experiments suggested that BoNT/X intoxication might be reducing the endocytosis of cell surface proteins. To quantify the phenotype, I repeated the experiments and used flow cytometry to measure the surface levels and amount of endocytosis. WGA binding was reduced by approximately 50% in BoNT/X intoxicated cells and only a third of the WGA was endocytosed compared to GFP and MUT BoNT/X transfected cells. All flow

cytometry analysis was performed after signal intensity was normalised to GFP-only control cells. Taken together, my results suggest that there is a global change in the levels of glycosylated proteins at the cell surface and that endocytosis is also altered in the intoxicated cells (Figure 4.2E).

4.3.3 The endocytic trafficking of many proteins is perturbed in BoNT/X intoxicated cells.

My WGA experiments suggest that there was a global change in endocytic trafficking in intoxicated cells. To validate this observation, I have examined the steady-state distribution of the selection of proteins that traffic over the cell surface (CD63, CD-MPR, CI-MPR, TGN46, and EGF-R). These proteins traffic via a range of different intracellular pathways and are endocytosed by clathrin and non-clathrin-mediated endocytosis (Sorkin and Goh, 2008, Dahms et al., 2008) so should provide good coverage of the post-Golgi pathways which may be impacted by the toxin.

4.3.3.1 The cell surface and total levels of CD63 are reduced by BoNT/X intoxication

To determine if the trafficking of late endosomal/lysosomal proteins are perturbed in BoNT/X treated cells I decided to examine the localisation and trafficking of CD63. CD63 is a late endosomal/lysosomal protein that traffics over the cell surface. It is enriched in lipid microdomains at the cell surface and is internalized by clathrin and caveolae-mediated endocytosis (Kiss and Botos, 2009). I performed uptake experiments using an anti-CD63 antibody that would bind CD63 at the cell surface and be internalized. The surface levels of CD63 are less than the TF-R so a longer uptake was performed (30 minutes at 37°C) (Figure 4.3A). Almost no anti-CD63 antibody was taken up in the intoxicated cells. In contrast, cells transfected with MUT BoNT/X showed abundant signal in endosomes. This observation suggests that CD63 is most likely absent from the cell surface in intoxicated cells. In order to verify these findings, I sought to determine the surface and total levels of CD63 by flow cytometry. Cells were stained for surface CD63 at 4°C to prevent internalization, washed and the appropriate secondary antibody was used (Figure 4.3B). The geometric mean was calculated for each sample and normalised to the GFP control. The surface levels of

CD63 were remarkably reduced in the intoxicated cells, which supported our anti-CD63 antibody uptake assay.

As observed in Chapter 3, the levels of steady-state TF-R in BoNT/X transfected cells were reduced. Thus, I decided to measure the total levels of CD63 in cells intoxicated with BoNT/X. After normalizing the GFP-signal of each transfected condition to GFP-only control, I could see that the levels of CD63 were reduced by more than half compared to MUT BoNT/X and GFP-only transfected cells. When taken all experiments into account, it was clear that the endocytic trafficking of CD63 is severely perturbed and its levels are reduced suggesting that the trafficking of lysosomal proteins may be perturbed by the toxin.

4.3.3.2 The surface levels of the Mannose 6-Phosphate receptor are reduced in intoxicated cells

To assess if BoNT/X perturbs the trafficking between the TGN, endosomes, and lysosomes I decided to examine the localisation and trafficking of the Mannose 6-phosphate receptor (MPR), CI-MPR, and CD-MPR. Both receptors mediate the transport of newly synthesized lysosomal enzymes from the TGN to a pre-lysosomal compartment in the endocytic route and prevent its transport to the surface. This is an important step as it prevents the delivery of protein-degrading enzymes to the extracellular environment. The MPR recycles constitutively between the TGN, endosomal compartment, and cell surface. At the plasma membrane, the CI-MPR binds and facilitates the internalization of extracellular ligands that prevent mislocalisation of the enzymes. I found that anti-CI-MPR and anti-CD-MPR antibody uptake was reduced in intoxicated cells suggesting that their levels at the cell surface might be reduced (Figure 4.3C). To directly measure the cell surface levels of CI-MPR I incubated the transfected cells with an anti-CI-MPR antibody on ice and then analysed the amount of antibody binding using flow cytometry (Figure 4.3D). The levels of the CI-MPR on the cell's surface were markedly reduced and the total levels of CI-MPR were also perturbed. To confirm this observation, I also performed steady-state localization of CI-MPR and CD-MPR by microscopy. I found that both proteins were markedly reduced in cells transfected with the WT BoNT/X, compared to the control cells (Figure 3.3). These findings suggest that trafficking between the TGN and late endosomes is

perturbed in cells intoxicated with BoNT/X. In addition, they may also help explain why the levels of CD63 in late endosomes and lysosomes are reduced in intoxicated cells.

4.3.3.3 The levels of TGN46 at the cell surface are reduced

To determine if the trafficking between the TGN, endosomes, and the cell surface was perturbed in intoxicated cells, I investigated the internalization of TGN46 by performing an antibody uptake assay. HeLa cells were grown on coverslips and transfected with the wild type and the mutant BoNT/X. The cells were then incubated with TGN46 antibody at 37°C for 20 minutes to allow for uptake. At the end of the incubation period, cells were washed, fixed, permeabilised, and appropriate secondary labelling antibody Alexa594 was added before imaged by fluorescence microscopy (Figure 4.3E). Inactive BoNT/X showed intracellular puncta staining within the cytoplasm and perinuclear compartments. However, there was virtually no TGN46 antibody uptake detected in cells transfected with the active BoNT/X suggesting that TGN46 was absent from the plasma membrane. To further verify the results, I next determined the steady-state subcellular localization of TGN46 in cells transfected with the wild type and mutant BoNT/X (Figure 3.3). Cells transfected with the wild type BoNT/X had reduced levels of the protein. These experiments suggest that BonT/X intoxication may be inhibiting the delivery of the TGN46 to the cell surface either via blocking its endocytic recycling or transport from the TGN.

4.3.4 The surface levels of the Epidermal Growth Factor Receptor are reduced but total levels are not dramatically altered

The majority of the cargo proteins examined so far are rapidly removed from the cell surface under normal conditions. Thus, I wanted to examine the localisation and trafficking of a protein that spends more of its time at the cell surface. The epidermal growth factor receptor (EGF-R) regulates several key events in cell growth, differentiation, survival, and migration (Wieduwilt and Moasser, 2008). EGFR is internalized mainly by clathrin-mediated endocytosis but can also be endocytosed by non-clathrin-mediated endocytosis (Sorkin & Goh, 2009). Recycling of the EGF-R can

occur via two distinct pathways, a rapid pathway through early endosomes and a slower pathway which begins mostly occurs from multivesicular bodies.

To investigate the internalization of the EGF-R an antibody uptake assay was performed. HeLa cells were grown on coverslips and transfected with the wild type and the mutant BoNT/X. The cells were then incubated with the anti-EGF-R antibody at 37°C for 20 minutes to allow for uptake. At the end of the incubation period, cells were washed, fixed, permeabilised, and labelled with secondary antibody conjugated to Alexa594 was (Figure 4.3F). Strong cell surface labelling was observed in the cells transfected with the inactive construct and in addition, some punctate structures were visible suggesting that the antibody may have been endocytosed. However, in the cells expressing the active toxin, the surface levels of antibody staining seemed reduced. To validate this observation, I used flow cytometry to measure the surface levels of the EGF-R (Figure 4.3G). In support of my previous results, I see a significant reduction in the cell surface levels of the receptor in the intoxicated cells. However, the total levels of the receptor are unaltered in contrast to what we see for most of the other proteins examined. As a control, I also repeated some of these experiments using WT and MUT BoNT/D (Supplemental Figure 1).

4.4 Discussion

4.4.1 Summary of results

In summary, I have shown that in BoNT/X intoxicated cells there is a dramatic alteration in the trafficking of endosomal proteins. For example, there is no transferrin uptake and the cell surface level of the receptor are drastically reduced. I also observed that the overall surface levels of glycosylated proteins are significantly reduced in intoxicated cells. Finally, I also observed a significant reduction in the cell surface levels of several specific receptors (CD63, MPR, and TGN46) and a reduction in their levels.

4.4.2 Why does BoNT/X intoxication cause a global reduction in cell surface proteins?

Taken together, my results indicate that there is a dramatic reduction in the surface levels of many proteins in BoNT/X intoxicated cells. For example, the TF-R is reduced ten-fold and WGA binding is reduced two-fold. For the majority of proteins, their surface levels are tightly regulated by the interplay of many processes including biosynthetic transport, endocytic uptake, recycling, and degradation. Disruption of any of these processes can cause a dramatic change in surface levels (Piga et al., 1990) (Takahashi et al., 2012) (Shi and Grant, 2013). At present, it is unclear which of these processes are most dramatically affected by BoNT/X intoxication. As VAMPs 3, 4 and Ykt6 are being simultaneously cleaved by the toxin it is likely that multiple pathways are being perturbed simultaneously. To explore this further, I have determined whether BoNT/X intoxication blocks the delivery of newly synthesized proteins to the cell surface (see Chapter 5).

It is also worth noting that the total levels of several other proteins (CD63, MPR, TGN46, and EGF-R) are being significantly reduced by the toxin. One interpretation of this observation is the recycling of these receptors is being perturbed and they are being directed for degradation in lysosomes (Peden et al., 2004). To directly test this hypothesis, intoxicated cells could be treated with protease inhibitors or drugs which inhibit endosomal acidification and lysosomal transport (Huss and Wieczorek, 2009). One would predict that these treatments should help protect the levels of these molecules in intoxicated cells. Surprisingly, the total levels of the EGF-R were not dramatically altered by BoNT/X intoxication even though the surface levels of the receptor were significantly reduced. At present, it is unclear why this may be the case. It is possible that the receptor is becoming internalised and trapped in a compartment that cannot fuse with lysosomes and/or the EGF-R is more resistant to proteolytic destruction. As mentioned in previous chapters, it would be very informative to perform rescue experiments with toxin-resistant SNARE molecules. This would allow these phenotypes to be directly assigned to the loss of a specific SNARE.

4.4.3 Why is the TF-R so dramatically affected by BoNT/X intoxication?

One of the most striking observations in this chapter is the almost complete loss of TF uptake in intoxicated cells. Further analysis of this defect showed that the TF-R is lost from the cell surface and the total levels of the receptor are significantly reduced. This phenotype is specific to the BoNT/X (cleaves of VAMPs 3, 4, and Ykt6) as BoNT/D (cleaves VAMPs3) does not cause a similar phenotype. At present, it is unclear why the TF-R is so vulnerable to BoNT/X intoxication. However, the receptor rapidly recycles over the cell surface and it is estimated that all of the receptors transit the cell surface every 10-20 minutes (Straley and Green, 2000) (Maxfield and McGraw, 2004). Thus, it is likely that the very dynamic nature of the receptor's trafficking makes it very vulnerable to perturbations in intracellular trafficking. In the longer term, it will be if interest to use techniques such as immuno-electron microscopy to localise the TF-R in the intoxicated cells.

4.4.4 Long term BoNT/X intoxication is likely to be incompatible with cell survival

As discussed earlier there is a dramatic reduction in the levels of cell surface proteins in BoNT/X intoxicated cells. At the time points used in my experiments, the majority of the cells are still viable. However, it is clear that gross cell morphology is becoming altered in some of the intoxicated cells. Based on the dramatic reduction in cell surface proteins we would predict that BoN/T intoxication is incompatible with cell survival. For example, the direct effect of loss of TF-R is the loss of iron uptake. Iron is a vital element for several metabolic pathways and physiological processes (Steere et al., 2012). Other than delivery and transfer of iron, Transferrin itself plays a crucial role in other biological functions in maintaining the health of the cell, such as preventing the formation of reactive oxygen species and acting as a protective scavenger towards free toxic iron (Grant and Donaldson, 2009). It is also very likely that the transport of essential key metabolites, such as amino acids and sugar, that are vital for cellular repair and survival are disrupted. It would be interesting to determine whether amino acid transporters, the solute carriers (SLC) family proteins are affected. It would also be interesting to determine if regulated trafficking through the endosomal system is also affected. One important example of this is the regulation of the mammalian insulin-

dependent sugar transporter, GLUT4 vesicular trafficking is affected in sugar transport on the surface of fat and muscle cells. The integrity of active ion-channels on the plasma membrane is crucial for maintaining equilibrium against changing electrochemical gradients. Therefore, possible disruption of these active transport mechanisms such as the sodium-potassium channel pump for mediating ion homeostasis across the membrane and extracellular environment also needs to be considered.

4.4.5 Could the changes in cell morphology be due to alterations in integrin trafficking?

Based on our microscopy experiments it is apparent the intoxicated cells often appear smaller and less well spread out. One of the main proteins that play a major role in migration, survival, and motility is integrins. Integrins are a family of single-pass type I transmembrane proteins, composed of heterodimers with two glycoprotein subunits α and β, that are expressed in all metazoans (Humphries et al., 2006). These cell-surface-adhesion family of proteins serves as receptors that play a mechanical role as cellular anchors and a biochemical role for transmission of chemical signals spatially and temporally that determine cellular responses such as migration, survival, cellular differentiation, and motility within the cell as well as to its surroundings (Calderwood, 2004). As most cell surface proteins are being down-regulated we could speculate that some of the cell-rounding observed in intoxicated cells could be due to the loss of integrins from the cell surface. Therefore, it would be interesting to measure the surface levels of integrins in intoxicate cells.

Figure 4.1 Transferrin receptor trafficking is severely perturbed in BoNT/X intoxicated cells.

(A) To determine the effect of BoNT/X on receptor-mediated endocytic trafficking, HeLa-M cells were grown on coverslips and transiently transfected with recombinant WT BoNT/X or MUT BoNT/X. As a control, cells were also transfected with WT BoNT/D or MUT BoNT/D constructs. The cells were then incubated with transferrin-AlexaFluor 647 for 10 minutes at 37℃. Scale bar 20 μm. Similar experiments were performed and analysed using flow cytometry (n=4). Error bars represent SEM. ****$P \leq 0.0001$.

To determine the surface levels of transferrin receptors on the cell surface, HeLa-M cells were grown and transfected with recombinant WT or MUT BoNT/X GFP-tagged constructs. Cells were harvested and stained with the anti-TF-R antibody at 4^{o}C in suspension. Cells were then fixed and the levels of transferrin receptor were measured by flow cytometry (n=4). ****$P \leq 0.0001$. Error bars represent SEM. As a control, surface levels of transferrin receptor on HeLa-M cells transfected with WT BoNT/D or MUT BoNT/D constructs were also measured by flow cytometry (n=4). Error bars represent SEM. ns, not significant.

(B) To determine the subcellular distribution of transferrin receptor (TF-R) in cells transfected with the BoNT/X, HeLa-M cells were grown on coverslips and transiently transfected with recombinant WT BoNT/X or MUT BoNT/X. As a control, cells were also transfected with WT BoNT/D or MUT BoNT/D. Scale bar 20 μm.

(C) HeLa-M cells transfected with recombinant WT BoNT/X and MUT BoNT/X were fixed, permeabilised, and stained with an anti-CD71 antibody. An appropriate secondary antibody was used and the total TF-R levels were measured by flow cytometry (n=4). Error bars represent SEM. ***$P \leq 0.001$.

(A)

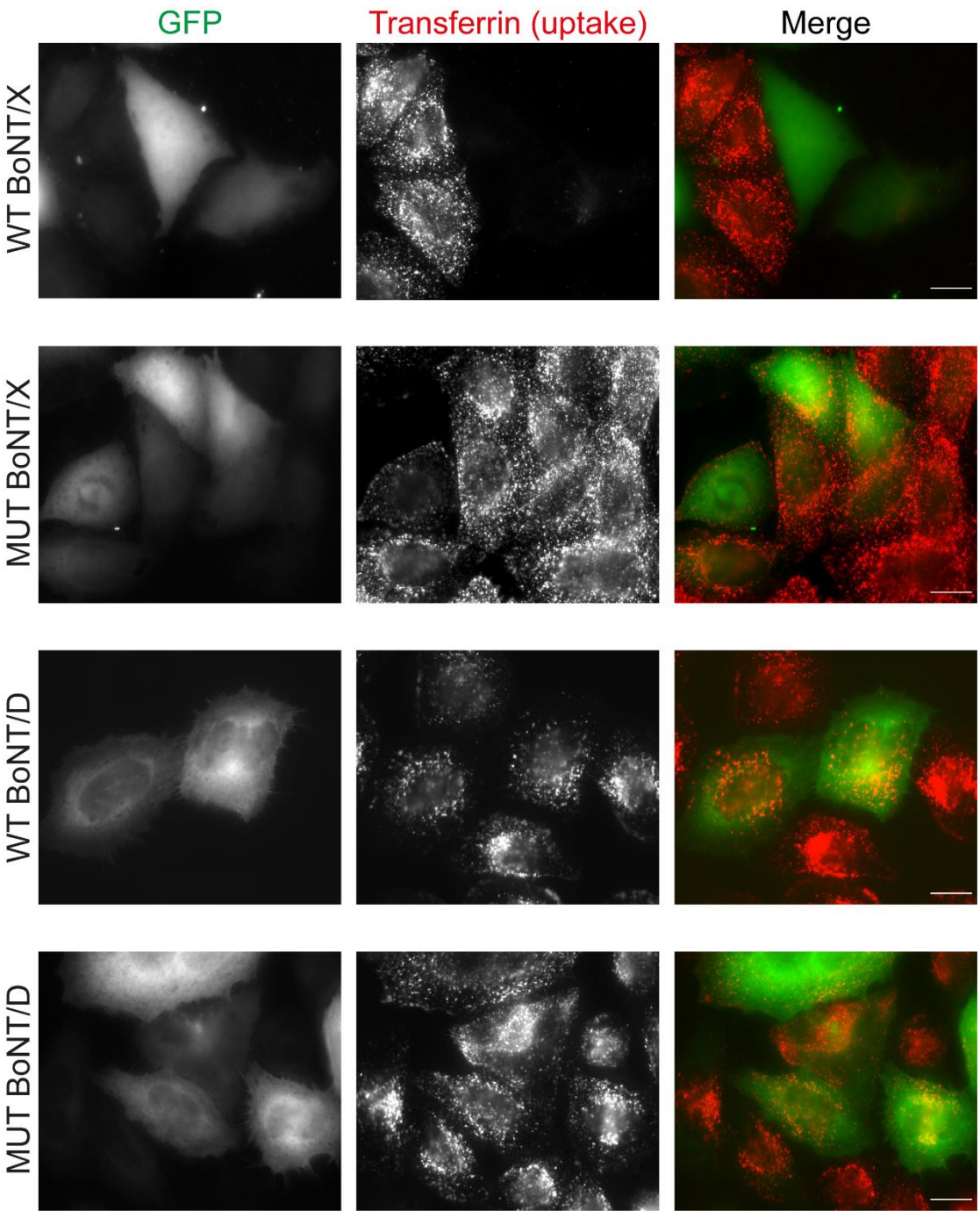
GFP
Transferrin (uptake)
Merge
WT BoNT/X
MUT BoNT/X
WT BoNT/D
MUT BoNT/D

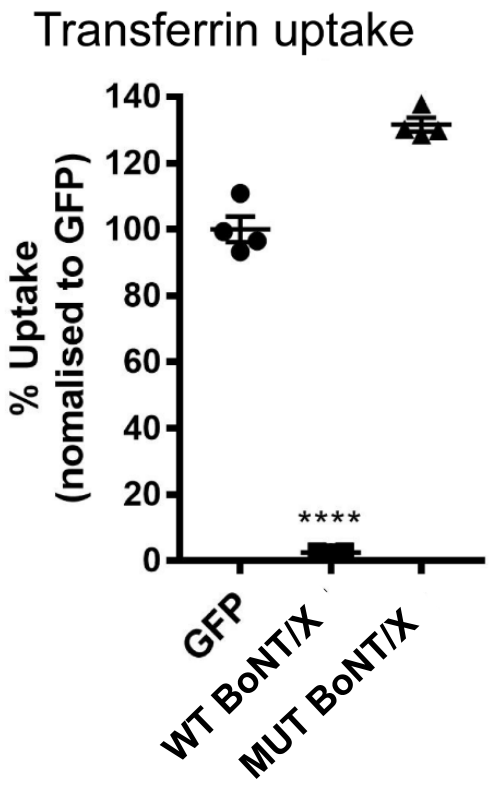
Transferrin uptake
% Uptake (nomalised to GFP)
140
120
100
80
60
40
20
0
****
GFP
WT BoNT/X
MUT BoNT/X

Surface TF-R

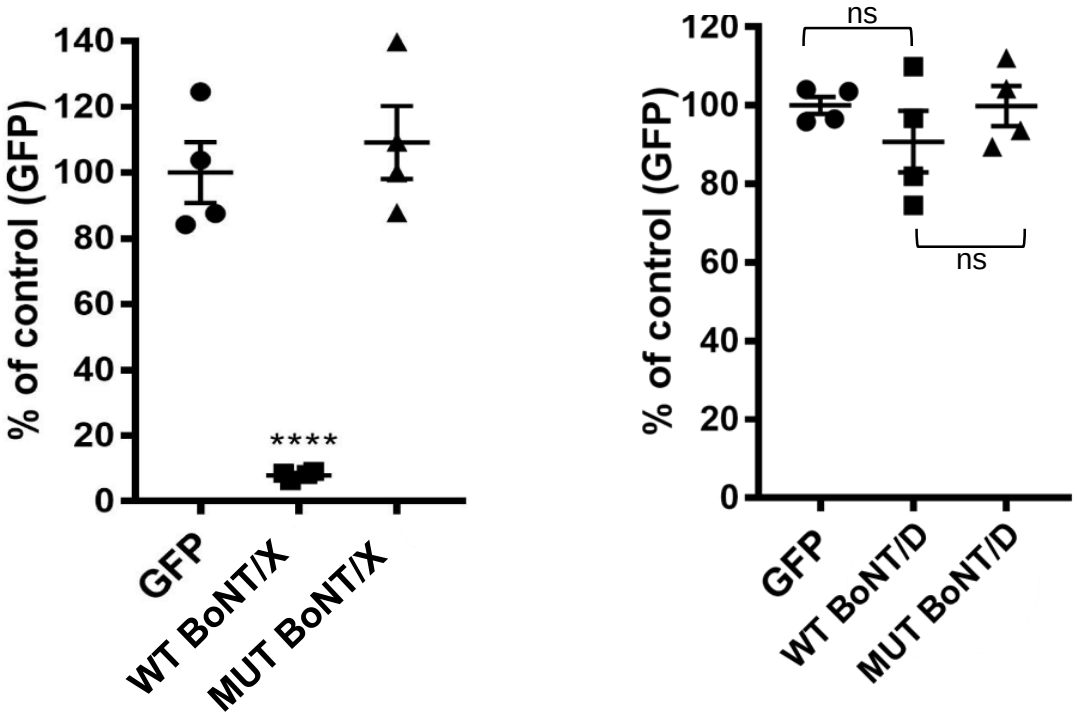
% of control (GFP)
140
120
100
80
60
40
20
0
****
GFP
WT BoNT/X
MUT BoNT/X
% of control (GFP)
120
100
80
60
40
20
0
ns
ns
GFP
WT BoNT/D
MUT BoNT/D

(B)

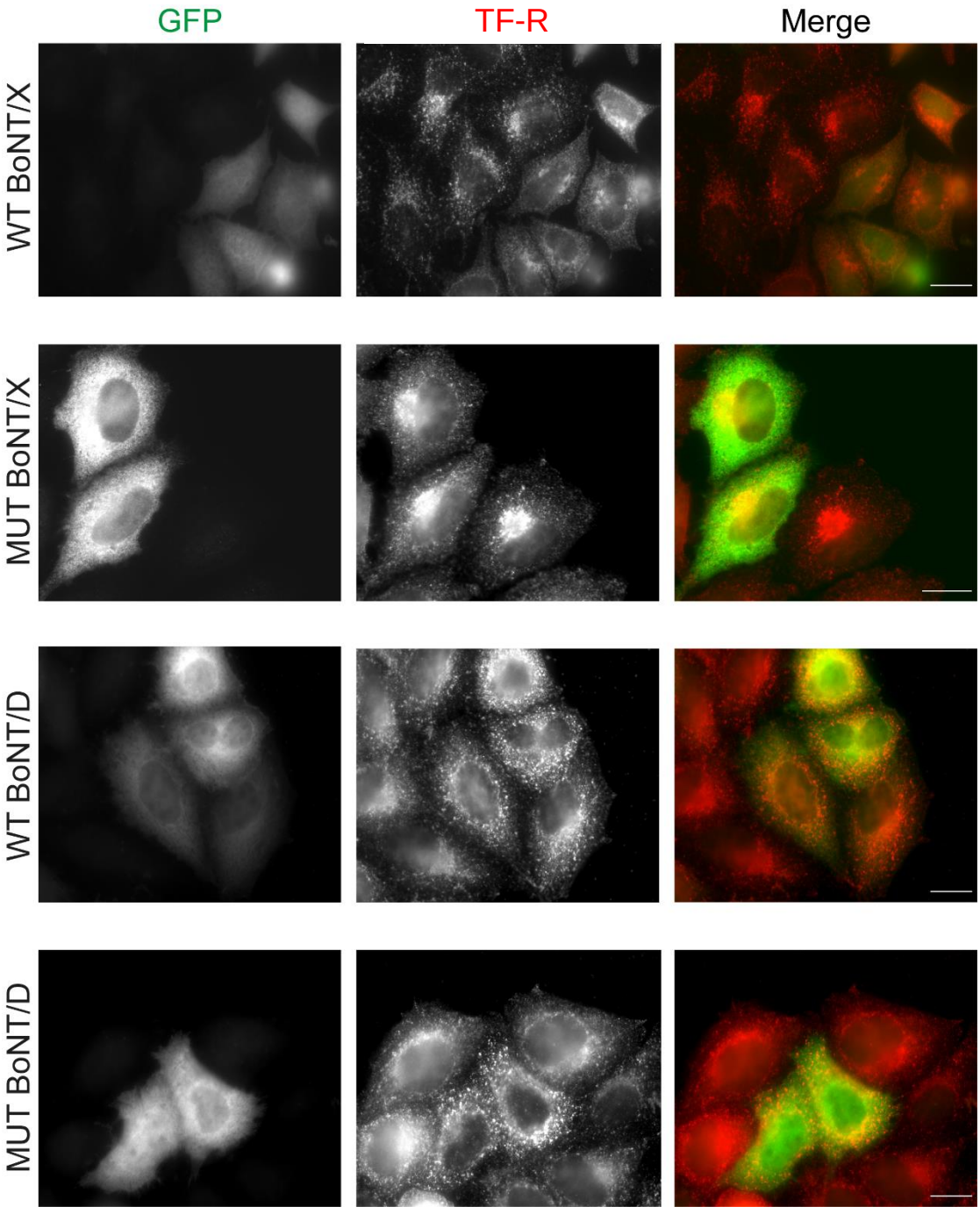

(C)

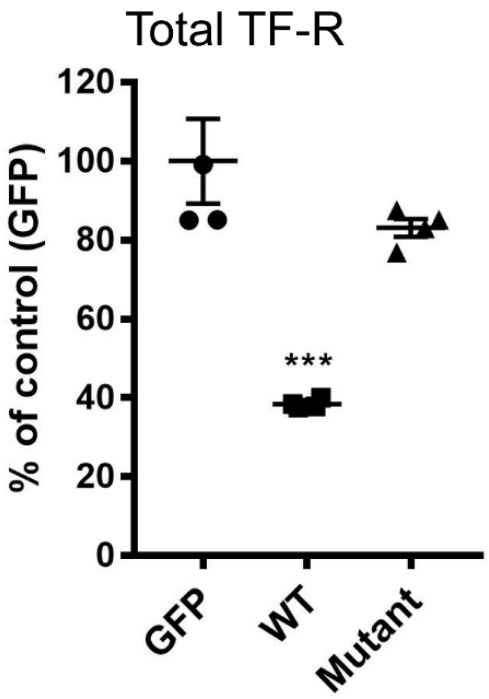

Figure 4.2 BoNT/X intoxication reduces the levels of glycosylated proteins at the cell surface and perturbs their endocytosis

(A) To develop an assay to measure WGA binding and endocytosis a series of pilot experiments were performed and analysed by fluorescence microscopy.

HeLa-M cells were transiently transfected with WT, MUT BoNT/X, or GFP vector. The cells were then either incubated with WGA at (B) 4°C or (C) 37°C before being washed and fixed. (D) To remove surface-bound WGA the cells were also washed with 0.1M N-acetyl-D-glucosamine (D-GlcNAc) for 5 minutes at 4°C. Scale bar 20 µm.

(E) Once optimal conditions had been established the experiments were repeated as above and WGA binding and endocytosis were measured and quantified using flow cytometry (n=4). Error bars represent SEM. ****$P \leq 0.0001$.

(A)

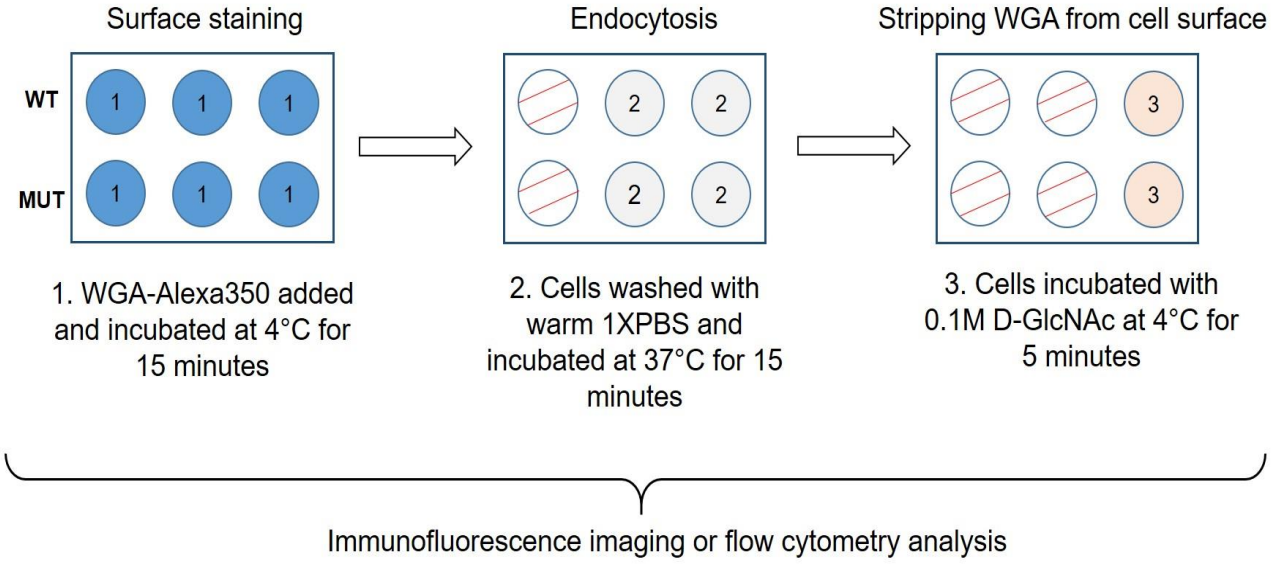
Surface staining
Endocytosis
Stripping WGA from cell surface
WT
MUT
1
2
3
1. WGA-Alexa350 added and incubated at 4°C for 15 minutes
2. Cells washed with warm 1XPBS and incubated at 37°C for 15 minutes
3. Cells incubated with 0.1M D-GlcNAc at 4°C for 5 minutes
Immunofluorescence imaging or flow cytometry analysis

(B)

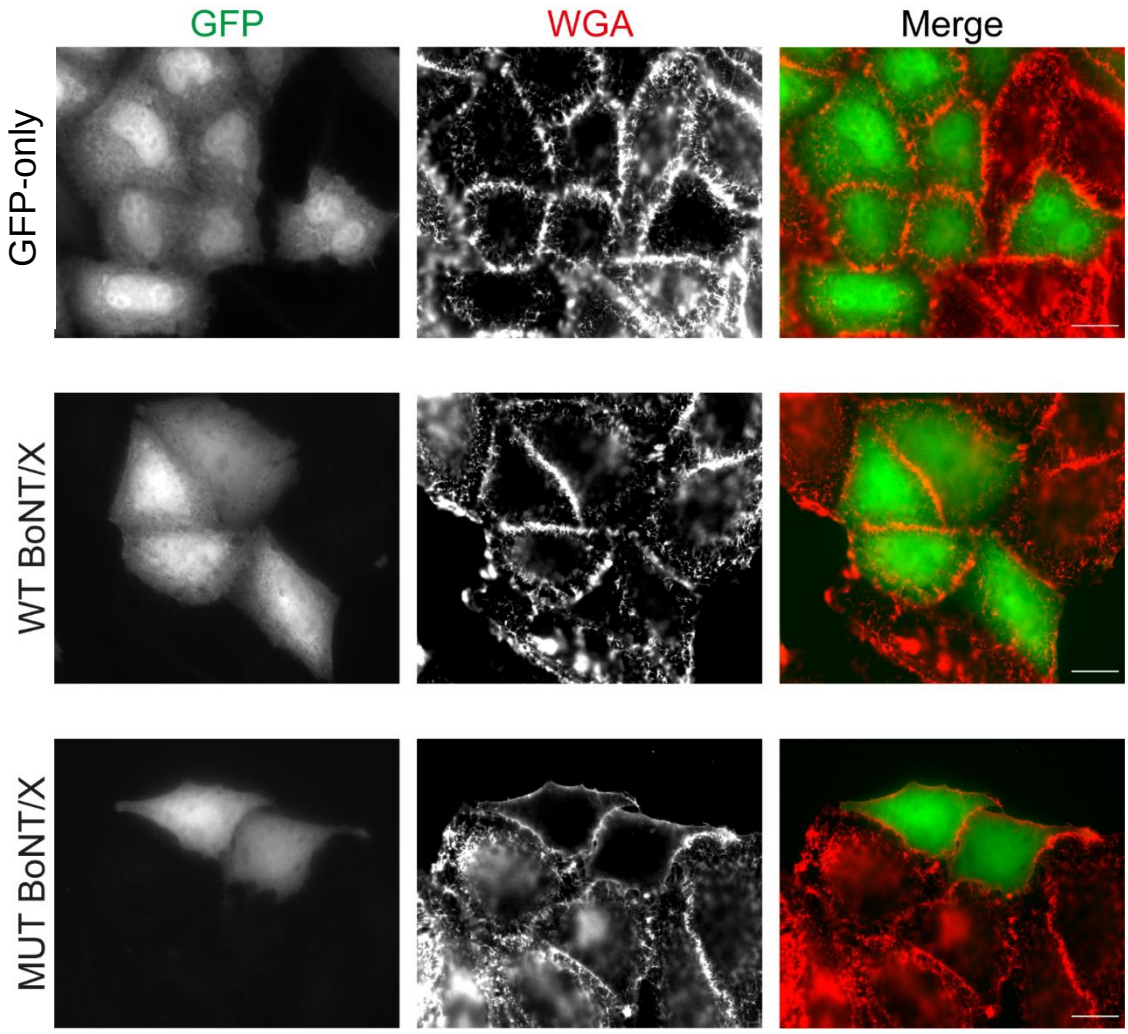

Incubation at 4°C

(C)

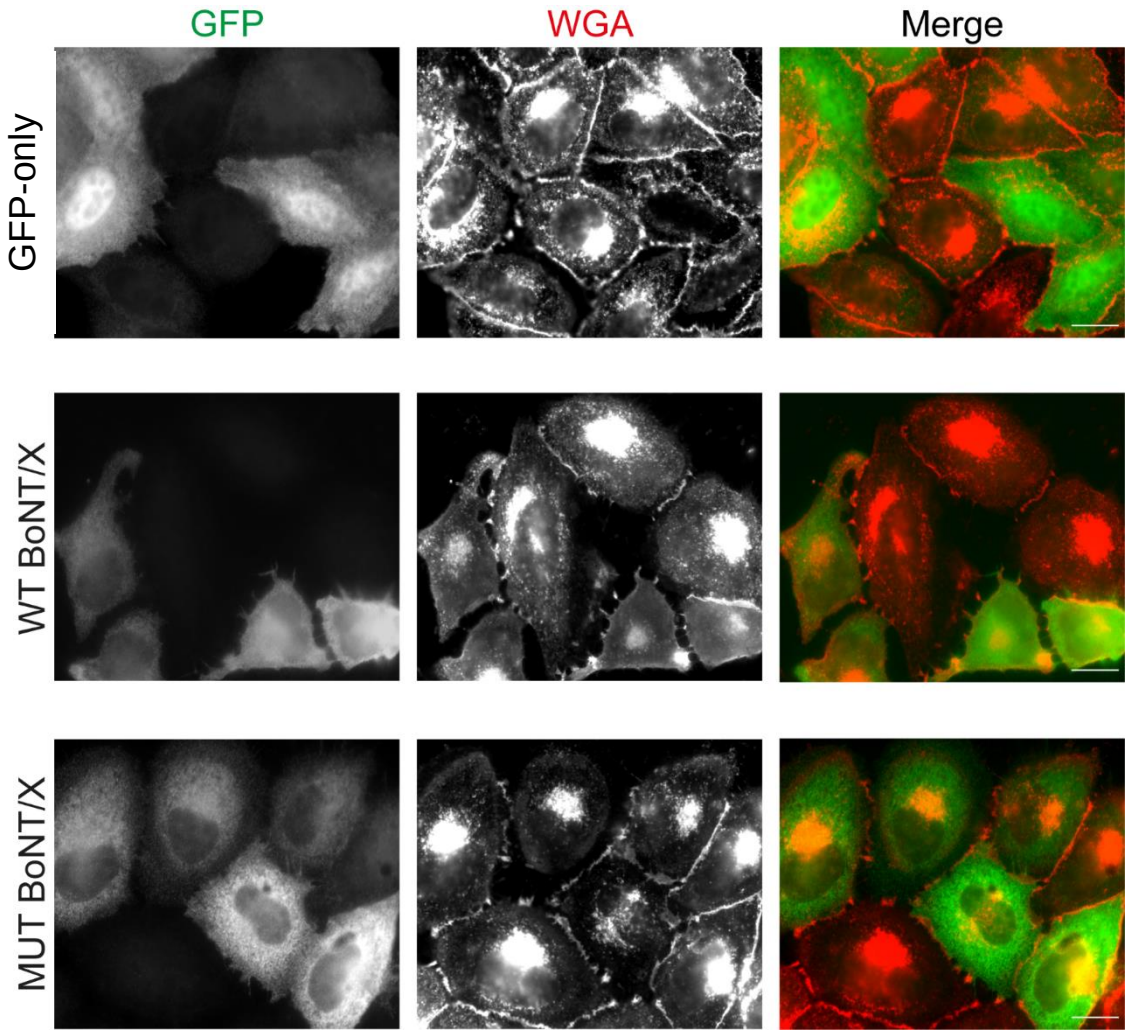

Incubation at 37°C

(D)

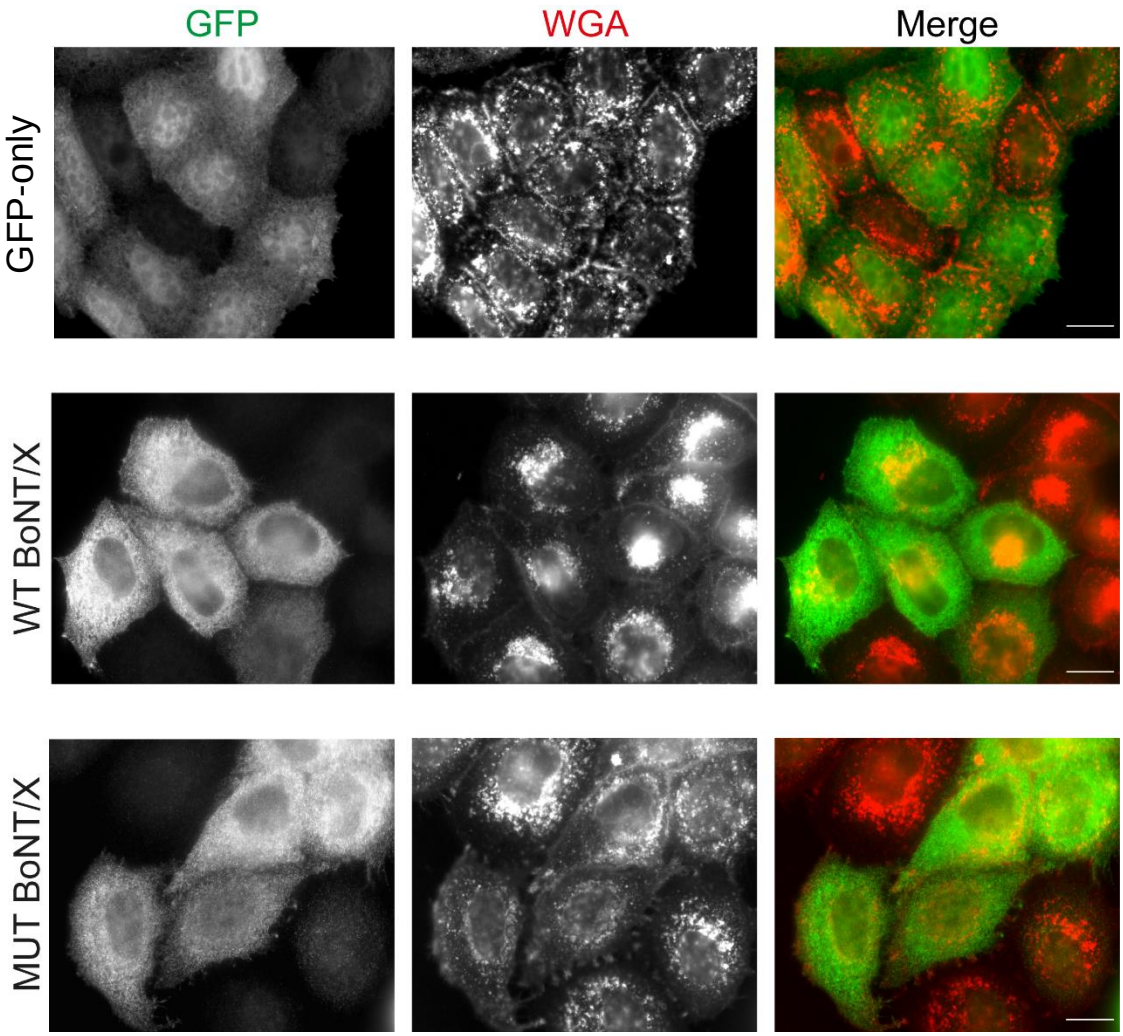

Treatment with 0.1M D-GlcNAc for 5 minutes at 4℃

(E)

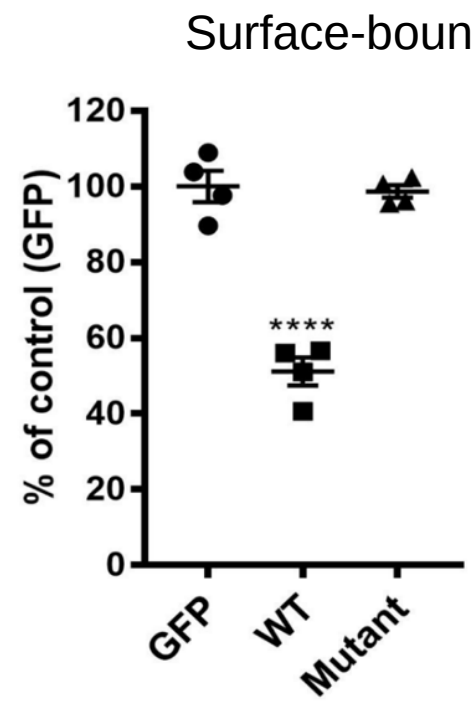
Surface-bound WGA
% of control (GFP)
120
100
80
60
40
20
0
****
GFP
WT
Mutant

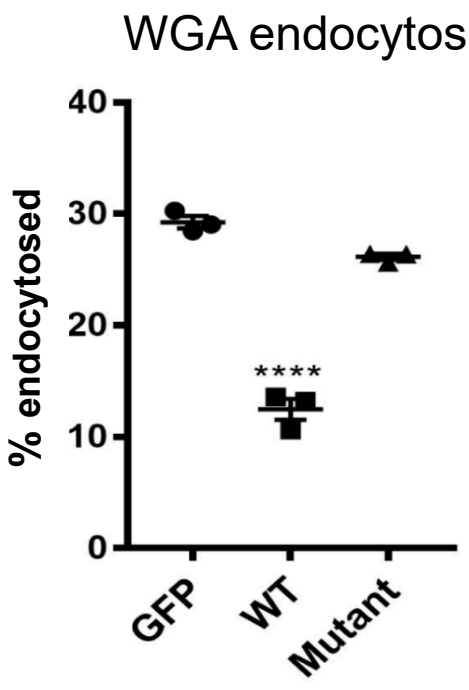
WGA endocytosis
% endocytosed
40
30
20
10
0
****
GFP
WT
Mutant

Figure 4.3 Endomembrane trafficking is perturbed in BoNT/X intoxicated cells

(A) To determine the effect of BoNT/X on endocytic trafficking of CD63 HeLa-M cells were grown on coverslips and were transiently transfected with recombinant WT BoNT/X in MUT BoNT/X GFP-tagged constructs. The cells were incubated with an anti-CD63 antibody and allowed to be internalized for 15 minutes at 37^{o}C. Cells were then fixed, permeabilised and an appropriate secondary antibody was added. Scale bar 20 µm.

(B) To determine the surface levels of CD63 in cells transfected with the BoNT/X, HeLa-M cells were grown and transfected with recombinant WT or MUT BoNT/X GFP-tagged constructs. Cells were harvested and stained with the anti-CD63 antibody at 4^{o}C in suspension. Cells were then fixed and an appropriate secondary antibody was added. The levels of surface CD63 were measured by flow cytometry (n=4). Error bars represent SEM. ****$P \leq 0.0001$. A similar experiment was conducted to quantify total CD63 levels. However, the cells were first fixed and permeabilised before the immunolabelling was performed. The levels of total CD63 were measured by flow cytometry (n=4). Error bars represent SEM. ****$P \leq 0.0001$.

(C) To determine the effect of BoNT/X on Cl-MPR and CDMPR, HeLa-M cells were grown on coverslips and were transiently transfected with recombinant WT BoNT/X or MUT BoNT/X GFP-tagged constructs. The cells were incubated with fluorescently labelled anti-ClMPR and anti-CDMPR antibody respectively and allowed to be internalized for 15 minutes at 37^{o}C. Scale bar 20 µm.

(D) To determine the surface levels of CI-MPR in cells transfected with the BoNT/X, HeLa-M cells were grown and transfected with recombinant WT and MUT BoNT/X GFP-tagged constructs Cells were stained and harvested with the anti-CI-MPR antibody at 4 ^{o}C in suspension. Cells were then fixed and an appropriate secondary antibody was added. The levels of surface CI-MPR were measured by flow cytometry (n=4). Error bars represent SEM. ****$P \leq 0.0001$. A similar experiment was repeated to quantify total CI-MPR and total CI-MPR levels. However, the cells were fixed and permeabilised before immunolabeling was performed. The levels of total CI-MPR were measured by flow cytometry (n=4). Error bars represent SEM. **$P \leq 0.01$; ***$P \leq 0.001$.

(E) To determine the effect of active BoNT/X light chain on receptor-mediated endocytic trafficking of Golgi marker, TGN46, HeLa-M cells were grown on coverslips and transiently transfected with WT or MUT BoNT/X GFP-tagged constructs. The cells were incubated with an anti-TGN46 antibody and allowed to be internalized for 15 minutes at 37^{o}C. Cells were then fixed, permeabilised and an appropriate secondary antibody was added. Scale bar 20 µm.

(F) To determine the effect of active BoNT/X light chain on receptor-mediated endocytic trafficking of a receptor that was not totally dependent on clathrin-mediated processes, EGFR, HeLa-M cells were grown on coverslips and transiently transfected with WT BoNT/X or MUT BoNT/X GFP-tagged constructs. The cells were incubated

with an anti-EGFR antibody and allowed to be internalized for 15 minutes at 37ºC. Cells were then fixed, permeabilised and an appropriate secondary antibody was added. Scale bar 20 µm.

(G) To determine the surface levels of EGF-R in cells transfected with the BoNT/X, HeLa-M cells were grown and transfected with recombinant WT or MUT BoNT/X GFP-tagged constructs. Cells were harvested and stained with the anti-EGF-R antibody at 4ºC in suspension. Cells were then fixed and an appropriate secondary antibody was added. The levels of surface EGF-R were measured by flow cytometry (n=4). Error bars represent SEM. ***$P \leq 0.001$. A similar experiment was conducted to quantify total EGF-R expression. However, the cells were first fixed and permeabilised before the immunolabelling was performed. The levels of total EGF-R were measured by flow cytometry (n=4). Error bars represent SEM. ns, not significant.

(A)

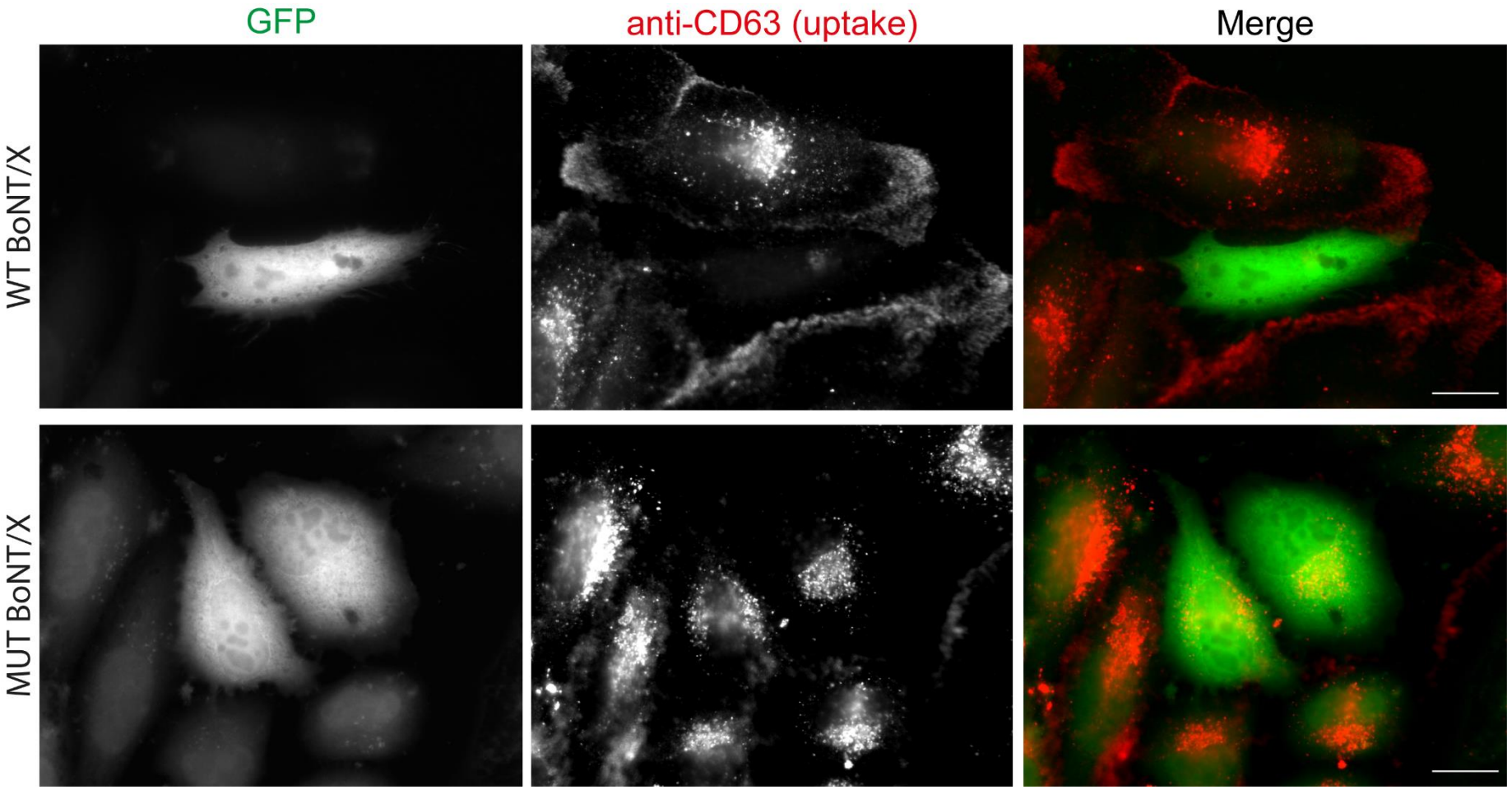

(B)

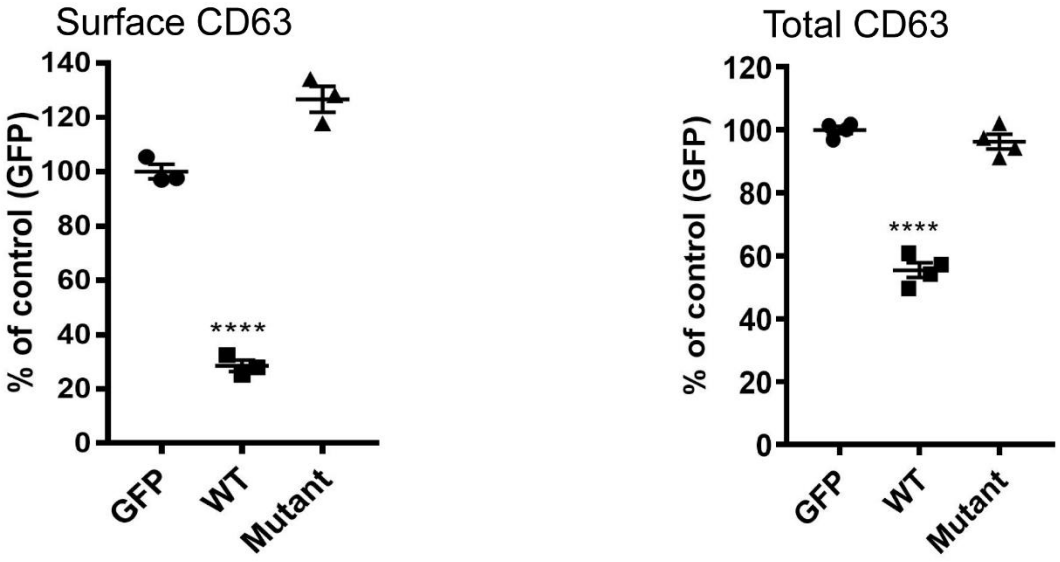
Surface CD63
% of control (GFP)
140
120
100
80
60
40
20
0
****
GFP
WT
Mutant
Total CD63
% of control (GFP)
120
100
80
60
40
20
0
****
GFP
WT
Mutant

(C)

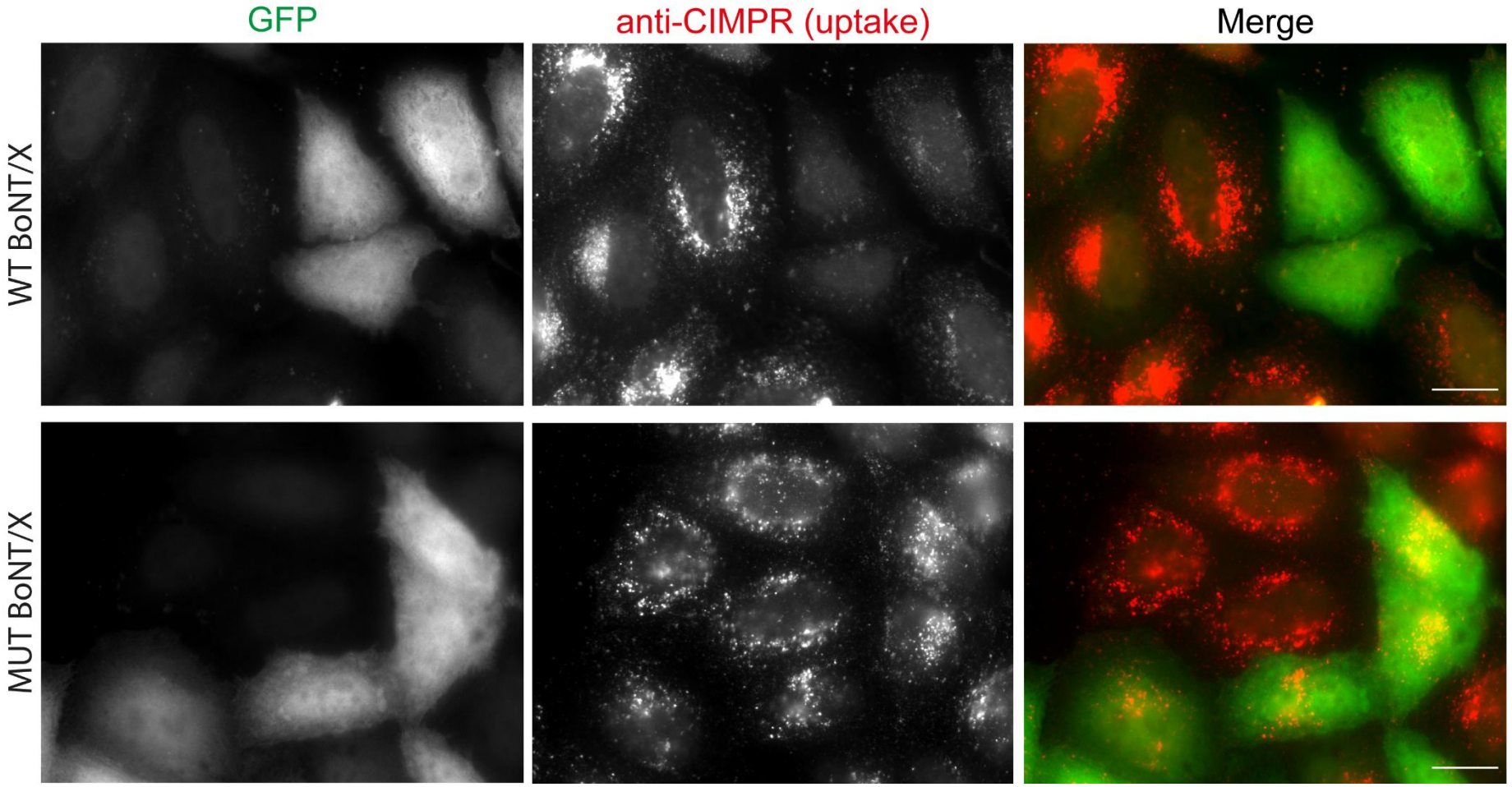

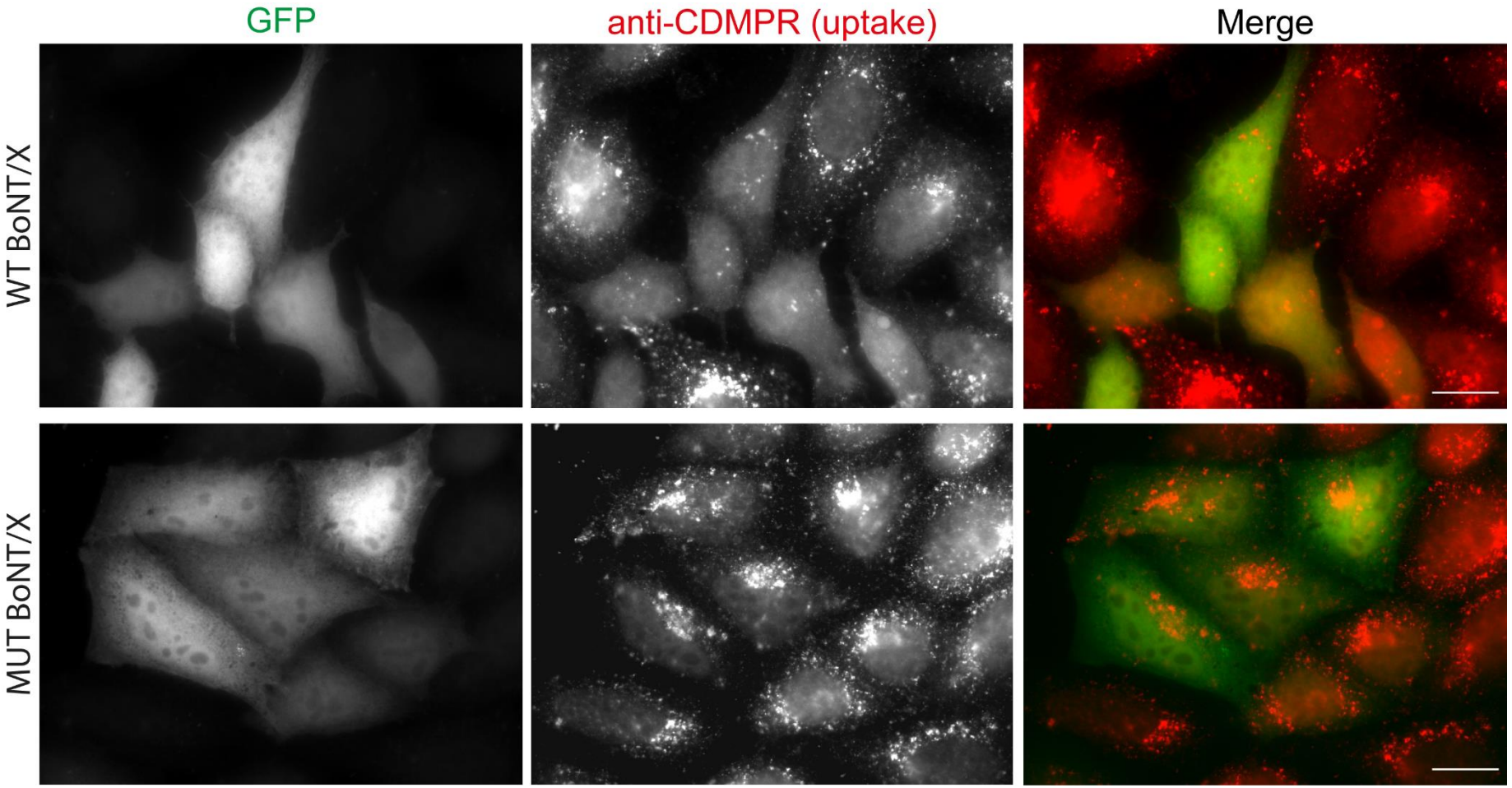
GFP
anti-CDMPR (uptake)
Merge
WT BoNT/X
MUT BoNT/X

(D)

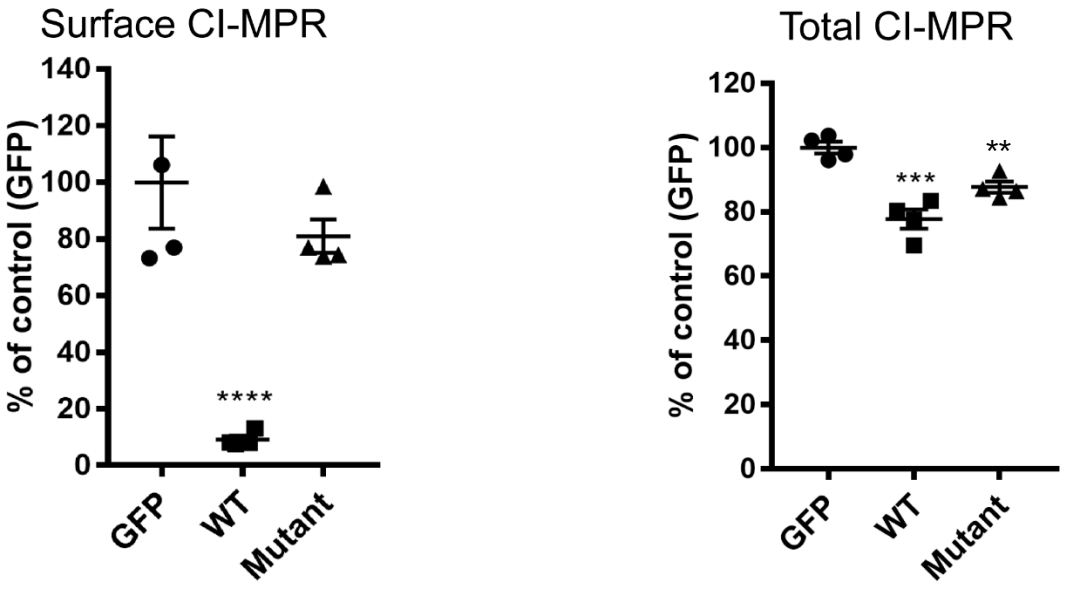
Surface CI-MPR
% of control (GFP)
140
120
100
80
60
40
20
0
****
GFP
WT
Mutant
Total CI-MPR
% of control (GFP)
120
100
80
60
40
20
0
***
**
GFP
WT
Mutant

(E)

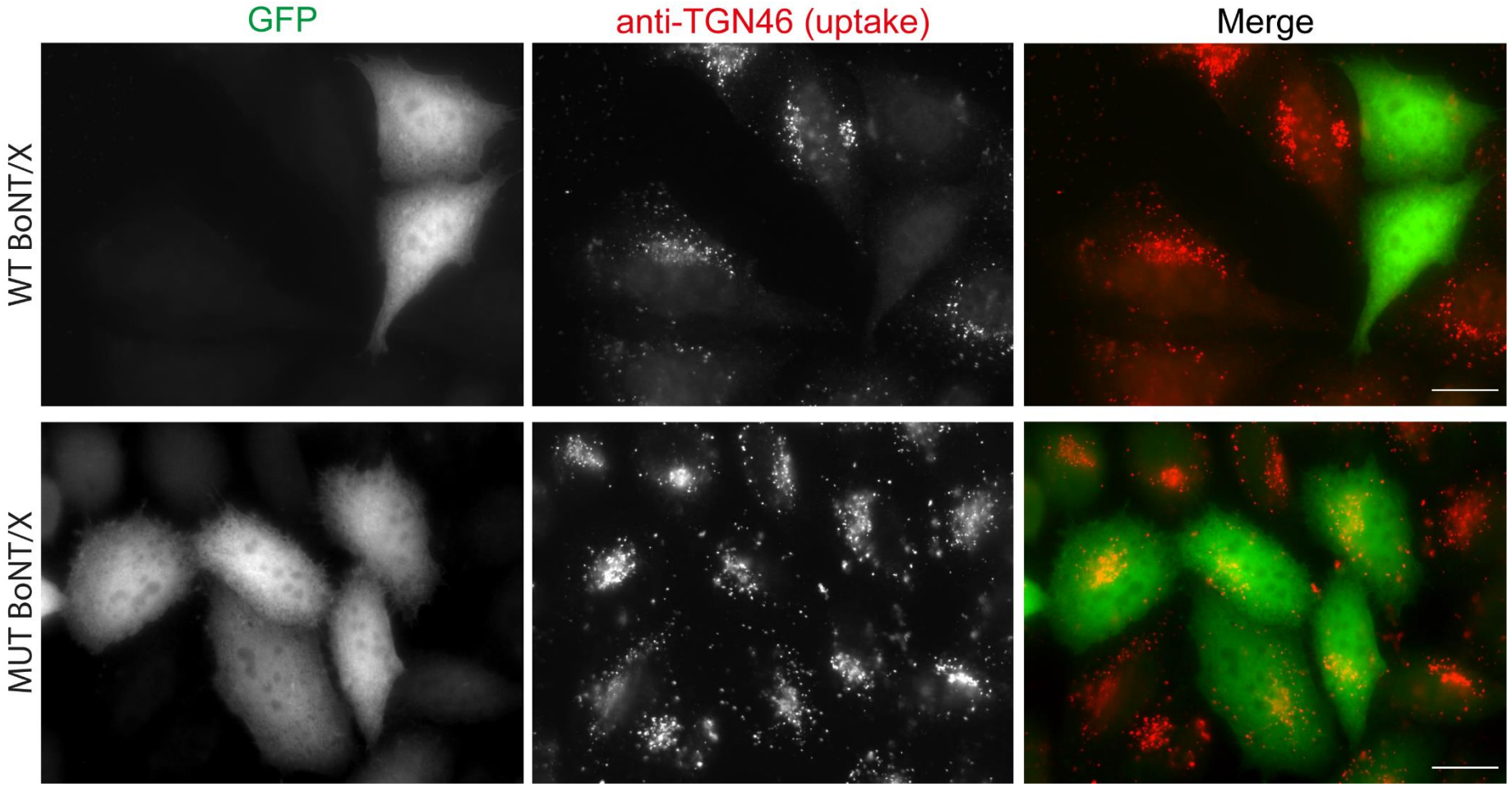

(F)

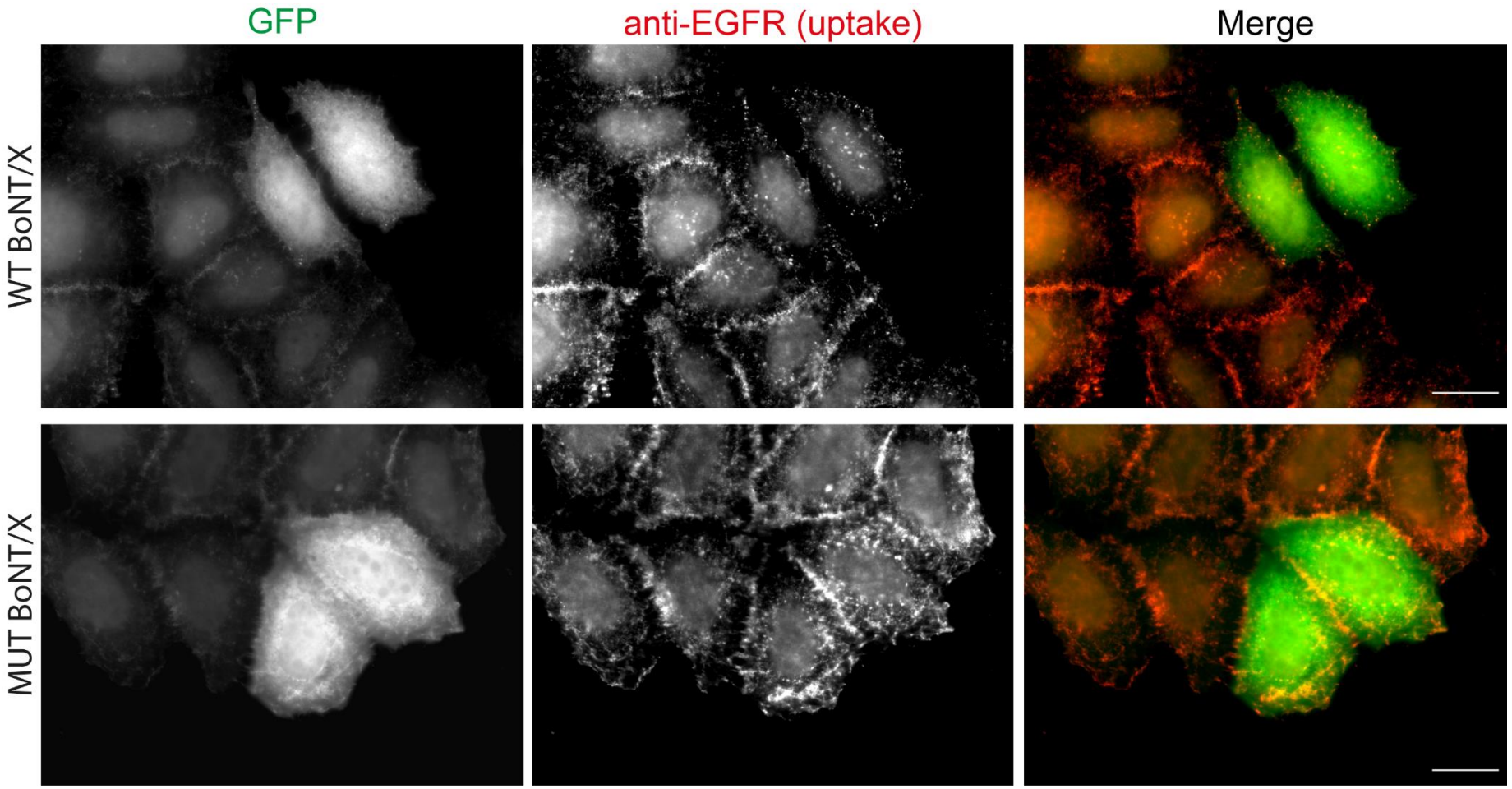

(G)

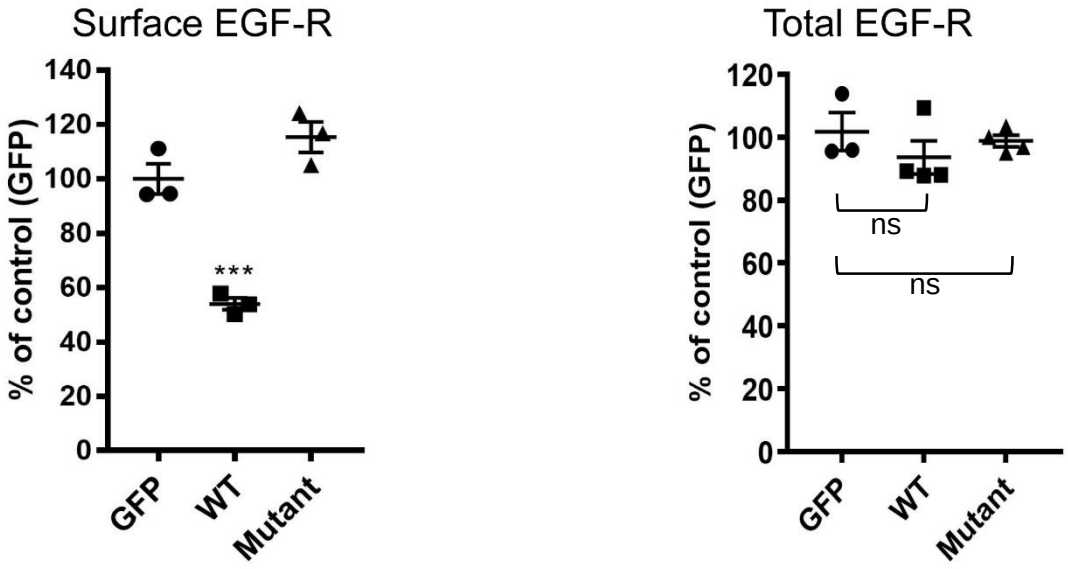
Surface EGF-R
% of control (GFP)
140
120
100
80
60
40
20
0
***
GFP
WT
Mutant
Total EGF-R
% of control (GFP)
120
100
80
60
40
20
0
ns
ns
GFP
WT
Mutant

Chapter 5: BoNT/X blocks the delivery of newly synthesised proteins to the cell surface

5.1 Introduction

It has long been established that BoNT serotypes A through G block regulated exocytosis of synaptic vesicles (Neale 1999). However, these BoNTs do not inhibit constitutive secretion. For example, work by Li Sheng Peng demonstrated that secretion of Luciferase in neurons was not blocked by treatment with BoNT/C and E (Peng et al., 2013). My work has shown that BoNT/X cleaves VAMPs 3, 4, and Ykt6 and intoxicated cells show a significant reduction in the levels of cell surface proteins. Thus, it is possible that the cleavage of BoNT/X blocks the delivery of newly synthesised proteins to the cell surface. For example, yeast Ykt6 is required for multiple transport steps including ER to Golgi transport (Kweon, Rothe, Conibear & Stevens, 2003) and more recently, our lab has shown that it is capable of forming SNARE complexes that drive the fusion of secretory vesicles with the plasma membrane in Drosophila cells (Gordon, Chia, Jayawardena, Antrobus, Bard & Peden, 2017).

5.2 Chapter aims

In this chapter, we aim to determine whether BoNT/X intoxication blocks constitutive secretion. We have determined whether BoNT/X blocks:

1) secretion of soluble cargo.
2) secretion of membrane-bound cargo.

5.3 Results

5.3.1 BoNT/X blocks constitutive secretion of soluble cargo

BoNT/X intoxication significantly reduces the levels of cell surface proteins. Thus, the toxin may be blocking pathways important for the delivery of newly synthesised proteins with the PM. To address this, I have used a fluorescence-based secretion assay to directly measure whether BoNT/X blocks constitutive secretion/exocytosis. The method used was developed by a former student in the lab (Gordon et al., 2010a). The reporter construct encodes EGFP linked to 4 F36M domains (mutant FK506- and rapamycin binding protein) (Figure 5.1A). When expressed in cells the F36M domains form ligand reversible dimers in the endoplasmic reticulum that cannot be secreted. The addition of Rapamycin or AP21998 releases the interactions between the F36M domains making the protein soluble. A pulse of the reporter is created that exits the endoplasmic reticulum and moves towards the Golgi to be secreted into the media. Secretion can be measured using either microscopy or flow cytometry. HeLa-M secretory reporter cells were transiently transfected in duplicate with mCherry-tagged WT and MUT BoNT/X. One sample was treated with Rapamycin for 120 minutes and while the other was used as a control. The cells were then fixed and a residual GFP signal was observed using a fluorescent microscope (Figure 5.1B, C). In parallel, the levels of secretion in the transfected cells were quantified using flow cytometry. (Figure 5.1D).

In the cells expressing BoNT/X, I observed that the reporter construct failed to be trafficked to the Golgi and was retained in the ER in small punctate structures found throughout the cytoplasm. In contrast, cells expressing the inactive version of the toxin, the secretory reporter accumulated in the Golgi and was lost from the ER. In support of these results, we observed that there was almost no secretion in intoxicated cells as measured by flow cytometry. In BoNT/X intoxicated cells only a small amount of the reporter was secreted (10%) compared to mock and MUT BoNT/X transfected cells where around 80% was secreted. Taken together, my data suggests that BoNT/X intoxication leads to a robust block in the delivery of newly synthesised proteins to the cell surface.

5.3.2 Development of a new flow cytometry-based assay for measuring the constitutive secretion of transmembrane anchored cargo

To investigate the effect of BoNT/X intoxication on transmembrane anchored proteins I developed a simple assay utilising GFP tagged recombinant proteins. The first reporter was based on CD8α. CD8 is a transmembrane glycoprotein that is normally expressed on the surface of immune cells. The protein is not expressed in HeLa-M cells so its cell surface levels can be monitored using antibodies that detect the extracellular domain of this protein. The second reporter developed was based on murine CD63 a protein that is localized to endosomes, lysosomes, and the cell surface. The surface levels of murine CD63 can be determined using a mouse-specific anti-CD63 antibody.

To test whether the delivery of membrane proteins to the cell surface was being blocked by BoNT/X, I co-transfected the active and inactive toxin with either CD8α-GFP or mCD63-GFP. As the reporter constructs were GFP tagged I used a non-fluorescent version of the toxin and assumed that both constructs were being transfected simultaneously into the cells. 24 hours after transfection the cells were incubated with anti-CD8 or CD63 antibodies at 4°C. The cells were fixed, stained, and imaged using a confocal microscope (Figure 5.2A and B). Cells expressing the inactive toxin showed strong plasma membrane staining for both GFP and extracellular antibodies. However, this cell surface staining was absent for both CD8 and CD63 in the intoxicated cells. In addition, the majority of the CD8 and CD63 staining was present on intracellular structures which resemble the ER and Golgi (Figure 5.2 A and B). This data suggests that BoNT/X is blocking the transport of both soluble and transmembrane-based cargo from the ER and/or Golgi. To quantitatively measure the amount of CD8 and CD63 on the cell surface I repeated the experiments by flow cytometry. The level of surface staining was normalised to mock-transfected cells. A significant drop in CD8 (1.4%) and CD63 (6.7%) surface levels was observed for cells expressing the active toxin. However, the surface levels of CD8 and CD63 were not as dramatically impacted by the expression of the inactive toxin (Figure 5.2C).

5.4 Discussion

5.4.1 Summary of results

To summarize, I have shown that recombinant BoNT/X completely blocks the transport of newly synthesised proteins to the cell surface. We find that in intoxicated cells both soluble and membrane-anchored proteins accumulate in structures that resemble compartments of the early biosynthetic pathway. These observations were taken together with my results from my previous chapters strongly suggest that the observed reduction in cell surface proteins is predominantly caused by a block in their biosynthetic transport.

5.4.2 Which SNARE is responsible for the block in ER to Golgi transport?

To my knowledge, this is the first time that a BoNT has been shown to block constitutive secretion. My data suggests that the block is occurring early in the biosynthetic pathway as the reporter constructs accumulate in structures that resemble the ER and intermediate compartment. Based on the current literature, it is most likely that the block in transport is being caused by the loss of Ykt6 and not VAMPs 3 and 4; because Ykt6 has been shown to act early in the biosynthetic pathway (McNew et al., 1997) and VAMPs 3/4 are localised to post-Golgi membranes and their disruption does not lead to a defect in secretion (Gordon et al., 2017, Joshi et al., 2018).

Ykt6 is an unusual R-SNARE as it does not possess a transmembrane domain but is anchored to membranes by farnesylation and palmitoylation. Ykt6 has a longin domain and has been shown to be required for ER to Golgi transport (Fukasawa et al., 2004, Hasegawa et al., 2004). Biochemical studies suggest a distinct GS15/Syn5/GS28/Ykt6 SNARE complex on COPI positive vesicular-tubular structure in the medial cisternae of the Golgi (Xu et al., 2002) and it can bind the tethering factor P115/USO1 (Sztul and Lupashin, 2009, Grabski et al., 2012). Based on the current literature, one would predict that in intoxicated cells, the reporter constructs should accumulate in transport vesicles which should be unable to fuse with the intermediate compartment or Golgi. If we examine the localisation of the reporter constructs in the intoxicated cells, we see a

range of phenotypes from being trapped in vesicles to structures that resemble the ER and intermediate compartment. At present, it is unclear why we are observing these slightly different phenotypes. In the future, it may be of interest to examine the localisation of these constructs in conjunction with markers of the ER and intermediate compartment such as ERGIC53. In addition, it might be of interest to examine the morphology of these structures using high-resolution imagining such as immuno-electron microscopy.

Ykt6 has been shown to function redundantly with Sec22B in ER to Golgi transport in yeast, drosophila, and mammalian cells (Hasegawa et al., 2003, Daste et al., 2015a, Gordon et al., 2017). Thus, it is a little surprising that I observed such a robust block in transport when Sec22B is not targeted by the toxin. It is possible that the acute nature of BoNT/X intoxication does not give the cell enough time for Sec22B to compensate for the loss of Ykt6. In the future, it will be important to determine that this phenotype is directly caused by the loss of Ykt6 and is not the result of non-specific protease activity. At the end of my Ph.D. I attempted to generate BoNT/X resistant versions of Ykt6 by mutating the cleavage site. These constructs are resistant to BoNT/X but appear to be non-functional suggesting that an alternate approach may be needed to be to address this question. As this work is still very preliminary, I decided not to include it in the thesis.

5.4.3 The development of a new assay for measuring the biosynthetic transport of membrane proteins

Many assays have been developed to measure the biosynthetic transport of proteins. A combination of yeast genetics, cloning, and biochemical approaches has allowed many core components of this pathway to be identified. The early work by George Palade and colleagues on protein secretion established that newly synthesised secretory proteins pass through a series of endomembrane organelles on their way to the extracellular space (Palade, 1975a). Studies involving yeast, *Saccharomyces cerevisiae*, identification of the genes that were defective in *sec* mutants revealed an array of proteins involved at multiple stages of the secretory pathway (Novick et al., 1980) (Bonifacino and Glick, 2004). Other techniques involved in-vitro assay for protein

transport between donor and acceptor Golgi compartments. This cell-free assay allowed the measurement of transport between cisternae of mammalian Golgi complex. Combined with classical protein purification, this has led to the identification of various components involved in vesicle budding and fusion (Balch et al., 1984). However, the utility of these assays is often limited because laborious normalisation procedures and time-consuming imaging approaches must be used. In addition, for many of these assays to work effectively clonal reporter lines must be made which is very time-consuming. The system I have developed offers an alternate approach that allows protein transport to be rapidly quantified using flow cytometry. By overexpressing a foreign protein that was either not native to the cell or from a different species we were able to measure the cell surface levels of the transfected proteins relatively easily. In addition, because the cargo protein has a fluorescent tag it makes the normalisation and quantitation relatively straightforward. For example, non-specific changes in reporter construct transcription/translation can be easily determined by alterations in the GFP signal. By utilising several cargo molecules that have different trafficking itineraries it may be possible to gain specific information regarding which post-Golgi pathways are being perturbed. However, this is not very relevant for BoNT/X as it appears to block all trafficking from the ER. There are some limitations of this assay. For example, the assay must be performed at 4°C while surface staining is carried out and the reporter constructs used have to be resistant to trypsinisation. In addition, it utilises over-expressed proteins rather than following endogenous cargo proteins.

In summary, I have developed a robust and highly reproducible assay that allows for the transport of newly synthesized proteins to be measured by using several different methods such as flow cytometry and fluorescent microscopy. This approach is easily adapted so should be useful for studying the transport of a wide range of cargo molecules in combination with chemical and forward genetic screens.

Figure 5.1 BoNT/X expression blocks constitutive secretion.

(A) Schematic of the reporter construct used to measure secretion (SS-signal sequence, eGFP-enhanced green fluorescent protein, FM-FKBP mutated, FCS-furin cleavage sequence, hGH-human growth hormone, and numbers represent amino acids. Secretory reporter cells were treated either with (red) or without AP21998 (blue) for 120 minutes and their mean fluorescent intensity measured using flow cytometry. A significant decrease in intracellular GFP is observed in cells treated with AP21998.

(B) and (C) To determine if the active BoNT/X had an effect on constitutive secretion, secretory reporter cells were grown on coverslips and were either mock-transfected (PEI) or transiently transfected with mCherry-tagged WT- and MUT BoNT/X overnight. The next day the cells were incubated with 2 µM Rapamycin for 120 minutes at 37℃. The cells were then fixed with PFA and imaged using a wide-field immunofluorescence microscope. Scale bar 20 µm.

(D) To quantify secretion, secretory reporter cells were transfected with cherry tagged WT- and MUT BoNT/X. The next day the cells were trypsinised and treated either with (blue) or without (red) 2 µM Rapamycin for 120 minutes at 37℃ and their mean fluorescence intensity was determined by flow cytometry. The amount of GFP secreted was calculated by dividing the mean fluorescence intensity of the treated and untreated samples. Error bars represent the experimental range. Error bars represent SEM of four repeats. ****$P \leq 0.0001$.

(A)

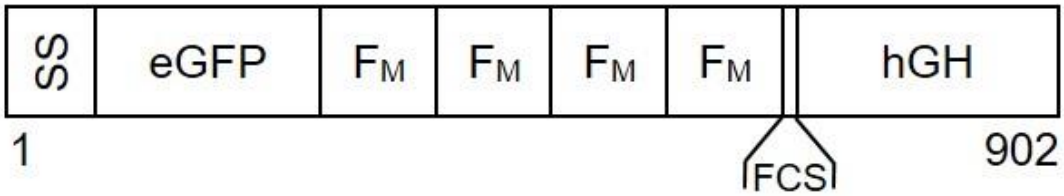
SS
eGFP
FM
FM
FM
FM
hGH
1
FCS
902

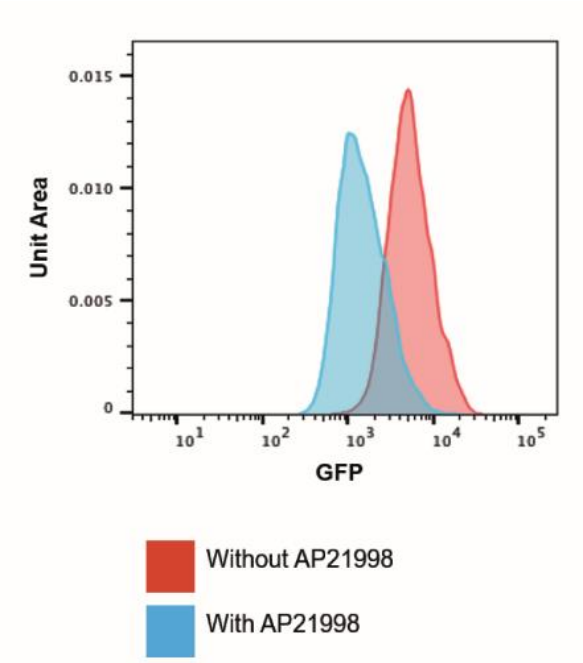
Unit Area
0.015
0.010
0.005
0
10^1
10^2
10^3
10^4
10^5
GFP
Without AP21998
With AP21998

(B)

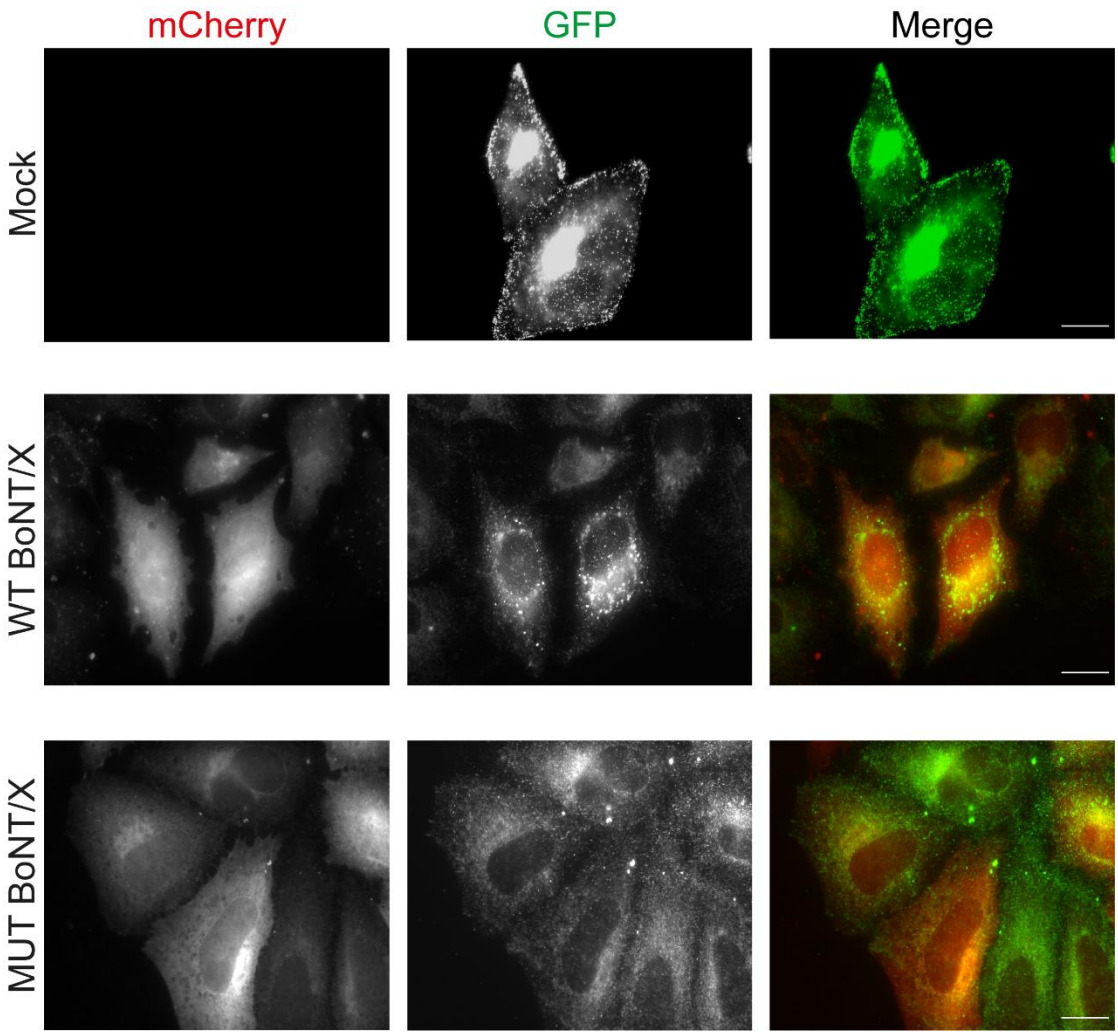

Before the addition of 2 μM Rapamycin

(C)

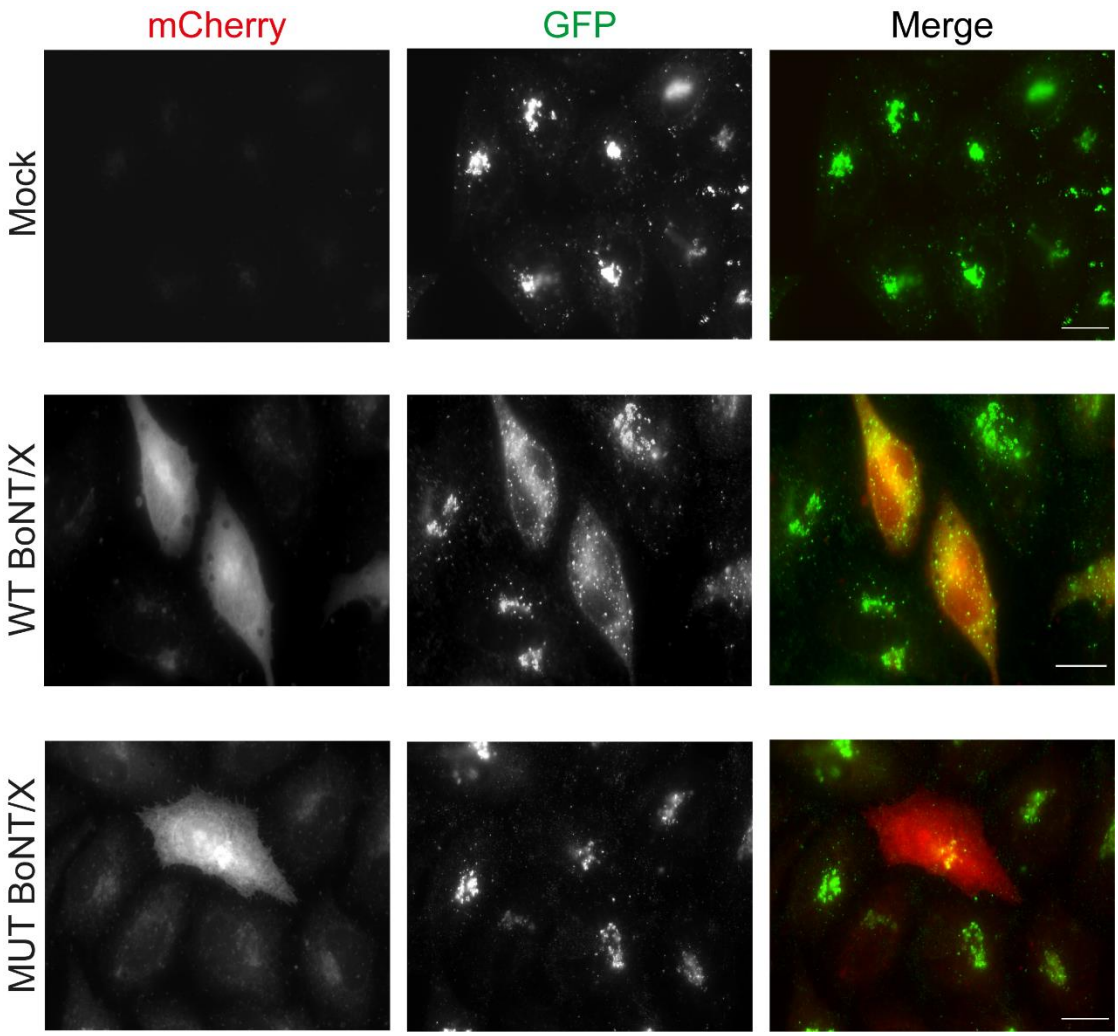

At 120 minutes after the addition of 2 μM Rapamycin

(D)

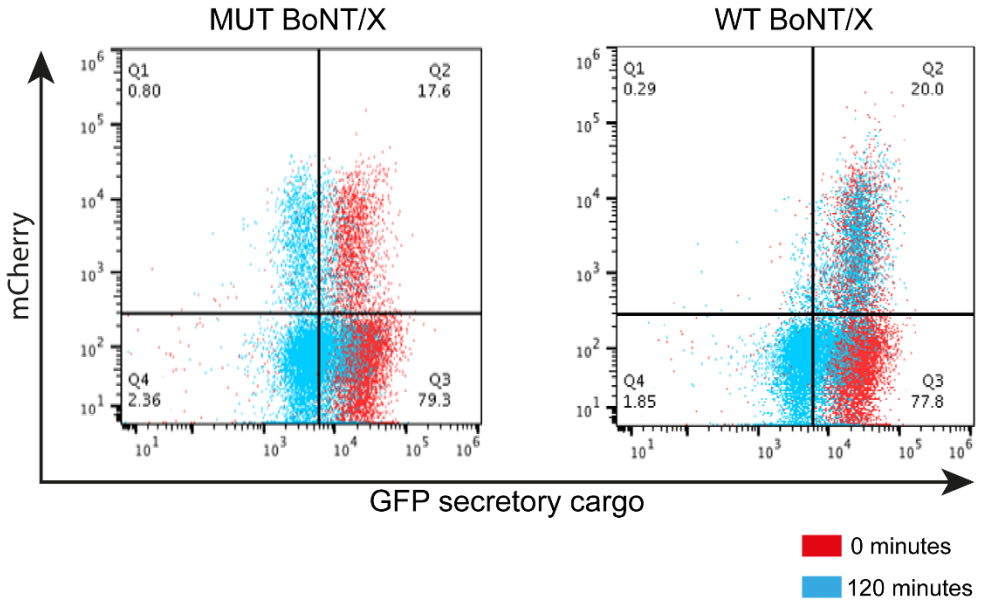

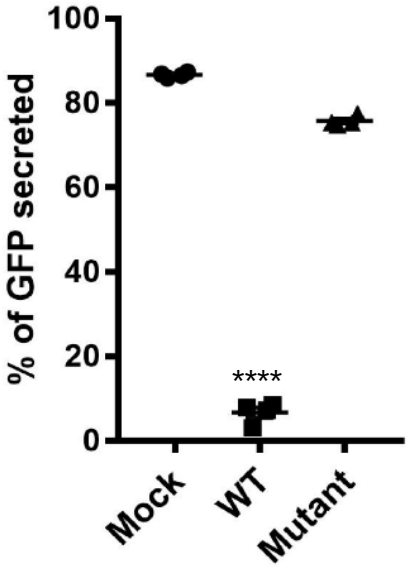

Figure 5.2 BoNT/X blocks the delivery of newly synthesized membrane proteins to the cell surface.

(A) To determine if BoNT/X blocks the delivery of CD8 to the cell surface HeLa-M cells were grown on coverslips and co-transfected with WT or MUT BoNT/X and eGFP-CD8a. To detect surface expression of CD8 the cells were labelled with the anti-CD8 antibody at 4ºC before being fixed. Scale bar 20 µm.

(B) To determine if BoNT/X blocks the delivery of CD63 to the cell surface, HeLa-M cells were grown on coverslips and co-transfected with the WT or MUT BoNT/X and mCD63-GFP. To detect surface expression of CD63 the cells were labelled with a species-specific anti-CD63 antibody at 4ºC before being fixed. Scale bar 20 µm.

(C) To measure the surface levels of CD8 and CD63 in BoNT/X intoxicated cells the cells were prepared as in (A)/(B) except the cell surface labelling was performed in suspension. The cells were then washed and their mean fluorescence intensity was determined using flow cytometry. Cell surface levels were normalised to the mock-transfected control. Error bars represent the SEM of four repeats. ****$P \leq 0.0001$.

(A)

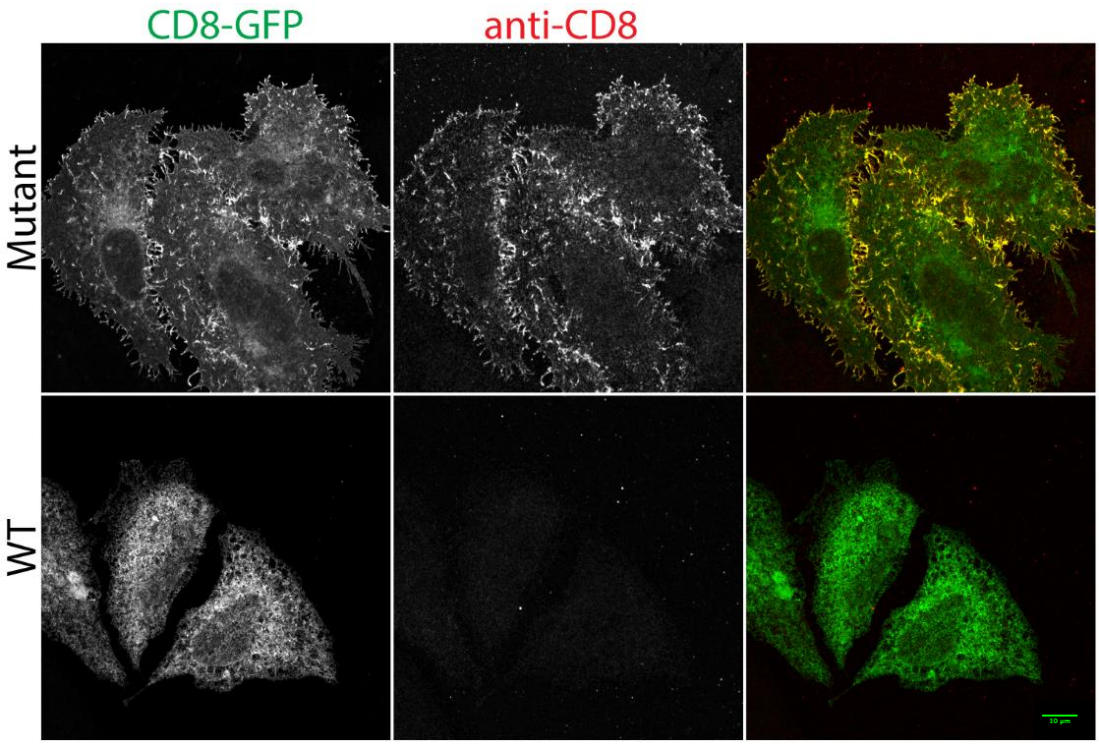

(B)

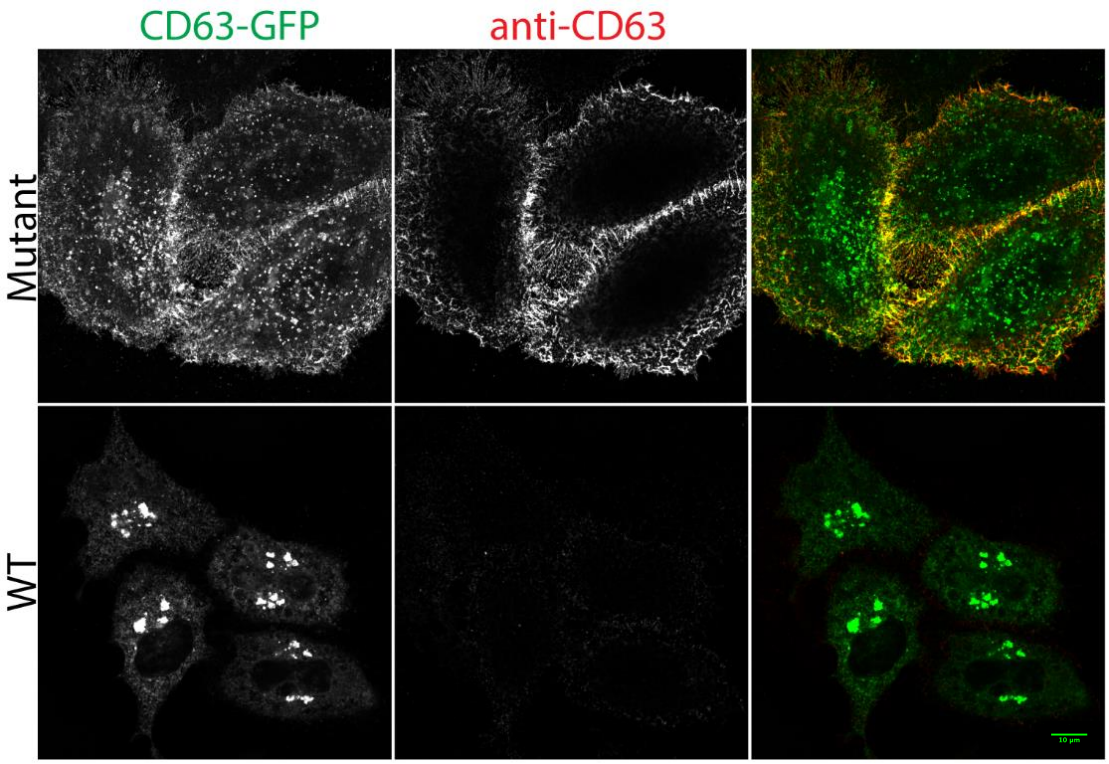

(C)

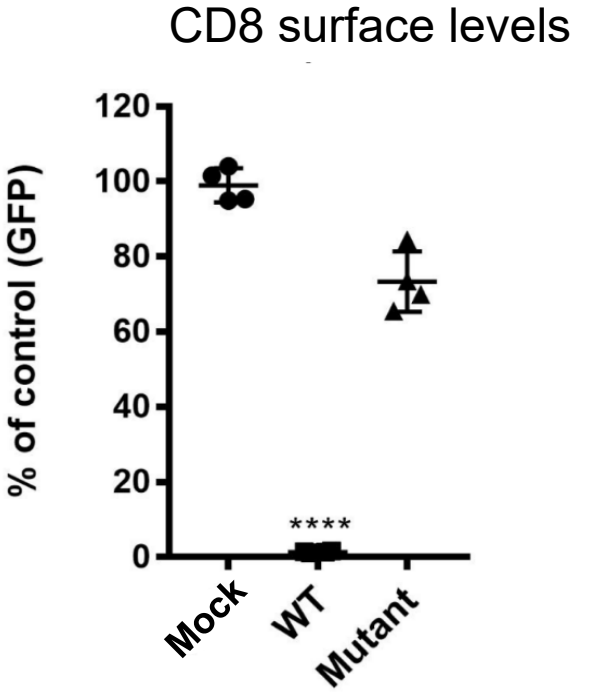
CD8 surface levels
% of control (GFP)
120
100
80
60
40
20
0
****
Mock
WT
Mutant

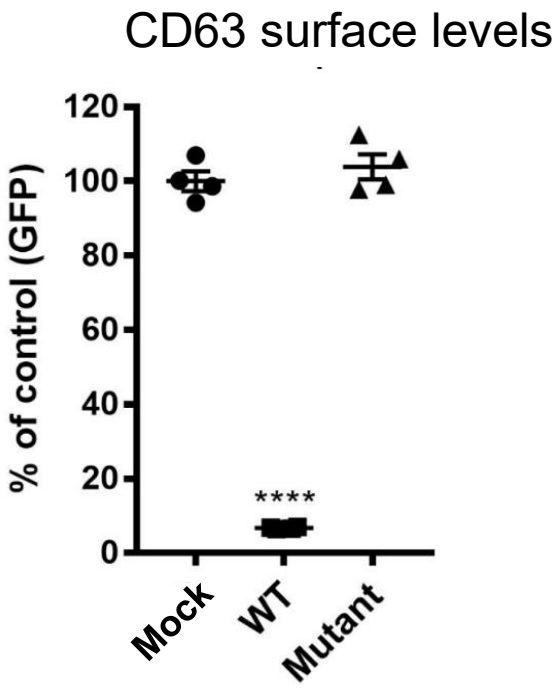
CD63 surface levels
% of control (GFP)
120
100
80
60
40
20
0
****
Mock
WT
Mutant

Chapter 6: Discussion

6.1 Introduction

BoNT/X was only recently discovered so almost nothing is known about its impact on intracellular trafficking. The studies performed thus far have predominantly focused on determining its substrate specificity in relation to neuronal physiology. Given that BoNT/X is capable of cleaving recombinant VAMPs 1-5 and Ykt6 it is likely that it will have a significant impact on intracellular trafficking. The goal of this study was to validate and extend BoNT/X's substrate specificity by looking at endogenous SNAREs and determine its effect on intracellular trafficking using a range of quantitative endocytic and biosynthetic transport assays. I have found that BoNT/X is capable of cleaving VAMPs 3, 4, and Ykt6 in vivo and that the loss of these SNAREs leads to a robust block in biosynthetic transport and causes pleiotropic defects in endocytic trafficking. In particular, I observed an almost complete loss of the TF-R from the cell surface and a reduction in the total levels of many proteins which are localised to endocytic organelles.

6.2 Are the defects in endocytic trafficking indirect?

As previously discussed, I have observed a range of striking endocytic defects in BoNT/X intoxicated cells. Thus, on the surface, it would appear that the loss of VAMPs 3, 4, and Ykt6 are severely perturbing endocytic trafficking. However, I have also shown that BoNT/X blocks the transport of newly synthesised proteins from the ER. Thus, it is plausible that many of the endocytic phenotypes I observe are just a consequence of the potent block in biosynthetic transport. For example, the reduction in cell surface levels for many receptors could simply be explained by inhibition in their delivery to the cell surface combined with their normal endocytosis and turnover in lysosomes. In support of this hypothesis, I found that the intoxicated cells were still capable of endocytosis as measured by WGA uptake. In principle, it should be relatively straightforward to determine whether the endocytic defects are being caused by a block in biosynthetic transport. For example, one could simply deplete Ykt6 using

RNAi and determine if the levels of the TF-R are reduced. Surprisingly, very little work has been performed on investigating the crosstalk between biosynthetic and endocytic pathways.

In the future, it will be of interest to develop novel ways to acutely manipulate the activity of BoNT/X. Having the ability to acutely manipulate the activity of BoNT/X would allow one to determine where the defect in trafficking was first occurring and make it less likely that you are measuring indirect phenotypes and changes due to compensation. For example, Alice Ting at Stanford University is attempting to develop photoactivatable versions of these toxins. In addition, it may be possible to generate cell lines expressing versions of BoNT/X which are under the control of a degron-based system. Degrons are small molecules composed of either structural motifs, exposed amino acid or short amino acid sequences which regulate protein degradation rates (Johnson et al., 1990, Varshavsky, 2019). The engineered version of this system is by genetically fusing a ligand-responsive destabilisation domain (DD) to the protein of interest (ref (Banaszynski et al., 2006). The DD used is a mutated FKBP12; (12 kDa FK506- and rapamycin-binding protein). The mutation causes the FKBP to degrade rapidly by the ubiquitination pathway in the absence of its ligand. Shld1, is a cell-permeable rapamycin analogue, FKBP ligand that protects the DD domain from degradation. With the active BoNT/X light chain as the protein of interest, we attempted to produce a DD-GFP-tagged BoNT/X light chain construct. The initial idea was to make a stable cell line that would express the BoNT/X light chain that would be degradable or switched-off because of the DD tag. By adding a stabilising ligand to the system, Sheild1 (Shld1), the protein would be stabilised so switched-on allowing us to control the activity of the toxin.

After initial trials, I was unable to produce this stable cell line most likely attributed to the potential leakiness of the system that may have caused degradation of the BoNT/X light chain to be insufficient, thus causing the light chain to be expressed regardless of the absence of the ligand, causing the cells to always appear sickly and dying in culture. The possible leakiness of the system, even minimal, is cytotoxic to cells because of the nature of the active BoNT/X light chain. It may also be possible to regulate the activity of these toxins by acutely regulating their localisation by using systems like the knock sideways approach. One could envisage restricting the toxin to the surface of

mitochondria and only releasing the toxin into the cytoplasm in the presence of a drug or a photoactivatable protease. One of the major challenges we face with this type of approach is it only takes a small number of molecules to intoxicate the cell. Thus, the targeting mechanism must be incredibly efficient.

6.3 Could the observed phenotypes be due to no-specific protease activity?

As discussed earlier, it is possible that the observed defects in trafficking in BoNT/X intoxicated cells could be caused by the non-specific protease activity of the toxin. As far as we are aware the recombinant toxin has similar activity as the bacterially expressed protein. For example, we do not see cleavage of VAMP7, 8, and Sec22B in intoxicated cells. However, we cannot rule out that BoNT/X may be cleaving other proteins. In general, the Botulinum field does not worry about this issue and it is assumed that these toxins are incapable of cleaving proteins that do not have homology with SNAREs. However, BoNT/X has a broader specificity than other botulinum molecules so it is possible it could be less selective. In theory, the simplest way to address this would be to perform a rescue experiment using a cleavage-resistant R-SNARE. This has successfully been performed for VAMPs 1-3 and the Tetanus light chain. Tetanus cleaves VAMPs 1-3 at R66-A67 and substituting these residues for valine (V) and tryptophan (W) completely abolished SNARE cleavage (Degtyar et al., 2013, Hoogstraaten et al., 2020). At the end of my Ph.D. I tried generating a panel of similar mutants for VAMP3 and Ykt6 (Q76V and F77W) (Supplemental Figure 2A). Initially, I designed my mutants based on VAMP8's sequence as this SNARE is not cleaved by BoNT/X. Surprisingly, these mutants did not block cleavage (RA residues replaced with KT), indicating that the difference at the cleavage site is not the reason why VAMP8 cannot be cleaved. However, when I introduced the VW mutant into VAMP3 and Ykt6 at the cleavage site, then I saw some evidence of protection (Supplemental Figure 2B). However, these mutants did not appear to traffic correctly and or protect against BoNT/X intoxication (Supplemental Figure 2C). Thus, we may need to take a different approach. For example, it may be possible to abolish the interaction between the SNARE and the toxin by mutating residues in the VAMP which are involved in SNARE binding (exosite). It may also be possible to make a VAMP3/VAMP8 exosite hybrid that is functional but not recognised by the toxin.

Another approach that may be worth exploring is to simply overexpress the SNARE of interest with the aim to overwhelm the activity of the toxin. These types of experiments may now be feasible as my lab has developed ways to transfect very low levels of the toxin into cells and still get robust intoxication.

6.4 Can we alter the specificity of BoNT/X by changing its localisation?

BoNT/X is a very interesting and exciting molecule as it cleaves a wider repertoire of R-SNAREs. However, its usefulness for investigating the physiological role of R-SNAREs is also reduced because of this property. The fact that is capable of cleaving multiple R-SNAREs makes the interpretation of the data generated by this toxin problematic as one can never be entirely sure which SNARE is causing the phenotype. Thus, it would be very useful to manipulate the specificity of BoNT/X so it only cleaves one R-SNARE at a time. The specificity of botulinum light chains can be re-engineered and there are versions of BoNT/E which have been altered so it can cleave SNAP23 as well as SNAP25 (Chen and Barbieri, 2009). However, the work involved in generating these molecules is significant. While working on my Ph.D. I had the idea so that the specificity of the toxin could potentially be altered by changing its localisation. For example, if you tethered the toxin to the ER it might not be able to cleave post-Golgi SNAREs or if you localise the toxin to the PM it might not be able to block ER to Golgi trafficking. In collaboration with several undergraduate students in the lab, I have attempted these experiments. Our initial experiments indicate that the toxin can be localised to the ER (Supplemental Figure 3). However, it still appears to be active and able to cleave post-Golgi SNAREs. At present, it is unclear why the ER localised toxin is still capable of cleaving Ykt6. However, our preliminary data suggest that it is the case as the transfected cells are still changing in morphology. Our attempt to generate PM localised versions of the toxin was also fruitless. We observed that the palmitoylated version of the toxin was able to inhibit its own trafficking and never reached the PM.

6.5 Is the loss of VAMP3 and VAMP4 important for the intoxicated phenotypes?

We have shown that there is a robust loss of VAMP3 and VAMP4 in intoxicated cells. VAMP3 can be found in smaller vesicles and the perinuclear region. In sorting endosomes, it preferentially segregates into tubular membranes to facilitate fusion with endocytic recycling and the Golgi (McMahon et al., 1993). VAMP3 has been well documented to regulate integrins, transferrin, and TF-R to the plasma membrane (Galli et al., 1994, McMahon et al., 1993), α-granule transport in platelets (Feng et al., 2002, Polgár et al., 2002) and retrograde transport of M6PR to the Golgi (Ganley et al., 2008). VAMP4 is broadly expressed and localised to the TGN where a majority is targeted to the tubular and vesicular membrane. It is also present on clathrin-coated and noncoated vesicles on endosomes (Advani et al., 1998). However, SNARE depletion via knockdown barely results in detectable phenotypes (Bethani et al., 2009). Furthermore, VAMP3/VAMP4 knockout mice are viable and do not appear to display any dramatic phenotypes (Yang et al., 2001a) (VAMP4 personal communication with Dr. Peden). siRNA targeted at VAMP3 or VAMP4 alone failed to block secretion (Gordon et al., 2010b). We are unable to conclude at this time that the phenotype is attributed to VAMP3/VAMP4 is the simultaneous loss of Ykt6 is likely to dominate the phenotype. Therefore, to test this hypothesis, we would need to develop a testing strategy using a version of the toxin that either does not cleave Ykt6 or a cleave-resistant Ykt6 protein construct as a phenotype rescue experiment.

6.6 Is BoNT/X a useful molecule for studying SNARE biology?

The work presented in this thesis demonstrates that BoNT/X causes the rapid cleavage of VAMP3, VAMP4, and Ykt6 in HeLa-M cells. The transfected cells become rapidly intoxicated and show a range of striking phenotypes from defects in biosynthetic transport through to blocks in endocytic uptake and recycling. These phenotypes are unique to BoNT/X and are not observed in cells when other bacterial toxins are used such as BoNT/D which just cleaves VAMP3. The specificity of this toxin still needs to be fully explored and it is possible that some of the observed phenotypes could be caused by off-target protease activity. However, this toxin does not cleave Sec22B, VAMP7, and VAMP8 suggesting that it has some specificity. The cytotoxicity seen in intoxicated cells is dose-dependent and in the future, it will be important to further

explore this and determine the optimal amount of toxin to be used. Many of the limitations of this toxin can be overcome if we can develop cleavage-resistant SNAREs or engineered versions of the toxin that alter it specifically. Thus, in the longer term, this molecule may be a very useful tool for acutely manipulating SNARE function.

BoNT/A has been exploited for its analgesic effect by inhibition of specific pain transmitters and mediators which promoted muscle relaxation. Due to its apparent cytotoxicity, data suggests that BoNT/X may not be used like Botox®, but this feature may prove useful for the targeted treatment of cancers of primary central nervous system tumours such as neuroblastoma. BoNT/C which cleaves SNAP25 and Syntaxin1 caused apoptotic death in differentiated human neuroblastoma cells in culture, where the ubiquitous loss of SNAP23 was observed (Rust et al., 2016, Arsenault et al., 2014). Therefore, BoNT/X may have a promising future as a highly toxic payload that can be used in cancer therapy.

Supplemental Figures

Supplemental Figure 1 Cleavage of VAMP3 by BoNT/D does not affect the distribution and morphology of major trafficking compartments.

To determine the effect of VAMP3 cleavage had on the main trafficking components, HeLa-M cells were grown on coverslips and were transiently transfected with recombinant WT BoNT/D or MUT BoNT/D. The cells were then fixed and stained with the indicated compartment-specific markers and imaged under fluorescence microscopy. Scale bar 20 μm.

Supplemental Figure 1

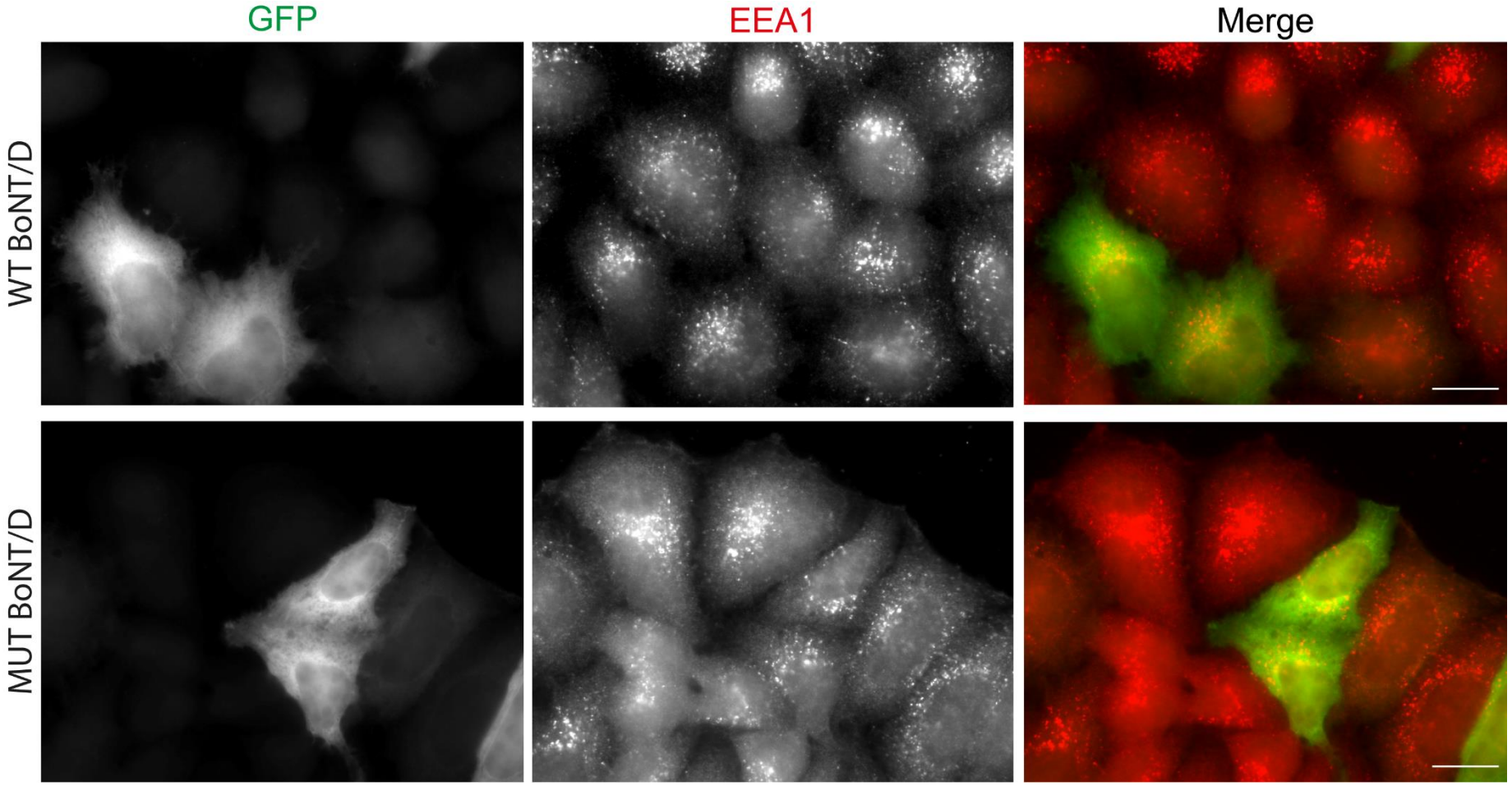

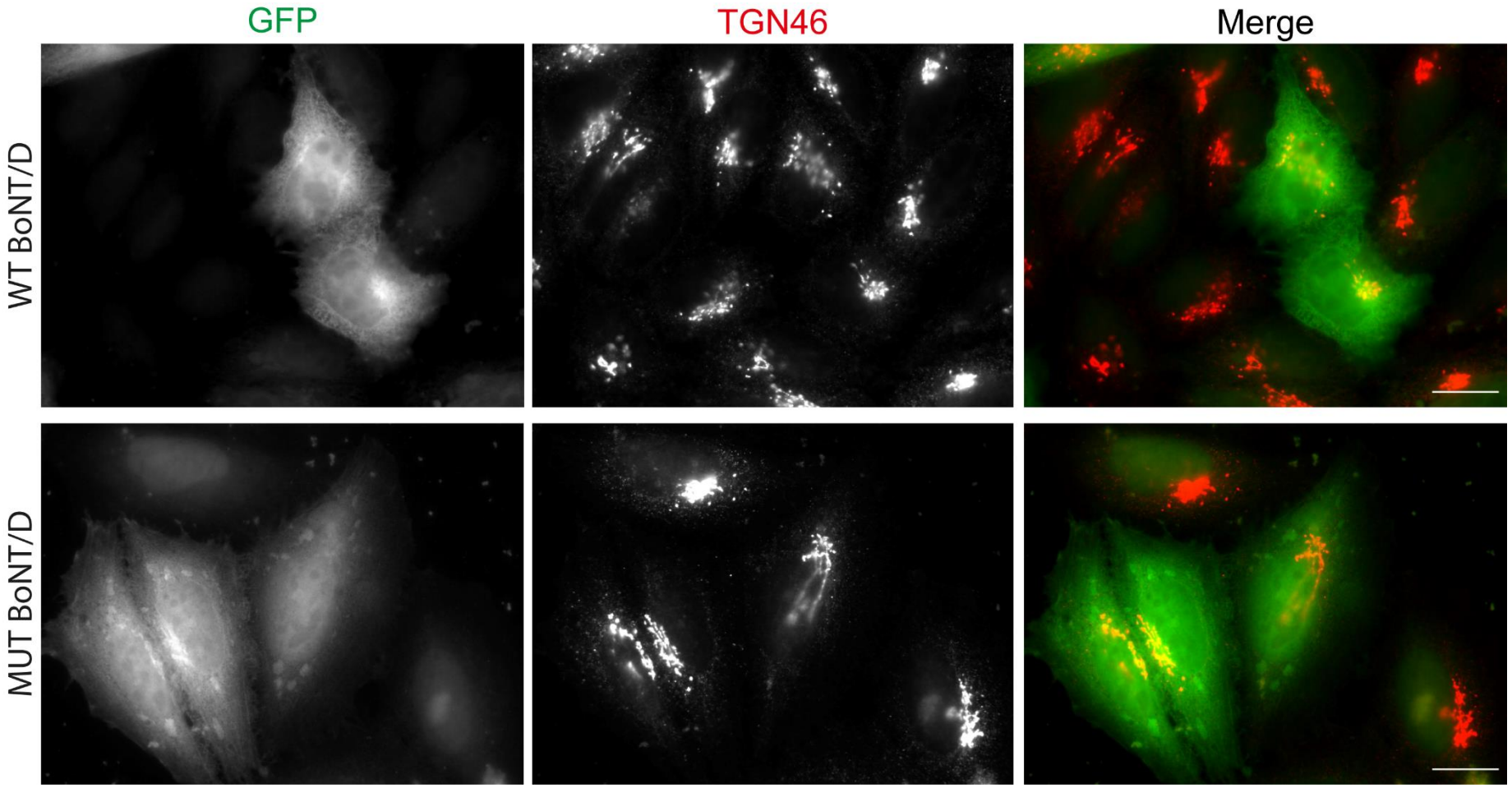
GFP
TGN46
Merge
WT BoNT/D
MUT BoNT/D

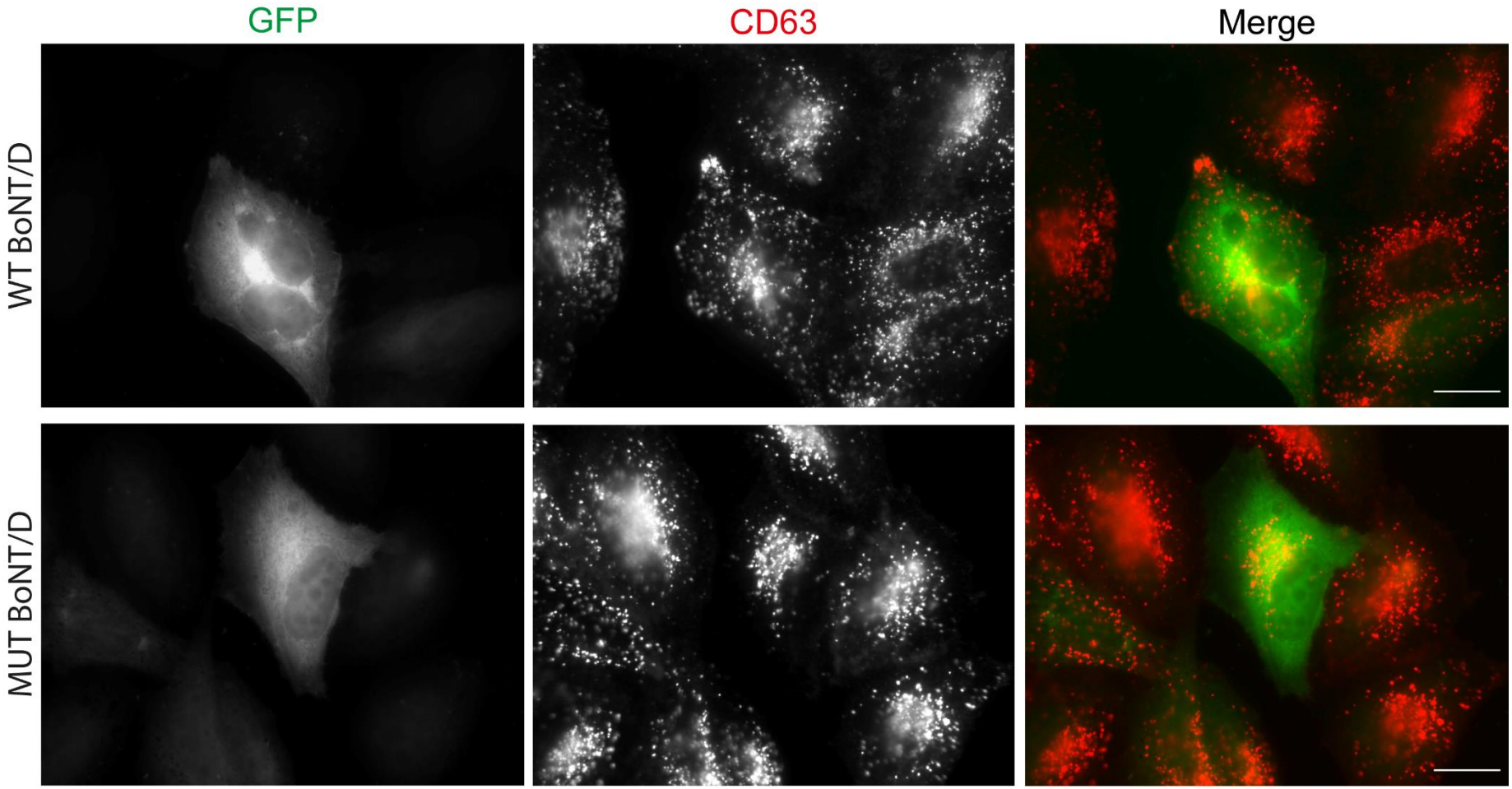
GFP
CD63
Merge
WT BoNT/D
MUT BoNT/D

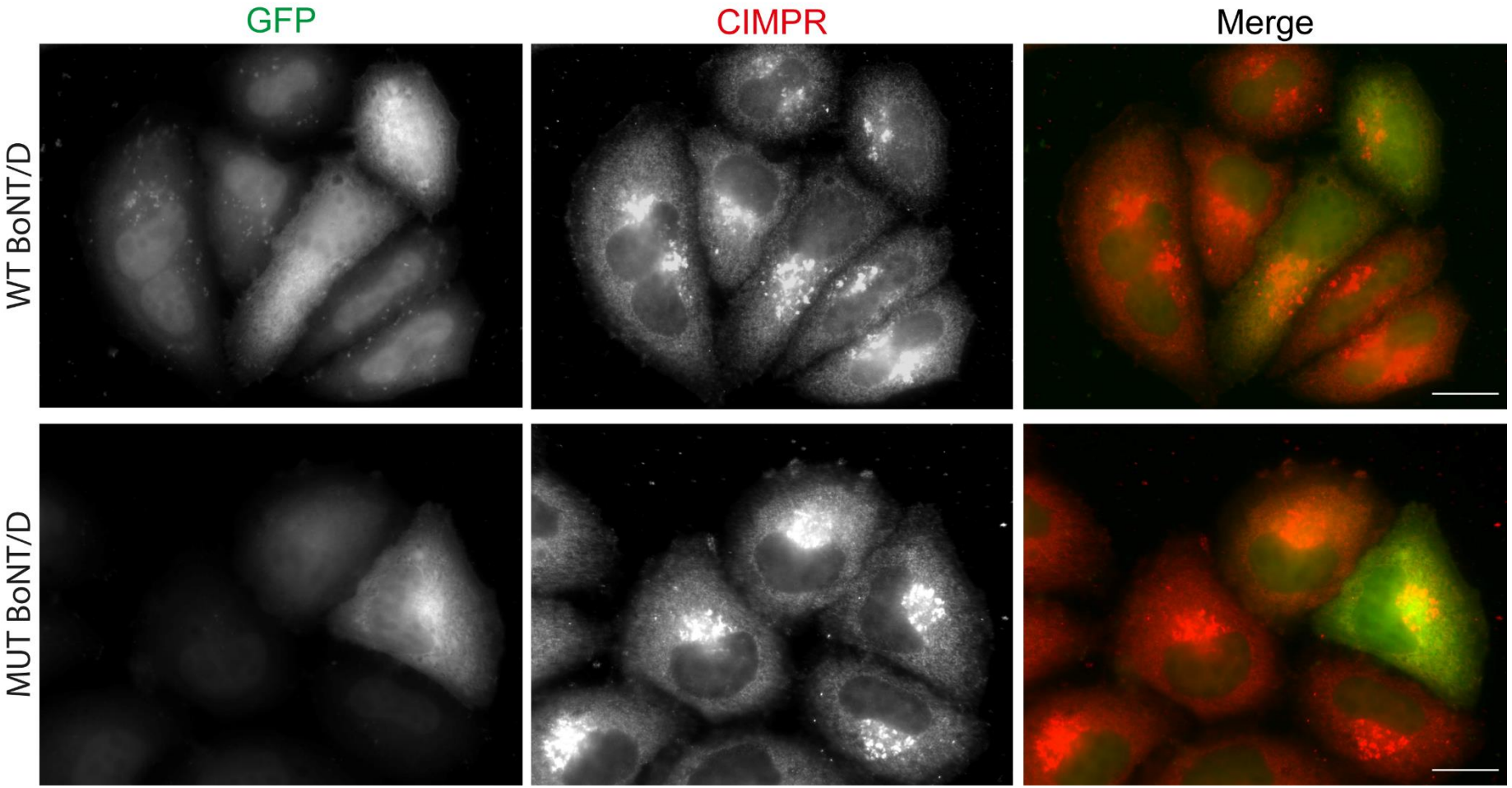
GFP
CIMPR
Merge
WT BoNT/D
MUT BoNT/D

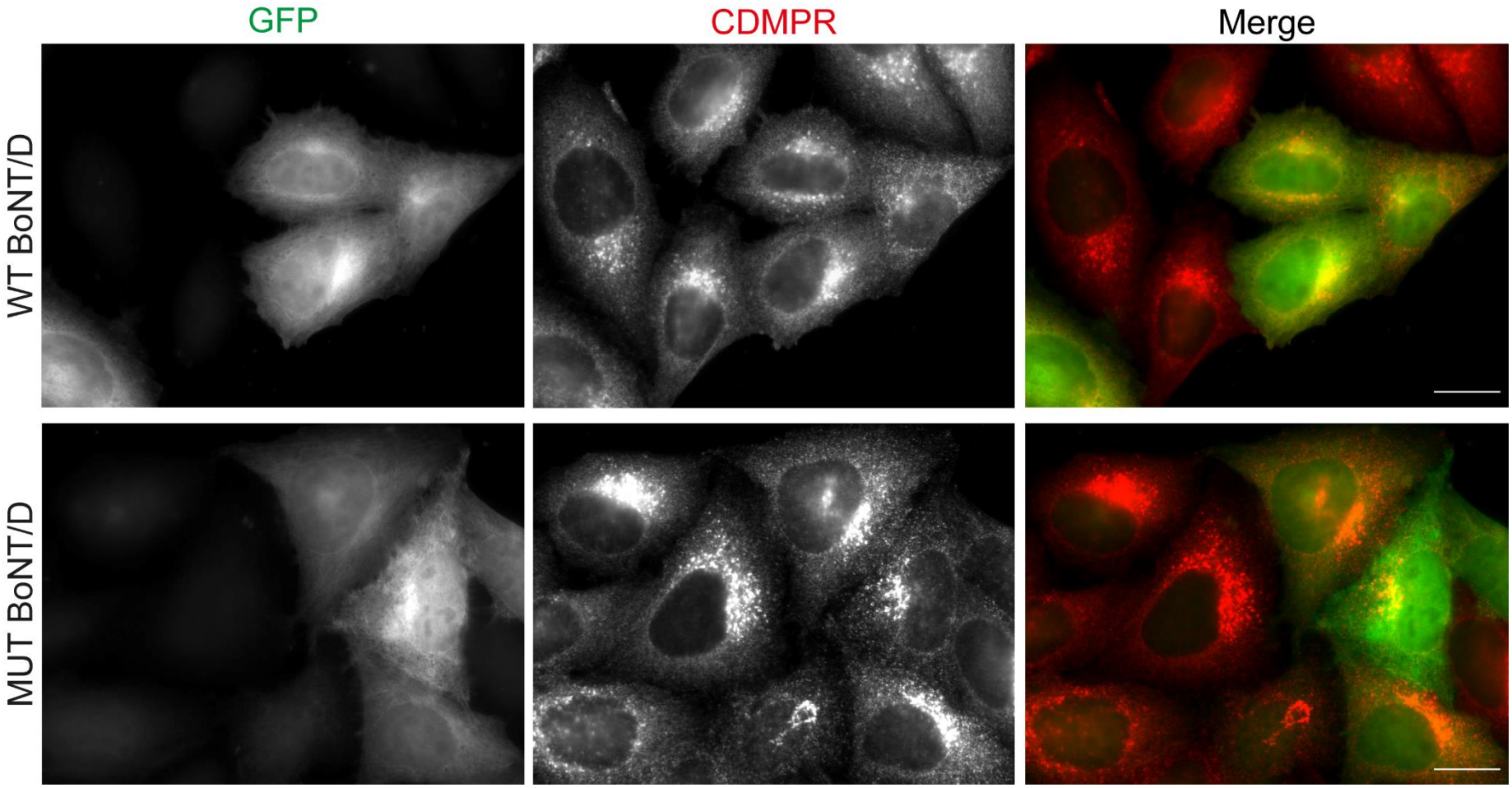
GFP
CDMPR
Merge
WT BoNT/D
MUT BoNT/D

Supplemental Figure 2 Cleave-resistant VAMP3 mutants showed some VAMP3 expression in BoNT/X transfected HeLa-M cells.

A) Schematic of mutated VAMP3 cleavage site on the SNARE motif, where the peptide sequence R66-A67 was substituted with VW. This HA-tagged mutant VAMP3 construct was expressed on the pEGFP-C3 backbone.

B) HeLa-M cells were transiently transfected with pEGFP-HA-mutant VAMP3 construct using PEI and incubated overnight. Scale bar 10 µm.

C) To determine whether VAMP3 expression could be recovered by a cleave-resistant VAMP3 mutant, HeLa-M cells were transiently co-transfected with either mcherry-tagged WT BoNT/X or mcherry-tagged MUT BoNT/X and pEGFP-HA-vwMUT VAMP3 overnight. Scale bar 10 µm.

(A)

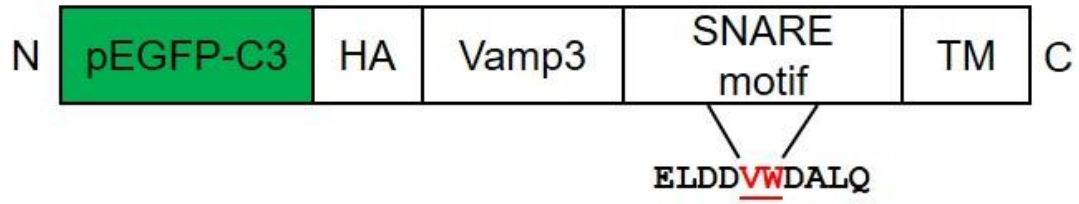

(B)

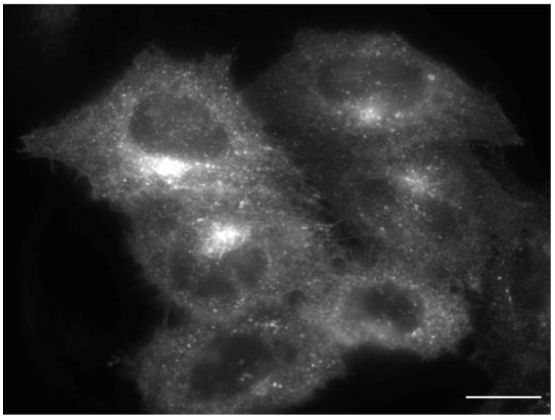

(C)

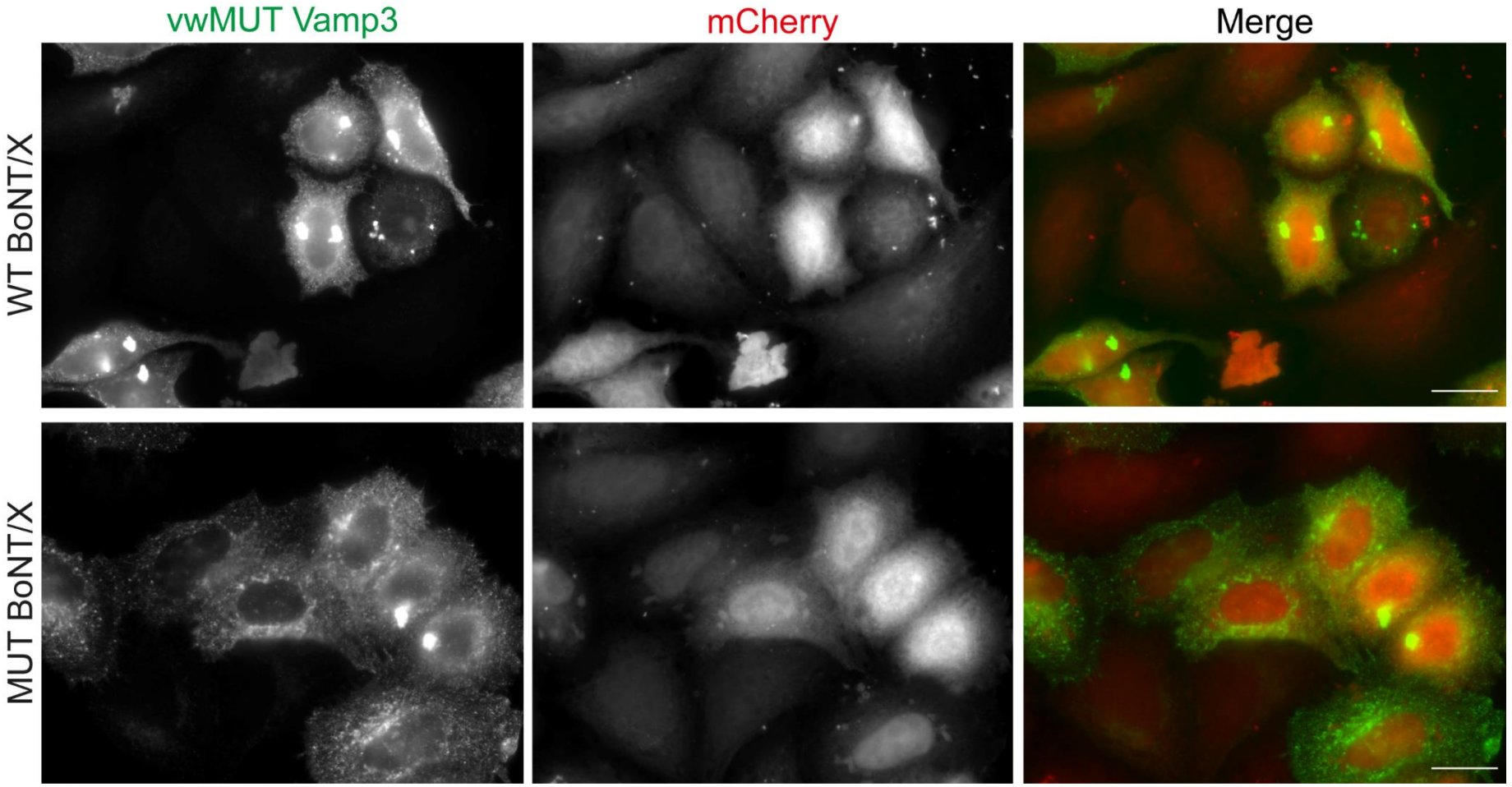

Supplemental Figure 3 Anchoring BoNT/X to different membranes.

(A) Schematic of plasmids created to anchor the WT and MUT BoNT/X light chain to the surface membrane protein. The top drawing shows the WT and MUT BoNT/X expressed with CD8 on a pIRESNeo vector. The bottom drawing shows WT and MUT BoNT/X expressed with an STX19 palmitoylation tail on a pEFGP vector backbone.

(B) Schematic of plasmids created to anchor the WT and MUT BoNT/X light chain to the endoplasmic reticulum membrane compartment expressed on a pEGFP vector backbone.

(C) HeLa-M cells were transiently transfected with the different constructs that anchor the BoNT/X light chain to different membrane locations.

(A)

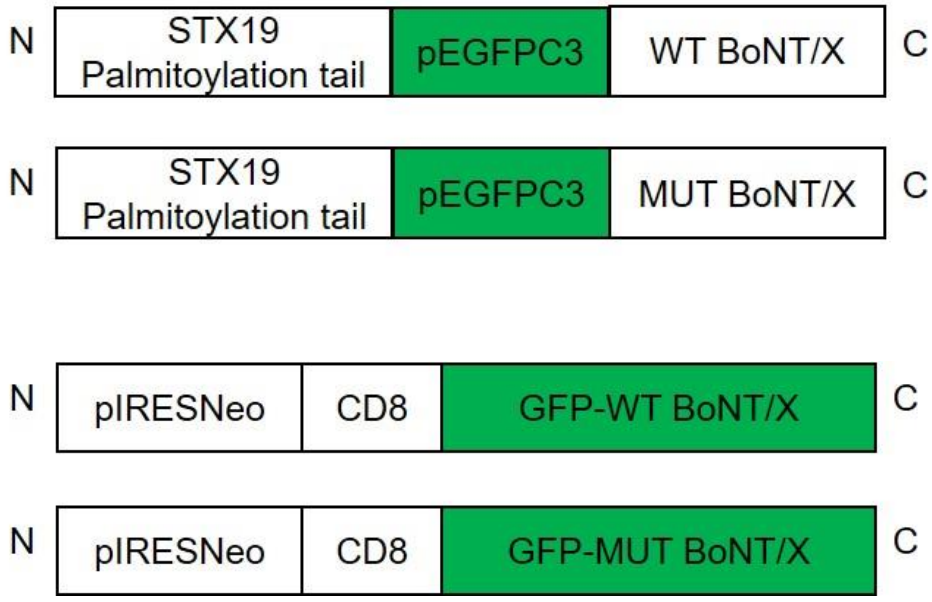
N
STX19
Palmitoylation tail
pEGFPC3
WT BoNT/X
C
N
STX19
Palmitoylation tail
pEGFPC3
MUT BoNT/X
C
N
pIRESNeo
CD8
GFP-WT BoNT/X
C
N
pIRESNeo
CD8
GFP-MUT BoNT/X
C

(B)

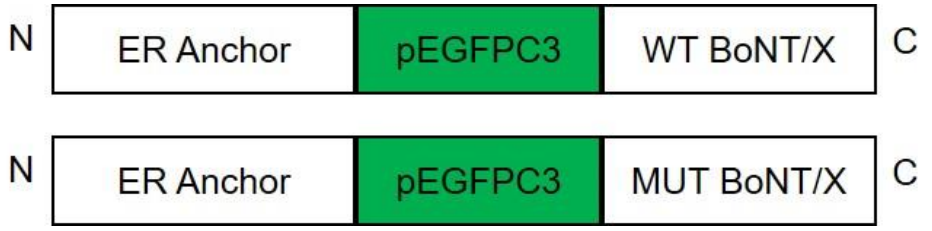
N
ER Anchor
pEGFPC3
WT BoNT/X
C
N
ER Anchor
pEGFPC3
MUT BoNT/X
C

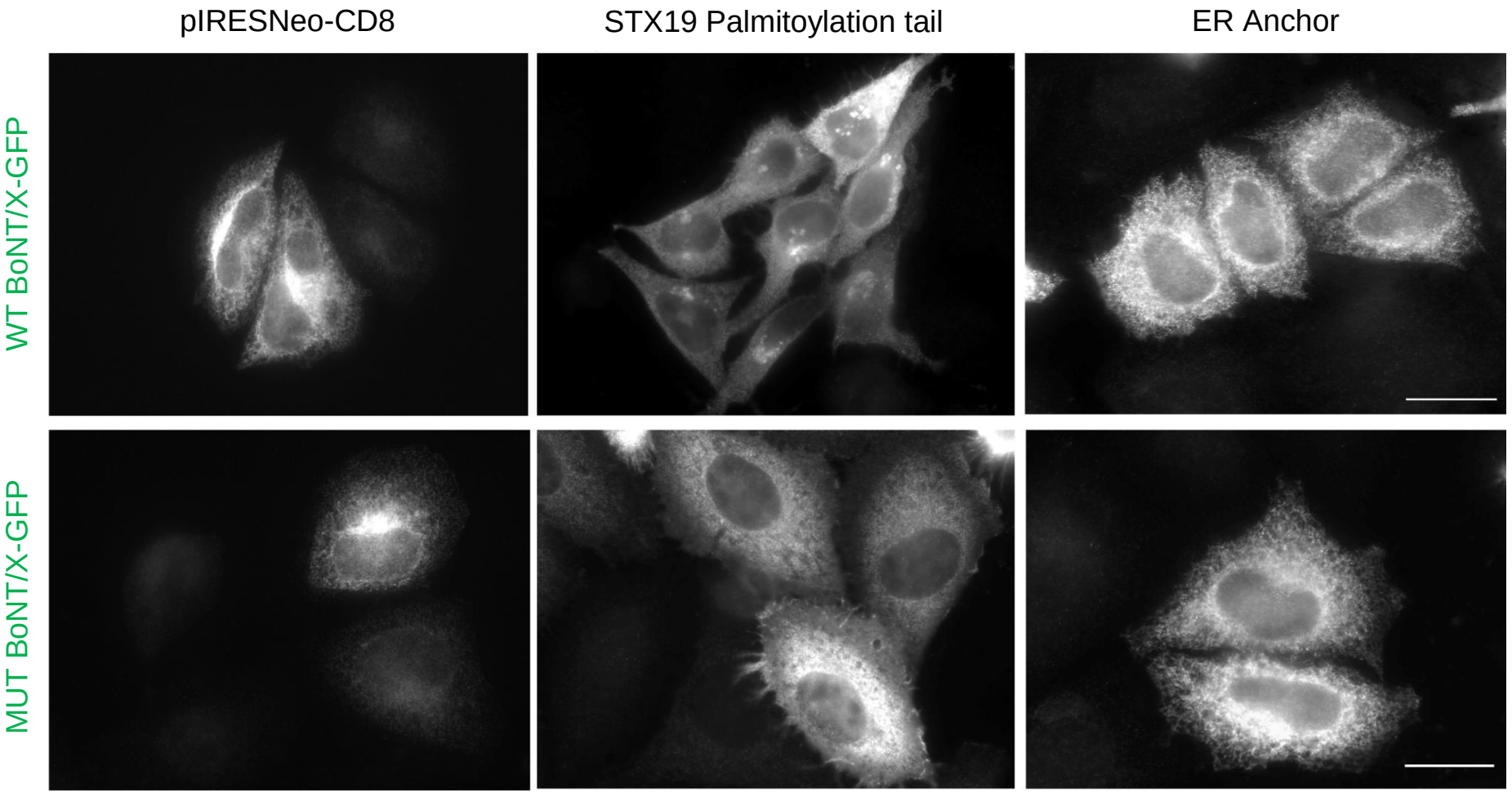
pIRESNeo-CD8
STX19 Palmitoylation tail
ER Anchor
WT BoNT/X-GFP
MUT BoNT/X-GFP

Bibliography

ADVANI, R. J., BAE, H.-R., BOCK, J. B., CHAO, D. S., DOUNG, Y.-C., PREKERIS, R., YOO, J.-S. & SCHELLER, R. H. 1998. Seven Novel Mammalian SNARE Proteins Localize to Distinct Membrane Compartments. *Journal of Biological Chemistry,* 273**,** 10317-10324.

ADVANI, R. J., YANG, B., PREKERIS, R., LEE, K. C., KLUMPERMAN, J. & SCHELLER, R. H. 1999. VAMP-7 mediates vesicular transport from endosomes to lysosomes. *The Journal of cell biology,* 146**,** 765-776.

AGUADO, F., GOMBAU, L., MAJÓ, G., MARSAL, J., BLANCO, J. & BLASI, J. 1997. Regulated Secretion Is Impaired in AtT-20 Endocrine Cells Stably Transfected with Botulinum Neurotoxin Type A Light Chain. *Journal of Biological Chemistry,* 272**,** 26005-26008.

ALLEN, L.-A. H., YANG, C. & PESSIN, J. E. 2002. Rate and extent of phagocytosis in macrophages lacking vamp3. *Journal of leukocyte biology,* 72**,** 217-221.

AND, R. C. L. & SCHELLER, R. H. 2000. Mechanisms of Synaptic Vesicle Exocytosis. *Annual Review of Cell and Developmental Biology,* 16**,** 19-49.

ARNON, S. S., SCHECHTER, R., INGLESBY, T. V., HENDERSON, D. A., BARTLETT, J. G., ASCHER, M. S., EITZEN, E., FINE, A. D., HAUER, J., LAYTON, M., LILLIBRIDGE, S., OSTERHOLM, M. T., O'TOOLE, T., PARKER, G., PERL, T. M., RUSSELL, P. K., SWERDLOW, D. L., TONAT, K. & BIODEFENSE, F. T. W. G. O. C. 2001. Botulinum Toxin as a Biological WeaponMedical and Public Health Management. *JAMA,* 285**,** 1059-1070.

ARSENAULT, J., CUIJPERS, S. A., FERRARI, E., NIRANJAN, D., RUST, A., LEESE, C., O'BRIEN, J. A., BINZ, T. & DAVLETOV, B. 2014. Botulinum protease-cleaved SNARE fragments induce cytotoxicity in neuroblastoma cells. *J Neurochem,* 129**,** 781-91.

ARSENAULT, J., FERRARI, E., NIRANJAN, D., CUIJPERS, S. A. G., GU, C., VALLIS, Y., O'BRIEN, J. & DAVLETOV, B. 2013. Stapling of the botulinum type A protease to growth factors and neuropeptides allows selective targeting of neuroendocrine cells. *Journal of Neurochemistry,* 126**,** 223-233.

AUGUSTIN, I., ROSENMUND, C., SÜDHOF, T. C. & BROSE, N. 1999. Munc13-1 is essential for fusion competence of glutamatergic synaptic vesicles. *Nature,* 400**,** 457-461.

AURELI, P., FENICIA, L., PASOLINI, B., GIANFRANCESCHI, M., MCCROSKEY, L. M. & HATHEWAY, C. L. 1986. Two Cases of Type E Infant Botulism Caused by Neurotoxigenic Clostridium butyricum in Italy. *The Journal of Infectious Diseases,* 154**,** 207-211.

BADE, S., RUMMEL, A., REISINGER, C., KARNATH, T., AHNERT-HILGER, G., BIGALKE, H. & BINZ, T. 2004. Botulinum neurotoxin type D enables cytosolic delivery of enzymatically active cargo proteins to neurones via unfolded translocation intermediates. 91**,** 1461-1472.

BAKER, R. W., JEFFREY, P. D., ZICK, M., PHILLIPS, B. P., WICKNER, W. T. & HUGHSON, F. M. 2015. A direct role for the Sec1/Munc18-family protein Vps33 as a template for SNARE assembly. *Science,* 349**,** 1111-1114.

BALCH, W. E., DUNPHY, W. G., BRAELL, W. A. & ROTHMAN, J. E. 1984. Reconstitution of the transport of protein between successive compartments of the Golgi measured by the coupled incorporation of N-acetylglucosamine. *Cell,* 39**,** 405-16.

BANASZYNSKI, L. A., CHEN, L.-C., MAYNARD-SMITH, L. A., OOI, A. G. L. & WANDLESS, T. J. 2006. A rapid, reversible, and tunable method to regulate protein function in living cells using synthetic small molecules. *Cell,* 126**,** 995-1004.

BAS, L., PAPINSKI, D., LICHEVA, M., TORGGLER, R., ROHRINGER, S., SCHUSCHNIG, M. & KRAFT, C. 2018. Reconstitution reveals Ykt6 as the autophagosomal SNARE in autophagosome-vacuole fusion. *J Cell Biol,* 217**,** 3656-3669.

BAUMERT, M., MAYCOX, P. R., NAVONE, F., DE CAMILLI, P. & JAHN, R. 1989. Synaptobrevin: an integral membrane protein of 18,000 daltons present in small synaptic vesicles of rat brain. *The EMBO journal,* 8**,** 379-384.

BECKERS, C. J. M., BLOCK, M. R., GLICK, B. S., ROTHMAN, J. E. & BALCH, W. E. 1989. Vesicular transport between the endoplasmic reticulum and the Golgi stack requires the NEM-sensitive fusion protein. *Nature,* 339**,** 397-398.

BEHRENDORFF, N., DOLAI, S., HONG, W., GAISANO, H. Y. & THORN, P. 2011. Vesicle-associated membrane protein 8 (VAMP8) is a SNARE (soluble N-ethylmaleimide-sensitive factor attachment protein receptor) selectively required for sequential granule-to-granule fusion. *The Journal of biological chemistry,* 286**,** 29627-29634.

BENNETT, M., CALAKOS, N. & SCHELLER, R. 1992. Syntaxin: a synaptic protein implicated in docking of synaptic vesicles at presynaptic active zones. 257**,** 255-259.

BETHANI, I., WERNER, A., KADIAN, C., GEUMANN, U., JAHN, R. & RIZZOLI, S. O. 2009. Endosomal Fusion upon SNARE Knockdown is Maintained by Residual SNARE Activity and Enhanced Docking. *Traffic,* 10**,** 1543-1559.

BINZ, T. 2013. Clostridial neurotoxin light chains: devices for SNARE cleavage mediated blockade of neurotransmission. *Curr Top Microbiol Immunol,* 364**,** 139-57.

BINZ, T. & RUMMEL, A. 2009a. Cell entry strategy of clostridial neurotoxins. 109**,** 1584-1595.

BINZ, T. & RUMMEL, A. 2009b. Cell entry strategy of clostridial neurotoxins. *J Neurochem,* 109**,** 1584-95.

BLASI, J., CHAPMAN, E. R., LINK, E., BINZ, T., YAMASAKI, S., DE CAMILLI, P., SÜDHOF, T. C., NIEMANN, H. & JAHN, R. 1993. Botulinum neurotoxin A selectively cleaves the synaptic protein SNAP-25. *Nature,* 365**,** 160-3.

BLOCK, M. R., GLICK, B. S., WILCOX, C. A., WIELAND, F. T. & ROTHMAN, J. E. 1988a. Purification of an N-ethylmaleimide-sensitive protein catalyzing vesicular transport. 85**,** 7852-7856.

BLOCK, M. R., GLICK, B. S., WILCOX, C. A., WIELAND, F. T. & ROTHMAN, J. E. 1988b. Purification of an N-ethylmaleimide-sensitive protein catalyzing vesicular transport. *Proceedings of the National Academy of Sciences,* 85**,** 7852-7856.

BOCK, J. B., MATERN, H. T., PEDEN, A. A. & SCHELLER, R. H. 2001. A genomic perspective on membrane compartment organization. *Nature,* 409**,** 839-841.
BOMBARDIER, J. P. & MUNSON, M. 2015. Three steps forward, two steps back: mechanistic insights into the assembly and disassembly of the SNARE complex. *Current opinion in chemical biology,* 29**,** 66-71.
BONFANTI, L., MIRONOV, A. A., JR., MARTÍNEZ-MENÁRGUEZ, J. A., MARTELLA, O., FUSELLA, A., BALDASSARRE, M., BUCCIONE, R., GEUZE, H. J., MIRONOV, A. A., JR. & LUINI, A. 1998. Procollagen Traverses the Golgi Stack without Leaving the Lumen of Cisternae: Evidence for Cisternal Maturation. *Cell,* 95**,** 993-1003.
BONIFACINO, J. S. & GLICK, B. S. 2004. The mechanisms of vesicle budding and fusion. *Cell,* 116**,** 153-66.
BRANDHORST, D., ZWILLING, D., RIZZOLI, S. O., LIPPERT, U., LANG, T. & JAHN, R. 2006. Homotypic fusion of early endosomes: SNAREs do not determine fusion specificity. 103**,** 2701-2706.
BRÖCKER, C., ENGELBRECHT-VANDRÉ, S. & UNGERMANN, C. 2010. Multisubunit Tethering Complexes and Their Role in Membrane Fusion. *Current Biology,* 20**,** R943-R952.
BROOKS, V. B., CURTIS, D. R. & ECCLES, J. C. 1955. Mode of action of tetanus toxin. *Nature,* 175**,** 120-1.
BRUNT, J., CARTER, A. T., STRINGER, S. C. & PECK, M. W. 2018. Identification of a novel botulinum neurotoxin gene cluster in Enterococcus. 592**,** 310-317.
CALDERWOOD, D. A. 2004. Integrin activation. *Journal of Cell Science,* 117**,** 657-666.
CALZOLARI, A., LAROCCA, L. M., DEAGLIO, S., FINISGUERRA, V., BOE, A., RAGGI, C., RICCI-VITANI, L., PIERCONTI, F., MALAVASI, F., DE MARIA, R., TESTA, U. & PALLINI, R. 2010. Transferrin receptor 2 is frequently and highly expressed in glioblastomas. *Translational oncology,* 3**,** 123-134.
CARR, C. M. & RIZO, J. 2010. At the junction of SNARE and SM protein function. *Current Opinion in Cell Biology,* 22**,** 488-495.
CAVALIER-SMITH, T. 1975. The origin of nuclei and of eukaryotic cells. *Nature,* 256**,** 463-468.
CAVALIER-SMITH, T. 1987. The origin of eukaryotic and archaebacterial cells. *Ann N Y Acad Sci,* 503**,** 17-54.
CHEN, S. & BARBIERI, J. T. 2009. Engineering botulinum neurotoxin to extend therapeutic intervention. *Proceedings of the National Academy of Sciences of the United States of America,* 106**,** 9180-9184.
CHEN, X., TOMCHICK, D. R., KOVRIGIN, E., ARAÇ, D., MACHIUS, M., SÜDHOF, T. C. & RIZO, J. 2002. Three-Dimensional Structure of the Complexin/SNARE Complex. *Neuron,* 33**,** 397-409.
COCUCCI, E., RACCHETTI, G., RUPNIK, M. & MELDOLESI, J. 2008. The regulated exocytosis of enlargeosomes is mediated by a SNARE machinery that includes VAMP4. 121**,** 2983-2991.
COSEN-BINKER, L. I., BINKER, M. G., WANG, C.-C., HONG, W. & GAISANO, H. Y. 2008. VAMP8 is the v-SNARE that mediates basolateral exocytosis in a

mouse model of alcoholic pancreatitis. *The Journal of Clinical Investigation,* 118**,** 2535-2551.
CRAIK, CHARLES S., PAGE, MICHAEL J. & MADISON, EDWIN L. 2011. Proteases as therapeutics. *Biochemical Journal,* 435**,** 1-16.
CROSS, J. A. & DODDING, M. P. 2019. Motor–cargo adaptors at the organelle–cytoskeleton interface. *Current Opinion in Cell Biology,* 59**,** 16-23.
D'SOUZA-SCHOREY, C. & CHAVRIER, P. 2006. ARF proteins: roles in membrane traffic and beyond. *Nature Reviews Molecular Cell Biology,* 7**,** 347-358.
DAHMS, N. M., OLSON, L. J. & KIM, J. J. 2008. Strategies for carbohydrate recognition by the mannose 6-phosphate receptors. *Glycobiology,* 18**,** 664-78.
DASTE, F., GALLI, T. & TARESTE, D. 2015a. Structure and function of longin SNAREs. *Journal of Cell Science,* 128**,** 4263-4272.
DASTE, F., GALLI, T. & TARESTE, D. 2015b. Structure and function of longin SNAREs. 128**,** 4263-4272.
DE DUVE, C. 2007. The origin of eukaryotes: a reappraisal. *Nature Reviews Genetics,* 8**,** 395-403.
DEGTYAR, V., HAFEZ, I. M., BRAY, C. & ZUCKER, R. S. 2013. Dance of the SNAREs: assembly and rearrangements detected with FRET at neuronal synapses. *J Neurosci,* 33**,** 5507-23.
DIETRICH, L. E., PEPLOWSKA, K., LAGRASSA, T. J., HOU, H., ROHDE, J. & UNGERMANN, C. 2005. The SNARE Ykt6 is released from yeast vacuoles during an early stage of fusion. *EMBO Rep,* 6**,** 245-50.
DIETRICH, L. E. P., BOEDDINGHAUS, C., LAGRASSA, T. J. & UNGERMANN, C. 2003. Control of eukaryotic membrane fusion by N-terminal domains of SNARE proteins. *Biochimica et Biophysica Acta (BBA) - Molecular Cell Research,* 1641**,** 111-119.
DILCHER, M., KÖHLER, B. & VON MOLLARD, G. F. 2001. Genetic interactions with the yeast Q-SNARE VTI1 reveal novel functions for the R-SNARE YKT6. *J Biol Chem,* 276**,** 34537-44.
DUGGAN, M. J., QUINN, C. P., CHADDOCK, J. A., PURKISS, J. R., ALEXANDER, F. C. G., DOWARD, S., FOOKS, S. J., FRIIS, L. M., HALL, Y. H. J., KIRBY, E. R., LEEDS, N., MOULSDALE, H. J., DICKENSON, A., GREEN, G. M., RAHMAN, W., SUZUKI, R., SHONE, C. C. & FOSTER, K. A. 2002. Inhibition of Release of Neurotransmitters from Rat Dorsal Root Ganglia by a Novel Conjugate of a Clostridium botulinumToxin A Endopeptidase Fragment and Erythrina cristagalliLectin. *Journal of Biological Chemistry,* 277**,** 34846-34852.
EDUPUGANTI, O. P., OVSEPIAN, S. V., WANG, J., ZURAWSKI, T. H., SCHMIDT, J. J., SMITH, L., LAWRENCE, G. W. & DOLLY, J. O. 2012. Targeted delivery into motor nerve terminals of inhibitors for SNARE-cleaving proteases via liposomes coupled to an atoxic botulinum neurotoxin. 279**,** 2555-2567.
FADER, C. M., SÁNCHEZ, D. G., MESTRE, M. B. & COLOMBO, M. I. 2009. TI-VAMP/VAMP7 and VAMP3/cellubrevin: two v-SNARE proteins involved in specific steps of the autophagy/multivesicular body pathways. *Biochimica et Biophysica Acta (BBA) - Molecular Cell Research,* 1793**,** 1901-1916.

FASSHAUER, D., SUTTON, R. B., BRUNGER, A. T. & JAHN, R. 1998. Conserved structural features of the synaptic fusion complex: SNARE proteins reclassified as Q- and R-SNAREs. *Proceedings of the National Academy of Sciences of the United States of America,* 95**,** 15781-15786.

FENG, D., CRANE, K., ROZENVAYN, N., DVORAK, A. M. & FLAUMENHAFT, R. 2002. Subcellular distribution of 3 functional platelet SNARE proteins: human cellubrevin, SNAP-23, and syntaxin 2. *Blood,* 99**,** 4006-4014.

FERRO-NOVICK, S. & BROSE, N. 2013. Traffic control system within cells. *Nature,* 504**,** 98-98.

FIELDS, I. C., SHTEYN, E., PYPAERT, M., PROUX-GILLARDEAUX, V., KANG, R. S., GALLI, T. & FÖLSCH, H. 2007. v-SNARE cellubrevin is required for basolateral sorting of AP-1B-dependent cargo in polarized epithelial cells. *The Journal of cell biology,* 177**,** 477-488.

FISCHER, A. 2013. Synchronized chaperone function of botulinum neurotoxin domains mediates light chain translocation into neurons. *Curr Top Microbiol Immunol,* 364**,** 115-37.

FONFRIA, E., DONALD, S. & CADD, V. A. 2016. Botulinum neurotoxin A and an engineered derivate targeted secretion inhibitor (TSI) A enter cells via different vesicular compartments. *Journal of Receptors and Signal Transduction,* 36**,** 79-88.

FRANK, S. P. C., THON, K.-P., BISCHOFF, S. C. & LORENTZ, A. 2011. SNAP-23 and syntaxin-3 are required for chemokine release by mature human mast cells. *Molecular Immunology,* 49**,** 353-358.

FRIEND , D. S. & FARQUHAR , M. G. 1967. FUNCTIONS OF COATED VESICLES DURING PROTEIN ABSORPTION IN THE RAT VAS DEFERENS. *The Journal of Cell Biology,* 35**,** 357-376.

FUKASAWA, M., VARLAMOV, O., ENG, W. S., SÖLLNER, T. H. & ROTHMAN, J. E. 2004. Localization and activity of the SNARE Ykt6 determined by its regulatory domain and palmitoylation. *Proceedings of the National Academy of Sciences of the United States of America,* 101**,** 4815-4820.

GALLI, T., CHILCOTE, T., MUNDIGL, O., BINZ, T., NIEMANN, H. & DE CAMILLI, P. 1994. Tetanus toxin-mediated cleavage of cellubrevin impairs exocytosis of transferrin receptor-containing vesicles in CHO cells. *Journal of Cell Biology,* 125**,** 1015-1024.

GANLEY , I. G., ESPINOSA , E. & PFEFFER , S. R. 2008. A syntaxin 10–SNARE complex distinguishes two distinct transport routes from endosomes to the trans-Golgi in human cells. *Journal of Cell Biology,* 180**,** 159-172.

GIMENEZ, D. F. & CICCARELLI, A. S. 1970. Another type of Clostridium botulinum. *Zentralbl Bakteriol Orig,* 215**,** 221-4.

GONZALEZ, L. C., WEIS, W. I. & SCHELLER, R. H. 2001. A Novel SNARE N-terminal Domain Revealed by the Crystal Structure of Sec22b. 276**,** 24203-24211.

GORDON, D. E., BOND, L. M., SAHLENDER, D. A. & PEDEN, A. A. 2010a. A Targeted siRNA Screen to Identify SNAREs Required for Constitutive Secretion in Mammalian Cells. 11**,** 1191-1204.

GORDON, D. E., BOND, L. M., SAHLENDER, D. A. & PEDEN, A. A. 2010b. A Targeted siRNA Screen to Identify SNAREs Required for Constitutive Secretion in Mammalian Cells. *Traffic,* 11**,** 1191-1204.
GORDON, D. E., CHIA, J., JAYAWARDENA, K., ANTROBUS, R., BARD, F. & PEDEN, A. A. 2017. VAMP3/Syb and YKT6 are required for the fusion of constitutive secretory carriers with the plasma membrane. *PLOS Genetics,* 13**,** e1006698.
GORDON, D. E., MIRZA, M., SAHLENDER, D. A., JAKOVLESKA, J. & PEDEN, A. A. 2009. Coiled-coil interactions are required for post-Golgi R-SNARE trafficking. *EMBO reports,* 10**,** 851-856.
GRABSKI, R., HAY, J. & SZTUL, E. 2012. Tethering factor P115: a new model for tether-SNARE interactions. *Bioarchitecture,* 2**,** 175-180.
GRANDO, S. A. & ZACHARY, C. B. 2018. The non-neuronal and nonmuscular effects of botulinum toxin: an opportunity for a deadly molecule to treat disease in the skin and beyond. *British Journal of Dermatology,* 178**,** 1011-1019.
GRANT, B. D. & DONALDSON, J. G. 2009. Pathways and mechanisms of endocytic recycling. *Nature Reviews Molecular Cell Biology,* 10**,** 597-608.
GROSS, J. C., CHAUDHARY, V., BARTSCHERER, K. & BOUTROS, M. 2012. Active Wnt proteins are secreted on exosomes. *Nat Cell Biol,* 14**,** 1036-45.
GUO, J. & CHEN, S. 2013. Unique Substrate Recognition Mechanism of the Botulinum Neurotoxin D Light Chain. 288**,** 27881-27887.
GUO, W., GRANT, A. & NOVICK, P. 1999. Exo84p Is an Exocyst Protein Essential for Secretion. 274**,** 23558-23564.
GUPTA, R. S. & BRIAN GOLDING, G. 1996. The origin of the eukaryotic cell. *Trends in Biochemical Sciences,* 21**,** 166-171.
HALL, J. D., MCCROSKEY, L. M., PINCOMB, B. J. & HATHEWAY, C. L. 1985. Isolation of an organism resembling Clostridium barati which produces type F botulinal toxin from an infant with botulism. *Journal of clinical microbiology,* 21**,** 654-655.
HALLETT, M., ALBANESE, A., DRESSLER, D., SEGAL, K. R., SIMPSON, D. M., TRUONG, D. & JANKOVIC, J. 2013. Evidence-based review and assessment of botulinum neurotoxin for the treatment of movement disorders. *Toxicon,* 67**,** 94-114.
HASEGAWA, H., YANG, Z., OLTEDAL, L., DAVANGER, S. & HAY, J. C. 2004. Intramolecular protein-protein and protein-lipid interactions control the conformation and subcellular targeting of neuronal Ykt6. *Journal of Cell Science,* 117**,** 4495-4508.
HASEGAWA, H., ZINSSER, S., RHEE, Y., VIK-MO, E. O., DAVANGER, S. & HAY, J. C. 2003. Mammalian ykt6 is a neuronal SNARE targeted to a specialized compartment by its profilin-like amino terminal domain. *Mol Biol Cell,* 14**,** 698-720.
HATHEWAY, C. L. 1994. Immunogenicity of the neurotoxins of Clostridium botulinum. *Therapy with Botulinum Toxin***,** 93-107.
HE, B. & GUO, W. 2009. The exocyst complex in polarized exocytosis. *Current opinion in cell biology,* 21**,** 537-542.

HILL, K. K., SMITH, T. J., HELMA, C. H., TICKNOR, L. O., FOLEY, B. T., SVENSSON, R. T., BROWN, J. L., JOHNSON, E. A., SMITH, L. A., OKINAKA, R. T., JACKSON, P. J. & MARKS, J. D. 2007. Genetic diversity among Botulinum Neurotoxin-producing clostridial strains. *Journal of bacteriology,* 189**,** 818-832.

HONG, W. 2005. SNAREs and traffic. *Biochimica et Biophysica Acta (BBA) - Molecular Cell Research,* 1744**,** 120-144.

HONG, W. & LEV, S. 2014. Tethering the assembly of SNARE complexes. *Trends in Cell Biology,* 24**,** 35-43.

HOOGSTRAATEN, R. I., VAN KEIMPEMA, L., TOONEN, R. F. & VERHAGE, M. 2020. Tetanus insensitive VAMP2 differentially restores synaptic and dense core vesicle fusion in tetanus neurotoxin treated neurons. *Scientific Reports,* 10**,** 10913.

HOPKINS, C. R. 1983. Intracellular routing of transferrin and transferrin receptors in epidermoid carcinoma A431 cells. *Cell,* 35**,** 321-30.

HUMPHRIES, J. D., BYRON, A. & HUMPHRIES, M. J. 2006. Integrin ligands at a glance. *Journal of Cell Science,* 119**,** 3901-3903.

HUSS, M. & WIECZOREK, H. 2009. Inhibitors of V-ATPases: old and new players. *Journal of Experimental Biology,* 212**,** 341-346.

IKEZAWA, M., TAJIKA, Y., UENO, H., MURAKAMI, T., INOUE, N. & YORIFUJI, H. 2018. Loss of VAMP5 in mice results in duplication of the ureter and insufficient expansion of the lung. *Developmental Dynamics,* 247**,** 754-762.

JAHN, R., LANG, T. & SÜDHOF, T. C. 2003. Membrane fusion. *Cell,* 112**,** 519-33.

JAHN, R. & SCHELLER, R. H. 2006. SNAREs — engines for membrane fusion. *Nature Reviews Molecular Cell Biology,* 7**,** 631-643.

JANKOVIC, J. 2017. Botulinum toxin: State of the art. 32**,** 1131-1138.

JÉKELY, G. 2003. Small GTPases and the evolution of the eukaryotic cell. *BioEssays,* 25**,** 1129-1138.

JOHNSON, E. A. & MONTECUCCO, C. 2008. Chapter 11 Botulism. *Handbook of Clinical Neurology.* Elsevier.

JOHNSON, E. S., GONDA, D. K. & VARSHAVSKY, A. 1990. Cis-trans recognition and subunit-specific degradation of short-lived proteins. *Nature,* 346**,** 287-291.

JOSHI, S., BANERJEE, M., ZHANG, J., KESARAJU, A., POKROVSKAYA, I. D., STORRIE, B. & WHITEHEART, S. W. 2018. Alterations in platelet secretion differentially affect thrombosis and hemostasis. *Blood advances,* 2**,** 2187-2198.

JUN, Y. & WICKNER, W. 2019. Sec17 (α-SNAP) and Sec18 (NSF) restrict membrane fusion to R-SNAREs, Q-SNAREs, and SM proteins from identical compartments. *Proceedings of the National Academy of Sciences,* 116**,** 23573-23581.

KAISER, C. A. & SCHEKMAN, R. 1990. Distinct sets of SEC genes govern transport vesicle formation and fusion early in the secretory pathway. *Cell,* 61**,** 723-733.

KAKINUMA, H., MARUYAMA, H., TAKAHASHI, H., YAMAKAWA, K. & NAKAMURA, S. 1996. The first case of type B infant botulism in Japan. 38**,** 541-543.

KEAN, M. J., WILLIAMS, K. C., SKALSKI, M., MYERS, D., BURTNIK, A., FOSTER, D. & COPPOLINO, M. G. 2009. VAMP3, syntaxin-13 and SNAP23 are involved in secretion of matrix metalloproteinases, degradation of the extracellular matrix and cell invasion. *Journal of Cell Science,* 122**,** 4089-4098.

KISS, A. L. & BOTOS, E. 2009. Endocytosis via caveolae: alternative pathway with distinct cellular compartments to avoid lysosomal degradation? *Journal of cellular and molecular medicine,* 13**,** 1228-1237.

KIYATKIN, N., MAKSYMOWYCH, A. B. & SIMPSON, L. L. 1997. Induction of an immune response by oral administration of recombinant botulinum toxin. *Infection and immunity,* 65**,** 4586-4591.

KLOEPPER, T. H., KIENLE, C. N. & FASSHAUER, D. 2007. An elaborate classification of SNARE proteins sheds light on the conservation of the eukaryotic endomembrane system. *Molecular biology of the cell,* 18**,** 3463-3471.

KWEON, Y., ROTHE, A., CONIBEAR, E. & STEVENS, T. H. 2003. Ykt6p is a multifunctional yeast R-SNARE that is required for multiple membrane transport pathways to the vacuole. *Mol Biol Cell,* 14**,** 1868-81.

LAUFMAN, O., HONG, W. & LEV, S. 2013. The COG complex interacts with multiple Golgi SNAREs and enhances fusogenic assembly of SNARE complexes. 126**,** 1506-1516.

LEGGETT, J., HARPER, E., WAITE, E., MARKS, P., MARTINEZ, A. & LIGHTMAN, S. 2013. GHRH receptor-targeted botulinum neurotoxin selectively inhibits pulsatile GH secretion in male rats. *Endocrinology,* 154**,** 3305-18.

LOW, S. H., LI, X., MIURA, M., KUDO, N., QUIÑONES, B. & WEIMBS, T. 2003. Syntaxin 2 and Endobrevin Are Required for the Terminal Step of Cytokinesis in Mammalian Cells. *Developmental Cell,* 4**,** 753-759.

LUFTMAN, K., HASAN, N., DAY, P., HARDEE, D. & HU, C. 2009. Silencing of VAMP3 inhibits cell migration and integrin-mediated adhesion. *Biochemical and Biophysical Research Communications,* 380**,** 65-70.

LUO, G., ZHANG, J. & GUO, W. 2014. The role of Sec3p in secretory vesicle targeting and exocyst complex assembly. *Mol Biol Cell,* 25**,** 3813-22.

MA, H., MENG, J., WANG, J., HEARTY, S., DOLLY, J. O. & O'KENNEDY, R. 2014. Targeted delivery of a SNARE protease to sensory neurons using a single chain antibody (scFv) against the extracellular domain of P2X3 inhibits the release of a pain mediator. *Biochemical Journal,* 462**,** 247-256.

MACDONALD, C., MUNSON, M. & BRYANT, N. J. 2010. Autoinhibition of SNARE complex assembly by a conformational switch represents a conserved feature of syntaxins. *Biochemical Society transactions,* 38**,** 209-212.

MALHOTRA, V., ORCI, L., GLICK, B. S., BLOCK, M. R. & ROTHMAN, J. E. 1988. Role of an N-ethylmaleimide-sensitive transport component in promoting fusion of transport vesicles with cisternae of the Golgi stack. *Cell,* 54**,** 221-227.

MALHOTRA, V., SERAFINI, T., ORCI, L., SHEPHERD, J. C. & ROTHMAN, J. E. 1989. Purification of a novel class of coated vesicles mediating biosynthetic protein transport through the Golgi stack. *Cell,* 58**,** 329-336.

MALLARD , F. D. R., TANG , B. L., GALLI , T., TENZA , D. L., SAINT-POL , A. S., YUE , X., ANTONY , C., HONG , W., GOUD , B. & JOHANNES , L. 2002. Early/recycling endosomes-to-TGN transport involves two SNARE complexes and a Rab6 isoform. *Journal of Cell Biology,* 156**,** 653-664.
MANCIAS, J. D. & GOLDBERG, J. 2007. The Transport Signal on Sec22 for Packaging into COPII-Coated Vesicles Is a Conformational Epitope. *Molecular Cell,* 26**,** 403-414.
MANSFIELD, M. J., ADAMS, J. B. & DOXEY, A. C. 2015. Botulinum neurotoxin homologs in non-Clostridium species. 589**,** 342-348.
MARTIN, W. & MÜLLER, M. 1998. The hydrogen hypothesis for the first eukaryote. *Nature,* 392**,** 37-41.
MARTINEZ-ARCA, S., RUDGE, R., VACCA, M., RAPOSO, G., CAMONIS, J., PROUX-GILLARDEAUX, V., DAVIET, L., FORMSTECHER, E., HAMBURGER, A., FILIPPINI, F., D'ESPOSITO, M. & GALLI, T. 2003. A dual mechanism controlling the localization and function of exocytic v-SNAREs. *Proceedings of the National Academy of Sciences of the United States of America,* 100**,** 9011-9016.
MASUYER, G., ZHANG, S., BARKHO, S., SHEN, Y., HENRIKSSON, L., KOŠENINA, S., DONG, M. & STENMARK, P. 2018. Structural characterisation of the catalytic domain of botulinum neurotoxin X - high activity and unique substrate specificity. *Scientific Reports,* 8**,** 4518.
MATSUI, T., JIANG, P., NAKANO, S., SAKAMAKI, Y., YAMAMOTO, H. & MIZUSHIMA, N. 2018. Autophagosomal YKT6 is required for fusion with lysosomes independently of syntaxin 17. *J Cell Biol,* 217**,** 2633-2645.
MAXFIELD, F. R. & MCGRAW, T. E. 2004. Endocytic recycling. *Nat Rev Mol Cell Biol,* 5**,** 121-32.
MAYLE, K. M., LE, A. M. & KAMEI, D. T. 2012. The intracellular trafficking pathway of transferrin. *Biochimica et biophysica acta,* 1820**,** 264-281.
MCCROSKEY, L. M., HATHEWAY, C. L., FENICIA, L., PASOLINI, B. & AURELI, P. 1986. Characterization of an organism that produces type E botulinal toxin but which resembles Clostridium butyricum from the feces of an infant with type E botulism. 23**,** 201-202.
MCMAHON, H. T. & MILLS, I. G. 2004. COP and clathrin-coated vesicle budding: different pathways, common approaches. *Curr Opin Cell Biol,* 16**,** 379-91.
MCMAHON, H. T., USHKARYOV, Y. A., EDELMANN, L., LINK, E., BINZ, T., NIEMANN, H., JAHN, R. & SÜDHOF, T. C. 1993. Cellubrevin is a ubiquitous tetanus-toxin substrate homologous to a putative synaptic vesicle fusion protein. *Nature,* 364**,** 346-349.
MCNEW, J. A., SOGAARD, M., LAMPEN, N. M., MACHIDA, S., YE, R. R., LACOMIS, L., TEMPST, P., ROTHMAN, J. E. & SÖLLNER, T. H. 1997. Ykt6p, a prenylated SNARE essential for endoplasmic reticulum-Golgi transport. *J Biol Chem,* 272**,** 17776-83.
MIMA, J., HICKEY, C. M., XU, H., JUN, Y. & WICKNER, W. 2008. Reconstituted membrane fusion requires regulatory lipids, SNAREs and synergistic SNARE chaperones. *Embo j,* 27**,** 2031-42.
MONTAGNAC, G., ECHARD, A. & CHAVRIER, P. 2008. Endocytic traffic in animal cell cytokinesis. *Current Opinion in Cell Biology,* 20**,** 454-461.

MONTAL, M. 2010. Botulinum Neurotoxin: A Marvel of Protein Design. 79**,** 591-617.
MONTECUCCO, C. & MOLGÓ, J. 2005. Botulinal neurotoxins: revival of an old killer. *Curr Opin Pharmacol,* 5**,** 274-9.
MONTECUCCO, C. & RASOTTO, M. B. 2015. On botulinum neurotoxin variability. *mBio,* 6**,** e02131-14.
MONTECUCCO, C. & SCHIAVO, G. 1994. Mechanism of action of tetanus and botulinum neurotoxins. *Mol Microbiol,* 13**,** 1-8.
MOREIRA, D. & LÓPEZ-GARCÍA, P. 1998. Symbiosis Between Methanogenic Archaea and δ-Proteobacteria as the Origin of Eukaryotes: The Syntrophic Hypothesis. *Journal of Molecular Evolution,* 47**,** 517-530.
MURARO, L., TOSATTO, S., MOTTERLINI, L., ROSSETTO, O. & MONTECUCCO, C. 2009. The N-terminal half of the receptor domain of botulinum neurotoxin A binds to microdomains of the plasma membrane. *Biochemical and Biophysical Research Communications,* 380**,** 76-80.
NAUMANN, M., BOO, L. M., ACKERMAN, A. H. & GALLAGHER, C. J. 2013. Immunogenicity of botulinum toxins. *Journal of neural transmission (Vienna, Austria : 1996),* 120**,** 275-290.
NETO, H. & GOULD, G. W. 2011. The regulation of abscission by multi-protein complexes. 124**,** 3199-3207.
NICHOLSON-FISH, J. C., KOKOTOS, A. C., GILLINGWATER, T. H., SMILLIE, K. J. & COUSIN, M. A. 2015. VAMP4 Is an Essential Cargo Molecule for Activity-Dependent Bulk Endocytosis. *Neuron,* 88**,** 973-984.
NOVICK, P., FIELD, C. & SCHEKMAN, R. 1980. Identification of 23 complementation groups required for post-translational events in the yeast secretory pathway. *Cell,* 21.
NUGENT, M., WANG, J., LAWRENCE, G., ZURAWSKI, T., GEOGHEGAN, J. A. & DOLLY, J. O. 2017. Conjugate of an IgG Binding Domain with Botulinum Neurotoxin A Lacking the Acceptor Moiety Targets Its SNARE Protease into TrkA-Expressing Cells When Coupled to Anti-TrkA IgG or Fc-βNGF. *Bioconjugate Chemistry,* 28**,** 1684-1692.
O'LEARY, V. B., OVSEPIAN, S. V., RAGHUNATH, A., HUO, Q., LAWRENCE, G. W., SMITH, L. & DOLLY, J. O. 2011. Innocuous full-length botulinum neurotoxin targets and promotes the expression of lentiviral vectors in central and autonomic neurons. *Gene Therapy,* 18**,** 656-665.
OHYA, T., MIACZYNSKA, M., COSKUN, U., LOMMER, B., RUNGE, A., DRECHSEL, D., KALAIDZIDIS, Y. & ZERIAL, M. 2009. Reconstitution of Rab- and SNARE-dependent membrane fusion by synthetic endosomes. *Nature,* 459**,** 1091-7.
OKA, T., UNGAR, D., HUGHSON, F. M. & KRIEGER, M. 2004. The COG and COPI complexes interact to control the abundance of GEARs, a subset of Golgi integral membrane proteins. *Molecular biology of the cell,* 15**,** 2423-2435.
OYLER, G. A., HIGGINS, G. A., HART, R. A., BATTENBERG, E., BILLINGSLEY, M., BLOOM, F. E. & WILSON, M. C. 1989. The identification of a novel synaptosomal-associated protein, SNAP-25,

differentially expressed by neuronal subpopulations. *The Journal of cell biology,* 109**,** 3039-3052.
PAGAN, J. K., WYLIE, F. G., JOSEPH, S., WIDBERG, C., BRYANT, N. J., JAMES, D. E. & STOW, J. L. 2003. The t-SNARE Syntaxin 4 Is Regulated during Macrophage Activation to Function in Membrane Traffic and Cytokine Secretion. *Current Biology,* 13**,** 156-160.
PALADE, G. 1975a. Intracellular aspects of the process of protein synthesis. *Science,* 189**,** 347-58.
PALADE, G. 1975b. Intracellular aspects of the process of protein synthesis. 189**,** 347-358.
PANTANO, S., MONTECUCCO, C. J. C. & SCIENCES, M. L. 2014. The blockade of the neurotransmitter release apparatus by botulinum neurotoxins. 71**,** 793-811.
PANTAZOPOULOU, A. & GLICK, B. S. 2019. A Kinetic View of Membrane Traffic Pathways Can Transcend the Classical View of Golgi Compartments. *Frontiers in Cell and Developmental Biology,* 7.
PEARSE, B. M. F. & ROBINSON, M. S. 1990. Clathrin, Adaptors, and Sorting. 6**,** 151-171.
PEDEN, A. A., PARK, G. Y. & SCHELLER, R. H. 2001. The Di-leucine Motif of Vesicle-associated Membrane Protein 4 Is Required for Its Localization and AP-1 Binding. 276**,** 49183-49187.
PEDEN, A. A., SCHONTEICH, E., CHUN, J., JUNUTULA, J. R., SCHELLER, R. H. & PREKERIS, R. 2004. The RCP-Rab11 complex regulates endocytic protein sorting. *Molecular biology of the cell,* 15**,** 3530-3541.
PENG, L., LIU, H., RUAN, H., TEPP, W. H., STOOTHOFF, W. H., BROWN, R. H., JOHNSON, E. A., YAO, W.-D., ZHANG, S.-C. & DONG, M. 2013. Cytotoxicity of botulinum neurotoxins reveals a direct role of syntaxin 1 and SNAP-25 in neuron survival. *Nature communications,* 4**,** 1472-1472.
PIGA, M., SATTA, L., CORRIAS, M., MONTALDO, C., LOI, G. L. & MADEDDU, G. 1990. Simultaneous 99mTc double labelling of the hepatic reticuloendothelial system and of the red blood cells: a simplified method for the detection of liver hemangiomas. *J Nucl Med Allied Sci,* 34**,** 77-80.
PIRAZZINI, M., ROSSETTO, O., ELEOPRA, R. & MONTECUCCO, C. 2017. Botulinum Neurotoxins: Biology, Pharmacology, and Toxicology. *Pharmacological reviews,* 69**,** 200-235.
PIRAZZINI, M., TEHRAN, D. A., LEKA, O., ZANETTI, G., ROSSETTO, O. & MONTECUCCO, C. 2016. On the translocation of botulinum and tetanus neurotoxins across the membrane of acidic intracellular compartments. *Biochimica et Biophysica Acta (BBA) - Biomembranes,* 1858**,** 467-474.
POCARD, T., LE BIVIC, A., GALLI, T. & ZURZOLO, C. 2007. Distinct v-SNAREs regulate direct and indirect apical delivery in polarized epithelial cells. 120**,** 3309-3320.
POLGÁR, J. N., CHUNG, S.-H. & REED, G. L. 2002. Vesicle-associated membrane protein 3 (VAMP-3) and VAMP-8 are present in human platelets and are required for granule secretion. *Blood,* 100**,** 1081-1083.

POULAIN, B. & HUMEAU, Y. 2003. [Mode of action of botulinum neurotoxin: pathological, cellular and molecular aspect]. *Ann Readapt Med Phys,* 46**,** 265-75.

PROCINO, G., BARBIERI, C., TAMMA, G., DE BENEDICTIS, L., PESSIN, J. E., SVELTO, M. & VALENTI, G. 2008. AQP2 exocytosis in the renal collecting duct -- involvement of SNARE isoforms and the regulatory role of Munc18b. *Journal of cell science,* 121**,** 2097-2106.

PRYOR, P. R., MULLOCK, B. M., BRIGHT, N. A., LINDSAY, M. R., GRAY, S. R., RICHARDSON, S. C. W., STEWART, A., JAMES, D. E., PIPER, R. C. & LUZIO, J. P. 2004. Combinatorial SNARE complexes with VAMP7 or VAMP8 define different late endocytic fusion events. *EMBO reports,* 5**,** 590-595.

RAINGO, J., KHVOTCHEV, M., LIU, P., DARIOS, F., LI, Y. C., RAMIREZ, D. M. O., ADACHI, M., LEMIEUX, P., TOTH, K., DAVLETOV, B. & KAVALALI, E. T. 2012. VAMP4 directs synaptic vesicles to a pool that selectively maintains asynchronous neurotransmission. *Nature neuroscience,* 15**,** 738-745.

RAO, S. K., HUYNH, C., PROUX-GILLARDEAUX, V., GALLI, T. & ANDREWS, N. W. 2004. Identification of SNAREs Involved in Synaptotagmin VII-regulated Lysosomal Exocytosis. 279**,** 20471-20479.

REALES, E., SHARMA, N., LOW, S. H., FÖLSCH, H. & WEIMBS, T. 2011. Basolateral Sorting of Syntaxin 4 Is Dependent on Its N-terminal Domain and the AP1B Clathrin Adaptor, and Required for the Epithelial Cell Polarity. *PLOS ONE,* 6**,** e21181.

REN, B., AZZEGAGH, Z., JARAMILLO, ANA M., ZHU, Y., PARDO-SAGANTA, A., BAGIRZADEH, R., FLORES, JOSE R., HAN, W., TANG, Y.-J., TU, J., ALANIS, DENISE M., EVANS, CHRISTOPHER M., GUINDANI, M., ROCHE, PAUL A., RAJAGOPAL, J., CHEN, J., DAVIS, C. W., TUVIM, MICHAEL J. & DICKEY, BURTON F. 2015. SNAP23 is selectively expressed in airway secretory cells and mediates baseline and stimulated mucin secretion. *Bioscience Reports,* 35.

ROBINSON, M. S. 2004. Adaptable adaptors for coated vesicles. *Trends Cell Biol,* 14**,** 167-74.

RODKEY, T. L., LIU, S., BARRY, M. & MCNEW, J. A. 2008. Munc18a scaffolds SNARE assembly to promote membrane fusion. *Molecular biology of the cell,* 19**,** 5422-5434.

ROSSETTO, O., PIRAZZINI, M. & MONTECUCCO, C. 2014. Botulinum neurotoxins: genetic, structural and mechanistic insights. *Nature Reviews Microbiology,* 12**,** 535-549.

RUIZ-MARTINEZ, M., NAVARRO, A., MARRADES, R. M., VIÑOLAS, N., SANTASUSAGNA, S., MUÑOZ, C., RAMÍREZ, J., MOLINS, L. & MONZO, M. 2016. YKT6 expression, exosome release, and survival in non-small cell lung cancer. *Oncotarget,* 7**,** 51515-51524.

RUMMEL, A. 2017. Two Feet on the Membrane: Uptake of Clostridial Neurotoxins. *In:* BARTH, H. (ed.) *Uptake and Trafficking of Protein Toxins.* Cham: Springer International Publishing.

RUMMEL, A., MAHRHOLD, S., BIGALKE, H. & BINZ, T. 2004. The HCC-domain of botulinum neurotoxins A and B exhibits a singular ganglioside binding site displaying serotype specific carbohydrate interaction. 51**,** 631-643.
RUST, A., DORAN, C., HART, R., BINZ, T., STICKINGS, P., SESARDIC, D., PEDEN, A. A. & DAVLETOV, B. 2017. A Cell Line for Detection of Botulinum Neurotoxin Type B. *Frontiers in pharmacology,* 8**,** 796-796.
RUST, A., LEESE, C., BINZ, T. & DAVLETOV, B. 2016. Botulinum neurotoxin type C protease induces apoptosis in differentiated human neuroblastoma cells. *Oncotarget,* 7**,** 33220-33228.
RYU, J.-K., MIN, D., RAH, S.-H., KIM, S. J., PARK, Y., KIM, H., HYEON, C., KIM, H. M., JAHN, R. & YOON, T.-Y. 2015. Spring-loaded unraveling of a single SNARE complex by NSF in one round of ATP turnover. *Science (New York, N.Y.),* 347**,** 1485-1489.
SACHER, M., JIANG, Y., BARROWMAN, J., SCARPA, A., BURSTON, J., ZHANG, L., SCHIELTZ, D., YATES, J. R., 3RD, ABELIOVICH, H. & FERRO-NOVICK, S. 1998. TRAPP, a highly conserved novel complex on the cis-Golgi that mediates vesicle docking and fusion. *The EMBO journal,* 17**,** 2494-2503.
SANGER, A., HIRST, J., DAVIES, A. K. & ROBINSON, M. S. 2019. Adaptor protein complexes and disease at a glance. *Journal of Cell Science,* 132**,** jcs222992.
SATO, M., YOSHIMURA, S., HIRAI, R., GOTO, A., KUNII, M., ATIK, N., SATO, T., SATO, K., HARADA, R., SHIMADA, J., HATABU, T., YORIFUJI, H. & HARADA, A. 2011. The Role of VAMP7/TI-VAMP in Cell Polarity and Lysosomal Exocytosis in vivo. 12**,** 1383-1393.
SCALES, S. J., PEPPERKOK, R. & KREIS, T. E. 1997. Visualization of ER-to-Golgi Transport in Living Cells Reveals a Sequential Mode of Action for COPII and COPI. *Cell,* 90**,** 1137-1148.
SCHIAVO, G., MATTEOLI, M. & MONTECUCCO, C. 2000. Neurotoxins Affecting Neuroexocytosis. 80**,** 717-766.
SCHIAVO, G., POULAIN, B., ROSSETTO, O., BENFENATI, F., TAUC, L. & MONTECUCCO, C. 1992a. Tetanus toxin is a zinc protein and its inhibition of neurotransmitter release and protease activity depend on zinc. *The EMBO journal,* 11**,** 3577-3583.
SCHIAVO, G. G., BENFENATI, F., POULAIN, B., ROSSETTO, O., DE LAURETO, P. P., DASGUPTA, B. R. & MONTECUCCO, C. 1992b. Tetanus and botulinum-B neurotoxins block neurotransmitter release by proteolytic cleavage of synaptobrevin. *Nature,* 359**,** 832-835.
SCHOCH, S., DEÁK, F., KÖNIGSTORFER, A., MOZHAYEVA, M., SARA, Y., SÜDHOF, T. C. & KAVALALI, E. T. 2001. SNARE Function Analyzed in Synaptobrevin/VAMP Knockout Mice. 294**,** 1117-1122.
SCHRAW, T. D., RUTLEDGE, T. W., CRAWFORD, G. L., BERNSTEIN, A. M., KALEN, A. L., PESSIN, J. E. & WHITEHEART, S. W. 2003. Granule stores from cellubrevin/VAMP-3 null mouse platelets exhibit normal stimulus-induced release. *Blood,* 102**,** 1716-1722.

SCOTT, A. B., ROSENBAUM, A. & COLLINS, C. C. 1973. Pharmacologic Weakening of Extraocular Muscles. *Investigative Ophthalmology & Visual Science,* 12**,** 924-927.
SCOTT, B. L., VAN KOMEN, J. S., IRSHAD, H., LIU, S., WILSON, K. A. & MCNEW, J. A. 2004. Sec1p directly stimulates SNARE-mediated membrane fusion in vitro. *The Journal of cell biology,* 167**,** 75-85.
SHARMA, N., LOW, S. H., MISRA, S., PALLAVI, B. & WEIMBS, T. 2006. Apical targeting of syntaxin 3 is essential for epithelial cell polarity. *The Journal of cell biology,* 173**,** 937-948.
SHEN, J., TARESTE, D. C., PAUMET, F., ROTHMAN, J. E. & MELIA, T. J. 2007. Selective Activation of Cognate SNAREpins by Sec1/Munc18 Proteins. *Cell,* 128**,** 183-195.
SHI, A. & GRANT, B. D. 2013. Interactions between Rab and Arf GTPases regulate endosomal phosphatidylinositol-4,5-bisphosphate during endocytic recycling. *Small GTPases,* 4**,** 106-9.
SHITARA, A., SHIBUI, T., OKAYAMA, M., ARAKAWA, T., MIZOGUCHI, I., SAKAKURA, Y. & TAKUMA, T. 2017. VAMP4 and its cognate SNAREs are required for maintaining the ribbon structure of the Golgi apparatus. *Journal of Oral Biosciences,* 59**,** 192-196.
SHONE, C. C., HAMBLETON, P. & MELLING, J. 1985. Inactivation of Clostridium botulinum type A neurotoxin by trypsin and purification of two tryptic fragments. 151**,** 75-82.
SHONE, C. C., HAMBLETON, P. & MELLING, J. 1987. A 50-kDa fragment from the NH2-terminus of the heavy subunit of Clostridium botulinum type A neurotoxin forms channels in lipid vesicles. 167**,** 175-180.
SIKORRA, S., HENKE, T., GALLI, T. & BINZ, T. 2008. Substrate recognition mechanism of VAMP/synaptobrevin-cleaving clostridial neurotoxins. *The Journal of biological chemistry,* 283**,** 21145-21152.
SIMONS, K. & TOOMRE, D. 2000. Lipid rafts and signal transduction. *Nature Reviews Molecular Cell Biology,* 1**,** 31-39.
SIMPSON, L. L. 2000. Identification of the characteristics that underlie botulinum toxin potency: implications for designing novel drugs. *Biochimie,* 82**,** 943-53.
SMITH, T. J., LOU, J., GEREN, I. N., FORSYTH, C. M., TSAI, R., LAPORTE, S. L., TEPP, W. H., BRADSHAW, M., JOHNSON, E. A., SMITH, L. A. & MARKS, J. D. 2005. Sequence variation within botulinum neurotoxin serotypes impacts antibody binding and neutralization. *Infection and immunity,* 73**,** 5450-5457.
SØGAARD, M., TANI, K., YE, R. R., GEROMANOS, S., TEMPST, P., KIRCHHAUSEN, T., ROTHMAN, J. E. & SÖLLNER, T. 1994. A rab protein is required for the assembly of SNARE complexes in the docking of transport vesicles. *Cell,* 78**,** 937-48.
SÖLLNER, T., WHITEHEART, S. W., BRUNNER, M., ERDJUMENT-BROMAGE, H., GEROMANOS, S., TEMPST, P. & ROTHMAN, J. E. 1993. SNAP receptors implicated in vesicle targeting and fusion. *Nature,* 362**,** 318-324.
SORKIN, A. & GOH, L. K. 2008. Endocytosis and intracellular trafficking of ErbBs. *Exp Cell Res,* 314**,** 3093-106.

STEEGMAIER, M., KLUMPERMAN, J., FOLETTI, D. L., YOO, J. S. & SCHELLER, R. H. 1999. Vesicle-associated membrane protein 4 is implicated in trans-Golgi network vesicle trafficking. *Molecular biology of the cell,* 10**,** 1957-1972.

STEERE, A. N., BYRNE, S. L., CHASTEEN, N. D. & MASON, A. B. 2012. Kinetics of iron release from transferrin bound to the transferrin receptor at endosomal pH. *Biochimica et biophysica acta,* 1820**,** 326-333.

STRALEY, K. S. & GREEN, S. A. 2000. Rapid transport of internalized P-selectin to late endosomes and the TGN: roles in regulating cell surface expression and recycling to secretory granules. *The Journal of cell biology,* 151**,** 107-116.

SÜDHOF, T. C., BAUMERT, M., PERIN, M. S. & JAHN, R. 1989. A synaptic vesicle membrane protein is conserved from mammals to Drosophila. *Neuron,* 2**,** 1475-1481.

SÜDHOF, T. C. & ROTHMAN, J. E. 2009. Membrane fusion: grappling with SNARE and SM proteins. *Science (New York, N.Y.),* 323**,** 474-477.

SUTTON, R. B., FASSHAUER, D., JAHN, R. & BRUNGER, A. T. 1998. Crystal structure of a SNARE complex involved in synaptic exocytosis at 2.4 Å resolution. *Nature,* 395**,** 347-353.

SZTUL, E. & LUPASHIN, V. 2009. Role of vesicle tethering factors in the ER–Golgi membrane traffic. *FEBS Letters,* 583**,** 3770-3783.

TAKAHASHI, M., TAJIKA, Y., KHAIRANI, A. F., UENO, H., MURAKAMI, T. & YORIFUJI, H. 2013. The localization of VAMP5 in skeletal and cardiac muscle. *Histochemistry and Cell Biology,* 139**,** 573-582.

TAKAHASHI, S., KUBO, K., WAGURI, S., YABASHI, A., SHIN, H.-W., KATOH, Y. & NAKAYAMA, K. 2012. Rab11 regulates exocytosis of recycling vesicles at the plasma membrane. *Journal of Cell Science,* 125**,** 4049-4057.

TAKÁTS, S., GLATZ, G., SZENCI, G., BODA, A., HORVÁTH, G. V., HEGEDŰS, K., KOVÁCS, A. L. & JUHÁSZ, G. 2018. Non-canonical role of the SNARE protein Ykt6 in autophagosome-lysosome fusion. *PLoS Genet,* 14**,** e1007359.

TOCHIO, H., TSUI, M. M. K., BANFIELD, D. K. & ZHANG, M. 2001. An Autoinhibitory Mechanism for Nonsyntaxin SNARE Proteins Revealed by the Structure of Ykt6p. 293**,** 698-702.

TRAN, T. H. T., ZENG, Q. & HONG, W. 2007. VAMP4 cycles from the cell surface to the trans-Golgi network via sorting and recycling endosomes. 120**,** 1028-1041.

TRIMBLE, W. S., COWAN, D. M. & SCHELLER, R. H. 1988a. VAMP-1: a synaptic vesicle-associated integral membrane protein. *Proceedings of the National Academy of Sciences of the United States of America,* 85**,** 4538-4542.

TRIMBLE, W. S., COWAN, D. M. & SCHELLER, R. H. 1988b. VAMP-1: a synaptic vesicle-associated integral membrane protein. *Proceedings of the National Academy of Sciences,* 85**,** 4538-4542.

VAROQUEAUX, F., SIGLER, A., RHEE, J.-S., BROSE, N., ENK, C., REIM, K. & ROSENMUND, C. 2002. Total arrest of spontaneous and evoked synaptic transmission but normal synaptogenesis in the absence of Munc13-mediated vesicle priming. *Proceedings of the National Academy of Sciences of the United States of America,* 99**,** 9037-9042.

VARSHAVSKY, A. 2019. N-degron and C-degron pathways of protein degradation. *Proceedings of the National Academy of Sciences,* 116**,** 358-366.
VAZQUEZ-CINTRON, E. J., BESKE, P. H., TENEZACA, L., TRAN, B. Q., OYLER, J. M., GLOTFELTY, E. J., ANGELES, C. A., SYNGKON, A., MUKHERJEE, J., KALB, S. R., BAND, P. A., MCNUTT, P. M., SHOEMAKER, C. B. & ICHTCHENKO, K. 2017. Engineering Botulinum Neurotoxin C1 as a Molecular Vehicle for Intra-Neuronal Drug Delivery. *Scientific reports,* 7**,** 42923-42923.
VERDERIO, C., ROSSETTO, O., GRUMELLI, C., FRASSONI, C., MONTECUCCO, C. & MATTEOLI, M. 2006. Entering neurons: botulinum toxins and synaptic vesicle recycling. *EMBO reports,* 7**,** 995-999.
WALL, A. A., CONDON, N. D., YEO, J. C., HAMILTON, N. A. & STOW, J. L. 2015. Chapter 1 - Dynamic imaging of the recycling endosomal network in macrophages. *In:* GUO, W. (ed.) *Methods in Cell Biology.* Academic Press.
WANG, C.-C., NG, C. P., LU, L., ATLASHKIN, V., ZHANG, W., SEET, L.-F. & HONG, W. 2004. A Role of VAMP8/Endobrevin in Regulated Exocytosis of Pancreatic Acinar Cells. *Developmental Cell,* 7**,** 359-371.
WARD, D. M., PEVSNER, J., SCULLION, M. A., VAUGHN, M. & KAPLAN, J. 2000. Syntaxin 7 and VAMP-7 are soluble N-ethylmaleimide-sensitive factor attachment protein receptors required for late endosome-lysosome and homotypic lysosome fusion in alveolar macrophages. *Molecular biology of the cell,* 11**,** 2327-2333.
WATSON, R. T. & PESSIN, J. E. 2001. Intracellular organization of insulin signaling and GLUT4 translocation. *Recent Prog Horm Res,* 56**,** 175-93.
WEIDMAN, P. J., MELANÇON, P., BLOCK, M. R. & ROTHMAN, J. E. 1989. Binding of an N-ethylmaleimide-sensitive fusion protein to Golgi membranes requires both a soluble protein(s) and an integral membrane receptor. *Journal of Cell Biology,* 108**,** 1589-1596.
WHYTE, J. R. & MUNRO, S. 2002. Vesicle tethering complexes in membrane traffic. *J Cell Sci,* 115**,** 2627-37.
WIEDUWILT, M. J. & MOASSER, M. M. 2008. The epidermal growth factor receptor family: biology driving targeted therapeutics. *Cellular and molecular life sciences : CMLS,* 65**,** 1566-1584.
WILLIAMS, D. & PESSIN, J. E. 2008. Mapping of R-SNARE function at distinct intracellular GLUT4 trafficking steps in adipocytes. *The Journal of cell biology,* 180**,** 375-387.
WILLIAMSON, C. H. D., VAZQUEZ, A. J., HILL, K., SMITH, T. J., NOTTINGHAM, R., STONE, N. E., SOBEK, C. J., COCKING, J. H., FERNÁNDEZ, R. A., CABALLERO, P. A., LEISER, O. P., KEIM, P. & SAHL, J. W. 2017. Differentiating Botulinum Neurotoxin-Producing Clostridia with a Simple, Multiplex PCR Assay. *Applied and environmental microbiology,* 83**,** e00806-17.
WILSON, D. W., WHITEHEART, S. W., WIEDMANN, M., BRUNNER, M. & ROTHMAN, J. E. 1992. A multisubunit particle implicated in membrane fusion. *Journal of Cell Biology,* 117**,** 531-538.
WILSON, D. W., WILCOX, C. A., FLYNN, G. C., CHEN, E., KUANG, W.-J., HENZEL, W. J., BLOCK, M. R., ULLRICH, A. & ROTHMAN, J. E. 1989. A

fusion protein required for vesicle-mediated transport in both mammalian cells and yeast. *Nature,* 339**,** 355-359.
XU, Y., MARTIN, S., JAMES, D. E. & HONG, W. 2002. GS15 Forms a SNARE Complex with Syntaxin 5, GS28, and Ykt6 and Is Implicated in Traffic in the Early Cisternae of the Golgi Apparatus. *Molecular Biology of the Cell,* 13**,** 3493-3507.
YAMAMOTO, H., IDA, T., TSUTSUKI, H., MORI, M., MATSUMOTO, T., KOHDA, T., MUKAMOTO, M., GOSHIMA, N., KOZAKI, S. & IHARA, H. 2012. Specificity of botulinum protease for human VAMP family proteins. 56**,** 245-253.
YANG, C., MORA, S., RYDER, J. W., COKER, K. J., HANSEN, P., ALLEN, L.-A. & PESSIN, J. E. 2001a. VAMP3 Null Mice Display Normal Constitutive, Insulin- and Exercise-Regulated Vesicle Trafficking. *Molecular and Cellular Biology,* 21**,** 1573-1580.
YANG, C., MORA, S., RYDER, J. W., COKER, K. J., HANSEN, P., ALLEN, L. A. & PESSIN, J. E. 2001b. VAMP3 null mice display normal constitutive, insulin- and exercise-regulated vesicle trafficking. *Molecular and cellular biology,* 21**,** 1573-1580.
YU, H., RATHORE, S. S. & SHEN, J. 2013. Synip Arrests Soluble N-Ethylmaleimide-sensitive Factor Attachment Protein Receptor (SNARE)-dependent Membrane Fusion as a Selective Target Membrane SNARE-binding Inhibitor. *Journal of Biological Chemistry,* 288**,** 18885-18893.
YU, I.-M. & HUGHSON, F. M. 2010. Tethering Factors as Organizers of Intracellular Vesicular Traffic. 26**,** 137-156.
ZENG, Q., SUBRAMANIAM, V. N., WONG, S. H., TANG, B. L., PARTON, R. G., REA, S., JAMES, D. E. & HONG, W. 1998. A Novel Synaptobrevin/VAMP Homologous Protein (VAMP5) Is Increased during In Vitro Myogenesis and Present in the Plasma Membrane. 9**,** 2423-2437.
ZENG, Q., TRAN, T. T. H., TAN, H.-X. & HONG, W. 2003. The Cytoplasmic Domain of Vamp4 and Vamp5 Is Responsible for Their Correct Subcellular Targeting: THE N-TERMINAL EXTENSION OF VAMP4 CONTAINS A DOMINANT AUTONOMOUS TARGETING SIGNAL FOR THE TRANS-GOLGI NETWORK. 278**,** 23046-23054.
ZHANG, S., MASUYER, G., ZHANG, J., SHEN, Y., LUNDIN, D., HENRIKSSON, L., MIYASHITA, S.-I., MARTÍNEZ-CARRANZA, M., DONG, M. & STENMARK, P. 2017. Identification and characterization of a novel botulinum neurotoxin. *Nature Communications,* 8**,** 14130.
ZHAO, M., WU, S., ZHOU, Q., VIVONA, S., CIPRIANO, D. J., CHENG, Y. & BRUNGER, A. T. 2015. Mechanistic insights into the recycling machine of the SNARE complex. *Nature,* 518**,** 61-67.